universität wien

DISSERTATION / DOCTORAL THESIS

Titel der Dissertation /Title of the Doctoral Thesis

„From local to global: Dissecting the molecular mechanisms of olfactory map formation in *Drosophila*“

verfasst von / submitted by

Rashmit Kaur

angestrebter akademischer Grad / in partial fulfilment of the requirements for the degree of

Doctor of Philosophy (PhD)

Wien, 2018/ Vienna 2018

Studienkennzahl lt. Studienblatt / degree programme code as it appears on the student record sheet:	A 794 685 437
Dissertationsgebiet lt. Studienblatt / field of study as it appears on the student record sheet:	Biologie/ Biology
Betreut von / Supervisor:	Univ.-Prof. Dr. Thomas Hummel

“God is in the details”

Preface

This thesis contains the results of 4 research projects summarized below. All projects include productive collaborations within the Department of Neurobiology and with other research groups. Author contributions are detailed at the end of each thesis chapter.

1) ***Commissural interneurons instruct bilaterality in olfactory circuit organization***. **Kaur R.**, Surala M., Hoger S., Grössmann N., Grimm A., Timaeus L., Kallina W., and Hummel T. (2018, submitted); described in chapter 2.
Although not the first experiments performed in my studies, this project defines the core of my PhD research. Intrigued by the fact that direct bilateral sensory connection is a feature unique to Diptera, I decided to determine the developmental mechanisms underlying inter-hemispheric connectivity using Neuroglian function as a critical genetic tool. I started the analysis of Neuroglian expression and loss-of function, and initiated the RNAi approach to identify the cell type specific requirement. I found that bilaterally projecting local interneurons are crucial for interhemispheric connectivity in the olfactory system. Here I could propose a novel developmental mechanism to induce the formation of commissural fibers during brain evolution.

2) ***Synaptic recognition identity in the Drosophila olfactory system is mediated by non-apoptotic caspase function***. Scheper C., **Kaur R.**, Timaeus L., Niehues S., Peters U. and Hummel T. (in preparation); described in chapter 3.
Previous analysis by C. Scheper has identified a non-apoptotic function of Dark, a central regulator in caspase activation, in *Drosophila* sensory neuron connectivity. In follow-up studies I could determine the relative contribution of different initiator caspases in modulating axonal pathfinding and target cell recognition. In addition, in a series of clonal conditions I could show how caspase activity affects the expression of cell adhesion molecules in the context of inter-axonal communication.

3) ***The chromatin modulator Psc coordinates synaptic and sensory identity in the Drosophila olfactory system*.** Aydemir Ö., **Kaur R.**, Steffes G., Kuhlmann B., Grimm A., Alenius M., Moore A., and Hummel T. (in preparation); described in chapter 4.

Identified by Ö. Aydemir in a genetic screen for regulators of olfactory receptor neuron development, the chromatin modulator Psc was shown to play a critical role in neuronal connectivity and odorant receptor expression. However, it was unclear why loss of Psc affects only a defined subset of sensory neurons and how synaptic and sensory identity are coordinated. Here I could show in a series of loss- and gain-of-function experiments that Psc controls a specific lineage-related identity by maintaining the expression of Svp, a member of the steroid receptor gene superfamily. Furthermore, I could demonstrate that neuronal connectivity and odorant receptor selection define two independent events in sensory neuron differentiation.

4) ***High-resolution ultramicroscopy of the developing and adult nervous system of optically-cleared Drosophila melanogaster.*** Pende M., Becker K., Wanis M., Saghafi S., **Kaur R.**, Hahn C., Pende N., Foroughipour M., Hummel T. and Dodt H.U. (Nature Communications, 2018); described in chapter 5.

A major challenge in the analysis of *Drosophila* olfactory system development is separate preparation of sensory neurons and synaptic brain regions during pupal stages, which makes the direct visualization of peripheral and central organization at sufficient spatial resolution difficult. To improve the imaging methodology I teamed up with the group of Prof. Hans-Ulrich Dodt, an expert in ultramicroscopy at the TU Vienna, to develop a new protocol for high-resolution imaging of *Drosophila* whole mount pupae and adult flies.

Acknowledgements

I am indebted to many people.

First and foremost, I am thankful to my supervisor Prof. Thomas Hummel for providing me this opportunity to do research under his guidance. He is not only a brilliant mentor but also a wonderful human being, who taught me perseverance and due diligence to details. I would like to thank you very much for all your support and understanding over these past few years. It has been a period of intense learning for me, not only in scientific arena, but also at a personal level. I will be always grateful for this extraordinary experience.

Many thanks to Prof. Axel Schmid, Prof. Harald Tichy and their lab colleagues for the warm welcome to the department. Prof. Ulrich Technau for kind advices and motivation. Prof. Dietmar Schmucker and Prof. Ruth Herbst for their time to review my work and inputs.

I am very thankful to the support staffs, the real backbone, of the department for their generous assistance. I am really amazed how much you guys work to keep the lab running. Alex- you are my super woman and you are flawless. We are such a good team. Thank you so much for helping me out with hundreds of dissections, several recombinations and constant support without questioning. I wish that I could learn planning things from you. Wolfgang- for never saying no and initiating the backfill work, Sigi- for rearing the flies so well, Dani- for taking care of mol-bio lab, Andreas- for helping with all the technical issues to and at last I cannot thank enough Maria in words. She made my stay possible in Vienna. Thank you so much Maria for taking care of all the bureaucratic issues, which gave me headache most of the time.

To Lorin, Abhi and GG for all the fun and collaborative environment from the initial days in the lab. You guys were excellent squad. I am thankful to Abhi, who helped me to get started in Münster and for his kind introduction to mol-bio lab. Thank you Lorin for introducing me to the other flies than *D. melanogaster*. I really admire your passion towards nature so much. GG! My special thanks to you for your unconditional support, for always taking my side in silly things, for your advices, for

several productive discussions, for keeping a scientific check on me, for always listening to my nonsense without getting bored and telling me what is right or wrong. I do not want to imagine my lab life without you not being around. To all of my wonderful current and former lab-members, especially to Ursula, Niki, Michi and Sebastian for your valuable associations and contributions on the projects. Including Deniz, Laura, Elisabeth, Michael Sackel, Ameya, Selen, Shilpa, Ali and Lubana for the delightful tea sessions, lab birthday celebrations, hikes, outings and memorable evenings. I will definitely miss you all.

Getting through my dissertation required more than academic support, I have many people to thank. I cannot begin to express my gratitude for their friendship. Purva, Tripti, Sakku, and Manika for being my pillar of support outside the lab, for keeping a constant check on me and never leaving me alone, no matter whichever corner of the world you all are in. I would like to thank my youngest buddy Rohan for being himself and such a wonderful child. You are the best addition in my life in Vienna and I will always cherish the moments I have spent with you. Thank you Mamta for welcoming me in your lovely family, letting me spoil Rohan, for your motivations and always telling me not to worry. I would also like to thank Katha, Astrid, Andrea and Bernd who opened both their home and heart to me right from the beginning and for hearing me patiently all the time. Because of you all I can call Austria as my second home. My special thanks to Ani for being so patient with me. You were always there through my thick and thin. You kept me going…

Most importantly, none of this could have happened without the support of my family. Thanks to my Papuda and Mamuda for their immense patience, encouragement, and kindness throughout last years. Thank you for allowing me my freedom and letting me wander around to pursue my goals. Thanks to my crazy siblings Ritta, Guru and Veer for their love and support.

This dissertation would have not been possible without the environment and resources of the University of Vienna.

I dedicate this thesis to the underprivileged children who cannot afford or are denied education.

Table of Contents

Zusammenfassung

Sensorische Systeme übertragen wichtige Informationen aus der Umwelt in neuronale Aktivität des Gehirns und ermöglichen damit eine entsprechende Verhaltensreaktion von Tieren. Die Wahrnehmung komplexer Informationen aus der Umwelt ist in mehrere parallele Signalwege organisiert, die oft in einem definierten räumlichen Muster im Gehirn angeordnet sind. So bildet zum Beispiel zu den olfaktorischen System jede Klasse von Geruchsrezeptoren eine eigene sensorischen Nervenbahn in höhere Integrationszentren wie die Pilzkörper in Insekten oder der olfaktorische Kortex in *Säugetieren*. Zusätzlich sind verschiedene Geruchsqualitäten, welche die Wahrnehmung von Nahrung oder soziale Interaktionen vermitteln, nicht nur in den peripheren Wahrnehmungsfeldern sondern auch in synaptische Gehirnregionen räumlich getrennt. Auf welche Weise sich die neuronale und molekulare Identität der Nervenbahnen und synaptischen Domänen während der Entwicklung von sensorischen Schaltkreisen herausbildet, stellt ein zentrales Forschungsthema in den Neurowissenschaften dar. Bilaterale Integration von sensorischer Aktivität zwischen den Gehirnhälften mittels separater Kommissuren ist ein gemeinsames Prinzip in der Organisation von Nervensystemen. In welchem Schritt entlang der peripher-zentralen Achse jedoch die bilaterale Repräsentation benötigt wird, kann sich in verschiedenen sensorischen Systemen grundlegend unterscheiden. So ist beispielsweise im primären olfaktorischen Zentrum vieler Arten (wie beim Antennallobus in Insekten oder dem Riechkolben in Säugetieren) die Organisation der ankommenden sensorischen Neurone strikt unilateral, während in höheren Geruchszentren wie dem Pilzkörper bzw. dem piriformen Kortex interhemisphärische Verbindungen ausgebildet werden. In der Evolution des Nervensystems können neuartige kommissurale Verbindungen, die eine Verknüpfung der beiden Hemisphären unterstützen wie das Corpus Callosum in höheren Säugetieren, recht schnell auftreten. Allerdings sind die Entwicklungsmechanismen, die einer Ausbildung solcher symmetrischer Verbindungen zugrunde liegen, weitestgehend unbekannt.

In meinem PhD Projekt habe ich die molekularen Mechanismen untersucht, die in Drosophila an drei unterschiedlichen Schritten den Aufbau des olfaktorischen Systems kontrollieren: Domänen-spezifische Segregation der Axone (1), synaptische

Spezifität von sensorischen Kanälen (2) und die Bildung eines bilateralen Netzwerks (3). (1) Ausgehend von der Beobachtung, dass der Verlust des Caspase-Regulators Dark zu einer spezifischen Veränderungen in der Projektion und synaptischen Verschaltung von olfaktorischen Rezeptorneuronen führt, habe ich die Funktion von Caspasen in einem Mechanismus unabhängig von einer Zelltod-Induktion charakterisiert. Dabei konnte ich zeigen, dass die relative Aktivität von Caspasen zur Expression von Zelladhäsionsmolekülen führt, die eine definierte Erkennungsidentität in der Projektion und Synaptogenese von Neuronen bedingt. (2) In einem zweiten Projekt konnte ich neue Transkriptionsfaktoren in der neuronalen Differenzierung des Geruchssystems analysieren. Nach der Notch-Rezeptor induzierten Diversifizierung von neuronalen Vorläuferzellen stablilisiert der Chromatin-Regulator PSC die molekulare Identität der sensorischen Rezeptoren mittels *Seven-up* Expression. (3) In meinem primären Forschungsprojekt konnte ich einen neuen Entwicklungsmechanismus identifizieren, durch den bilateral-symmetrische Gehirnregionen in Drosophila miteinander verknüpft werden. Die antennale Kommissur, bei der es sich um eine evolutionäre Neubildung im Stammbaum der Fliegen handelt, entsteht durch die Projektion eines kontralateralen Axons der sensorischen Neurone. Der Verlust des Zelladhäsionsmoleküles Neuroglian führt zu einen Rückbildung des bilateralen Schaltkreises in eine unilateral Repräsentation der sensorischen Information. Die Anwendung der RNA-Interferenz Methode zeigte nicht nur eine zell-autonome Neuroglian Funktion in sensorischen Neuronen sondern auch in einer neuen Klasse von “kommissuralen Pionierneuronen” [cPINs]. Vor dem Einwachsen der sensorischen Nervenzellen bilden cPINs eine dendritische Verzweigung im ipsilateralen Zielgebiet und einen kommissuralen Trakt aus. Basierend auf diesen Ergebnissen postuliere ich ein Entwicklungsmodell, in dem cPINs mittels Neuroglian die ipsilateral Zielzellerkennung von Axonen verhindert und damit eine kontralaterale Projektion ermöglichen. Da sich cPINs im adulten Nervensystem in bilaterale inhibitorische Interneurone differenzieren, zeigen diese Ergebnisse wie ein einzelner Zelltyp die funktionelle Organisation von neuronalen Netzwerken zwischen den Gehirnhemispheren kontrollieren kann.

Synopsis

Sensory systems map features of the external world into internal representations within the brain, thus allowing animals to respond appropriately to important environmental signals. The perception of complex environmental information is organized into multiple parallel pathways, which in many cases are arranged in a defined spatial pattern. For example in the olfactory system, each odorant receptor type forms a distinct sensory channel towards the higher integration centers like insect mushroom bodies or mammalian olfactory cortex. In addition, different odor qualities associated with food perception versus social interaction are spatially separated not only in the peripheral receptive fields but also in distinct olfactory brain regions. How distinct channel and domain identity is specified during sensory map formation defines a central topic in developmental circuit neuroscience.

Bilateral integration of hemispheric sensory activity via distinct commissural fiber tracts is a common principle in nervous system organization, although the position along the peripheral-central axis, at which bilateral representation is required, can differ quite substantially. For example, in most olfactory systems the first processing center, the olfactory bulb in mammals and antennal lobe in insects, define regions of strict unilateral sensory input and interhemispheric connections are established in central olfactory association domains like piriform cortex/mushroom bodies in mammals and insects, respectively. Interestingly, novel commissural tracts supporting bilateral integration can evolve quite rapidly like the corpus callosum in mammals, but the developmental mechanisms underlying the formation of homotopic connections between brain hemispheres are mostly unknown.

In my PhD project, I have explored the molecular mechanism involved in three distinct developmental steps in *Drosophila* olfactory map formation: domain-specific axon segregation, synaptic specificity of sensory channels and bilateral circuit assembly. (1) Starting with the observation that loss of *Death-associated apaf-1 related killer* [Dark], the main regulator of initiator caspases, results in a specific switch in olfactory receptor neuron [ORN] axon segregation and targeting, I determined how the non-apoptotic function of caspases provides axonal recognition identity. Here I could show that the cell-intrinsic levels of the caspases specify the

expression of adhesion molecules in an ORN class specific manner, thereby providing novel insights in the regulatory mechanisms linking domain and synaptic identity. (2) To learn more about the unique coordination of receptor expression and synaptic partner choice I characterized the interplay among different transcription factors in lineage-related ORN differentiation. Following the initial Notch-mediated diversification of precursor siblings via *Seven-up* activation, the chromatin-modulator PSC is subsequently required to stabilize ORN identity and allowing the appropriate olfactory receptor choice during late ORN development.

(3) In my main project I could identify a novel mechanism by which pairs of homotopic synaptic glomeruli across brain hemispheres are integrated into a bilateral olfactory map. The olfactory commissure, an evolutionary novelty in higher dipteran flies, results from an additional contralateral projection of each ORN. Loss of the cell adhesion molecule Neuroglian leads to a switch of the bilateral into a unilateral olfactory circuit. Cell-type specific RNAi revealed that, in addition to a cell-autonomous function in ORNs, Neuroglian is required in a novel class of "commissural pioneering interneurons" [cPINs]. Before ORN axon innervation, cPINs not only extend processes within the ipsi-lateral target field but also establish a pioneer commissural tract. I propose a model in which cPINs prevent ipsi-lateral target recognition via Neuroglian thereby facilitating contra-lateral projections of in-growing ORN axons. As cPINs subsequently develop in bilateral inhibitory interneurons, these findings demonstrate how a single cell type can organize the functional assembly of interhemispheric brain circuits.

Chapter 1

Introduction

1.1 Sensory systems

Organisms are challenged with complex and dynamic sensory stimuli in their natural surroundings. This requires external sensory organs to perceive environmental cues and a central nervous system to process, deduce and induce behavioral responses. Mostly stereotypic and dedicated neural circuits are formed for distinct sensory modalities during nervous system development. In each sensory modality the stimulus is mapped onto the central nervous system precise synaptic connections in the transition from periphery to the brain [1]. Beside strictly topographic connections, in which the spatial pattern of peripheral activation is maintained in central synaptic areas, integration and processing of sensory information often requires convergent and divergent connectivity pattern, a basic design exhibited by most sensory systems [1].

Evolutionary distant species, such as mammals and insects, show similar structural and functional principles in sensory circuit organization, raising the question about conserved molecular programs. During development, various processes coordinate with each other to specify sensory neurons and the precise synaptic connections with the distinct target cells in the central nervous system. A detailed understanding of the factors and mechanisms underlying the development of sensory circuits' organization is one of the main topics of contemporary developmental neuroscience.

1.2 The olfactory system

Among different sensory modalities, olfaction is fundamental to all animal species, for their behavioral responses to potential mate, communication, food and navigation [2]. It also exhibits a high degree of evolutionary conservation throughout the animal kingdom with respect to its overall circuit architecture and share common aspects which are fundamental to information processing [2]. Interestingly, olfaction evolved earlier than any other sensory modalities, approximately 500 million years ago, thus

the most ubiquitous and ancient of all senses [3]. Partly due to its anatomical accessibility, and modularity, it has long been appreciated as a well-suited model system for addressing questions pertinent to sensory system organization and development. Despite these advantages, research on chemical senses like olfaction is less well understood and has been rather slow in comparison to other sensory systems such as vision and hearing, the modalities more crucial to survival of *Homo Sapiens* [4]. In this thesis I addressed central aspects of olfactory system organization and development utilizing the genetic model *Drosophila.*

In flies, olfaction begins from peripheral sensory organs, such as olfactory epithelium in mammals and a pair of antenna and maxillary palp in insects and [Fig1]. The olfactory system encounters enormous number of distinct stimuli. Hence in order to increase the chemical detection coverage and accurate recognition of an odor, olfactory sensory system has evolved to express a rather rich repertoire of sensory receptor molecules, the "Olfactory Receptor" [OR] that are localized on the dendrites of the olfactory receptor neurons [2,5]. A glimpse into the richness of ORs is provided by the sheer size of the OR gene family: approximately 60 in *Drosophila*, 170 in honey bee and 1000 in mouse [6–8]. ORs are G-protein coupled receptors exhibiting seven trans-membrane domains, however insect ORs are evolutionary distinct from mammalian ORs [8,9]. These studies showed that individual olfactory receptor neurons [ORNs], anatomically similar in insects and mammals, choose to express only one *OR* gene [6,10]. ORNs expressing a given OR are restricted to defined expression "zones" in the peripheral sensory organs [6,11,12] [Fig 1]. Most individual odors activate multiple ORs, where some ORs are broadly tuned responding to several odors and others are tuned narrowly, therefore an individual stimulus is encoded by combined activity of multiple ORs [5,13]. This appears to be essential requirement for discriminatory capacity of sensory system as it enables animals to differentiate many more odors than the number of ORs expressed.

Although the molecular and cellular organization of the insect and mammalian system is remarkably similar, the developmental control mechanisms underlying olfactory circuit formation are quite different. In flies the expression of an OR is based on deterministic principles, vertebrates on the other hand exhibit a powerful stochastic choice process in complemented by feedback regulation [14]. Further, the functional

ORs localize in growing ORN axons to determine their synaptic specificity in the mouse olfactory brain center [15], whereas the *Drosophila* OR genes are expresses after ORN connectivity has been established, raising the questing of how monospecific OR selection and axonal connectivity are precisely coupled in ORN development. In this dissertation I am addressing the role of the transcriptional regulators Psc and Svp in the coordinated differentiation of "sensory specificity" and "synaptic identity" in Drosophila ORNs [Fig 1].

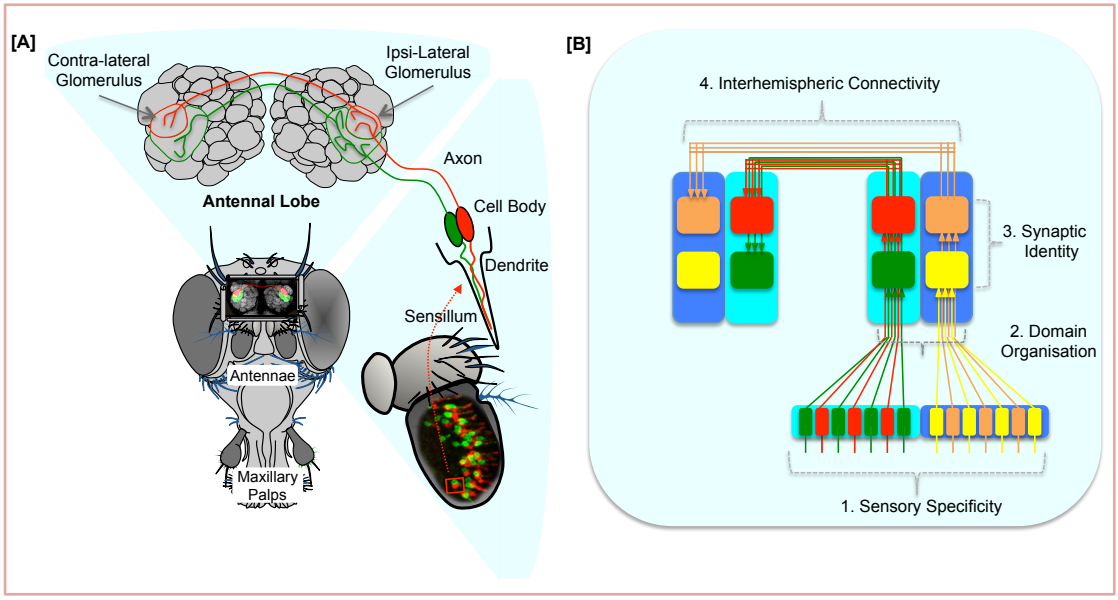

Figure 1: The *Drosophila* olfactory system. [A] Anatomical organization of the adult AL of *Drosophila* showing the projections of olfactory receptor neurons [ORNs, red and green] from the antenna into the AL in the brain [figure adapted from 16]. In the AL, sensory neurons segregate in a class-specific manner in both hemispheres. [B] Schematic drawing of global organization of ORN projections into the AL and the key features of the olfactory map, numbered as 1-4. The cell-bodies of the ORNs are located in stereotyped combination [red and green ORN] within a single unit called sensillum and are grouped into classes according to the olfactory receptor [OR] they express on their dendrites [Sensory Specificity]. Different morphological sensilla are enriched on the medial and lateral surface of the antenna and this segregation of sensilla type on the antenna is apparent in the AL [cyan and blue, respectively], in which ORNs send their axons to the AL and they segregate into distinct projection domains [Domain Organization]. All ORNs of the same OR class [e.g. green] converge onto the same glomerulus [Synaptic Identity]. Most ORN classes [e.g. green and red] send a projection across the commissure and innervate the corresponding homologous glomerulus in the contra-lateral AL [Interhemispheric connectivity], whereas few of the ORN class show unilateral innervation [e.g. yellow].

In both insects and vertebrates, there is massive convergence of ORNs onto the primary olfactory or processing center (the insect antennal lobe [AL] and the vertebrate olfactory bulb [OB]). Both AL and OB harbors synaptic connections that are organized into spatially segregated and discrete units of neuropile known as

"glomeruli," a key evolutionarily conserved feature and one of the most distinctive structure in the brain [17] [Fig 1]. In general, the olfactory system has a remarkably stereotypic organization into a discrete neuronal map [18] where distributed ORNs in the periphery expressing the same type of OR converge onto the same glomeruli, displaying precise synaptic identity [6,19] [Fig 1]. This is in contrast to the other sensory modalities like visual system, which exhibit continuous topographic mapping between the receptive and target fields in order to conserve the spatial information of the stimuli [18]. In mouse, ORNs expressing the same OR are found within specific epithelium zone but without any within-zone spatial organization [11,12]. ORNs project their axons ipsilaterally and innervate stereotypic pair of glomeruli, creating a mirror- symmetric organization of isofunctional or homologous glomerular pair on the OB [19]. Thus, each OB possess duplicated glomerular map with intrabulbar connection [20]. Similarly in *Drosophila*, there appears to be the conservation of sensilla-type zonal organization at the level of antennal lobe [Fig 1B] [21,22].

The AL contains synaptic connections between axons of ORNs and dendrites of second-order neurons. Odor information is modulated by diverse population of local interneurons [LN] having heterogeneous neurite arborizations throughout the AL [23,24]. Information is transmitted further upstream to the secondary olfactory centers via output neuron (projection neuron in insects and mitral/tufted cells in vertebrates). The majority of projection neurons [PNs] shows uniglomerular dendritic innervation in the glomerulus and have axonal innervation ipsilaterally to the higher processing centers; the lateral horn [LH] and Mushroom body [MB] in insects and multiple cortical regions collectively referred as olfactory cortex in mammals, showing a massive divergence from the primary processing centers to the secondary olfactory centers [24,25]. Depending on the nature of the stimuli these higher order innervations form parallel channels [26,27]. For example, food and pheromone sensing odors are represented in spatially distinct region on the AL. Further in the higher brain centers, specially pheromone sensing olfactory channels has stereotyped wiring patterns in the LH [26]. However, the food odor sensing channel shows less deterministic innervation pattern in the MB calyx [28]. The extent of deterministic innervations in the two of the higher brain centers, MB and LH, indicates their involvement processes underlying learned and innate behaviors, respectively [28,29]. Likewise in *Bombyx mori,* PN representing sex pheromones send axons to the distinct area in the lateral protocerebrum [30]. Similar segregation of the different olfactory

channels and dichotomous organization is seen in mammals where ORNs originating from the nasal epithelium process general odors and some pheromones, while the vomeronasal organ are more specific to the pheromone sensation [31]. Like *Drosophila,* the PNs from mammalian OB relays the information relevant for learnt and innate behavior show diffused and stereotypic innervation, respectively, to the olfactory cortex [32,33]. Aforementioned spatial segregation is seen at both primary and secondary olfactory centers in insects and vertebrates. Is spatial segregation a key for "synaptic specificity" of ORNs? What are the underlying molecular mechanisms that control the segregation of different sensory channels in the central brain? In this dissertation I have addressed the cellular and molecular mechanisms regulating the organization of different sensory channels into distinct "projection domains" in the AL [Fig 1].

Besides spatial organization of the olfactory map, another conserved feature of olfactory system across the animal kingdom is its bilateral organization [34,35]. The stereotyped position of identified glomeruli is not only preserved between individuals but also between the two brain hemispheres with in the same individual, creating a bilaterally symmetric olfactory sensory maps [19,34,35]. Organisms with bilateral symmetry, integration between left and right hemipshere is important for processing lateralized sensory and motor functions [36]. In nature, animals face the challenge to process dynamic sensory inputs emanating from different directions fast and efficiently, which could be facilitated by specific connectivity between the two hemispheres [37]. Such interhemispheric communication is mediated via axonal connections known as commissures, which are present throughout vertebrates and insects [36,38]. In vertebrates three main telencephalon commissures are the anterior commissure [interconnecting the olfactory system and a part of limbic system], the hippocampal commissure [interconnecting a part of limbic system] and the corpus callosum [interconnecting the large part of cortical area]. The corpus callosum is exclusively present in placental mammals and described as true "evolutionary novelty" [39,40] It is crucial for information transfer between various cortical regions, and is believed to be important for lateralized brain function [40]. In the olfactory sensory system of vertebrates and insects, the primary processing center shows define regions of strict unilateral sensory inputs and the interhemispheric connections are established further higher up in the olfactory association domains, like piriform cortex

and mushroom bodies in mammals and insects, respectively [34,41]. Interhemispheric interaction between two the hemispheres is physiologically important, for e.g. it is involved in the recall of memory established by unilateral olfactory conditioning [34,42]. A prominent exception to this unilateral olfactory representation is the "olfactory commissure" in flies, which has evolved during the transition from basal Nematocera mosquito-like species to more recent, fast and agile Brachycera [35] [Fig 1]. Most Dipterans exhibit direct connection between primary processing centers via ORN axons, a feature not yet observed in any other sensory system. What are the underlying molecular mechanisms involved in the formation of such "evolutionary innovation"? In the third part of my PhD project I have addressed the molecular mechanisms, which triggers the formation of novel commissural tracts.

The main aim of my PhD thesis was to gain novel developmental insights into synaptic organization of bilateral olfactory maps. The plethora of genetic tools in *Drosophila* to visualize subset of olfactory cells and to modulate their gene functions allowed my to experimentally address the molecular mechanisms of 3 developmental processes:

i. The coordination of synaptic and sensory identity in ORN differentiation.
ii. The non-apoptotic role of caspases in segregation of ORN axons into distinct projection domains.
iii. The cellular interactions in bilateral olfactory map formation.

1.3 Olfactory receptor neuron specification

Generally, the emergence of the overall distribution of ORNs and the expression of specific ORs involve multiple underlying players. In mice, the nasal epithelium is in direct contact with the environment and within the epithelium about 10^6 ORNs are grouped into more than thousand different classes according to their OR expression [8,19]. All neurons expressing the same OR are located within the OE in a zonal manner, but within each zone ORNs are randomly distributed [11,12]. Using the zone-specific marker, the epithelium can be divided into dorsomedial [D] and ventrolateral [V] zones. The OR genes are phylogenetically divided into distinct classes: The class I ORs, evolutionary more ancient "fish-type" while class II ORs are

the “terrestrial type” which have undergone massive expansive and constitute 90% of the OR genes [14] [see section 1.4, Fig 6A].

In rodents, the OR choice is stochastic where single OR genes are expressed in monoallelic manner and this leads to genetic basis for the axonal projection of ORNs to the OB [43]. The expression of various OR genes, which are usually arranged in clusters is controleed by the combinatorial code of multiple negative and positive signals that orchestrate the expression of a single OR per ORN thereby ensuring the “One Neuron - One Receptor” rule [10] [Fig 2]. A recent model suggest that positive regulation of OR gene choice is mediated via *cis*-acting “locus control region” [LCR]; a regulatory region that controls multiple genes, clustered at a specific genetic locus [10,43]. Certain transcription-activating factors upon binding to LCR, forming a holocomplex, could physically interacts with the remote promoter site by looping out the intervening DNA [10,43] [Fig 2]. Such LCRs are often found in the OR promtor regions and are known to be composed of homeodomain-like and O/E- like sequences and that could act as enhancers [44]. Two homeodomin factors Emx2 and Lhx2 have been shown to bind to the identified regulatory sequence and their loss could substantially affect OR expression [45,46]. These regulatory sequences are found for every *Or* gene, although their arrangement and number could differ from gene to gene, thus they may represent a unique code for each OR [47]. This LCR-promoter interaction alone does not inhibit the activation of second OR. Once the functional OR protein is made, it prevents the activation of OR protein from another gene cluster, by producing inhibitory signals causing degradation of the activation complex [10,48] [Fig 2]. Although, how this inhibitory signal works is not yet established. OR-mediated negative feedback is uncoupled to G-protein signaling as ORNs expressing ORs with mutated G-protein signaling motifs still exhibit this endogenous sensory identity [49,50]. In addition, *Or* gene choice restriction is also imposed by the positional information of ORN within the olfactory epithelium and is regulated by zone-specific transcription factors like Msh homeobox 1 [Msx1] and forkhead box protein G1 [Foxg1] [51,52].

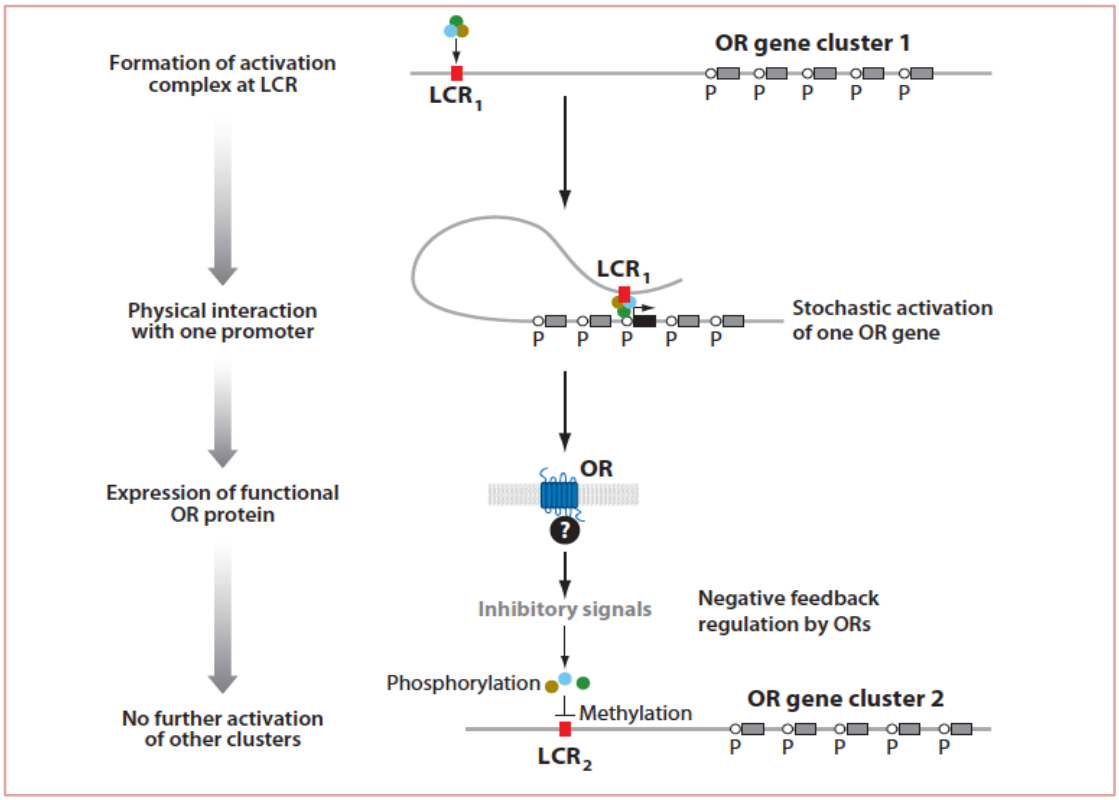

Figure 2: Monogenic and monoallelic OR expression in mouse olfactory system. Once the activation complex is formed in the *cis*-acting locus control region [LCR], it binds to a single promoter [P] which is randomly selected from OR gene cluster. Once the functional OR protein is expressed it transmits an unknown inhibitory signal and silence the activation of any other OR gene cluster [figure taken from 43]**.**

In addition to the above mentioned *in cis* action modality, *Or* gene expression is controlled via extensive interchromosomal interactions [53]. Together with so called prototypical enhancers like *H* enhancer [10], additional OR enhancers, the Greek Islands were recently discovered which function in trans by forming a complex network of interchromosomal interactions [53,54]. These islands are co-bound by two transcription factors Lhx2 and Ebf forming a multi-enhancer interchromosomal hub and has a critical and ubiquitous role as key regulator of OR expression [54].

The fly olfactory system differs from its mouse counterpart in some respect but exhibits broadly similar underlying molecular regulations. Fly ORNs are housed in olfactory sensilla on the two main olfactory appendages, the antennae and the maxillary palps [55]. Each sensilla can be divided into three main morphological classes - basiconic, trichoid and ceoloconic which contains stereotypic combination of up to four ORNs [55]. Basiconic and trichoid sensilla contain ORNs expressing one

of the *Or* genes, which are seven transmembrane G-protein coupled receptors, whereas the coeloconic sensilla contains ionotropic receptors [Irs] related to ionotropic glutamate receptor [56,57]. The sensilla types are specified by the basic helix-loop-helix (bHLH) transcription factors Atonal and Amos [58–60]. Atonal specifies the coeloconic sensilla and basiconic sensilla on antenna and maxillary palp, respectively, whereas Amos specifies basiconic and trichoid sensilla on the antenna [58,59,61,62]. The expression levels of another transcription factor Lozenge regulates differentiation of basiconic and trichoid sensilla: high-level of which leads to basiconic whereas low level gives rise to trichoid sensilla [63]. Within antenna, different *Or* genes segregate in different regions along the proximal-distal and dorso-ventral axes, similar to zonal organization in the vertebrate OE [64]. Each of the approximately 1300 ORNs, typically express only one OR or IR in addition to another common co-receptor Or83b and Ir8a/Ir25a respectively [6,64–67]. However, unlike mouse, *Drosophila* olfactory system seems to lack the negative feedback mechanism to ensure "One Neuron-One Receptor" rule. Transgenic expression of ectopic *Or* gene during development does not change or perturb the endogenous OR expression [68]. Furthermore, ORNs in which the *Or* gene has been removed can still connect to their cognate target but do not respond to the odor stimulus [68]. ORNs in each sensillum are derived from a common sensory organ precursor cell [SOP], which in series of division give rise to differentiated ORNs and support cells in each sensillum according to the $Notch^{ON}$ [high Notch activity] and $Notch^{OFF}$ [low Notch activity] activity [69] [Fig 3]. Notch mediated cell-cell signaling among the SOP progenies controls the initial ORN diversification [69]. In addition, ORN specification are epigenetically regulated by Notch signaling via chromatin regulation, where chromatin modifiers Hamlet [Ham] and C-terminal-binding protein [CtBP] are expressed in subsets of ORNs [70]. Ham represses Notch signaling by forming complex with CtBP. This leads to a reduction in H3K4 (activating) methylation and increase in H3K27 (repressing) methylation around Notch target genes [70]. In addition, *Or* expression in $Notch^{ON}$ ORNs is also regulated by the transcriptional corepressor Atrophin [71]. Regulation of CO_2 sensing receptors, Gr21a and Gr63a, is also shown to be mediated by chromatin modifying protein MMB/dREAM complex which consists of several transcription and chromatin remolding factors [72]. dREAM complex has also been shown to regulate *Or* expression by downregulating H3K9 methylation [72].

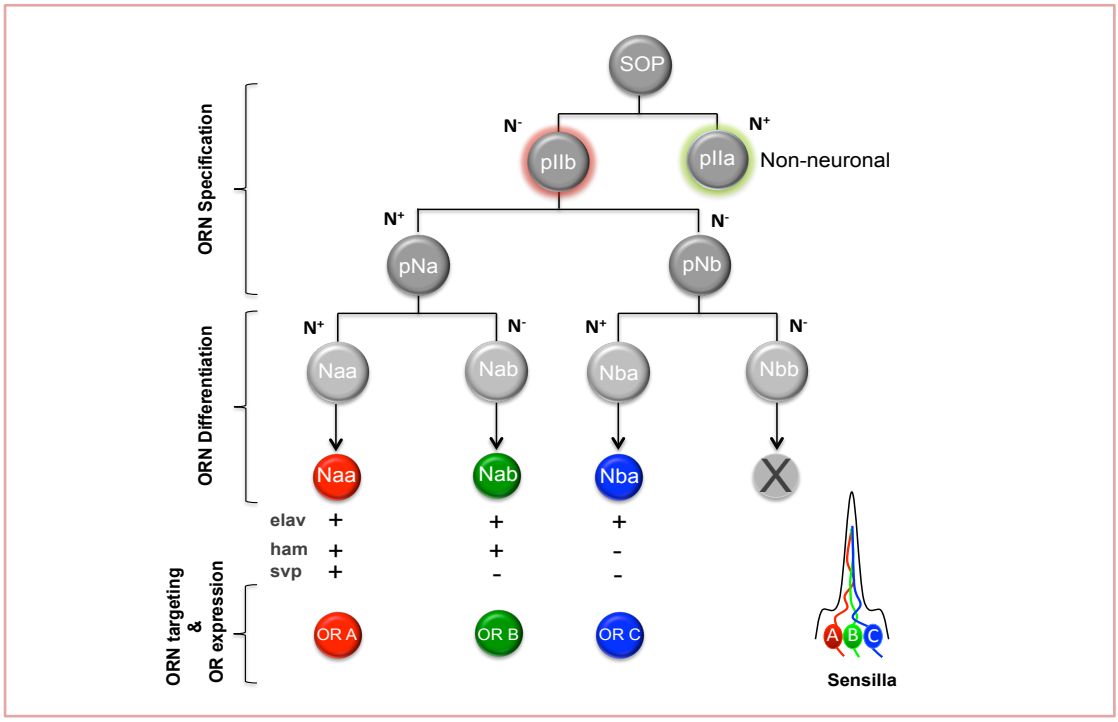

Figure 3: Iterative Notch signaling delineates ORN identity in *Drosophila.* ORNs within a sensillum are related by lineage and acquire different identities via differential activity of Notch. The SOP divides to create two intermediate precursor cells, pIIa [green circle, Notch high (N^+)] and pIIb [red circle, Notch low (N^-)], which will undergo multiple rounds of asymmetric cell division to generate non-neuronal support cells and ORNs, respectively. In a specific ORN lineage, pIIb further divides asymmetrically and gives rise to second level of intermediate precursor cells named pNa (N^+) and pNb (N^-). Post-mitotic cells can be identified by the expression of *elav*. In the next step ORNs differentiate, thus resulting in three neurons [A, B and C, in this example] with distinct OR expression [red, green and blue] and axonal targeting preference. ORNs derived from Naa identity can be identified by the expression of *svp* and *ham* is shown to be expressed in pNa and its sibling Naa and Nab [Figure adapted from 68,69].

Subset of ORNs are dependent on a POU domain transcription factor called Acj6 for *Or* expression in adult antenna and maxillary palp and in *acj6* mutants ORNs, the response profile of many ORNs are altered suggesting a change in ORN identity [74]. This was supported by the identification of an Acj6 binding site upstream of *Or* genes [75]. Besides Acj6, another POU domain transcription factor, Pdm3, could function independently or cooperatively with Acj6 to regulate specific *Or* expression [76]. Recently, it has been proposed that Acj6 and six novel transcription factors could form a combinatorial code to achieve specific *Or* gene expression [77].

The *Or* promoters appear to contain all the information required for the regulation of OR expression. Two cis-regulatory sequences named Dyad1 and Oligo1, are required

for the expression of ORs in maxillary palp and repression of same ORs in the antenna, respectively [14]. In addition to the combination of different transcription factors, microRNA *mir-279* has been shown to restrict the expression of CO2 sensing receptors, Gr21a and Gr63a to the antennal ORNs [78]. *miR-279* down regulates transcription factor Nerfin-1 and loss of *miR-279* leads to the expression of CO2 sensing ORNs in maxillary palp [78]. Another transcription factor Prospero has also been to shown to activate *miR-279* and restrict its expression in the antenna [79]. Unlike mammals, *Drosophila* ORNs are independent of OR function for axonal targeting in the AL but synaptic targeting is substantially regulated buy other factors that are involved in sensory specificity like, Acj6 and Pdm3, the transcription factors and Notch signaling [69,76,80]. Altogether, sensory specificity of ORNs appears to be deterministic in *Drosophila*, which is regulated by epigenetic modification of chromatin landscape of *Or* promoters, combinatorial code of transcription factors, and *cis*-regulatory elements. Unlike mouse olfactory system, where ORs are multifunctional as they control single receptor expression as well as regulate sensory axon targeting, how is OR class identity of each sensory neuron molecularly linked to synaptic connectivity is largely unknown.

1.4 Synaptic specificity of olfactory receptor neurons

A functional nervous system is determined by the precise connectivity between various neuronal types. The ORNs not only choose the OR in a stereotypic manner but also innervate to their specific glomeruli in class specific manner. The specificity of synaptic connections unfolds in various steps like pathway selection, target recognition and remodeling of synapses [81]. During development the differentiated neurons navigate through the environment with the aid of growth cones tipped at the edge of the extending axons. *En route,* they encounter several attractive and repulsive guidance cues which allows axons to sort out into distinct projection domains [82,83] probably based on the receptor they express.

In mice, each ORN expressing the same OR projects a single unbranched axons to the ipsilateral OB converging onto two glomeruli, creating a stereotyped mirror-symmetric lateral and medial map [19] [see section 1.5, Fig 8A]. In rodents, olfactory map formation involves a combination of global [genetically programed] and local

events [activity dependent], which are regulated in stepwise manner [Fig 4A]. For instance, an ORN axon is guided to form a coarse map by the combination of anterior-posterior [A-P] and dorsal-ventral [D-V] patterning factors [43]. This map gets further matured and refined by segregation of axons in an activity-dependent manner [43]. For A-P innervation, OR plays an essential role in axon targeting by regulating the transcript levels of axon guidance and sorting molecules by OR-derived cAMP levels [49,84].

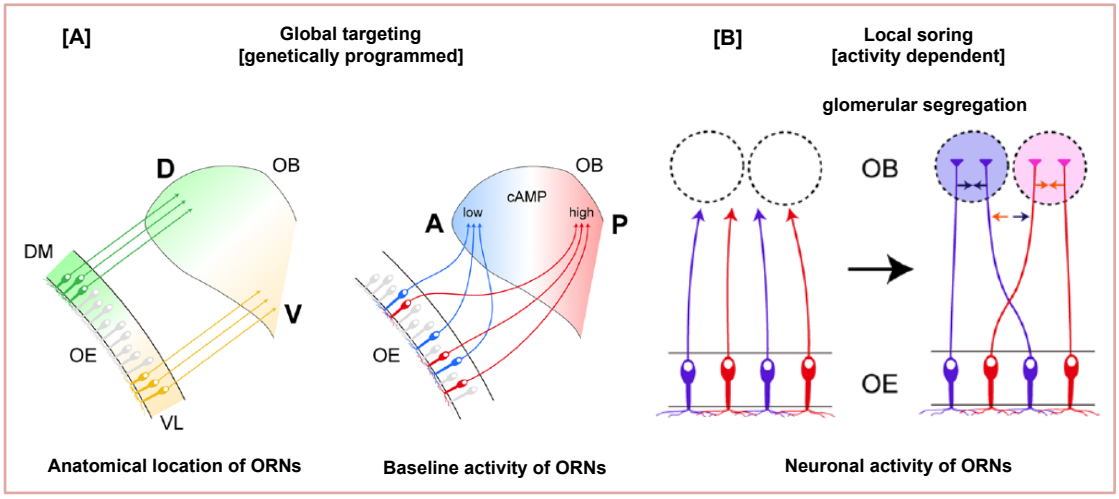

Figure 4: Stepwise regulation of olfactory map formation in the mouse olfactory bulb. [A] ORNs are guided from OE to the OB by the combination of A-P and D-V patterning factors. Anatomical location of ORNs within the OE influence the ORN innervation in the developing bulb and A-P innervation is achieved via OR activity derived cAMP signals. These two genetically programed factors form coarse olfactory map. [B] The coarse map is further refined in an activity dependent manner in the newborn [figure taken from 83].

Both, OR identity and OR protein levels directly affect cAMP signaling. A specific cAMP level in the ORNs correspond to a specific synaptic target region within the A-P axis; ORNs with high cAMP signaling project their axons to the posterior OB, whereas those with low levels innervate the anterior OB [49,86]. Furthermore, cAMP signaling has been shown to regulate the expression of axon guidance molecule in the ingrowing ORN termini, for e.g., Nrp1 receptor [anterior-low, posterior-high] and its repulsive ligand Sema3A [anterior-high, posterior-low], in a graded fashion to maintain the A-P topography of the OB map [49]. Along the A-P axis, the pre-target axon sorting also facilitates the map formation. Nrp1 and Sema3A is expressed in complementary manner, where Nrp1-low/Sema3A-high axons are sorted into central and Nrp1-high/Sema3A-low into outer lateral bundle [43,86] [Fig 5A]. In mature

ORNs, different level of ORs activity determines the expression levels of axon sorting molecules important for glomerular segregation. The adhesive Kirrel2 and Kirrel3 and repulsive ephrin-As and EphAs are expressed in complementary fashion in each subset of ORNs [84,87]. These aforementioned axon-sorting molecules whose expression levels are determined by OR-derived cAMP signals can be classified into two types:

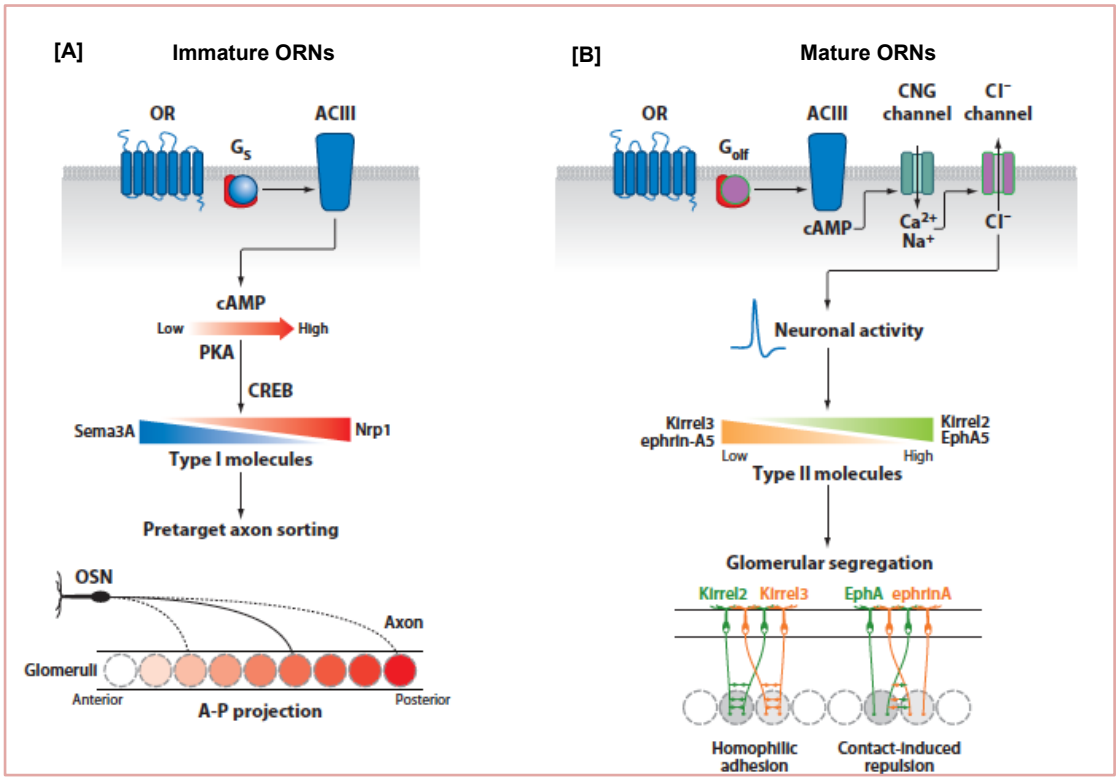

Figure 5: Activity dependent A-P innervation and axonal sorting of ORNs in the mouse olfactory system. [A] In developing ORNs, Nrp1 and Sema3A are expressed in complimentary fashion and regulate pre-target axon sorting. It is assumed that each OR generates a specific level of cAMP signal which further translates into the relative expression of these two molecules via cAMP dependent protein kinase A [PKA] and cAMP response element binding protein [CREB]. [B] In neonatal mouse, the differential activity of OR/ cAMP signals controls the expression of Kirrel2/3 and ephrin-A/EphA. These two cell adhesion molecules mediates intra-class homophilic adhesion and inter-class repulsion of ORN axons. Axon guidance and sorting molecules are divided into two types: type I, expressed in graded manner [e.g. Nrp1 and Sema3A] and type II, showing mosaic pattern [e.g. Kirrel2 and Kirrel3] [figure taken from 43].

Type I [expressed in graded manner in ORN termini] and Type II [expressed in a mosaic pattern in ORN termini] [Fig 5B]. In contrast to the A-P projection, ORNs projecting along the D-V axis are associated with the physical location of ORNs in the OE and the D-V guidance molecules are independent of OR signaling [10]. On the basis of the the zone-specific molecules for e.g., OCAM [V zone positive] and NQO1

[D zone positive] [88,89], OE can be divided into two non-overlapping D and V zones, where they appear as parallel stripes oriented along dorsomedial-ventrolateral axis. ORNs innervate the OB in a "zone-to-zone" manner, so that the glomerulus position on the D-V domain of the OB correspond to the ORN position in the OE [90] [Fig 6A].

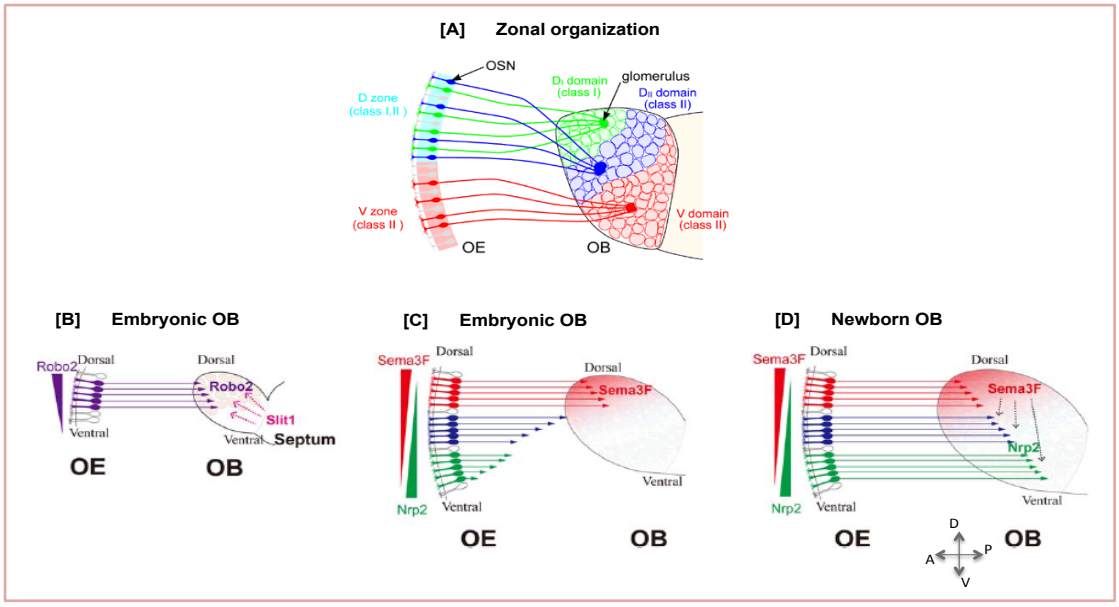

Figure 6: ORN axonal projections along the D-V axis in the mouse olfactory system. [A] Zone-to-zone innervation of ORNs. ORNs are arranged in the dorsomedial zone [D zone] and ventrolateral zone [V zone] in the OE and project their axons to the dorsal [D domain] and ventral [V domain] domain of the OB respectively. In D Zone although the class I and class II ORs are intermingled their segregation is specific in the target region [green and blue] in the OB. Class II ORs are mainly found in V zone. Each Or gene is distributed in continuous and overlapping fashion in the OE and project ventrally [red] in the OB. [B-D] Axonal projection of ORNs along the D-V axis. [B] ORNs innervate the OB sequentially as the ORNs from the D zone on the OE mature first. With the expression of slit from the septum, early born axons starts to express Robo2 during innervation in the anterodorsal domain of the OB. [C] Nrp2 and Sema3F are expressed in graded and complimentary manner in the ingrowing ORNs. The early-arrived ORNs from D-zone secrete Sema3F at the anterodorsal region of the OB, which prevent the late arriving [D] Nrp2 positive ORNs from V-zone from invading the dorsal region of the OB (figure [A] taken from http://www.coe.s.u-tokyo.ac.jp/integr-life/english/findings/research071107.html, figure [B-D] taken from 89]).

Misexpression of ORs from one zone to the other shifted the innervation of ORN axons accordingly along the D-V axis indicating that *Or* gene choice is not purely stochastic but depends on positional information [92]. The D domain of the OB is further divided into two, D_I and D_{II}, domains according to the expressed OR classes, which are arranged parallel with the A-P axis. D_I glomeruli expresses class I [fish – type] ORs, whereas D_{II} glomeruli represents class II [terrestrial – type] ORs [14,43] [Fig 6A]. Though the class I and class II ORs are intermingled in the D zone of OE, their innervation in the OB is separated. Class II ORs are expressed in V zone. During

development, ORNs from the D zone mature first and innervate the D domain in the OB first [93]. Later the glomerulus map expands ventrally [93]. Robo2 and Slit1 and the graded expression of Nrp2 and Sema3F has been shown to act in complementary fashion to contribute along the D-V axis projection [93] [Fig 6B-D]. However, *Gli3* mutant mouse lacks OB but ORN expressing the same OR can converge and rough map order is preserved [86,94]. Above-mentioned studies suggest a model in which segregation and then fasciculation of ORNs in projection domains via axon-axon interactions self-organize the olfactory map independent of target derived signals.

In *Drosophila*, like their mammalian counterpart, the ORN targeting is also achieved in a stepwise manner comprising axonal projection domain selection, inter and intra-axonal interactions for establishing glomerular boundaries and achieving synaptic specificity that ensures correct ORN wiring. However, in flies ORs play no role in axon targeting and it is dependent on target-derived cues. During *Drosophila* olfactory system development Atonal specified ORN axons circumscribe the proto-AL by 18 hour after pupa formation [APF] [95,96] [Fig 7A]. In the next two hours, axons defasiculate and segregate and into two distinct axonal bundles forming the two projection domains: one in dorsolateral [DL] and the other one in ventromedial [VM] direction, mainly innervating the posterior part of the AL [97] [Fig 7A]. Later, at 26 hr APF, Amos ORN axons approach the proto-AL extending along its anterior part [97] [Fig 7B]. Different studies using *atonal* mutants and cell specific ablation have demonstrated that Atonal ORNs initiate the patterning of the AL, hence called as "pioneer ORNs" and have a direct influence on the axonal targeting of late arriving Amos ORNs, hence called as "follower ORNs" [95,97]. In addition, *atonal* mutant flies lack coeloconic and basiconic sensilla on the antenna and maxillary palp, respectively, and perturb the axonal commissure of the remaining Amos ORNs [60,95,97]. ORN axons from maxillary palp innervate the AL at 30hr APF and they are further dependent on the antennal ORNs for their targeting, displaying a hierarchical innervation of neurons in olfactory map formation [98,99]. Further, ORNs expressing the same OR converge onto one of the 50 AL glomeruli and synapse on the dendrites of PN, establishing one to one synaptic connection [96]. Initial choice of projection domain plays a crucial role in accomplishing synaptic specificity of ORNs. Semaphorins [Sema] has been shown to play an essential role in the selection of projection domains, promoting axon-axon interactions of ORNs as

well as dendrites of PNs [100–102]. A transmembrane Sema-1a was shown to form a gradient along the DL-VM axis of the proto-AL and loss of Sema-1a causes PN dendrites to mistarget to VM glomeruli [103]. Whereas two secreted Semas, Sema-2a and Sema-2b, are also involved in PN dendrite targeting [101] forming a counter gradient suggesting, that secreted and membrane bound Semas interact to form coarse map of PN dendrites along one axis [104]. Like in PNs, Sema plays a crucial role for the selection of the correct projection domain in ORNs. Sema-2b, which signals via PlexB receptors, attracts and consolidates the ORN axons innervating the VM domain [100]. In addition to regulate OR expression, Joo et al., 2013 showed that Notch-signaling functions upstream of Sema-2b and restricts its expression to ORNs that choose the VM domain, consistent with the observation that $Notch^{ON}$ and $Notch^{OFF}$ ORNs are segregated with in the AL [69]. In addition to Semaphorins, a target-derived molecule that has been shown to affect the ingrowth and coarse targeting of ORNs is Hedgehog [Hh]. Hh signaling in the antennal anlage divides ORNs into two subsets having low and high level of patched receptors [105]. These differential expression of patched receptor in ORNs response to brain derived Hh for target selection [105]. The Robo receptors are a second class guidance molecules which are involved in the initial targeting of ORN axons [106]. *Drosophila* has three Robo [Robo, Robo2 and Robo3] and they all are expressed in discrete subsets of ORN axons that segregate from one another and take medial versus lateral pathways during ORN axonal ingrowth [107]. Loss and gain of function studies show mistargeting defects, suggesting crucial role of Robo signaling in ORN axon positioning in the AL [22,107]. After the initial trajectory choice, ORN axons surpass their putative target region and project contralaterally across the midline via olfactory commissure [Fig 7B]. Later, approximately 35hr APF, the protoglomeruli are formed where ORN axons and the PN dendrites start to assemble, and functional synapses mature [96,108,109] [Fig 7C].

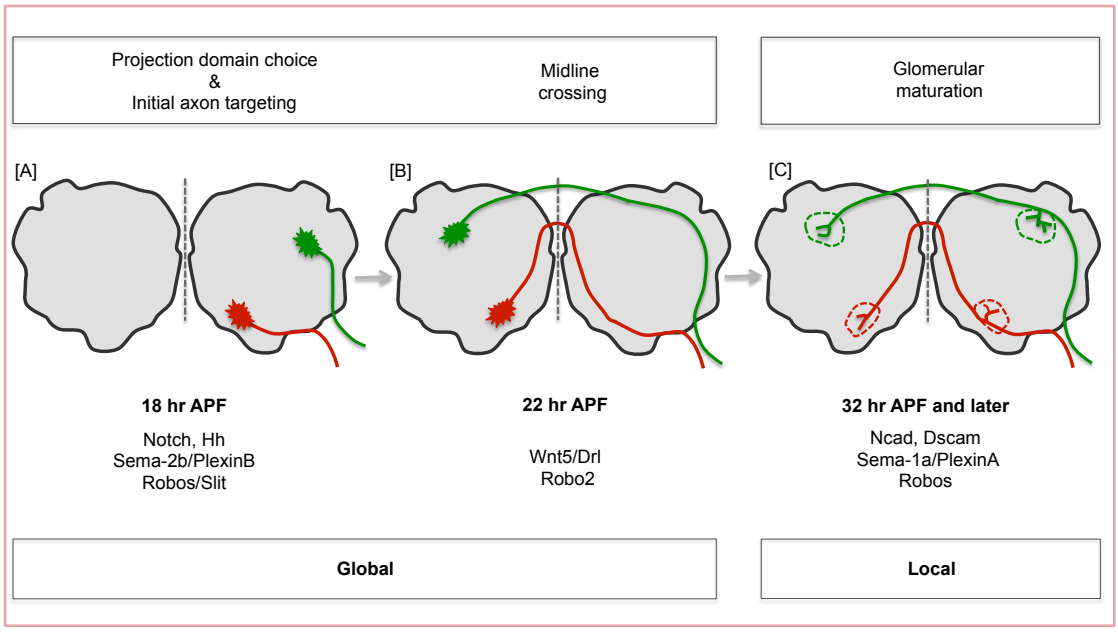

Figure 7: Stepwise regulation of olfactory map formation in the *Drosophila*. The adult olfactory map begins to assemble at the beginning of pupa formation. [A, B] Initial and global organization of ORN axon projections. [A] Atonal specified pioneer ORN axons from the antennal anlage start to innervate the proto-AL at 18 hr APF, followed by the axons of Amos specified ORNs and defasciculate into two main AL projections [red and green], dorsolateral [DL] and ventromedial [VM] based upon Sema-2b/Plexin-B, Notch and target derived Hh signaling. [B] In next two hours pioneer ORN axons cross the midline [gray dotted lines] to innervate the contra-lateral side forming olfactory commissures, followed by Amos ORN axons. Contra-lateral projections are mediated through various cell-cell interactions [neuron-neuron, neuron-glia] at the midline via Robo2/slit and Wnt5/Drl signaling and the formation of midline glia structure TIFR. [C] Local axon-axon interactions within the AL. By 35 hr APF protoglomerular formation begins, which is mediated by inter and intra axonal signaling under the control of N-cad, Dscam, Robo and Sema-1a/PlexinA. Commencement of synaptogenesis happens at 45 hr APF where ORN axons synapse with their class specific post-synaptic partners and form the spherical neuropil elements, called glomeruli [dotted circles]. For clarity ORN axons are represented only from right side of the brain.

Glomerulus convergence is dependent on N-cadherin [N-Cad], where *n-cad* mutant ORN axons correctly reach their target glomeruli but fail to coalesce into glomeruli [108]. This indicates that N-cad is involved in intraclass attraction during the convergence of ORN axons. Several other guidance molecules also play important role in the process of ORN axon targeting. Dscam, a Ig superfamily protein which signals through two downstream effectors Dock and Pak, is also required for ORN target specification [106,110,111]. Dscam generates approximately 38,000 alternative spliced isoforms [112]. Loss of *dscam* in ORN axons causes ectopic innervation and shows defects in both ipsi and contralateral innervation [110]. Although *dscam* null mutant show ectopic innervation, the axons can still converge together in class specific manner, indicating that targeting is independent on its diversity [110]. Like

Semas, Dscam and N-Cad have been shown to affect PN targeting, where *dscam* mutant PN dendrites fail to innervate the glomeruli and overexpression of *dscam* leads to positional shifts of the dendrites [108,114]. Sema-1a mediates interclass repulsion between classes of ORN that prevents axons to coalesce and ensures fine tuning of glomerular boundaries [102]. A lot is known regarding the molecular mechanisms involved in axon targeting and glomerular formation, but molecular determinants coupling the initial trajectory choice leading to precise synaptic specificity of ORNs remains elusive.

1.5 Inter and intra-hemispheric connectivity in olfactory circuit

Convergence of inputs from bilateral receptive fields is a common feature of insects' and vertebrates' sensory systems [42,115] which allows relative comparison of spatially distributed features relevant for higher order sensory processing such as localization of audition and visual depth perception [115]. Such interhemispheric connections have shown to be important in the context of olfaction, e.g. lateralization of odors, olfactory learning, and memory recall [34,42,116,117]. In rodents, broad olfactory system connectivity exists at two different levels: first, within the OB, where two isofunctional glomeruli are linked via a set of intrabulbar projections and second between the two OB via interhemispheric connections [20,34] [Fig 8]. The olfactory system components form functional units called olfactory column, with glomerulus at its apex, output neurons, like mitral/ tufted cells, lying directly beneath, and extending LNs like periglomerular and granule cells at its base [20] [Fig 8A]. The mirror symmetric maps on the OB are linked to one another through set of intrabulbar projections which is mediated by external tufted cells [20]. The external tufted cells further send axons to the internal plexiform layer beneath the isofunctional glomerulus on the opposite side of the OB [20], which results in a reciprocal connection between the glomerular pairs that receive innervation from ORNs expressing same the OR [20,118] [Fig 8A].

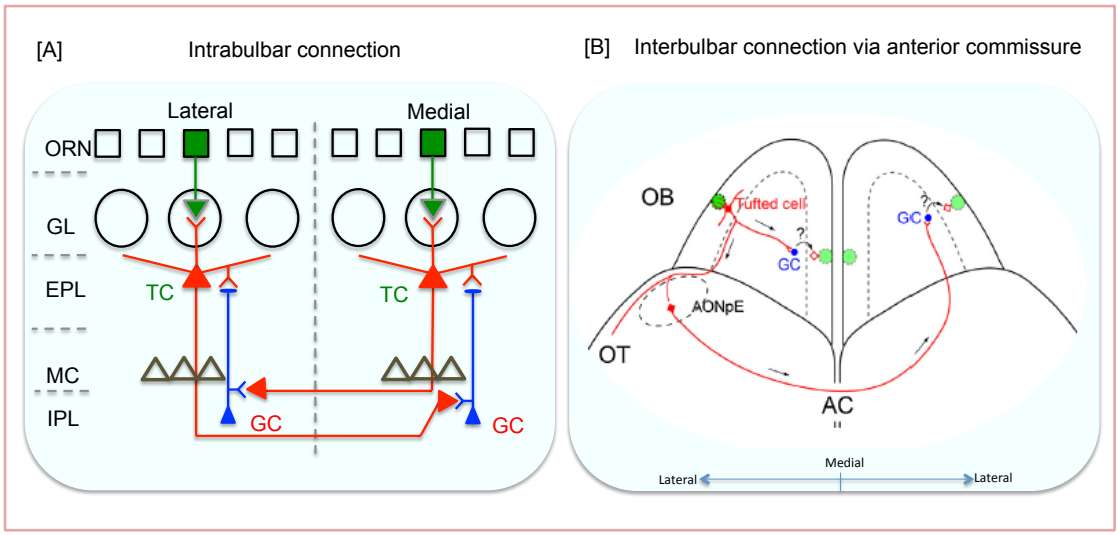

Figure 8: The intra and interbulbar circuit in the mouse olfactory system. [A] Schematic of neuronal wiring of intrabulbar connections within one OB. ORNs expressing the same OR [green] converge to form two isofunctional or homologous glomeruli [GL] on the medial and lateral in the two halves of each OB. Axons of tufted cells [TC, red] from a given glomerulus form an axonal projection in the internal plexiform layer [IPL] on the opposite side of the OB. In IPL, axons of TC form excitatory synapse onto the dendrites of the inhibitory granule cells [GC, blue]. The TC reciprocally connects these isofunctional glomeruli. [B] Schematic exhibiting interhemispheric connectivity of bilateral OB. In addition to intrabulbar connection via TC, they also project their axons to olfactory cortex including AON. Axons from AONpE project further through anterior commissure [AC] to the contralateral OB, where they target the isofunctional glomeruli. However, it is still unknown how GC modulates TC, question mark in [B]. EPL, external plexiform layer; MC, mitral cells; OT, olfactory tubercle. (figure [A] adapted from 24, figure [B] taken from 116]).

These intrabulbar connections are highly dependent on neuronal activity for projection refinements, suggesting that odor induced activity shapes not only the glomerular boundaries but also the internal circuit of the bulb [118]. Further axons of mitral and tufted cells fasciculate and form lateral olfactory tract extending multiple collaterals that project to the distinct regions in the olfactory cortex including piriform cortex, cortical amygdala, anterior olfactory nucleus, etc. [24,32] [Fig 8B]. Both mitral and tufted cells synapse on to different regions of the olfactory cortex implying that different aspects of odor information processed by mitral and tufted cells are differentially processed by distinct cortical regions [24]. Although the bilateral OBs lack direct connections between them, the anterior olfactory nucleus [AON] is a region of the olfactory cortex which is known to contain neurons that project contralaterally via the anterior commissure, connecting the two olfactory hemispheres of the brain [120,121] [Fig 8B]. AON is composed of two separate structures, the pars principalis [AONpP] and pars externa [AONpE] [121,122]. Neurons in the AONpE

gathers inputs from mitral/tufted cells ipsilaterally and project exclusively on to the granule cell on the contralateral side in topographically conserved manner [34,121] [Fig 8B]. The di-synaptic ipsilateral OB-AONpE-contralateral OB connection precisely link isofunctional glomerulus creating interhemispheric connectivity [24,34]. In addition, this interhemispheric connection was also shown to exchange olfactory information by regulating neuronal activity on the contralateral OB [34]. In addition to contralateral transfer of olfactory memory between the two hemisphere these inhibitory interbulbar connections is proposed to "enhance contrast between inputs to two nostrils and help the stereo sensation of an odor" [34,120].

Unlike mouse, *Drosophila* has evolved a direct connection between the two AL via sensory neurons where most of the ORN classes innervate onto homotypic regions on both side of the AL [61,123] [Fig 1A]. "Having bilateral rather than unilateral projections at sensory level may represent useful redundancy" [124]. In addition, bilateral inputs may also enhance the overall accuracy of navigation by the increasing the signal to noise ratio [125]. The bilateral innervation of the antennal ORNs seems to be restricted to higher Dipteran [35,123], however the underlying molecular mechanisms that might have been utilized during the evolution of contralateral connectivity of antennal ORN axons are still unclear. During first phase of development, the growing pioneer ORN axons starts to invade the ipsilateral AL at 18 hr APF and project to the contralateral AL crossing the midline approximately at 22hr APF [96,109]. By 32hr APF, the axons of follower ORNs arrives at the ipsilateral AL and soon starts to project across the olfactory commissure to innervate the contralateral AL [97] [Fig 7]. In the second phase of development, the ORN axons start to coalesce with the dendrites of PN and by 45hr APF most glomeruli appears with class specific ORN-PN recognition [108]. Finally, the expression of ORs occurs concomitantly with synaptogenesis at a late stage of AL development. In addition to ORN axons and PN dendrites, the AL also harbors the neurites of several uni- and bi-lateral LNs [23,126,127]. In contrast to the one to one ORN-PN connections, LNs show diversity and variability in their innervation pattern. Some LNs restrict their neurites to subsets of glomeruli, whereas others innervate more globally [23]. A midline glial structure, namely "transient interhemispheric fibrous ring" [TIFR], located between the two ALs, has been shown to have intimate cell-cell interactions with the ORN axon in the midline [128,129]. TIFR, whose morphogenesis is

dependent on Neuroglian, is transiently coupled with the developing olfactory commissural during metamorphosis and it's genetic ablation shows loss of the interhemispheric connections in all the bilateral ORN classes [128]. The TIFR associated glia cells express Derailed [Drl], a tyrosine kinase receptor, near the AL and its ligand Wnt5 is expressed in ORN axons. This ORN–glia interaction has been shown to contribute to the precise targeting of ORNs across the midline and to specific glomeruli within the ipsilateral AL [130]. In addition to the specification of ORN projection domain and positioning axons at the defined sites within the AL, the formation of olfactory commissures are also dependent on Robo signaling [106]. It is possible that TIFR may serve as a substrate for ORN axon crossing and may function nonautonomously to promote ORN axonal extension across the midline. My findings shed new insights into a simple mechanism where adhesion based developmental program is involved to switch a complete unilateral map to a bilateral circuit.

1.6 Aims of my research program

1.6.1. Understanding the coordination of synaptic and sensory identity in ORN differentiation

One of the main coordinators of sensory specificity and synaptic connectivity in the mouse olfactory system is the OR itself, where it plays an instructive role in ORN axon-targeting [19]. However, in the *Drosophila* olfactory system, sensory identity of ORNs is determined depending on the precursor they are derived from [69], and the factors that lead to the expression of a specific OR in lineage related ORNs remains elusive. The first aim of this study is to determine the function of Polycomb group gene *Posterior sex combs* [*Psc*] on the regulation of neuronal differentiation. Psc was identified in a mosaic screen for mutations that affect ORN development [131]. Loss of Psc affects class-specific OR choice [sensory differentiation] and targeting [synaptic differentiation], and differences in Psc level among lineage-related ORNs determine neuronal subtype diversification. Psc mutants show a switch in OR gene expression among lineage-related neurons. In addition, single cell analysis also revealed an axonal projection defect in which axon terminals fail to innervate the appropriate target glomerulus indicating a defect in synaptic identity. The further characterization of Psc function has been challenged by the fact that no OR-independent neuronal markers were available to determine how axonal connectivity and OR gene expression was mechanistically linked.

By analyzing a broad range of ORN classes in the Psc mutant background I realized the Psc affect all olfactory sensilla, which contain 3 different ORN classes but not the large population of 2-neuron sensilla. In a detailed lineage study, I could show that Psc regulates the differentiation of the $Notch^{ON}$ precursor Naa by suppressing the alternative default Nab fate. In the following series of LOF and GOF experiments I could determine 2 main steps of Psc function: 1) Specification of synaptic identity by maintenance of Svp expression; 2) Specification of sensory identity by suppression of the default OR gene, which seems sufficient to allow an alternative OR gene to become expressed. These data showed that ORN connectivity can be functionally separated from OR gene expression and Psc functions in two independent steps of ORN differentiation to coordinate both processes ensuring a precise coupling of

sensory neuron identity. Furthermore, the fact that the down-regulation of a given OR by ectopic Psc expression leads to the activation of an alternative OR indicating a feedback mechanism similar to ORN differentiation in vertebrates (Chapter 4) [Fig 9].

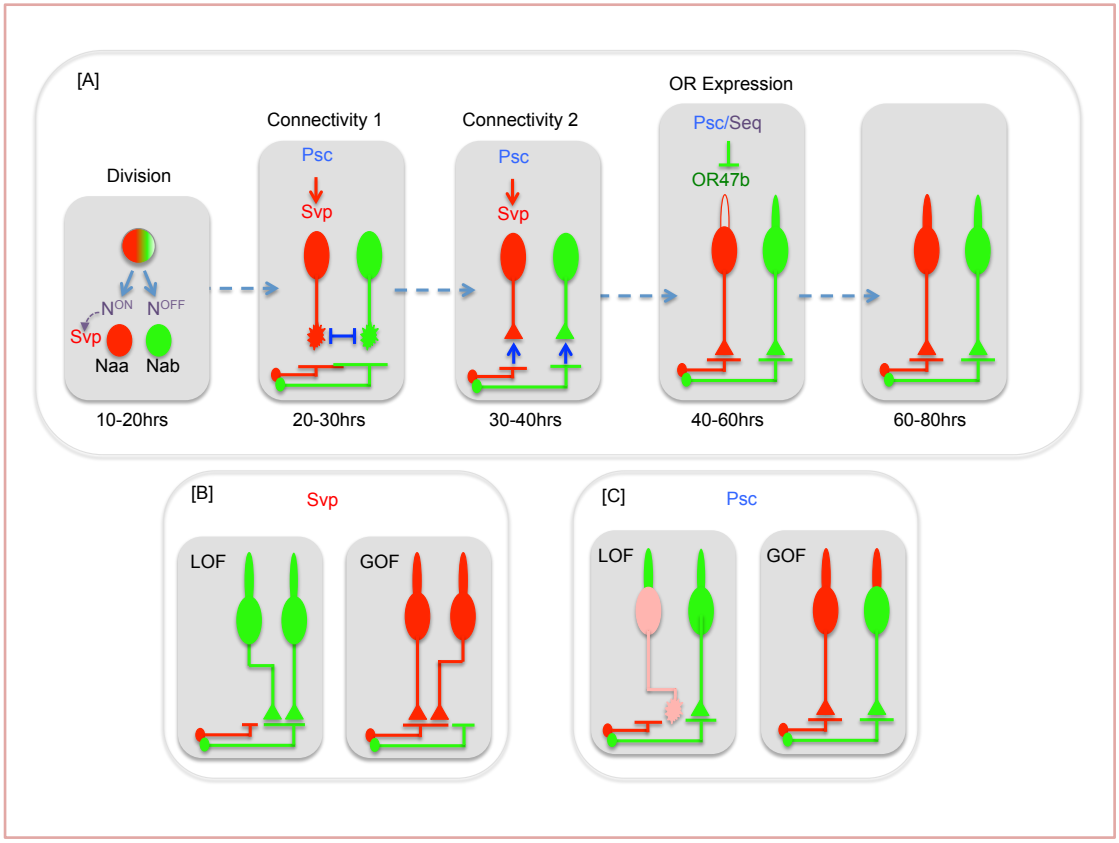

Figure 9: Psc coordinates synaptic and sensory identity in ORN differentiation. [A] Consecutive stages of wild type ORN development of at4 sensilla. In the final division of ORN precursor cells ["Division"] Notch [N] signaling diversifies the two siblings Naa and Nab through the activation of Svp. In the following phase of neuronal growth, inter-axonal signaling first leads to their segregation at the target field ["Connectivity 1"] and the subsequent synaptic partner matching ["Connectivity 2"]. During both steps of connectivity development Psc regulates the expression of Svp to maintain Naa identity. Following the formation of ORN connectivity, in the second half of pupa development sequential waves of OR expression can be observed starting with OR1 in Nab [OR47b, green] and OR2 in Naa [Or88a, red] expression as the final step of ORN differentiation. Here, Psc is critical for the suppression of OR1 in Naa. [B] Changes in Svp expression, either loss-of-function (LOF) or ectopic expression (GOF) leads to a complete switch in ORN identity, supporting its role as a read-out of Notch-mediated diversification. [C] Loss of Psc affect both steps in ORN differentiation in a distinct way: The down-regulation of Svp in Naa results in the loss of synaptic identity and a switch in OR expression due to the failure to suppress OR47b onset. On the other hand, Psc over-expression in Nab does not influence axon targeting due to the absence of Svp but suppresses OR47b in both precursor cells thereby allowing alternative OR gene selection, indicating independent functions of Psc in the context of synaptic and sensory identity.

1.6.2. Understanding the non-apoptotic role of caspases in segregation of ORN axons into distinct projection domains

In the second project I characterized a novel mechanism in *Drosophila* that controls the spatial sorting of ORN axons into different projection domains preceding the glomerulus-specific convergence. Are spatial segregation and precise target recognition interdependent process? Another mutation identified in the histological screen mentioned above affects the pro-apoptotic gene *Death-associated apaf-1 related killer* [Dark] [132]. In contrast to Psc mutants showing loss of synaptic identity, mutations in Dark lead to a defined switch of ORN axons to a specific new glomerulus. Interestingly, ectopic ORN innervation of Dark mutants is accompanied by a change from the medial to the lateral projection domain within the target region. I first addressed the question which components of the core-cell death pathway coordinate ORN axon pathfinding and targeting. Using loss-of-function mutations and RNAi approaches I found a partially redundant role of initiator caspases Dronc and Strica. Furthermore, the controlled reduction in Dronc activity by RNAi revealed the importance of definite level of its activity for spatial sorting and axonal convergence, whereas intermediate Dronc activity defines the axonal projection domain of ingrowing ORNs, loss of Dronc activity leads to a complete switch in ORN connectivity. Detailed clonal analysis confirmed the importance of cell-levels of caspase activity for ORN synaptic identity. To get insights into the non-apoptotic mechanism of neuronal caspase function I analyzed the expression of domain-specific cell surface molecule Connectin [Con]. Like *dark* [132], *dronc* mutant ORN axons showed ectopic Con expression, which directly correlated with the projection identity. Further experiments showed that ectopic Con expression can shift wild type axons to the lateral domain and Con downregulation via RNAi can suppress lateral targeting of caspase mutant ORN axons. From these results I could propose a model of neural wiring, in which the posttranslational modulation of cell surface molecules allows the transition from axonal pathfinding to synaptic connectivity (Chapter 3) [Fig. 10].

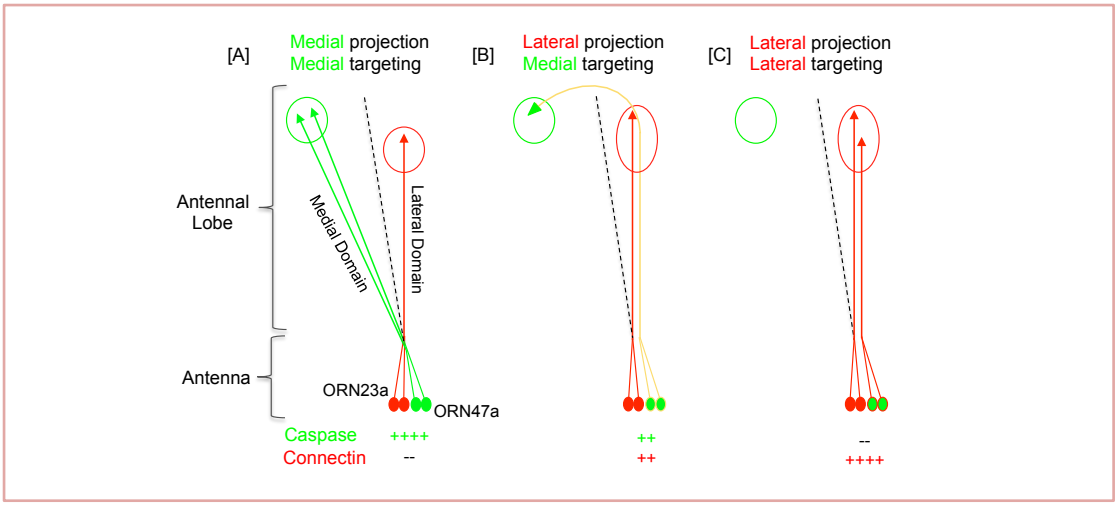

Figure 10: Caspase controls neuronal recognition in sequential manner where its differential activity mediates initial axon sorting into separate domains in the AL and subsequent target cell recognition via regulating the expression of cell adhesion molecule Connectin. [A] ORNs with high caspase levels remains in medial pathway and target the cognate glomerulus in medial domain, [B] whereas decrease in caspase activity to intermediate level shows axon projection defects where caspase mutant axons switch the domain from medial to lateral and [C] complete loss of Dronc shows projection as well as targeting defect from medial to lateral domain.

1.6.3. Understanding the cellular interactions in bilateral olfactory map formation

During the analysis of caspase-mutant ORNs I realized that the initial projection domain of ingrowing axons are maintained in the contralateral hemisphere of bilateral ORNs. Intrigued by the fact that bilateral connectivity of ORNs is unique feature of dipteran [Fig 1], the main goal of this study was to gain novel insights into the development of interhemispheric connection of the adult olfactory map. In this regard, I took a candidate RNAi approach and screened about 120 neuronal cell surface molecules in developing ORN. The screen resulted in the identification of evolutionary conserved cell-adhesion molecule Neuroglian [Nrg]. Loss of Nrg leads to a complete switch from bilateral to unilateral olfactory circuit, with ORNs having a precise ipsilateral innervation pattern. Targeted Nrg RNAi revealed a function not only in sequentially-ingrowing ORNs but also in a small cluster of a early-projecting commissural interneurons [cPINs]. Developmental studies showed that a key event in the transition from uni- to bilateral circuit formation is the suppression of ipsilateral axon targeting to allow contralateral innervation. To get further insights into the molecular mechanism of Nrg function in bi-lateral map formation, I analyzed a series of Nrg deletion constructs targeting extra- and intra- cellular domains for their

capacity to rescue the Nrg-mutant unilateral connectivity phenotype. I could show a differential requirement of molecular interactions with extra-and intracellular proteins in different neuronal types of bilateral olfactory system. Furthermore, single cell analysis of developing ORN axons and interaction of ORN axons and key cPINs provide an exciting working model for the rapid formation of brain commissures in nervous system evolution (Chapter 2) [Fig. 11].

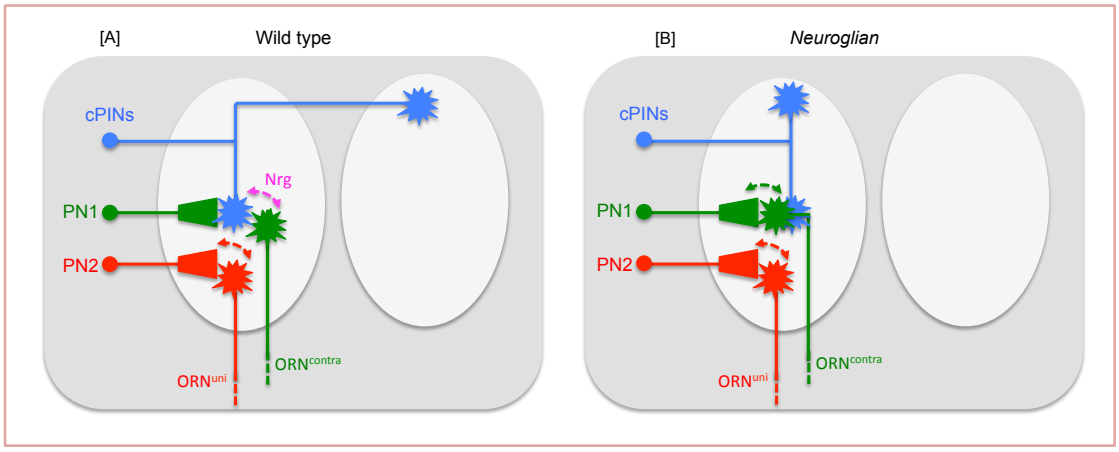

Figure 11: Neuroglian mediates bilateral connectivity of *Drosophila* olfactory circuit. [A] In wild type cPINs [blue] start to extend their neurites during the larval-pupal transition and innervate both ipsi- and contra-lateral AL prior to the ORN innervation. All the bilateral projecting ORNs [green] ignore the ipsilateral target [PN1] by sticking to cPINs via Nrg mediated adhesion [magenta arrow] and project contralaterally using cPINs as a bridge, whereas ORNs with unilateral innervation [red] directly innervate their respective target cell [PN2] [red arrow] [B] In Neuroglian mutant, bilateral map is switched to unilateral with precise ipsilateral targeting where cPINs fail to project contralaterally affecting the bilateral connectivity of all bilateral projecting ORNs.

1.6.4. Improving the optical clearing and imaging of whole mount Drosophila

In order to determine the OR expression in *psc*/ *svp* mutant and to investigate the positional information and frequency of *dark* mutant single cell clone, I processed and imaged the antennae and brains of each animal separately because of the long projection of ORNs, whose the cell bodies reside in the periphery and axons are sent to the developing center nervous system. This process of separate dissection and visualization of the appendages and neuronal circuit is quite laborious and error prone. Moreover, the dissected antennae have to be imaged immediately after the dissection, as the thick cuticle on the antenna is impermeable and is not amenable for standard tissue fixing protocols. In order to overcome such tedious process and to visualize intact animals, I collaborated with Marko Pende in Prof. Hans Unrich

Dodt's lab to develop a novel protocol "*FlyClear*" for optical clearing and high-resolution imaging of whole pupa and adult *Drosophila*. The *FlyClear* protocol showed preservation of endogenous fluorophores like eGFP and mCherry up to a month, and preserved the complete morphology of the adult fly (Chapter 5) [Fig. 12]. This novel tissue clearing technique will greatly facilitate the high-resolution analysis of global neural circuit organization in wild type and mutant *Drosophila*.

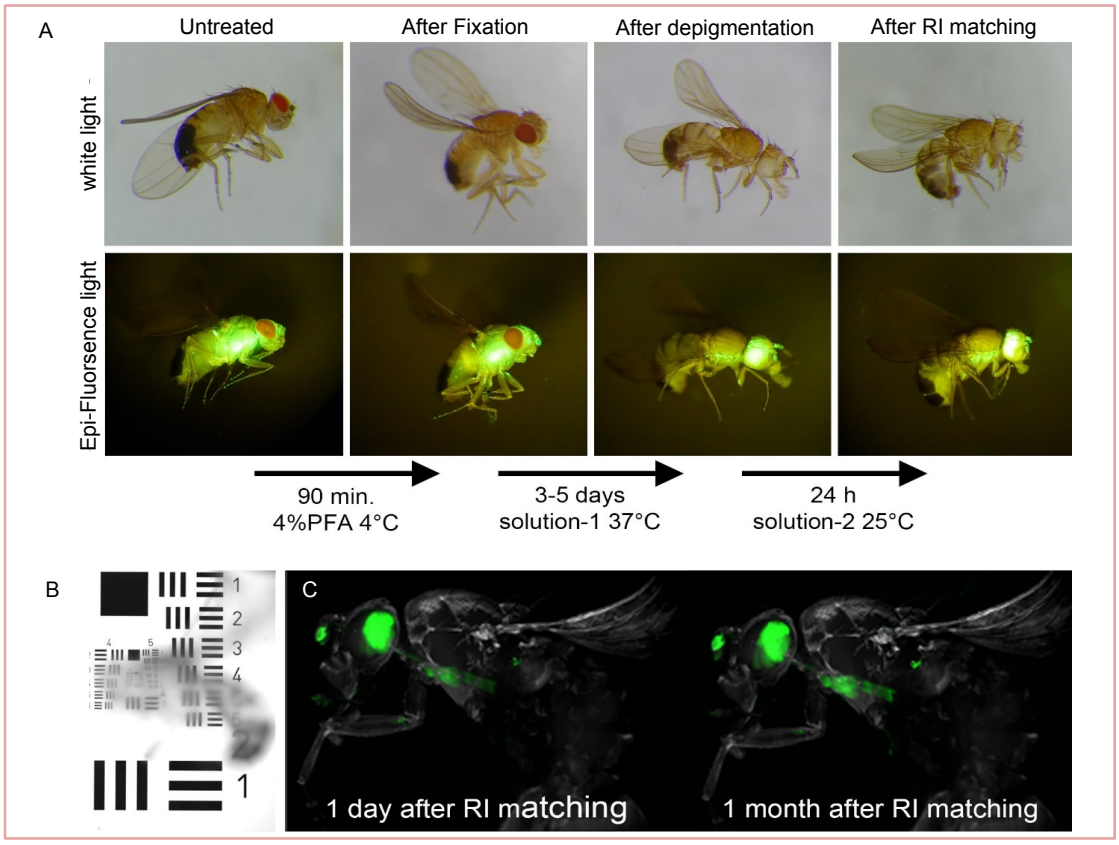

Figure 12: Workflow and properties of the *FlyClear* protocol. [A] Main steps of the *FlyClear* protocol; Initially, a fixed adult *Drosophila* is treated with *Solution-1* at 37°C for 3-5 days to remove pigment and lipid components, followed by washing with PBS. For refractive index matching as well as persevering the endogenous GFP signal, the sample is treated with *Solution-2* for 24 hours at 25°C. The specimens are kept for storage in *Solution-2* at 25°C. The upper panel shows a series of sample images obtained with a stereo-microscope white light. The same samples visualized with an epifluorescence microscope are shown in the corresponding images of the lower panel. [B] The wide field image of the cleared single adult fly placed on a USAF-chart in *Solution-2* demonstrates the high level of transparency. [C] Representative images demonstrating the GFP signal preservation after one day and after one month, recorded by light-sheet microscopy under identical conditions

1.7 References

1. Eric R. Kandel, James H. Schwartz, Thomas M. Jessell, Steven A. Siegelbaum AJH. Principles of Neural Science. Fifth Edit. McGraw Hill Professional; 2012.
2. Grabe V, Sachse S. Fundamental principles of the olfactory code. BioSystems. Elsevier Ireland Ltd; 2018;164: 94–101. doi:10.1016/j.biosystems.2017.10.010
3. Hara TJ. Olfaction and gustation in fish: an overview. Acta Physiol Scand. 1994;152: 207–17. doi:10.1111/j.1748-1716.1994.tb09800.x
4. Laissue PP, Vosshall LB. The Olfactory Sensory Map in. Brain Dev Drosoph melanogaster. 2008; 102–114. doi:10.1007/978-0-387-78261-4_7
5. Su CY, Menuz K, Carlson JR. Olfactory Perception: Receptors, Cells, and Circuits. Cell. 2009;139: 45–59. doi:10.1016/j.cell.2009.09.015
6. Vosshall LB, Wong AM, Axel R. An olfactory sensory map in the fly brain. Cell. 2000;102: 147–159. doi:10.1016/S0092-8674(00)00021-0
7. Robertson HM, Wanner KW. The chemoreceptor superfamily in the honey bee, Apis mellifera: Expansion of the odorant, but not gustatory, receptor family. Genome Res. 2006;16: 1395–1403. doi:10.1101/gr.5057506
8. Buck L, Axel R. A novel multigene family may encode odorant receptors: A molecular basis for odor recognition. Cell. 1991;65: 175–187. doi:10.1016/0092-8674(91)90418-X
9. Benton R, Sachse S, Michnick SW, Vosshall LB. Atypical membrane topology and heteromeric function of Drosophila odorant receptors in vivo. PLoS Biol. 2006;4: e20. doi:10.1371/journal.pbio.0040020
10. Serizawa S, Miyamichi K, Nakatani H, Suzuki M, Saito M, Yoshihara Y, et al. Negative Feedback Regulation Ensures the One Receptor-One Olfactory Neuron Rule in Mouse. Science (80-). 2003;302: 2088–2094. doi:10.1126/science.1089122
11. Ressler KJ, Sullivan SL, Buck LB. A zonal organization of odorant receptor gene expression in the olfactory epithelium. Cell. 1993;73: 597–609. doi:10.1016/0092-8674(93)90145-G
12. Vassar R, Ngai J, Axel R. Spatial segregation of odorant receptor expression in the mammalian olfactory epithelium. Cell. 1993;74: 309–18. doi:0092-8674(93)90422-M [pii]

13. Fişek M, Wilson RI. Stereotyped connectivity and computations in higher-order olfactory neurons. Nat Neurosci. 2013;17: 280–288. doi:10.1038/nn.3613
14. Fuss SH, Ray A. Mechanisms of odorant receptor gene choice in Drosophila and vertebrates. Mol Cell Neurosci. Elsevier Inc.; 2009;41: 101–112. doi:10.1016/j.mcn.2009.02.014
15. Mombaerts P. Axonal Wiring in the Mouse Olfactory System. Annu Rev Cell Dev Biol. 2006;22: 713–737. doi:10.1146/annurev.cellbio.21.012804.093915
16. Brochtrup A, Hummel T. Olfactory map formation in the Drosophila brain: Genetic specificity and neuronal variability. Curr Opin Neurobiol. Elsevier Ltd; 2011;21: 85–92. doi:10.1016/j.conb.2010.11.001
17. Shipley MT, Ennis M. Functional organization of olfactory system. J Neurobiol. 1996;30: 123–176. doi:10.1002/(SICI)1097-4695(199605)30:1<123::AID-NEU11>3.0.CO;2-N
18. Luo L, Flanagan JG. Development of continuous and discrete neural maps. Neuron. 2007;56: 284–300. doi:10.1016/j.neuron.2007.10.014
19. Mombaerts P, Wang F, Dulac C, Chao SK, Nemes A, Mendelsohn M, et al. Visualizing an olfactory sensory map. Cell. 1996;87: 675–686. doi:10.1016/S0092-8674(00)81387-2
20. Lodovichi C, Belluscio L, Katz LC. Functional topography of connections linking mirror-symmetric maps in the mouse olfactory bulb. Neuron. 2003;38: 265–276. doi:10.1016/S0896-6273(03)00194-6
21. Mori K. The Olfactory Bulb: Coding and Processing of Odor Molecule Information. Science (80-). 1999;286: 711–715. doi:10.1126/science.286.5440.711
22. Rodrigues V, Hummel T. Development of the Drosophila olfactory system. Adv Exp Med Biol. 2008;628: 82–101. doi:10.1007/978-0-387-78261-4_6
23. Chou YH, Spletter ML, Yaksi E, Leong JCS, Wilson RI, Luo L. Diversity and wiring variability of olfactory local interneurons in the Drosophila antennal lobe. Nat Neurosci. Nature Publishing Group; 2010;13: 439–449. doi:10.1038/nn.2489
24. Imai T. Construction of functional neuronal circuitry in the olfactory bulb. Semin Cell Dev Biol. Elsevier Ltd; 2014;35: 180–188. doi:10.1016/j.semcdb.2014.07.012
25. Liang L, Luo L. The olfactory circuit of the fruit fly Drosophila melanogaster.

Sci China Life Sci. 2010;53: 472–484. doi:10.1007/s11427-010-0099-z

26. Jefferis GSXE, Potter CJ, Chan AM, Marin EC, Rohlfing T, Maurer CR, et al. Comprehensive Maps of Drosophila Higher Olfactory Centers: Spatially Segregated Fruit and Pheromone Representation. Cell. 2007;128: 1187–1203. doi:10.1016/j.cell.2007.01.040
27. Wong AM, Wang JW, Axel R. Spatial representation of the glomerular map in the Drosophila protocerebrum. Cell. 2002;109: 229–241. doi:10.1016/S0092-8674(02)00707-9
28. Caron SJC, Ruta V, Abbott LF, Axel R. Random convergence of olfactory inputs in the Drosophila mushroom body. Nature. Nature Publishing Group; 2013;497: 113–117. doi:10.1038/nature12063
29. Heisenberg M. Mushroom body memoir: From maps to models. Nat Rev Neurosci. 2003;4: 266–275. doi:10.1038/nrn1074
30. Seki Y, Aonuma H, Kanzaki R. Pheromone processing center in the protocerebrum of Bombyx mori revealed by nitric oxide-induced anti-cGMP immunocytochemistry. J Comp Neurol. 2005;481: 340–351. doi:10.1002/cne.20392
31. Dulac C, Wagner S. Genetic Analysis of Brain Circuits Underlying Pheromone Signaling. Annu Rev Genet. 2006;40: 449–467. doi:10.1146/annurev.genet.39.073003.093937
32. Sosulski DL, Lissitsyna Bloom M, Cutforth T, Axel R, Datta SR. Distinct representations of olfactory information in different cortical centres. Nature. 2011;472: 213–219. doi:10.1038/nature09868
33. Kobayakawa K, Kobayakawa R, Matsumoto H, Oka Y, Imai T, Ikawa M, et al. Innate versus learned odour processing in the mouse olfactory bulb. Nature. 2007;450: 503–508. doi:10.1038/nature06281
34. Yan Z, Tan J, Qin C, Lu Y, Ding C, Luo M. Precise Circuitry Links Bilaterally Symmetric Olfactory Maps. Neuron. 2008;58: 613–624. doi:10.1016/j.neuron.2008.03.012
35. Stocker RF. The organization of the chemosensory system in Drosophila melanogaster: a review. Cell Tissue Res. 1994;275: 3–26. doi:10.1007/BF00305372
36. Suárez R, Gobius I, Richards LJ. Evolution and development of interhemispheric connections in the vertebrate forebrain. Front Hum Neurosci.

2014;8: 497. doi:10.3389/fnhum.2014.00497

37. Wilson RI. Early Olfactory Processing in *Drosophila* : Mechanisms and Principles. Annu Rev Neurosci. 2013;36: 217–241. doi:10.1146/annurev-neuro-062111-150533

38. Lovick JK, Ngo KT, Omoto JJ, Wong DC, Nguyen JD, Hartenstein V. Postembryonic lineages of the Drosophila brain: I. Development of the lineage-associated fiber tracts. Dev Biol. 2013;384: 228–57. doi:10.1016/j.ydbio.2013.07.008

39. Mihrshahi R. The Corpus Callosum as an Evolutionary Innovation. J Exp Zool B Mol Dev Evol. 2006;306: 1–7. doi:10.1002/jez.b.21085

40. van der Knaap LJ, van der Ham IJM. How does the corpus callosum mediate interhemispheric transfer? A review. Behav Brain Res. Elsevier B.V.; 2011;223: 211–221. doi:10.1016/j.bbr.2011.04.018

41. Aso Y, Hattori D, Yu Y, Johnston RM, Iyer NA, Ngo TTB, et al. The neuronal architecture of the mushroom body provides a logic for associative learning. Elife. 2014;3: e04577. doi:10.7554/eLife.04577

42. Strube-Bloss MF, Nawrot MP, Menzel R. Neural correlates of side-specific odour memory in mushroom body output neurons. Proc R Soc B Biol Sci. 2016;283: 20161270. doi:10.1098/rspb.2016.1270

43. Mori K, Sakano H. How is the olfactory map formed and interpreted in the mammalian brain? Annu Rev Neurosci. 2011;34: 467–99. doi:10.1146/annurev-neuro-112210-112917

44. Nishizumi H, Kumasaka K, Inoue N, Nakashima A, Sakano H. Deletion of the core-H region in mice abolishes the expression of three proximal odorant receptor genes in cis. Proc Natl Acad Sci U S A. 2007;104: 20067–20072. doi:10.1073/pnas.0706544105

45. Hirota J, Mombaerts P. The LIM-homeodomain protein Lhx2 is required for complete development of mouse olfactory sensory neurons. Proc Natl Acad Sci U S A. 2004;101: 8751–8755. doi:10.1073/pnas.0400940101

46. McIntyre JC, Bose SC, Stromberg AJ, McClintock TS. Emx2 stimulates odorant receptor gene expression. Chem Senses. 2008;33: 825–837. doi:10.1093/chemse/bjn061

47. Hoppe R, Breer H, Strotmann J. Promoter motifs of olfactory receptor genes expressed in distinct topographic patterns. Genomics. 2006;87: 711–723.

doi:10.1016/j.ygeno.2006.02.005

48. Lewcock JW, Reed RR. A feedback mechanism regulates monoallelic odorant receptor expression. Proc Natl Acad Sci. 2004;101: 1069–1074. doi:10.1073/pnas.0307986100
49. Imai T, Suzuki M, Sakano H. Odorant receptor-derived cAMP signals direct axonal targeting. Science (80-). 2006;314: 657–661. doi:10.1126/science.1131794
50. Nguyen MQ, Zhou Z, Marks CA, Ryba NJP, Belluscio L. Prominent Roles for Odorant Receptor Coding Sequences in Allelic Exclusion. Cell. 2007;131: 1009–1017. doi:10.1016/j.cell.2007.10.050
51. Duggan CD, DeMaria S, Baudhuin A, Stafford D, Ngai J. Foxg1 is required for development of the vertebrate olfactory system. J Neurosci. 2008;28: 5229–5239. doi:10.1523/JNEUROSCI.1134-08.2008
52. Norlin EM, Alenius M, Gussing F, Hägglund M, Vedin V, Bohm S. Evidence for gradients of gene expression correlating with zonal topography of the olfactory sensory map. Mol Cell Neurosci. 2001;18: 283–295. doi:10.1006/mcne.2001.1019
53. Markenscoff-Papadimitriou E, Allen WE, Colquitt BM, Goh T, Murphy KK, Monahan K, et al. Enhancer interaction networks as a means for singular olfactory receptor expression. Cell. 2014;159: 543–57. doi:10.1016/j.cell.2014.09.033
54. Monahan K, Schieren I, Cheung J, Mumbey-Wafula A, Monuki ES, Lomvardas S. Cooperative interactions enable singular olfactory receptor expression in mouse olfactory neurons. Elife. 2017;6: 8–11. doi:10.7554/eLife.28620
55. Shanbhag S., Müller B, Steinbrecht R. Atlas of olfactory organs of Drosophila melanogaster. Arthropod Struct Dev. 2000;29: 211–229. doi:10.1016/S1467-8039(00)00028-1
56. Clyne PJ, Warr CG, Freeman MR, Lessing D, Kim J, Carlson JR. A novel family of divergent seven-transmembrane proteins: candidate odorant receptors in Drosophila. Neuron. 1999;22: 327–38. doi:10.1016/S0896-6273(00)81093-4
57. Rytz R, Croset V, Benton R. Ionotropic Receptors (IRs): Chemosensory ionotropic glutamate receptors in Drosophila and beyond. Insect Biochem Mol Biol. Elsevier Ltd; 2013;43: 888–897. doi:10.1016/j.ibmb.2013.02.007

58. Jhaveri D, Sen A, Reddy GV, Rodrigues V. Sense organ identity in the Drosophila antenna is specified by the expression of the proneural gene atonal. Mech Dev. 2000;99: 101–11. doi:10.1016/S0925-4773(00)00487-1
59. Goulding SE, zur Lage P, Jarman AP. amos, a proneural gene for Drosophila olfactory sense organs that is regulated by lozenge. Neuron. 2000;25: 69–78. doi:10.1016/S0896-6273(00)80872-7
60. Gupta BP, Rodrigues V. Atonal is a proneural gene for a subset of olfactory sense organs in Drosophila. Genes Cells. 1997;2: 225–33. doi:10.1046/j.1365-2443.1997.d01-312.x
61. Couto A, Alenius M, Dickson BJ. Molecular, anatomical, and functional organization of the Drosophila olfactory system. Curr Biol. 2005;15: 1535–1547. doi:10.1016/j.cub.2005.07.034
62. Fishilevich E, Vosshall LB. Genetic and functional subdivision of the Drosophila antennal lobe. Curr Biol. 2005;15: 1548–1553. doi:10.1016/j.cub.2005.07.066
63. Reddy G V, Gupta B, Ray K, Rodrigues V. Development of the Drosophila olfactory sense organs utilizes cell-cell interactions as well as lineage. Development. 1997;124: 703–12. Available: http://www.ncbi.nlm.nih.gov/pubmed/9043085
64. Vosshall LB, Amrein H, Morozov PS, Rzhetsky A, Axel R. A spatial map of olfactory receptor expression in the Drosophila antenna. Cell. 1999;96: 725–736. doi:10.1016/S0092-8674(00)80582-6
65. Gao Q, Yuan B, Chess A. Convergent projections of Drosophila olfactory neurons to specific glomeruli in the antennal lobe. Nat Neurosci. 2000;3: 780–785. doi:10.1038/77680
66. Benton R, Vannice KS, Gomez-Diaz C, Vosshall LB. Variant Ionotropic Glutamate Receptors as Chemosensory Receptors in Drosophila. Cell. Elsevier Inc.; 2009;136: 149–162. doi:10.1016/j.cell.2008.12.001
67. Silbering AF, Rytz R, Grosjean Y, Abuin L, Ramdya P, Jefferis GSXE, et al. Complementary Function and Integrated Wiring of the Evolutionarily Distinct Drosophila Olfactory Subsystems. J Neurosci. 2011;31: 13357–13375. doi:10.1523/JNEUROSCI.2360-11.2011
68. Dobritsa AA, Van Der Goes Van Naters W, Warr CG, Steinbrecht RA, Carlson JR. Integrating the molecular and cellular basis of odor coding in the

Drosophila antenna. Neuron. 2003;37: 827–841. doi:10.1016/S0896-6273(03)00094-1

69. Endo K, Aoki T, Yoda Y, Kimura KI, Hama C. Notch signal organizes the Drosophila olfactory circuitry by diversifying the sensory neuronal lineages. Nat Neurosci. 2007;10: 153–160. doi:10.1038/nn1832
70. Endo K, Karim MR, Taniguchi H, Krejci A, Kinameri E, Siebert M, et al. Chromatin modification of Notch targets in olfactory receptor neuron diversification. Nat Neurosci. Nature Publishing Group; 2012;15: 224–233. doi:10.1038/nn.2998
71. Alkhori L, Öst A, Alenius M. The corepressor Atrophin specifies odorant receptor expression in Drosophila. FASEB J. 2014;28: 1355–1364. doi:10.1096/fj.13-240325
72. Sim CK, Perry S, Tharadra SK, Lipsick JS, Ray A. Epigenetic regulation of olfactory receptor gene expression by the Myb-MuvB/dREAM complex. Genes Dev. 2012;26: 2483–2498. doi:10.1101/gad.201665.112
73. Schmucker D, Hassan BA. Hamlet Notches fate. Nat Neurosci. Nature Publishing Group; 2012;15: 174–176. doi:10.1038/nn.3029
74. Clyne P, Certel S, de Bruyne M, Zaslavsky L, Johnson W, Carlson J. The odor-specificities of a subset of olfactory Neuron receptor neurons are governed by acj6, a POU domain transcription factor. Neuron. 1999;22: 339–347.
75. Bai L, Carlson JR. Distinct Functions of acj6 Splice Forms in Odor Receptor Gene Choice. J Neurosci. 2010;30: 5028–5036. doi:10.1523/JNEUROSCI.6292-09.2010
76. Tichy AL, Ray A, Carlson JR. A New Drosophila POU Gene, pdm3, Acts in Odor Receptor Expression and Axon Targeting of Olfactory Neurons. J Neurosci. 2008;28: 7121–7129. doi:10.1523/JNEUROSCI.2063-08.2008
77. Jafari S, Alkhori L, Schleiffer A, Brochtrup A, Hummel T, Alenius M. Combinatorial activation and repression by seven transcription factors specify Drosophila odorant receptor expression. PLoS Biol. 2012;10: e1001280. doi:10.1371/journal.pbio.1001280
78. Cayirlioglu P, Kadow IG, Zhan X, Okamura K, Suh GSB, Gunning D, et al. Hybrid neurons in a microRNA mutant are putative evolutionary intermediates in insect CO2 sensory systems. Science. 2008;319: 1256–60. doi:10.1126/science.1149483

79. Hartl M, Loschek LF, Stephan D, Siju KP, Knappmeyer C, Kadow ICG. A New Prospero and microRNA-279 Pathway Restricts CO2 Receptor Neuron Formation. J Neurosci. 2011;31: 15660–15673. doi:10.1523/JNEUROSCI.2592-11.2011
80. Komiyama T, Carlson JR, Luo L. Olfactory receptor neuron axon targeting: Intrinsic transcriptional control and hierarchical interactions. Nat Neurosci. 2004;7: 819–825. doi:10.1038/nn1284
81. Goodman CS, Shatz CJ. Developmental mechanisms that generate precise patterns of neuronal connectivity. Cell. 1993;72: 77–98. doi:10.1016/S0092-8674(05)80030-3
82. Kolodkin AL, Tessier-lavigne M. 1. Mechanisms and Molecules of Neuronal Wiring A Primer. 2011; 1–14. doi:10.1101/cshperspect.a001727
83. Dickson BJ. Molecular Mechanisms of Axon Guidance. Science (80-). 2002;298: 1959–1964. doi:10.1126/science.1072165
84. Serizawa S, Miyamichi K, Takeuchi H, Yamagishi Y, Suzuki M, Sakano H. A Neuronal Identity Code for the Odorant Receptor-Specific and Activity-Dependent Axon Sorting. Cell. 2006;127: 1057–1069. doi:10.1016/j.cell.2006.10.031
85. Takeuchi H, Sakano H. Neural map formation in the mouse olfactory system. Cell Mol Life Sci. 2014;71: 3049–57. doi:10.1007/s00018-014-1597-0
86. Imai T, Yamazaki T, Kobayakawa R, Kobayakawa K, Abe T, Suzuki M, et al. Pre-Target axon sorting establishes the neural map topography. Science (80-). 2009;325: 585–590. doi:10.1126/science.1173596
87. Cutforth T, Moring L, Mendelsohn M, Nemes A, Shah NM, Kim MM, et al. Axonal ephrin-As and odorant receptors: Coordinate determination of the olfactory sensory map. Cell. 2003;114: 311–322. doi:10.1016/S0092-8674(03)00568-3
88. Yoshihara Y, Kawasaki M, Tamada a, Fujita H, Hayashi H, Kagamiyama H, et al. OCAM: A new member of the neural cell adhesion molecule family related to zone-to-zone projection of olfactory and vomeronasal axons. J Neurosci. 1997;17: 5830–5842.
89. Gussing F, Bohm S. NQO1 activity in the main and the accessory olfactory systems correlates with the zonal topography of projection maps. Eur J Neurosci. 2004;19: 2511–8. doi:10.1111/j.0953-816X.2004.03331.x

90. Wang F, Nemes A, Mendelsohn M, Axel R. Odorant receptors govern the formation of a precise topographic map. Cell. 1998;93: 47–60. doi:10.1016/S0092-8674(00)81145-9
91. Nishizumi H, Sakano H. Developmental regulation of neural map formation in the mouse olfactory system. Dev Neurobiol. 2015;75: 594–607. doi:10.1002/dneu.22268
92. Miyamichi K. Continuous and Overlapping Expression Domains of Odorant Receptor Genes in the Olfactory Epithelium Determine the Dorsal/Ventral Positioning of Glomeruli in the Olfactory Bulb. J Neurosci. 2005;25: 3586–3592. doi:10.1523/JNEUROSCI.0324-05.2005
93. Takeuchi H, Inokuchi K, Aoki M, Suto F, Tsuboi A, Matsuda I, et al. Sequential arrival and graded secretion of Sema3F by olfactory neuron axons specify map topography at the bulb. Cell. 2010;141: 1056–1067. doi:10.1016/j.cell.2010.04.041
94. St. John JA, Clarris HJ, McKeown S, Royal S, Key B. Sorting and convergence of primary olfactory axons are independent of the olfactory bulb. J Comp Neurol. 2003;464: 131–140. doi:10.1002/cne.10777
95. Jhaveri D, Rodrigues V. Sensory neurons of the Atonal lineage pioneer the formation of glomeruli within the adult Drosophila olfactory lobe. Development. 2002;129: 1251–1260.
96. Jefferis GSXE, Vyas RM, Berdnik D, Ramaekers A, Stocker RF, Tanaka NK, et al. Developmental origin of wiring specificity in the olfactory system of Drosophila. Development. 2004;131: 117–30. doi:10.1242/dev.00896
97. Okumura M, Kato T, Miura M, Chihara T. Hierarchical axon targeting of Drosophila olfactory receptor neurons specified by the proneural transcription factors Atonal and Amos. Genes to Cells. 2016;21: 53–64. doi:10.1111/gtc.12321
98. Jefferis GSXE, Hummel T. Wiring specificity in the olfactory system. Semin Cell Dev Biol. 2006;17: 50–65. doi:10.1016/j.semcdb.2005.12.002
99. Sweeney LB, Couto A, Chou YH, Berdnik D, Dickson BJ, Luo L, et al. Temporal Target Restriction of Olfactory Receptor Neurons by Semaphorin-1a/PlexinA-Mediated Axon-Axon Interactions. Neuron. 2007;53: 185–200. doi:10.1016/j.neuron.2006.12.022
100. Joo W, Sweeney L, Liang L, Luo L. Linking cell fate, trajectory choice, and

target selection: Genetic analysis of sema-2b in olfactory axon targeting. Neuron. 2013;78: 673–686. doi:10.1016/j.neuron.2013.03.022

101. Sweeney LB, Chou YH, Wu Z, Joo W, Komiyama T, Potter CJ, et al. Secreted semaphorins from degenerating larval ORN axons direct adult projection neuron dendrite targeting. Neuron. Elsevier Inc.; 2011;72: 734–747. doi:10.1016/j.neuron.2011.09.026
102. Lattemann M, Zierau A, Schulte C, Seidl S, Kuhlmann B, Hummel T. Semaphorin-1a controls receptor neuron-specific axonal convergence in the primary olfactory center of Drosophila. Neuron. 2007;53: 169–84. doi:10.1016/j.neuron.2006.12.024
103. Komiyama T, Luo L. Intrinsic Control of Precise Dendritic Targeting by an Ensemble of Transcription Factors. Curr Biol. 2007;17: 278–285. doi:10.1016/j.cub.2006.11.067
104. Hong W, Luo L. Genetic control of wiring specificity in the fly olfactory system. Genetics. 2014;196: 17–29. doi:10.1534/genetics.113.154336
105. Chou YH, Zheng X, Beachy PA, Luo L. Patterning Axon Targeting of Olfactory Receptor Neurons by Coupled Hedgehog Signaling at Two Distinct Steps. Cell. 2010;142: 954–966. doi:10.1016/j.cell.2010.08.015
106. Jhaveri D, Saharan S, Sen A, Rodrigues V. Positioning sensory terminals in the olfactory lobe of Drosophila by Robo signaling. Development. 2004;131: 1903–12. doi:10.1242/dev.01083
107. Jhaveri D, Saharan S, Sen A, Rodrigues V. Positioning sensory terminals in the olfactory lobe of Drosophila by Robo signaling. Development. 2004;131: 1903–12. doi:10.1242/dev.01083
108. Hummel T, Zipursky SL. Afferent induction of olfactory glomeruli requires N-cadherin. Neuron. 2004;42: 77–88. doi:10.1016/S0896-6273(04)00158-8
109. Jhaveri D, Sen A, Rodrigues V. Mechanisms underlying olfactory neuronal connectivity in Drosophila-the atonal lineage organizes the periphery while sensory neurons and glia pattern the olfactory lobe. Dev Biol. 2000;226: 73–87. doi:10.1006/dbio.2000.9855
110. Hummel T, Vasconcelos ML, Clemens JC, Fishilevich Y, Vosshall LB, Zipursky SL. Axonal targeting of olfactory receptor neurons in Drosophila is controlled by Dscam. Neuron. 2003;37: 221–31. doi:10.1016/S0896-6273(02)01183-2

111. Ang L-H, Kim J, Stepensky V, Hing H. Dock and Pak regulate olfactory axon pathfinding in Drosophila. Development. 2003;130: 1307–16. doi:10.1242/dev.00356
112. Schmucker D, Clemens JC, Shu H, Worby CA, Xiao J, Muda M, et al. Drosophila Dscam is an axon guidance receptor exhibiting extraordinary molecular diversity. Cell. 2000;101: 671–684. doi:10.1016/S0092-8674(00)80878-8
113. Hattori D, Demir E, Kim HW, Viragh E, Zipursky SL, Dickson BJ. Dscam diversity is essential for neuronal wiring and self-recognition. Nature. 2007;449: 223–7. doi:10.1038/nature06099
114. Zhu H, Hummel T, Clemens JC, Berdnik D, Zipursky SL, Luo L. Dendritic patterning by Dscam and synaptic partner matching in the Drosophila antennal lobe. Nat Neurosci. 2006;9: 349–355. doi:10.1038/nn1652
115. Wilson DA. Binaral interactions in the rat piriform cortex. J Neurophysiol. 1997;78: 160–169. doi:10.1152/jn.1997.78.1.160
116. Kucharski D, Hall WG. New routes to early memories. Science (80-). 1987;238: 786–788. doi:10.1126/science.3672125
117. Barton RA, Clark DA. One nostril knows what the other learns. Nature. 2002;415: 9972–9972. doi:10.1038/419802a
118. Marks CA, Cheng K, Cummings DM, Belluscio L. Activity-dependent plasticity in the olfactory intrabulbar map. J Neurosci. 2006;26: 11257–66. doi:10.1523/JNEUROSCI.2805-06.2006
119. Belluscio L, Lodovichi C, Feinstein P, Mombaerts P, Katz LC. Odorant receptors instruct functional circuitry in the mouse olfactory bulb. Nature. 2002;419: 296–300. doi:10.1038/nature01001
120. Kikuta S, Sato K, Kashiwadani H, Tsunoda K, Yamasoba T, Mori K. Neurons in the anterior olfactory nucleus pars externa detect right or left localization of odor sources. Proc Natl Acad Sci. 2010;107: 12363–12368. doi:10.1073/pnas.1003999107
121. Scott JW, Ranier EC, Pemberton JL, Orona E, Mouradian LE. Pattern of rat olfactory bulb mitral and tufted cell connections to the anterior olfactory nucleus pars externa. J Comp Neurol. 1985;242: 415–24. doi:10.1002/cne.902420309
122. Brunjes PC, Illig KR, Meyer EA. A field guide to the anterior olfactory nucleus

(cortex). Brain Research Reviews. 2005. pp. 305–335. doi:10.1016/j.brainresrev.2005.08.005

123. Stocker RF, Lienhard MC, Borst A, Fischbach KF. Neuronal architecture of the antennal lobe in Drosophila melanogaster. Cell Tissue Res. 1990;262: 9–34. Available: http://www.ncbi.nlm.nih.gov/pubmed/2124174
124. Gaudry Q, Hong EJ, Kain J, de Bivort BL, Wilson RI. Asymmetric neurotransmitter release enables rapid odour lateralization in Drosophila. Nature. Nature Publishing Group; 2013;493: 424–8. doi:10.1038/nature11747
125. Louis M, Huber T, Benton R, Sakmar TP, Vosshall LB. Bilateral olfactory sensory input enhances chemotaxis behavior. Nat Neurosci. 2008;11: 187–199. doi:10.1038/nn2031
126. Das A, Sen S, Lichtneckert R, Okada R, Ito K, Rodrigues V, et al. Drosophila olfactory local interneurons and projection neurons derive from a common neuroblast lineage specified by the empty spiracles gene. Neural Dev. 2008;3: 1–17. doi:10.1186/1749-8104-3-33
127. Lai S-L, Awasaki T, Ito K, Lee T. Clonal analysis of Drosophila antennal lobe neurons: diverse neuronal architectures in the lateral neuroblast lineage. Development. 2008;135: 2883–2893. doi:10.1242/dev.024380
128. Chen W, Hing H. The L1-CAM, neuroglian, functions in glial cells for Drosophila antennal lobe development. Dev Neurobiol. 2008;68: 1029–1045. doi:10.1002/dneu.20644
129. Simon AF, Boquet I, Synguélakis M, Préat T. The Drosophila putative kinase linotte (derailed) prevents central brain axons from converging on a newly described interhemispheric ring. Mech Dev. 1998;76: 45–55. doi:10.1016/S0925-4773(98)00104-X
130. Yao Y, Wu Y, Yin C, Ozawa R, Aigaki T, Wouda RR, et al. Antagonistic roles of Wnt5 and the Drl receptor in patterning the Drosophila antennal lobe. Nat Neurosci. 2007;10: 1423–1432. doi:10.1038/nn1993
131. Aydemir Ö. Sensory and Synaptic Specification of the Olfactory Receptor Neurons in Drosophila melanogaster. WWU Münster. 2009.
132. Scheper C. The Role of Drosophila Apaf-1-related-killer (dark) in Establishing Synaptic Specificity in the Olfactory System. WWU Münster. 2009.

Chapter 2

Commissural interneurons instruct bilaterality in olfactory circuit organization

Rashmit Kaur[1], Michael Surala[1], Sebastian Hoger[1], Nicole Grössmann[2], Alexandra Grimm[1], Lorin Timaeus[1], Wolfgang Kallina[1], and Thomas Hummel[1*]

[1] Department of Neurobiology, University of Vienna, Althanstrasse 14A, 1090, Vienna, Austria

[2] Ludwig Boltzmann Institute , Health technology assessment , Garnisongasse7/20, 1090 Vienna, Austria

* Corresponding author: thomas.hummel@univie.ac.at

2.1 Summary

The two brain hemispheres of bilaterally-symmetric nervous systems are highly interconnected by distinct commissural tracts allowing the rapid exchange and integration of sensory and motor information [1,2]. The sudden appearance of novel interhemispheric connections during brain evolution like the innovation of the corpus callosum by placental mammals - according to T. H. Huxley "the greatest leap anywhere made by Nature in her brainwork"[3] - raises the question about the underlying developmental mechanism. The formation of bilateral circuits requires not only a variety of guidance cues and cellular interactions but also the precise regulation of ipsi- versus contralateral synaptic target recognition [4–6]. How is the global remodeling of multiple neural components into a bilateral brain circuit coordinated? Here we show that the induction of the olfactory commissure, an evolutionary novelty in dipteran flies for enhanced interhemispheric communication of sensory information [7], is controlled by the localized activity of a single cell adhesion molecule. Loss of the conserved Ig family member L1CAM/Neuroglian (Nrg), which affects corpus callosum development in mammals, leads to a complete reversal of the *Drosophila* bilateral into unilateral olfactory sensory map. Cell type-specific analysis revealed autonomous and non-autonomous Nrg functions in a small population of commissural pioneer interneurons, which not only prepattern the olfactory contralateral tracts but also prevent the targeting of ingrowing sensory axons to their ipsilateral synaptic partners. Subsequent hierarchical interactions between pioneer and follower axons via differential Nrg signaling control the sequential assembly of bilateral excitatory and inhibitory circuit elements. These findings revealed a novel developmental program for the induction of gross changes in brain connectivity. With the identification of dynamic bilateral sensory maps in more basal Dipteran species and conserved molecular and cellular organization of midline structures in vertebrates [2] our results will stimulate future comparative studies to determine how modulation of cell adhesion can trigger brain circuit evolution.

2.2 Results and Discussion

With a multitude of sensory class-specific synaptic glomeruli, interconnected by various types of modulatory interneurons, vertebrates and insects share main structural and functional features in olfactory circuit organization [8,9]. Although sensory representation in the majority of olfactory systems is strictly unilateral, flies have evolved a unique bilateral olfactory map in which sensory neurons (ORNs) target, in addition to the ipsilateral glomerulus, a homotopic synaptic region on the contralateral hemisphere via a commissural extension [10,11] (Fig. 1a, b). Within Diptera, unilateral axon labeling of antennal ORNs revealed a more dynamic uni- versus bilateral organization in Nematoceran species (Fig. 1c, Extended Data Fig. 1), and a prominent bilateral olfactory map in higher Brachycera (Fig. 1d, Extended Data Fig. 1) suggesting a flexible binary circuit design in early fly evolution [12].

To gain insights into the developmental mechanism underlying bilateral sensory map formation we performed a candidate gene approach in *Drosophila* using unilateral antennal labeling of mutants combined with targeted RNA interference (RNAi) in projecting ORNs. In both assays, loss of the Ig family member Neuroglian (Nrg) leads to a striking and highly-penetrant connectivity phenotype: axons of bilateral ORNs project only to their ipsilateral target glomerulus with a complete absence of a contralateral connection, thereby switching the olfactory sensory map back to the unilateral organization (Fig. 1e, f-i, l, m). A systematic analysis of multiple ORN classes in the *Nrg* mutant background showed that the majority of bilateral neuron classes display a precise ipsilateral connectivity pattern similar to unilateral ORN classes in wild type (Fig. 1 table, Extended Data Fig. 2). As terminal arborization remains confined within glomerular boundaries (Fig. 1j, k) and no changes in presynaptic density (Fig. 1n, o) of bilateral ORN axons within the ipsilateral hemisphere can be observed in *Nrg* mutants, these data indicate a sensitive developmental step in olfactory system formation to switch between a uni- versus bilateral state of circuit organization.

Besides ORNs, Nrg is expressed in various central neurons and glial cells [13] in the developing and adult olfactory system (Extended Data Fig. 3), raising the question about the underlying cellular interactions for bilateral circuit formation. We therefore

extended the targeted Nrg RNAi approach using a collection of developmental expression lines for different olfactory cell types. In contrast to a previous study [13], interfering with Nrg function in various olfactory glia types (via *repo-Gal4*, *442-Gal4*) did not affect the wild type connectivity pattern of bilateral ORNs (Extended Data Fig. 4). Similarly, developmental knock down of Nrg in projection neurons (PN, via *GH146-Gal4*), the main synaptic partner neurons of ORNs, has no effect on sensory axon targeting (Fig. 1p). However, loss of Nrg in a specific cluster of ventro-lateral (vl) interneurons (via *OK107-Gal4*, *OK371-Gal4*) results in a unilateral ORN connectivity phenotype (compare Fig. 1q and 1m). In the adult olfactory system, the vl-cluster contains different types of uni- and bilateral interneurons with specific dendritic arborizations [14,15] (Fig. 1r). *Nrg* mutant vl-cluster neurons fail to develop a contralateral projection but show no change of dendritic arborization within the ipsilateral hemisphere (Fig. 1s). These results identified Nrg function in olfactory interneurons as a central regulator of bilateral connectivity (Fig. 1t).

Pioneer sensory axons in the *Drosophila* olfactory system show high Nrg expression and segregate into a lateral and medial pathway while extending dorsally towards the midline (Fig. 2a). By the time of sensory neuron ingrowth, vl-interneurons have established a restricted dendritic arborization within the antennal lobe (AL) and a prominent midline commissure (Fig. 2b). To determine the neuronal diversity of commissural interneurons critical for bilateral circuit organization, we analyzed a collection of expression lines [16] (Fig. 2 c-i) and identified a small population of bilateral vl-interneurons which, upon Nrg knockdown, results in an unilateral ORN projection phenotype (Extended Data Fig. 5). Further developmental and clonal characterization revealed two main morphological classes of these commissural pioneer interneurons (cPINs), which prefigure the early sensory projections: the majority of cPINs (8-10 neurons) extends along the dorso-lateral pathway and forms a restricted commissural tract at the dorsal AL ("lateral cPINs", Fig. 2c, f, g, h). A smaller subset of cPINs (2-4 neurons) projects via the medial AL on the ipsi- as well as contralateral hemisphere ("medial cPINs", Fig 2c, f, i). The dendritic fields of lateral and medial cPINs remain separated in *Nrg* mutants but both classes of interneuron fail to extend a commissural tract (Fig. 2d, e). During wild type development, outgrowing cPINs establish an ipsilateral dendritic arbor and a commissural extension, which converge on the contralateral side (Fig. 2j-m"). In *Nrg*

mutants, the formation of ipsilateral processes is not affected but the contralateral extensions become rerouted and merge with the ipsilateral dendritic processes ("ipsilateral growth switch", Fig. 2n-q). As the entry side of ORN pioneer axons at the posterior AL is devoid of PN dendrites (Extended Data Fig. 6), the tight temporal and spatial coupling of cPIN-ORN growth pattern further supports a direct instructive role of olfactory interneurons in bilateral sensory neuron innervation.

To induce interhemispheric circuit organization, a likely cellular scenario would be the formation of a novel contralateral branch following the default developmental program of unilateral axon targeting (Fig. 3a-1). However, the comparison of initial axon targeting of uni- and bilateral pioneer neurons in wild type and *Nrg* mutants points towards an alternative developmental strategy to coordinate bilateral innervation (Fig. 3a-2). In wild type, axons of atonal-positive pioneer ORNs form a solid fiber track (Fig. 3b), which extends beyond the ipsilateral target region (Fig. 3c). After sending a commissural process across the dorsal midline (Fig. 3d), glomeruli are induced via bilateral axon convergence (Fig. 3e). In contrast, loss of Nrg result in a strong accumulation of pioneer axons at the ipsilateral prospective target side (Fig. 3f, g). During the period of contralateral axon projection in wild type, *Nrg* mutants show an accelerated glomerular convergence (Fig. 3h) but no obvious differences in glomerulus maturation (Fig. 3i). Single cell analysis revealed a highly dynamic growth cone morphology with a dense array of filopodia all along the AL surface (Fig. 3j-m). Here again, no signs of filopodia enrichment at the putative target region can be detected. During ipsilateral extension, single axons form the same amounts of filopodia in the central and dorsal AL domain (Fig. 3l, p). By the time of contralateral axon projection, the number of ipsilateral dorsal filopodia reduces and processes at the central synaptic target region are stabilized (Fig. 3m, q). In contrast, axons of unilateral ORN display a restricted field of filopodia during initial targeting and axon convergence (Fig. 3n-q). In the subsequent period of glomerulus assembly, *Nrg* mutants show an increased axonal restriction at the unilateral presynaptic region (Fig. 3s, u) compared to the bilateral innervation in wild type (Fig. 3r, t). These results show that the transient suppression of ipsilateral target site recognition defines a key event in bilateral map formation. Here, ipsilateral ORN-cPIN interaction shifts the primary ORN-PN recognition program to the contralateral hemisphere followed by ipsilateral axon targeting via the localized stabilization of axon collaterals. The

functional coupling of delayed axon targeting and contralateral growth by cPINs ensures an organized assembly of bilateral sensory circuits.

Neuron type-specific interference with Nrg function revealed not only a cell-autonomous role in cPINs and ORNs but also a strict hierarchy in their cellular interactions (Fig. 4b-m, summarized in a). The removal of Nrg from cPINs triggers unilateral targeting of all bilateral ORN classes (Fig. 4f, g) whereas the knock down of Nrg in ORNs has no effect on the bilateral organization of cPINs (Fig. 4h, k). Similarly, axons of follower ORNs rely on Nrg expression in cPINs and pioneer sensory neurons (Fig. 4j) but not vice versa (Fig. 4k, l), indicating a defined sequence of interneuronal interactions which correlates with the specific window of axon growth (Fig. 4a). Furthermore, bilateral serotonergic CSD neurons [17], which innervate the AL after sensory neurons, depend on Nrg specifically for the olfactory commissure but not for the development of an evolutionary more ancient protocerebral commissure [17] (Extended Data Fig. 7). As Nrg-mediated adhesion triggers different types of intracellular signaling pathways [18], we tested if the sequence of bilateral neuronal interactions involves distinct downstream effectors (Fig. 4r). Loss of the PDZ interacting domain has no effect on bilateral map formation (Fig. 4r, Extended Data Fig. 8) whereas the interference with Ankyrin binding specifically disrupts bilateral organization of follower ORNs (Fig. 4q'). The combined deletion of Ankyrin/PDZ interacting domains affects all bilateral ORN classes indicating partially redundant function in pioneer ORNs (Fig. 4p", q"). Bilateral cPIN development is mediated via Moesin interaction with the complete absence of a contralateral extension following the deletion of the corresponding intracellular domain (Fig. 4n'''). These results revealed distinct effector pathways in the Nrg-mediated hierarchical interactions to coordinate the bilateral assembly of key circuit components. Interestingly, cPINs subsequently develop into glutamatergic inhibitory interneurons of the adult olfactory system [19], indicating that an efficient bilateral odor representation requires the combined segregation of different types of modulatory interneurons along with sensory neurons.

Although a balanced activity of chemo-attraction and -repulsion has been a broadly accepted mechanism in bilateral circuit development for decades [4–6], recent studies on Netrin signaling have challenged the concept of long-range guidance also at the

midline and a critical role for cell adhesion have been shown in both vertebrates [20,21] and insects [22]. With the developmental switch mechanism between uni- and bilateral circuit organization described here, the evolutionary induction of Nrg expression in unilateral cPIN precursors would support novel cellular interactions. For example, persisting Nrg-positive larval commissures in close proximity to the developing adult olfactory system [23,24] could provide a permissive substrate for unilateral cPIN precursors to extend across the midline. A similar mechanism has been proposed for corpus callosum development with novel adhesive interactions of pioneer fibers with more ancient commissures of the hippocampus [2]. As sequential afferent interaction is a common theme not only among sensory neuron in insect and vertebrate olfactory systems development [25–27] but also corpus callosum formation [2,28], cPINs could have "highjacked" preexisting Nrg-mediated ORN interactions and thereby shifting unilateral olfactory circuit assembly to the contralateral hemisphere. In an alternative scenario, bilateral cPIN may have appeared de-novo and triggered interhemispheric connectivity of sensory neurons. Interestingly, the ventral AL neuroblast lineages generate a highly diverse population of bilateral neurons [15,23] and a recent study showed how changes in Hox gene expression within these progenitors result in major remodeling of brain circuit organization [29]. As the larval olfactory system in higher Dipterans display a unilateral connectivity pattern [30], an adult life style with highly agile flight behaviors seems to be a major determinant for the evolution of bilateral sensory representation. The enhanced sensitivity due to a higher degree of sensory convergence in bilateral versus unilateral olfactory circuits is accompanied by a substantial reduction in spatial information. It is tempting to speculate that the bilateral olfactory map became stabilized in the course of Dipteran evolution by strengthening directional sensitivity via lateralized synaptic differentiation [7].

2.3 Methods Summary

For developmental analysis of individual ORN axon targeting wild type single cell clones were generated using the Flybow (FB) construct [31] in combination with a heat induced *mFLP5* on 2nd chromosome. Flies expressing FB1.1B transgene under the control of *R86G11-Gal4* [16] were exposed to single heat shock for 90 minutes at 37°C to induce transient mFLP5 [31] activity between 0 to 5 hrs after pupa formation

(APF). Confocal images were processed and analyzed using ImageJ and Imaris 9.2 (Bitplane).

To characterize the neuronal morphology of cPIN, wild type single cell clones were generated using the hs-FLP and FRT/FLP system [32]. Wild type cPINs were labeled with *R19H07-Gal4* [16] driving the expression of UAS-mCD8::GFP [32]. II instar larvae were heat shocked for 20-30 minutes at 37°C. Pupae at the desired stage were dissected. The developmental pattern of pioneer ORNs, their synaptogenesis and LNs, in wild type and *Nrg* mutant background were analyzed in confocal image stacks of stained pupal and adult brains. *R86G11-Gal4* [16] and *R20F11-Gal4* [16] driver lines for ORNs and LNs were used respectively. *Nrg* mutant hemizygous males and heterozygous females (control), were preselected at third instar and separated in different food vials for both clonal and expression analysis. White pupae were selected for staging; pupae at desired age, and adult flies were dissected after eclosion.

2.4 Methods

Fly stocks and Genetics

Fly stocks and crosses were maintained in standard medium at 25°C unless stated otherwise. To discover molecules involved in bilateral sensory map formation, an RNAi screen was conducted against several cell adhesion molecules using *Pebbeled-Gal4* (a gift from L. Luo, ref. 25), details of the screen are available from the authors). To perform Nrg RNAi knockdown in ORNs, glia and antennal lobe associated neurons, the following stocks were obtained from Bloomington *Drosophila* Stock Center (BDSC) or received as gift: ORN drivers, *Sg18.1-Gal4* [33] (BDSC 6405), *atonal-Gal4* (a gift from B.A. Hassan), *amos-Gal4* (a gift from T. Chihara, ref. 26), ORN specific drivers and markers were kindly provided by B. Dickson and L. Vosshall [34,35]; LN drivers, *OK107-Gal4* (BDSC 854, ref. 14), *OK371-Gal4* (a gift from H. Aberle, ref. 14); Gal4 and LexA driver lines having expression in subset of LNs were selected based on expression pattern [16] and were obtained from BDSC; glia specific drivers, *repo-Gal4* (BDSC 7415), *442-Gal4* (a gift from T. Préat, ref. 13), PN specific *GH146-Gal4* [36], UAS-Nrg RNAi (BDSC 38215). Stocks used for Nrg mutant and intracellular domain deletion constructs (P[acman] constructs); nrg^{849} (BDSC 35827), nrg^{14} and P[acman] constructs were kindly provided by Jan Pielage (ref. 18). For visualizing axons, synaptic terminals and co-labeling of two distinct cell

types, reporters of different binary systems were used; UAS-*mCD8::GFP* [32], *UAS-Brp::GFP* (BDSC 36291), *UAS-mCherry* (BDSC 27392), *10XUAS-mCD8::RFP,13X LexAop2-mCD8::GFP* (BDSC 32229). For generating single cell clones *hs-mFLP5* [31] (BDSC 56799, BDSC 35534) and UAS-Flybow1.1B [31] (BDSC 56803) constructs were used.

Immunohistology

Primary antibodies used for in this study were: rat anti-cadherin-N extracellular domain (DN-Ex no.8; 1:10; DSHB), mouse anti-Flamingo (1:5, DSHB), mouse anti-Neuroglian-180 (1:10, DSHB), rabbit anti-GFP (1:1000 Invitrogen), mouse anti Fasciclin2 (1:5, DSHB). Secondary antibodies used were as follows: goat anti-rabbit Alexa 488 (1:500), goat anti-rat Alexa 568 (1:300), goat anti- rat Alexa 647 (1:500), goat anti-mouse Alexa 568 (1:300), Avidin Alexa 488 (1:40). For general nuclear staining, TOTO-3 (1:5000) was used. All the secondary antibodies were obtained from Invitrogen.

Dissection of the pupal and adult brains was carried out in 1x phosphate buffer saline (PBS) and fixed in 2% freshly prepared paraformaldehyde (prepared in 1x PBS) for 60 and 90 minutes at room temperature respectively. The fixative was removed, and the brains were washed four times with 0.1% PBTx (0.1% Triton X-100 in 1x PBS) for 15 minutes each at the room temperature. Blocking of the samples was performed for 60 minutes at room temperature in 10% Goat serum, prepared in 0.1% PBTx then incubated with primary antibody over night at 4°C. Following four time washing, 15 minutes each, samples were incubated with secondary antibody over night at 4°C. After four times washing, 15 minutes each, samples were mounted in Vectasheild (vector laboratories), an anti-fade mounting medium for confocal microscopy. Both primary and secondary antibodies were diluted in 10% Goat Serum. Fluorescent samples were analyzed using a Leica TCS SP5II confocal microscope. To process, analyze images, and quantify phenotypes the open source tool ImageJ, Adobe photoshop and Imaris (Bitplane) were used.

Unilateral antennal backfills

All the experiments were performed on adult flies. Mosquitoes (*A. arabiensis*) were kindly provided by IAEA, Seibersdorf Laboratories, Austria. Almost all diptera

species were collected within the state of Vienna area, with the exception of *Hermetia illucens*, which was caught in South Tyrol. Species identity of fly samples was performed by a diptera determination key to reach family level and further specific literature to refine the taxon. In cases where a genus level could not be reached or there were remaining uncertainties, the help of experts on the diptera-forum (www.diptera.info) was claimed. Living flies were first anthestized via CO_2 and then inserted into 200µl or 1000µl plastic pipette tips, where parts of the tips have been cut off according to the body size, so that the head could stick out of the tip. The flies were immobilized with plasticine. In a petri dish, the loaded pipette tip was placed on a plasticine cube with a small indentation for the fly head. To apply the tracer, a wall was built around the antenna with vaseline, creating a small cavity and leaving only one antenna exposed. In all flies, the right antenna was cut, at the base of the third segment, and completely submerged with a drop of neuronal backfill tracer - 2% neurobiotin (vector laboratories) diluted in millipore water. The cavity was then completely covered with vaseline to prevent desiccation and the petri dish was kept in 4°C for 90 minutes. Afterwards, the fly heads were removed and processed with above mentioned immunohistology process for visualization on the same day[37]. The DN-Cadherin as a general neuropil marker and anti-nrg to label the olfactory commissure.

2.5 Acknowledgements

We are grateful to B. A. Hassan, T. Chihara, J. Pielage, H. Aberle and T. Préat for providing critical reagents for this study. We would like to thank the Bloomington *Drosophila* Stock Center for *Drosophila* transgenic lines and Developmental Studies Hybridoma Bank for antibodies. We further thank L. Luo and Y. Chou for stimulating discussions and members of the Hummel laboratory for critical comments on the manuscript. DFG, Schram Foundation, ROL Research Platform Vienna University supported this work.

2.6 Author Contributions

R.K. performed the RNAi screen and all the RNAi experiments, analyzed Neuroglian mutation, performed P[acman] analysis. M.S. performed the developmental analysis of ORNs and analyzed single cell FLYBOW clones. S.H performed the LN specific RNAi screen and analyzed the development of LNs. N.G. analyzed the developmental

expression of early ORN specific Rubin-Gal4s. A.G. performed antibody staining. L.T. collected and identified Diptera species and performed antennal backfills. W.K. performed antennal backfills. R.K. and T.H. conceived the project, designed the experiments, data interpretation and manuscript preparation. T.H. collected and identified Diptera species, supervision, data interpretation and funding acquisition.

2.7 References

1. Aboitiz F, Montiel J. One hundred million years of interhemispheric communication: The history of the corpus callosum. Brazilian J Med Biol Res. 2003;36: 409–420. doi:10.1590/S0100-879X2003000400002
2. Suárez R, Gobius I, Richards LJ. Evolution and development of interhemispheric connections in the vertebrate forebrain. Front Hum Neurosci. 2014;8: 497. doi:10.3389/fnhum.2014.00497
3. TH Huxley. Man's Place in Nature. McMillan, London, UK. 1863.
4. Dickson BJ. Molecular Mechanisms of Axon Guidance. Science (80-). 2002;298: 1959–1964. doi:10.1126/science.1072165
5. Evans TA, Bashaw GJ. Axon guidance at the midline: of mice and flies. Curr Opin Neurobiol. 2010;20: 79–85. doi:10.1016/j.conb.2009.12.006
6. Chédotal A, Richards LJ. Wiring the brain: the biology of neuronal guidance. Cold Spring Harb Perspect Biol. 2010;2: 1–18. doi:10.1101/cshperspect.a001917
7. Gaudry Q, Hong EJ, Kain J, de Bivort BL, Wilson RI. Asymmetric neurotransmitter release enables rapid odour lateralization in Drosophila. Nature. Nature Publishing Group; 2013;493: 424–8. doi:10.1038/nature11747
8. Brochtrup A, Hummel T. Olfactory map formation in the Drosophila brain: Genetic specificity and neuronal variability. Curr Opin Neurobiol. Elsevier Ltd; 2011;21: 85–92. doi:10.1016/j.conb.2010.11.001
9. Imai T, Yamazaki T, Kobayakawa R, Kobayakawa K, Abe T, Suzuki M, et al. Pre-Target axon sorting establishes the neural map topography. Science (80-). 2009;325: 585–590. doi:10.1126/science.1173596
10. Stocker RF. The organization of the chemosensory system in Drosophila melanogaster: a review. Cell Tissue Res. 1994;275: 3–26. doi:10.1007/BF00305372

11. Vosshall LB, Amrein H, Morozov PS, Rzhetsky A, Axel R. A spatial map of olfactory receptor expression in the Drosophila antenna. Cell. 1999;96: 725–736. doi:10.1016/S0092-8674(00)80582-6
12. Wiegmann BM, Trautwein MD, Winkler IS, Barr NB, Kim J-W, Lambkin C, et al. Episodic radiations in the fly tree of life. Proc Natl Acad Sci U S A. 2011;108: 5690–5. doi:10.1073/pnas.1012675108
13. Chen W, Hing H. The L1-CAM, neuroglian, functions in glial cells for Drosophila antennal lobe development. Dev Neurobiol. 2008;68: 1029–1045. doi:10.1002/dneu.20644
14. Das A, Chiang A, Davla S, Priya R, Reichert H, VijayRaghavan K, et al. Identification and analysis of a glutamatergic local interneuron lineage in the adult Drosophila olfactory system. Neural Syst Circuits. BioMed Central Ltd; 2011;1: 4. doi:10.1186/2042-1001-1-4
15. Chou YH, Spletter ML, Yaksi E, Leong JCS, Wilson RI, Luo L. Diversity and wiring variability of olfactory local interneurons in the Drosophila antennal lobe. Nat Neurosci. Nature Publishing Group; 2010;13: 439–449. doi:10.1038/nn.2489
16. Jenett A, Rubin GM, Ngo TTB, Shepherd D, Murphy C, Dionne H, et al. A GAL4-Driver Line Resource for Drosophila Neurobiology. Cell Rep. The Authors; 2012;2: 991–1001. doi:10.1016/j.celrep.2012.09.011
17. Dacks AM, Christensen TA, Hildebrand JG. Phylogeny of a serotonin-immunoreactive neuron in the primary olfactory center of the insect brain. J Comp Neurol. 2006;498: 727–46. doi:10.1002/cne.21076
18. Siegenthaler D, Enneking EM, Moreno E, Pielage J. L1CAM/Neuroglian controls the axon-axon interactions establishing layered and lobular mushroom body architecture. J Cell Biol. 2015;208: 1003–1018. doi:10.1083/jcb.201407131
19. Liu WW, Wilson RI. Glutamate is an inhibitory neurotransmitter in the Drosophila olfactory system. Proc Natl Acad Sci. 2013;110: 10294–10299. doi:10.1073/pnas.1220560110
20. Varadarajan SG, Kong JH, Phan KD, Kao T-J, Panaitof SC, Cardin J, et al. Netrin1 Produced by Neural Progenitors, Not Floor Plate Cells, Is Required for Axon Guidance in the Spinal Cord. Neuron. 2017;94: 790–799.e3. doi:10.1016/j.neuron.2017.03.007

21. Dominici C, Moreno-Bravo JA, Puiggros SR, Rappeneau Q, Rama N, Vieugue P, et al. Floor-plate-derived netrin-1 is dispensable for commissural axon guidance. Nature. 2017;545: 350–354. doi:10.1038/nature22331
22. Akin O, Zipursky SL. Frazzled promotes growth cone attachment at the source of a Netrin gradient in the Drosophila visual system. Elife. 2016;5. doi:10.7554/eLife.20762
23. Lovick JK, Ngo KT, Omoto JJ, Wong DC, Nguyen JD, Hartenstein V. Postembryonic lineages of the Drosophila brain: I. Development of the lineage-associated fiber tracts. Dev Biol. 2013;384: 228–57. doi:10.1016/j.ydbio.2013.07.008
24. Hartenstein V, Younossi-Hartenstein A, Lovick JK, Kong A, Omoto JJ, Ngo KT, et al. Lineage-associated tracts defining the anatomy of the Drosophila first instar larval brain. Dev Biol. Elsevier; 2015;406: 14–39. doi:10.1016/j.ydbio.2015.06.021
25. Sweeney LB, Couto A, Chou YH, Berdnik D, Dickson BJ, Luo L, et al. Temporal Target Restriction of Olfactory Receptor Neurons by Semaphorin-1a/PlexinA-Mediated Axon-Axon Interactions. Neuron. 2007;53: 185–200. doi:10.1016/j.neuron.2006.12.022
26. Okumura M, Kato T, Miura M, Chihara T. Hierarchical axon targeting of Drosophila olfactory receptor neurons specified by the proneural transcription factors Atonal and Amos. Genes to Cells. 2016;21: 53–64. doi:10.1111/gtc.12321
27. Sakano H. Neural map formation in the mouse olfactory system. Neuron. Elsevier Inc.; 2010;67: 530–42. doi:10.1016/j.neuron.2010.07.003
28. Fame RM, MacDonald JL, Macklis JD. Development, specification, and diversity of callosal projection neurons. Trends Neurosci. Elsevier Ltd; 2011;34: 41–50. doi:10.1016/j.tins.2010.10.002
29. Sen S, Cao D, Choudhary R, Biagini S, Wang JW, Reichert H, et al. Genetic transformation of structural and functional circuitry rewires the Drosophila brain. Elife. 2014;3: 1–27. doi:10.7554/eLife.04407
30. Thum AS, Leisibach B, Gendre N, Selcho M, Stocker RF. Diversity, variability, and suboesophageal connectivity of antennal lobe neurons in D. melanogaster larvae. J Comp Neurol. 2011;519: 3415–32. doi:10.1002/cne.22713

31. Shimosako N, Hadjieconomou D, Salecker I. Flybow to dissect circuit assembly in the Drosophila brain. Methods Mol Biol. 2014;1082: 57–69. doi:10.1007/978-1-62703-655-9_4
32. Lee T, Luo L. Mosaic Analysis with a Repressible Cell Marker for Studies of Gene Function in Neuronal Morphogenesis. Neuron. 1999;22: 451–461. doi:10.1016/S0896-6273(00)80701-1
33. Jhaveri D, Sen A, Rodrigues V. Mechanisms underlying olfactory neuronal connectivity in Drosophila-the atonal lineage organizes the periphery while sensory neurons and glia pattern the olfactory lobe. Dev Biol. 2000;226: 73–87. doi:10.1006/dbio.2000.9855
34. Couto A, Alenius M, Dickson BJ. Molecular, anatomical, and functional organization of the Drosophila olfactory system. Curr Biol. 2005;15: 1535–1547. doi:10.1016/j.cub.2005.07.034
35. Vosshall LB, Wong AM, Axel R. An olfactory sensory map in the fly brain. Cell. 2000;102: 147–159. doi:10.1016/S0092-8674(00)00021-0
36. Stocker RF, Heimbeck G, Gendre N, de Belle JS. Neuroblast ablation in Drosophila P[GAL4] lines reveals origins of olfactory interneurons. J Neurobiol. 1997;32: 443–56. doi:10.1002/(SICI)1097-4695(199705)32
37. Solari P, Corda V, Sollai G, Kreissl S, Galizia CG, Crnjar R. Morphological characterization of the antennal lobes in the Mediterranean fruit fly Ceratitis capitata. J Comp Physiol A Neuroethol Sensory, Neural, Behav Physiol. Springer Berlin Heidelberg; 2016;202: 131–146. doi:10.1007/s00359-015-1059-7

Main Figure legends

Figure 1. Loss of Neuroglian results in a switch of bilateral into unilateral sensory map organization.

(a, b) Adult olfactory system of *Drosophila*. Sensory neurons from the antennae project via the antennal nerves to the bilateral antennal lobes (AL, dashed circle) (a). Schematic of a single olfactory receptor neuron (ORN) connecting to a synaptic glomerulus at the ipsilateral AL and a homotopic glomerulus in the contralateral hemisphere (b, Neuropil marker N-Cadherin in red). Scale bar = 100µm and 50µm for a and b respectively. (c-e) Uni- and bilateral olfactory map organization in Diptera.

Unilateral antennal backfill revealed a strict ipsilateral representation of ORN afferents in mosquitos (c). In contrast, in higher Brachyceran like *Drosophila* (d), the majority of ORNs project in a bilateral fashion as indicated by a large commissural tract and labeling of the contralateral AL. In contrast to wild type, *Drosophila* carrying a mutation in the cell adhesion molecule Nrg displays a strict unilateral afferent innervation (e). (f-i) Labeling of different bilateral ORN populations in *Drosophila* wild type (f, h) and *Nrg* mutants (g, i) identified not only the complete absence of the antennal commissure (f, g) but also the precise ipsilateral targeting and class-specific ORN axon convergence (asterisks in h, i). (j-k) *Nrg* mutants show a specific loss of bilateral ORN connectivity. (j) Wild type projections from a single olfactory sensillum (ac1) containing 2 bilateral (Ir92a, Ir31a yellow and green respectively, arrows indicate contralateral projections) and one unilateral (Ir75d, red) ORN classes. Note the higher degree of synaptic arborization within the ipsilateral glomerulus (left insets) compared to the contralateral target side (right insets). (k) In *Nrg* mutant, bilateral ORN axons show a normal level of ipsilateral arborization but fail to extend any contralateral process (yellow/green arrows, contralateral AL not shown). No changes in the connectivity of the unilateral ORN class can be detected. The table summarizes a systematic analysis of 19 ORN classes in *Nrg* mutants showing a complete switch of all bilateral (red and green) into unilateral ORNs (black) but no effect on unilateral ORN classes (blue). (l, m) The targeted Nrg RNAi in projecting ORNs uncovers a cell-autonomous function in sensory neurons visualized by the unilateral connectivity (Or47b in green). (n, o) Compared to wild type (n, n'), loss of Nrg (o, o') has no effect on the pre-synaptic differentiation at the ipsilateral target side as indicated by the localization of Bruchpilot protein. Green, Brp::GFP and Red, neuropil marker N-cadherin. (p, q) Targeted RNAi of Nrg in different cell types of the developing olfactory system. Removal of Nrg from projection neurons (PNs) does not influence bilateral ORN (green) connectivity (p, p'). In contrast, loss of Nrg in a cluster of ventro-lateral interneurons (vl-LNs) leads to a complete switch into unilateral ORN circuitry (q, q'). (r, s) In the adult olfactory system, a vl cluster (white arrow) of LNs displays, in addition to a broad ipsilateral arborization within the AL, a distinct commissural projection (inset r', r''). In *Nrg* mutant ipsilateral dendritic arborizations seems unaffected whereas the contralateral LN tract is missing (inset s', s''). Green, LNs. Red, all neurons. Blue, neuropil marker N-cadherin. (t) Schematics illustrating sensory map connectivity in the *Drosophila*

olfactory system. Within each pair of homotopic glomeruli, bilateral sensory input (red and orange ORNs) onto unilateral PNs is modified by different classes of bilateral LNs. Loss of Nrg in bilateral ORNs and LNs (but not PNs or midline glial cells) leads to a switch of the bilateral into a unilateral sensory representation. Dashed vertical white line indicates the midline, commissure position is highlighted by white box and a dotted circle shows glomerulus boundaries. Scale bar = 20μm for all images of adult ALs.

Figure 2. Commissural interneurons prepattern bilateral ORN projections.
(a-a'') At about 20hr APF, Nrg positive (arrowhead in a'') ORN pioneer axons enter the AL and segregate into a lateral and a medial fascicle (arrows in a, arrowheads in a'), which extend towards the dorsal midline of Nrg positive fibers (bracket in a''). (b-b'') At the time of ORN axon arrival, a ventro-lateral cluster (cell bodies indicated by arrowhead) of commissural pioneer interneurons (cPINs) has developed localized ipsilateral dendritic arborizations (dashed circle in b') and broad contralateral projection at the dorsal AL (arrowhead in b' and b''). ORN axons (arrow in b'') and the commissural tract of cPINs (bracket in b'') can be identified by their strong expression of the cell adhesion molecule Flamingo (Fmi in b''). (c-c''') Based on the spatial segregation of their dendritic fields in the adult AL, two main classes of cPINs, the lateral and the medial, can be recognized (lateral/medial domain, LD/MD). The cell bodies of both cPIN classes are in close proximity (inset, c'' and c''') but their commissural tracts in the dorsal AL remain separated (dashed box in c and brackets in c'). (d-e) In *Nrg* mutants, the dendritic field of each cPIN class in the ipsilateral AL (LD/MD) remains correctly positioned but the contralateral projection is missing (dashed boxes in d, e). (f-i) Wild type organization of cPIN classes. Before ORN axons arrival, dendritic fields of the cPIN classes segregate in the ipsi- and contralateral AL. (f, f') Both lateral and medial cPINs having distinct projection patterns. (g-h') Lateral cPINs possess a distinct ipsilateral dendritic field (arrows in g' and h') and a strong commissural tract, which terminate at the dorsal edge of the contralateral AL (arrowhead in h). In contrast, medial cPINs have a thin commissural tract, which extend to ventral region of the contralateral AL (i, i'). Development of cPIN in wild type (j-m'') and *Nrg* mutants (n-p). With the beginning of metamorphosis, cPINs start to extend to the dorsal AL midline (arrow in j') and ventral extensions of the ipsilateral dendritic arborizations become visible (green

arrowhead in j'). Following the initiation of the ipsilateral dendritic field (green arrowhead in k', k''), cPINs project a pioneer commissural track across the dorsal midline (red arrowhead, showing contralateral axon in k', k''), which grows along the medial surface of the contralateral AL (l', l'') to merge with the ipsilateral dendritic arborization at the time of ORN axon arrival (m', m''). In *Nrg* mutants, no changes can be observed for initiation of the dendritic field (green arrowhead in n) and the dorsal extension of cPINs within the ipsilateral AL (white arrowheads in n). However, the dorsal process loops back, extend ventrally and "self-merge" with the ventral ipsilateral processes (o), subsequently forming the appropriate dendritic field in the medial AL region (p). (q) Schematics summarize the growth pattern of lateral and medial cPIN classes in a wild type and *Nrg* mutant olfactory system. Dashed vertical white line indicates midline, developing AL is indicated by white dotted circle and LD and MD is indicated by red dotted line. Scale bar = and 10μm for all images of pupal and 20μm for adult (c-e) ALs.

Figure 3. Neuroglian suppresses ipsilateral ORN axon targeting.

(a) Two alternative developmental pathways to switch from unilateral to bilateral circuit assembly: (1) Following the ipsilateral ORN targeting to glomerulus-specific PNs, contralateral innervation is induced via a commissural branch (blue) across the midline (ML). (2) Direct contralateral projection via suppression of ipsilateral targeting followed by the induction of an ipsilateral synaptic collateral (blue). (b-i) Axon growth analysis of a single pioneer ORN class (Ir92a), which targets a ventral medial glomerulus (VM1, see Fig. 1). In wild type, pioneer Ir92a ORN axon enter the AL around 20 hr APF (b) and extend along the medial pathway to the dorsal AL with no signs of accumulation at the putative target region in the ventro-medial AL region (white line). Following midline crossing and extension to the contralateral target region (red line in d), ORN axons converge within the next 20hrs into spatially restricted synaptic glomeruli (e). (f-i) In *Nrg* mutants, ORN axons reach the AL within the temporal period of wild type axons. In contrast to the smooth ipsilateral extension of pioneer axons in wild type, loss of Nrg leads to an instant accumulation of pioneer axons at the prospective ventral target region (arrowhead in f). During the period of wild type dorsal extension and contralateral projection (25-30 hr APF), *Nrg* mutant pioneer axons converge prematurely at the target region (arrowheads in g, h), with no differences during the following period of glomerulus maturation (i). (j-q) Single cell

analysis of pioneer axon branch dynamics. During the period of ipsilateral growth, individual axons of bilateral ORNs induce a large number of lateral processes all along the medial AL neuropil (ventral, central and dorsal area in l) with no enrichment at the prospective target region (TR, red lines in j, high magnification in j'; quantification in p). Following the contralateral projection, the number of ipsilateral filopodia reduces at the dorsal AL and restricts to the prospective ventro-medial target region (k and m, quantification in q). In contrast to bilateral ORNs, axons of ingrowing unilateral ORNs aggregate at the prospective ventral target region with filopodia extending into multiple directions (n, o quantification in p and q). (r-u) Similarly to the sequence of axon projection, the presynaptic differentiation following contralateral projections, as indicated by the localization of Bruchpilot-GFP, is more restricted in *Nrg* mutants compared to wild type (r, s) but similar pattern of synaptic maturation is observed during glomerulus assembly (t, u). Scale bar = 10μm for all images of pupal ALs.

Figure 4. Differential Neuroglian signaling mediates hierarchical neuron interactions in bilateral circuit formation.

(a) Analysis of cell-type specific Nrg RNA interference to define autonomous and non-autonomous functions of sequentially ingrowing cPINs, pioneer and follower ORNs as well as serotonergic CSD neurons. The table summarizes the resulting connectivity phenotypes. (e-g) Removal of Nrg in developing cPINs does not only switch bilateral into unilateral interneurons (e) but also disrupt the bilateral projection of pioneer and follower ORNs (f and g, respectively, compare to wild type b-d). (h-j) Downregulation of Nrg in pioneer neurons interferes with their bilateral projection (i) as well as the projections of follower neurons (j), but has no effect on bilateral cPIN development (h). (k-m) Restricted removal of Nrg in late projecting bilateral ORN classes ("followers") transforms them into a unilateral projection type (m) but leave the bilateral organization of cPINs (k) and pioneer ORNs (l) unaffected, demonstrating a strict temporal hierarchy of Nrg-mediated interneuronal interactions in bilateral circuit formation. (n-r) Analysis of Nrg domain requirement for 2 classes of cPINs (n, o) and 2 classes of bilateral ORN types, pioneer ORNs (p) and follower ORNs (q). Removal of the consensus sequence for Ankyrin signaling (Δ*FIGQY*) strongly affects the bilateral projection of follower ORNs (q') but not pioneer ORNs (p') and cPINs (n', o'). The combined deletion of Ankyrin and PDZ binding (*TYV)*

domains (Δ*C*), switches all bilateral ORNs into a unilateral connectivity pattern (p'', q'') but does not interfere with bilateral cPIN development (n'', o''). The deletion of the Moesin binding domain (Δ*FERM*) leads to a complete unilateral connectivity pattern for all 4 classes of bilateral olfactory neurons (n'''-q'''). (r) Schematics illustrate domain organization of Nrg and the connectivity phenotype of the deletion mutants (top) and their quantification (bottom). Scale bar = 20µm for all images of adult ALs. Note – For the list of genotypes used in this study check the extended data table 1.

Extended Data Figure legends

Extended Data Figure 1. Uni- versus bilateral olfactory circuit organization within Diptera (a) Phylogenetic tree of Diptera consisting of the two suborders Nematocera (blue, including mosquitos, crane flies and black flies) and Brachycera (red, consisting of around 120 families, adopted from ref. 12). Different infraorders are indicated by boxes and families are grouped according to the ORN connectivity. (b) Following unilateral antennal nerve labeling backfills (right antenna) of 1-2 representative species for each of the analyzed 26 families, the contralateral AL innervation (dotted circle) was determined and classified into unilateral (no labeling), weak (white arrowhead) and strong bilateral innervation. Within Nematocera, a dynamic organization of uni- and bilateral olfactory map can be observed. In basal Brachycera ("Orthorrhapha"), the bilateral innervation of sensory neurons becomes more prominent and strong bilateral maps are found in all analyzed Schizophora species. Labeling: Anterograde backfill by neurobiotin (green) visualized by Avidin-AlexaFluor488, neuropil marker DN-Cadherin (blue), anti BP104 staining shows neuronal isoform specific Nrg (red).

Extended Data Figure 2. Comprehensive analysis of uni- and bilateral projecting antennal ORN axon in *Neuroglian* mutant (see also Table in Figure 1). (a-d) Bilateral olfactory map is disrupted in *Nrg* mutant: (a) ORN class specific analysis of bilateral Atonal-positive pioneer ORNs (red box) in wild type and *Nrg* mutant. In the wild type AL, ORN axons converge tightly onto their specific glomeruli. In *Nrg* mutants, the commissural tract is lost in all six ORN classes and axons innervate their cognate ipsilateral target. (b, c) Analysis of bilateral Amos-positive follower ORNs

(green box) in wild type and *Nrg* mutant. Like pioneers, wild type follower ORN axons innervate their respective ipsi- and contralateral glomerulus in the mirror symmetric AL. In *Nrg* mutants, most bilateral ORN classes precisely target the ipsilateral glomerulus. In a small subset of *Nrg* mutant ORN classes (Or23a, Or67b), axons occasionally overshoot their ipsilateral target glomerulus and terminate at the dorsal midline (arrowheads in c). (d) Unilateral projecting Atonal and Amos ORN classes are unaffected in *Nrg* mutant (Blue box). Atonal specific class is indicated by red and green line indicates Amos specific class within the blue box. Genotypes: Wild type: *nrg^{849}/+; UAS-mCD8::GFP; OR-Gal4* (on II or III) *or nrg^{849}/+; Or-mCD8::GFP;*(on II or III). *Nrg* mutant: *nrg^{849}/Y; UAS-mCD8::GFP; OR-Gal4* (on II or III) *or nrg^{849}/Y; Or-mCD8::GFP;*(on II or III). Labeling: All ORN axons are labeled by Or specific Gal4 driven UAS-mCD8::GFP or reporter lines which were stained with anti-GFP (in green), counterstained with neuropil marker DN-cadherin (red) and cell bodies are visualized with TOTO-3 (blue).

Extended Data Figure 3. Neuroglian expression during development. (a-f) During pupal development Nrg displays differential expression in the olfactory system. Analysis of Nrg expression in axons of Atonal-positive pioneer ORNs (a, b), and Amos-positive follower ORNs (c, d). Nrg (red) is strongly enriched on all the pioneer and follower ORN axons (green) during adult (a and c) and pupa (b and d) respectively. Nrg expression is seen on tightly fasciculated olfactory commissure fibers (few posterior Z- projections) in adult and pupa (white arrow head in a’’’- d’’’). (e-f) In early pupal development, strong Nrg expression can be observed in most commissural fibers (e) and a weak expression on unilateral projection neurons (f, cell bodies in white circle). Genotypes: (a-b’’’) *;UAS-mCD8::GFP; atonal-Gal4;* (c-d’’’) *;amos-Gal4; UAS-mCD8::GFP;* (e-f’’’) *UAS-mCD8::GFP; GH146-Gal4;*. Labeling: All neuronal axons are labeled by Gal4 driven UAS-mCD8::GFP which were stained with anti-GFP (in green), counterstained with neuropil marker DN-cadherin (blue) and anti BP104 staining shows neuronal isoform specific Nrg (red).

Extended Data Figure 4. Neuroglian expression in midline glia cells is dispensable for bilateral ORN connectivity. (a-b’’) Targeted Nrg RNAi in two different glia populations (*repo-Gal4 and 442-Gal4*) did not affect the bilateral connectivity (a’, a’’, b’, b’’) and the innervation pattern of ORN classes as compared

to wild type (a, b). (d) Quantification of bilateral connectivity of the analyzed ORN classes. Genotypes: (a, b) *;UAS-Nrg RNAi ; Or-mCD8::GFP/+* (a', b') *;UAS-Nrg RNAi; Or-mCD8::GFP/ repo-Gal4* (a'', b'') *;UAS-Nrg RNAi; Or-mCD8::GFP/ 442-Gal4*. Labeling: All neuronal axons are labeled by Or-mCD8::GFP reporter which were stained with anti-GFP (in green), counterstained with neuropil marker DN-cadherin (red), cell bodies are visualized with TOTO-3 (blue).

Extended Data Figure 5. Cell specific loss of Neuroglian in cPINs affects bilateral olfactory map formation. (a) Expression pattern of five identified Gal4 driver lines which lead to a UAS-RNAi phenotype in bilateral ORNs. These Gal4 lines were divided, based on the penetrance of the ORN connectivity phenotype, into two groups, strong (a1-a3) and weak (a4-a5). Gal4 lines a1 and a3 showed variable expression pattern, labeling cells from both ventro-lateral and lateral clusters during the development (data not shown). (b) Example of ORN connectivity phenotypes in a strong (*R59E08-Gal4*) and a weak (*R12C01-Gal4*) driver line for pioneer and follower ORNs. (c) Quantification of commissural phenotypes observed in cPINs and ORNs upon Nrg knockdown in cPINs. Genotypes: (a1-a5) *;UAS-mCD8::GFP; Rubin-Gal4;*. (b) *;UAS-Nrg RNAi; Or-mCD8::GFP/Rubin-Gal4* (c) For cPINs - *;UAS-mCD8::GFP/ UAS-Nrg RNAi; Rubin-Gal4*. For ORNs - same as b. Labeling: (a1-a5) cPINs are labeled by Gal4 driven UAS-mCD8::GFP which were stained with anti-GFP (in green), counterstained with neuropil marker DN-cadherin (blue). (b) ORN axons are labeled by Or reporter lines, which were stained with anti-GFP (in green), counterstained with neuropil marker DN-cadherin (red).

Extended Data Figure 6. Spatial segregation of PN and LN dendrites in the early AL. (a, b) During ORN axon ingrowth, the LN and PN dendritic fields are spatially segregated in AL. At 18 hr after pupa formation, axons of projection neurons (green) are seen to innervate the anterior AL densely (a) whereas the posterior part of the AL is mainly occupied by LN dendrites (b) and axons and dendrites of PNs and LNs do not overlap. White arrows indicate the entry site of ORN axons. LN and PN cell bodies are labeled in red and green respectively. Genotypes: *;;GH146-mCD8::GFP, c753-Gal4 UAS-CD2*. Labeling: PN axon are labeled by GH146 reporter which was stained with anti-GFP (in green), dendrites of LNs are labeled with c753-Gal4 driven UAS-CD2 (in red) stained with anti-CD2 antibody, AL is counterstained with neuropil marker DN-cadherin (red).

Extended Data Figure 7. Neuroglian affects olfactory commissure development of CSD neurons. (a) Neuronal morphology of CSD (contralaterally-projecting Serotonin-immunoreactive Deutocerebral) neuron. Each AL of *Drosophila* is innervated ipsi-and contralaterally by a pair of CSDs (white arrow). The dendrites of CSD neuron innervate the ipsilateral AL, branches to the higher brain center on both hemisphere via protocerebral commissure (PC, white arrow head), innervate the contralateral AL and subsequently project back to the ipsilateral AL via olfactory commissure (OC, red arrow head). (b-c) The filament-tracing module of Imaris (Bitplane) reveals the 3-D organization of CSD neuron in wild type and *Nrg* mutant. In wild type, both PC and OC are seen (b), whereas *Nrg* mutants show a specific loss of the OC (c). Genotypes: wild type: nrg^{849}/+;*UAS-mCD8::GFP; R37D04-Gal4, Nrg* mutant: nrg^{849}/Y; *UAS-mCD8::GFP; R37D04-Gal4* Labeling: (a) Dendrites of CSD neurons are labeled with *R37D04-Gal4* driven *UAS-mCD8::GFP* (in green) stained with anti-GFP antibody and AL is counterstained with neuropil marker DN-cadherin (blue).

Extended Data Figure 8. Intracellular TYV domain is dispensable for bilateral olfactory map formation. (a-d) The binding motif for PDZ domain containing protein is not required for bilateral projecting neurons of olfactory system as shown for mushroom body pathfinding (ref.18). (a, b) Axons of two bilateral projecting cPINs, (cPIN-1 and cPIN-2, see main figure 4) shows wild type like commissural projection (inset for cPIN1). (c-d) Axons of pioneer and follower ORN classes are also unaffected, showing bilateral innervation. Genotypes: (a-d) nrg^{14} /y; *P[*nrg^{180}*_ ΔTYV]; Or-Gal4 or Rubin-Gal4, UAS-mCD8::GFP*. Labeling: (a-d) Olfactory (cPINs and ORNs) neurons are labeled with Gal4 driven UAS-mCD8::GFP (in green) stained with anti-GFP antibody, AL is counterstained with neuropil marker DN-cadherin (blue) and mushroom body is visualized (as a control) using FasII (red, αβ axons).

Extended Data Table 1

1 a	*Pebbled-Gal4 UAS-mCD8::GFP;;*
1 b	Canton S

1 c, c’	*A. aarabiensis*
1 d, d’	Canton S
1 e, e’	*nrg^{849} ;;*
1 f	*nrg^{849} /x; UAS-mCD8::GFP/Sg18.1-Gal4 ;*
1 g	*nrg^{849} /y; UAS-mCD8::GFP/Sg18.1-Gal4 ;*
1 h	*nrg^{849} /x;; R17H02-Gal4 UAS-mcherry*
1 i	*nrg^{849} /y;; R17H02-Gal4 UAS-mcherry*
1 j	*;hsmFL5; UAS-Flybow 1.1B/ R86G11-Gal4*
1 k	*nrg^{849} /y; hsmFL5; UAS-Flybow 1.1B, R86G11-Gal4*
1 l	*;+/Sg18.1-Gal4 ;Or47b::mCD8GFP/+*
1 m	*;UAS-Nrg^{RNAi}/Sg18.1-Gal4 ;Or47b::mCD8GFP/+*
1 n, n’	*nrg^{849} /x; UAS-Brp::GFP/Or47b-Gal4 ;*
1 o, o’	*nrg^{849} /y; UAS-Brp::GFP/Or47b-Gal4 ;*
1p, p’	*;UAS-Nrg^{RNAi};Or47b::mCD8GFP/GH146-Gal4*
1 q, q’	*; UAS-Nrg^{RNAi};Or47b::mCD8GFP/+;OK107-Gal4*
1 r, r”	*; UAS-mCD8::GFP;;OK107-Gal4*
1 s-s”	*nrg^{849} /y; UAS-mCD8::GFP;;OK107-Gal4*

2 a, a’, a”	*UAS-mCD8GFP; UAS-mCD8GFP;atonal-Gal4*
2 b, b’, b”	*; UAS-mCD8GFP;;OK107-Gal4*
2 c, c’,c”, c”’	*13XLexAop2-mCD8::GFP,10XUASmCD8::RFP; R20F11-LexA; R19H07-Gal4*
2 d	*nrg^{849} /y; UAS-mCD8GFP; R20F11-Gal4*
2 e	*nrg^{849} /y; UAS-mCD8GFP; R19H07-Gal4*
2 f	*UAS-mCD8GFP; UAS-mCD8GFP; R12C01-Gal4*
2 g, g’	*UAS-mCD8GFP; UAS-mCD8GFP; R19H07-Gal4*
2 h	*hs-FLP;FRT42,UAS-mCD8GFP/FRT42,Gal80; R19H07-Gal4*
2 i, i’	*UAS-mCD8GFP; UAS-mCD8GFP; R20F11-Gal4*
2 j-m”	*UAS-mCD8GFP; UAS-mCD8GFP; R20F11-Gal4*
2 n,o,p	*nrg^{849} /y; UAS-mCD8GFP; R20F11-Gal4*

3 b-e	*nrg^{849}/x; UAS-mCD8::GFP; R86G11-Gal4*
3 f-i	*nrg^{849}/y; UAS-mCD8::GFP; R86G11-Gal4*
3 j-o	*;hsmFL5; UAS-Flybow 1.1B/ R86G11-Gal4*
3 r-t	*nrg^{849}/x; UAS-Brp::GFP/ R86G11-Gal4 ;*
3 s-u	*nrg^{849}/y; UAS-Brp::GFP/ R86G11-Gal4 ;*

4 b	*; R20F11-LexA/ CyO; 13XLexAop2-mCD8::GFP*
4 c	*;+/ CyO; ato-Gal4/ Or35a::mCD8-GFP*
4 d	*; CyO/amos-Gal4; Or47b::mCD8-GFP*
4 e	*;UAS-Nrg^{RNAi}/R20F11-LexA;13XLexAop2mCD8::GFP/R19H07-Gal4*
4 f	*;UAS-Nrg^{RNAi}; Or35a::mCD8-GFP; OK107-Gal4*
4 g	*;UAS-Nrg^{RNAi}; Or47b::mCD8-GFP; OK107-Gal4*
4 h	*;UAS-Nrg^{RNAi}/R20F11-LexA;13XLexAop2-mCD8::GFP/atonal-Gal4*
4 i	*;UAS-Nrg^{RNAi}; Or35a::mCD8-GFP; ato-Gal4*
4 j	*;UAS-Nrg^{RNAi}; Or47b::mCD8-GFP; ato-Gal4*
4 k	*Pebbled-Gal4;Nrg^{RNAi}/R20F11-LexA;13XLexAop2-mCD8::GFP*
4 l	*;UAS-Nrg^{RNAi}/amos-Gal4; Or35a::mCD8-GFP*
4 m	*;UAS-Nrg^{RNAi}/amos-Gal4; Or47b::mCD8-GFP*
4 n	*nrg^{14}/y; P[nrg_wt]; R12C01-Gal4, UAS-mCD8::GFP*
4 n’	*nrg^{14}/y;P[nrg^{180}_ΔFIGQY];R12C01-Gal4, UAS-mCD8::GFP*
4 n”	*nrg^{14}/y; P[nrg^{180}_ΔC]; R12C01-Gal4, UAS-mCD8::GFP*
4 n”’	*nrg^{14}/y; P[nrg_ ΔFERM]; R12C01-Gal4, UAS-mCD8::GFP*
4 o	*nrg^{14}/y; P[nrg_wt]/ UAS-mCD8::GFP; R19H07-Gal4*
4 o’	*nrg^{14}/y;P[nrg^{180}_ΔFIGQY]/UAS-mCD8::GFP; R19H0 -Gal4*
4 o”	*nrg^{14}/y; P[nrg^{180}_ ΔC]/ UAS-mCD8::GFP; R19H07-Gal4*
4 o”’	*nrg^{14}/y; P[nrg_ ΔFERM/ UAS-mCD8::GFP; R19H0 -Gal4*
4 p	*nrg^{14}/y; P[nrg_wt]/ UAS-mCD8::GFP; Ir92a-Gal4*
4 p’	*nrg^{14}/y; P[nrg^{180}_ ΔFIGQY]/ UAS-mCD8::GFP; Ir92a-Gal4*
4 p”	*nrg^{14}/y; P[nrg^{180}_ ΔC]/ UAS-mCD8::GFP; Ir92a-Gal4*

4 p”’	*nrg^{14}/y; P[nrg_ ΔFERM/ UAS-mCD8::GFP; Ir92a-Gal4*
4 q	*nrg^{14}/y; P[nrg_wt]; Or47b-Gal4, UAS-mCD8::GFP*
4 q’	*nrg^{14}/y; P[nrg^{180}_ ΔFIGQY]; Or47b-Gal4, UAS-mCD8::GFP*
4 q”	*nrg^{14}/y; P[nrg^{180}_ ΔC]; Or47b-Gal4, UAS-mCD8::GFP*
4 q”’	*nrg^{14}/y; P[nrg_ ΔFERM]; Or47b-Gal4, UAS-mCD8::GFP*

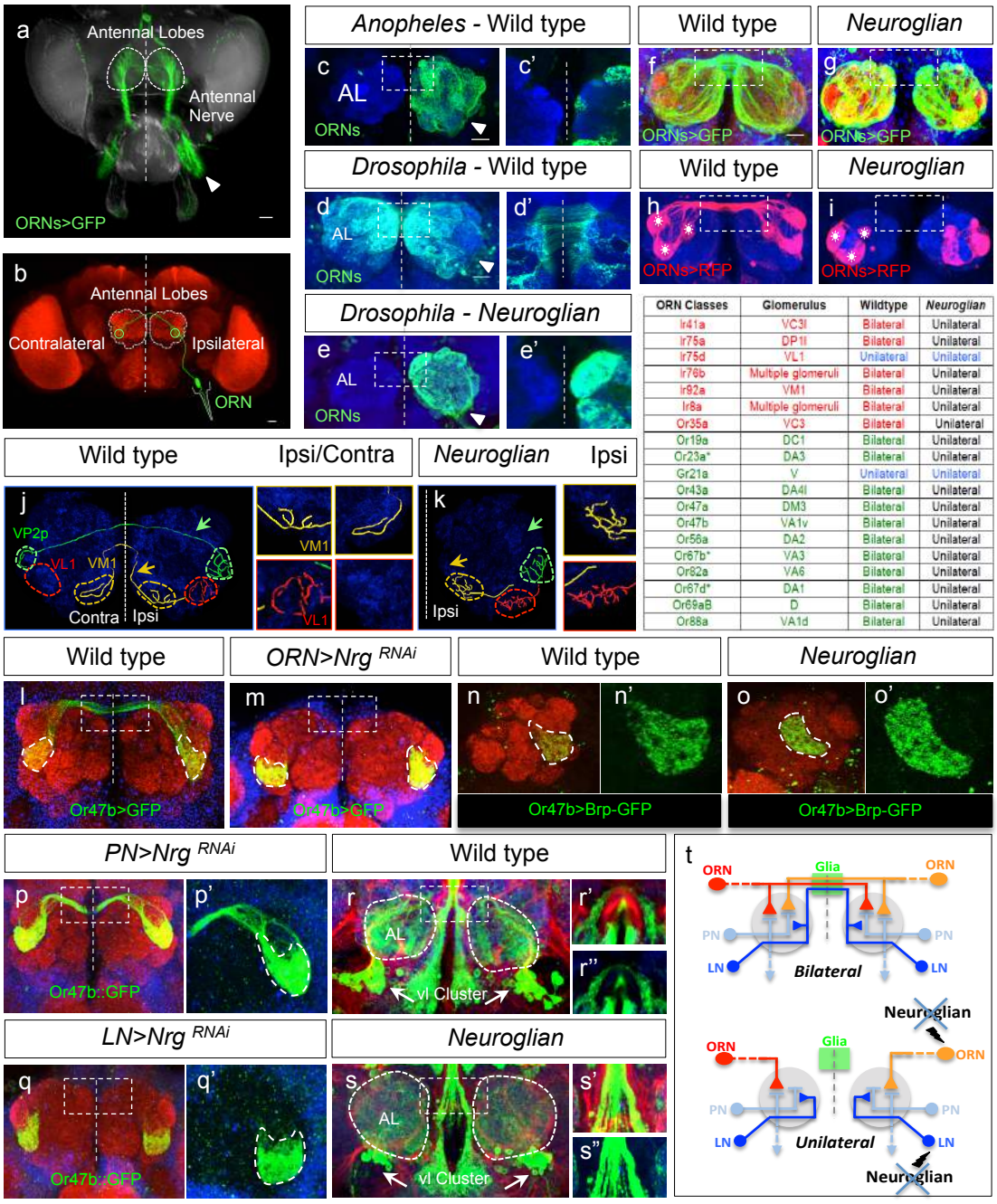

ORN Classes	Glomerulus	Wildtype	*Neuroglian*
Ir41a	VC3l	Bilateral	Unilateral
Ir75a	DP1l	Bilateral	Unilateral
Ir75d	VL1	Unilateral	Unilateral
Ir76b	Multiple glomeruli	Bilateral	Unilateral
Ir92a	VM1	Bilateral	Unilateral
Ir8a	Multiple glomeruli	Bilateral	Unilateral
Or35a	VC3	Bilateral	Unilateral
Or19a	DC1	Bilateral	Unilateral
Or23a*	DA3	Bilateral	Unilateral
Gr21a	V	Unilateral	Unilateral
Or43a	DA4l	Bilateral	Unilateral
Or47a	DM3	Bilateral	Unilateral
Or47b	VA1v	Bilateral	Unilateral
Or56a	DA2	Bilateral	Unilateral
Or67b*	VA3	Bilateral	Unilateral
Or82a	VA6	Bilateral	Unilateral
Or67d*	DA1	Bilateral	Unilateral
Or69aB	D	Bilateral	Unilateral
Or88a	VA1d	Bilateral	Unilateral

Figure 1

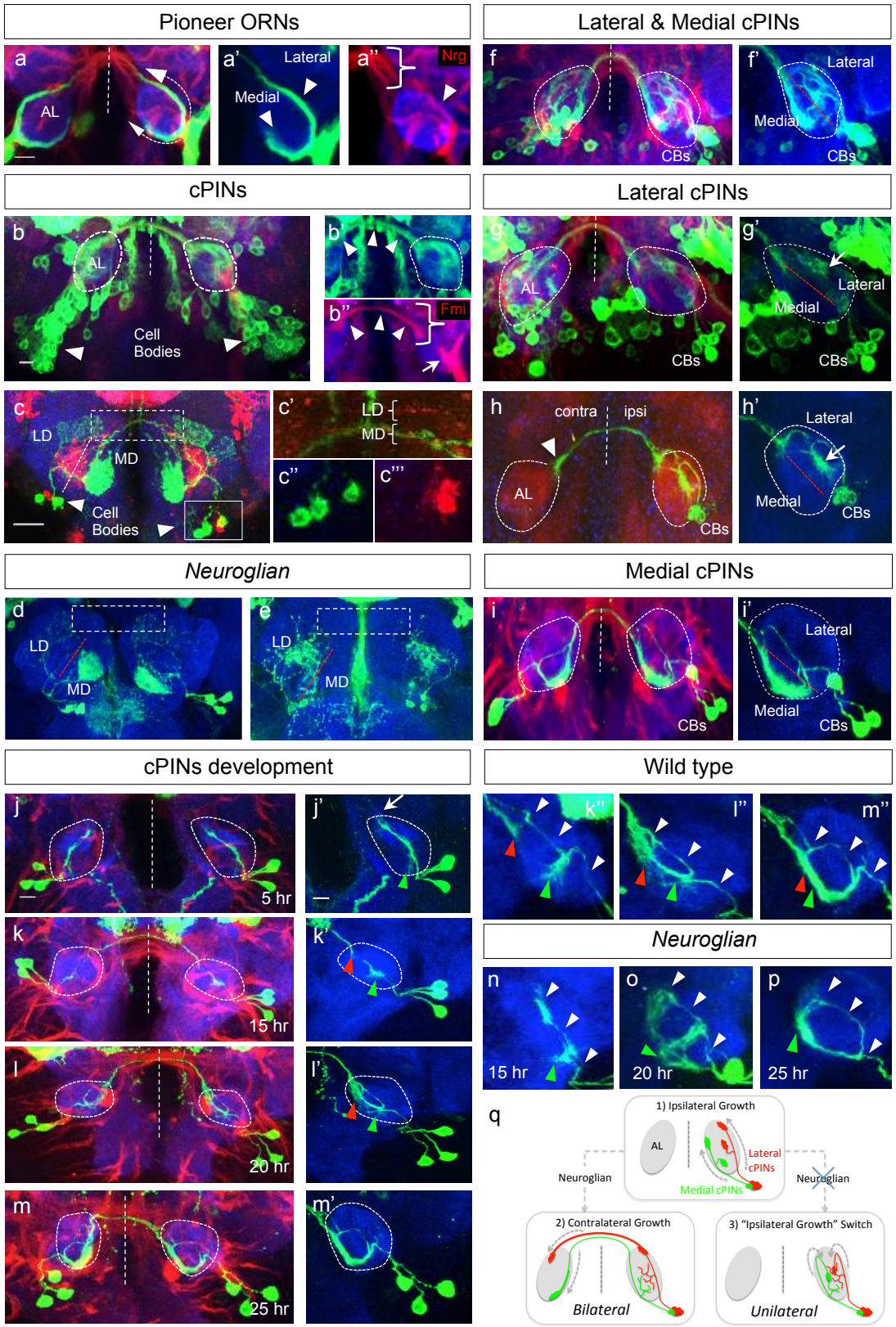
Pioneer ORNs
Lateral & Medial cPINs
cPINs
Lateral cPINs
Neuroglian
Medial cPINs
cPINs development
Wild type
Neuroglian
a
a'
a''
AL
Lateral
Medial
Nrg
f
f'
CBs
b
b'
b''
Cell Bodies
Fmi
g
g'
c
c'
c''
c'''
LD
MD
h
h'
contra
ipsi
d
e
i
i'
j
j'
k
k'
l
l'
m
m'
5 hr
15 hr
20 hr
25 hr
k''
l''
m''
n
o
p
q
1) Ipsilateral Growth
Lateral cPINs
Medial cPINs
Neuroglian
2) Contralateral Growth
Bilateral
3) "Ipsilateral Growth" Switch
Unilateral

Figure 2

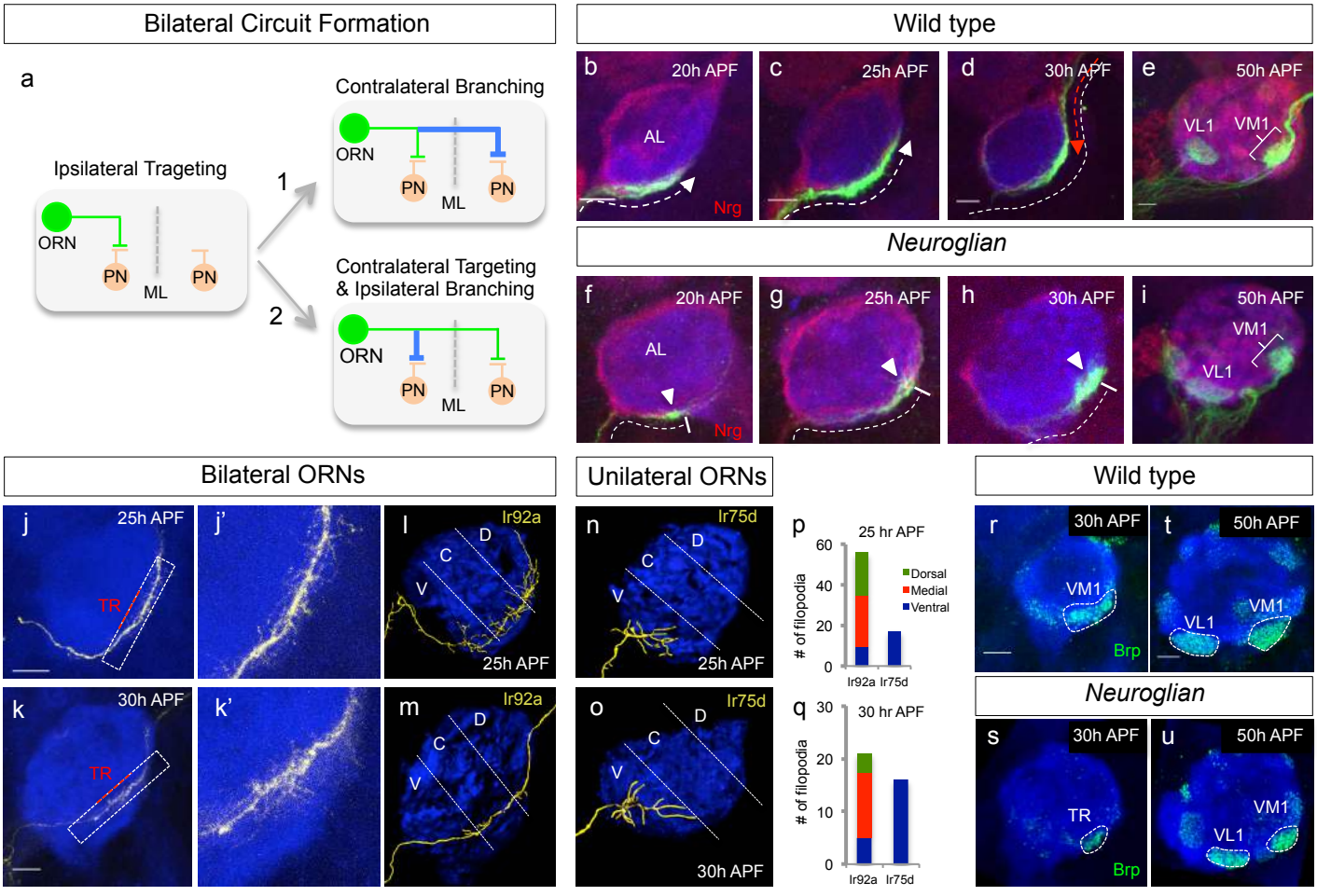
Bilateral Circuit Formation
a
Ipsilateral Trageting
ORN
PN
ML
PN
1
Contralateral Branching
ORN
PN
ML
PN
2
Contralateral Targeting
& Ipsilateral Branching
ORN
PN
ML
PN
Wild type
b
20h APF
AL
Nrg
c
25h APF
d
30h APF
e
50h APF
VL1
VM1
Neuroglian
f
20h APF
AL
Nrg
g
25h APF
h
30h APF
i
50h APF
VM1
VL1
Bilateral ORNs
j
25h APF
TR
j'
l
Ir92a
D
C
V
25h APF
k
30h APF
TR
k'
m
Ir92a
D
C
V
Unilateral ORNs
n
Ir75d
D
C
V
25h APF
o
Ir75d
D
C
V
30h APF
p
25 hr APF
60
40
20
0
# of filopodia
Dorsal
Medial
Ventral
Ir92a
Ir75d
q
30
20
10
0
# of filopodia
30 hr APF
Ir92a
Ir75d
Wild type
r
30h APF
VM1
Brp
t
50h APF
VM1
VL1
Neuroglian
s
30h APF
TR
Brp
u
50h APF
VM1
VL1

Figure 3

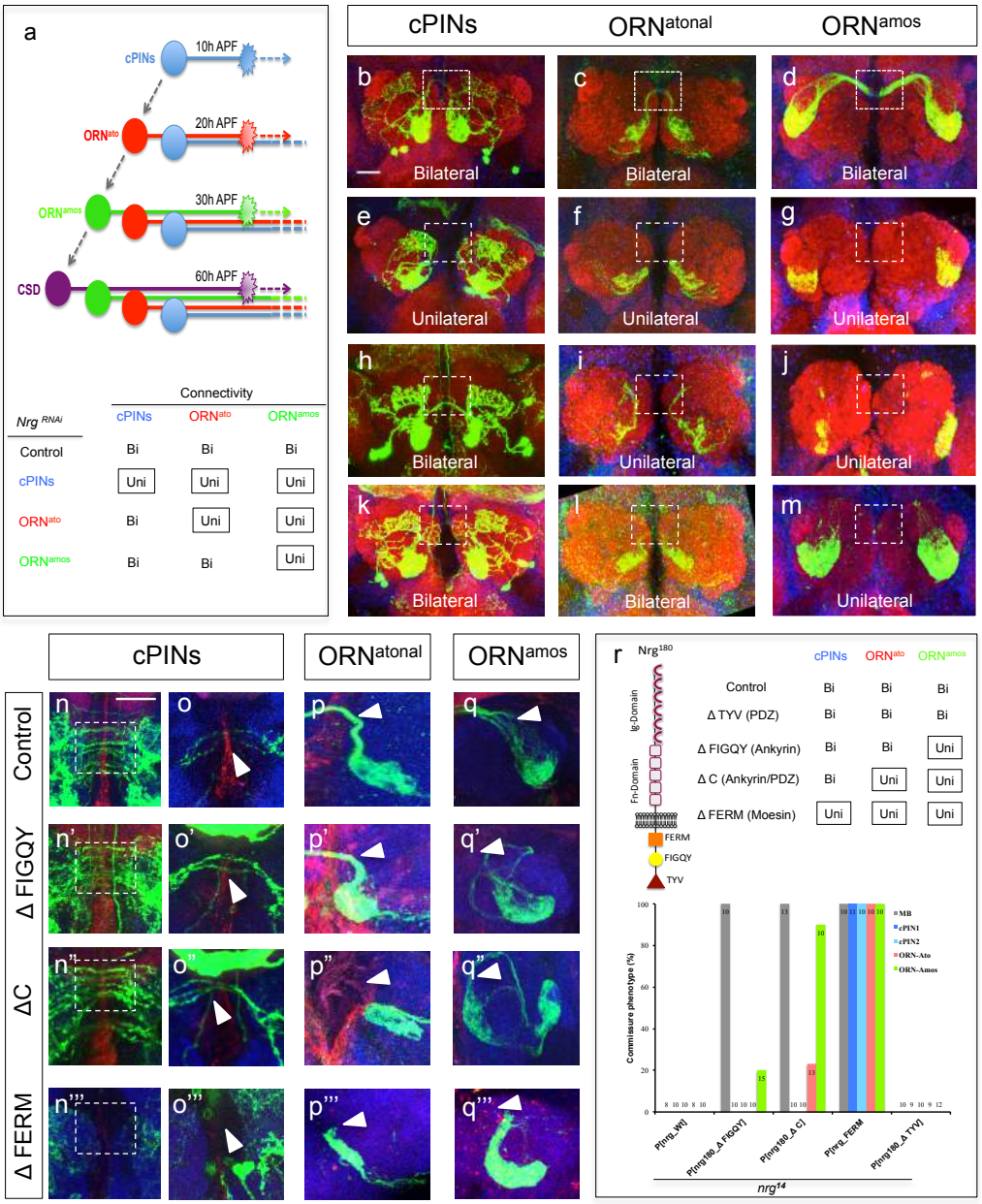
a
cPINs
10h APF
ORNato
20h APF
ORNamos
30h APF
CSD
60h APF
Connectivity
Nrg RNAi
cPINs
ORNato
ORNamos
Control
Bi
Bi
Bi
cPINs
Uni
Uni
Uni
ORNato
Bi
Uni
Uni
ORNamos
Bi
Bi
Uni
cPINs
ORNatonal
ORNamos
b
Bilateral
c
Bilateral
d
Bilateral
e
Unilateral
f
Unilateral
g
Unilateral
h
Bilateral
i
Unilateral
j
Unilateral
k
Bilateral
l
Bilateral
m
Unilateral
cPINs
ORNatonal
ORNamos
Control
Δ FIGQY
ΔC
Δ FERM
n
o
p
q
n'
o'
p'
q'
n''
o''
p''
q''
n'''
o'''
p'''
q'''
r
Nrg180
Ig-Domain
Fn-Domain
FERM
FIGQY
TYV
cPINs
ORNato
ORNamos
Control
Bi
Bi
Bi
Δ TYV (PDZ)
Bi
Bi
Bi
Δ FIGQY (Ankyrin)
Bi
Bi
Uni
Δ C (Ankyrin/PDZ)
Bi
Uni
Uni
Δ FERM (Moesin)
Uni
Uni
Uni
Commissure phenotype (%)
MB
cPIN1
cPIN2
ORN-Ato
ORN-Amos
P{nrg_WT}
P{nrg180_Δ FIGQY}
P{nrg180_Δ C}
P{nrg_FERM
P{nrg180_Δ TYV}
nrg14

Figure 4

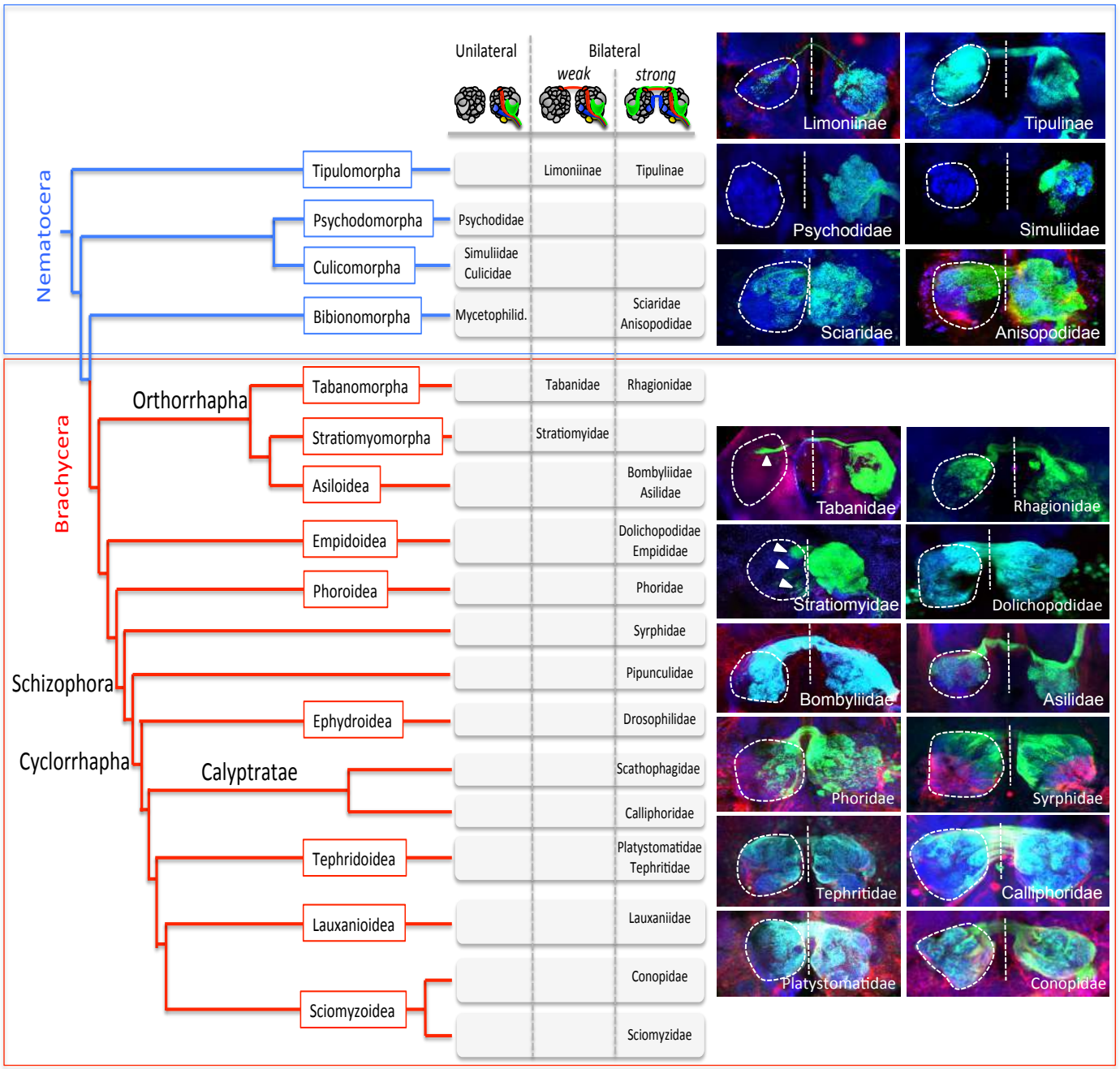

Extended Data Figure 1

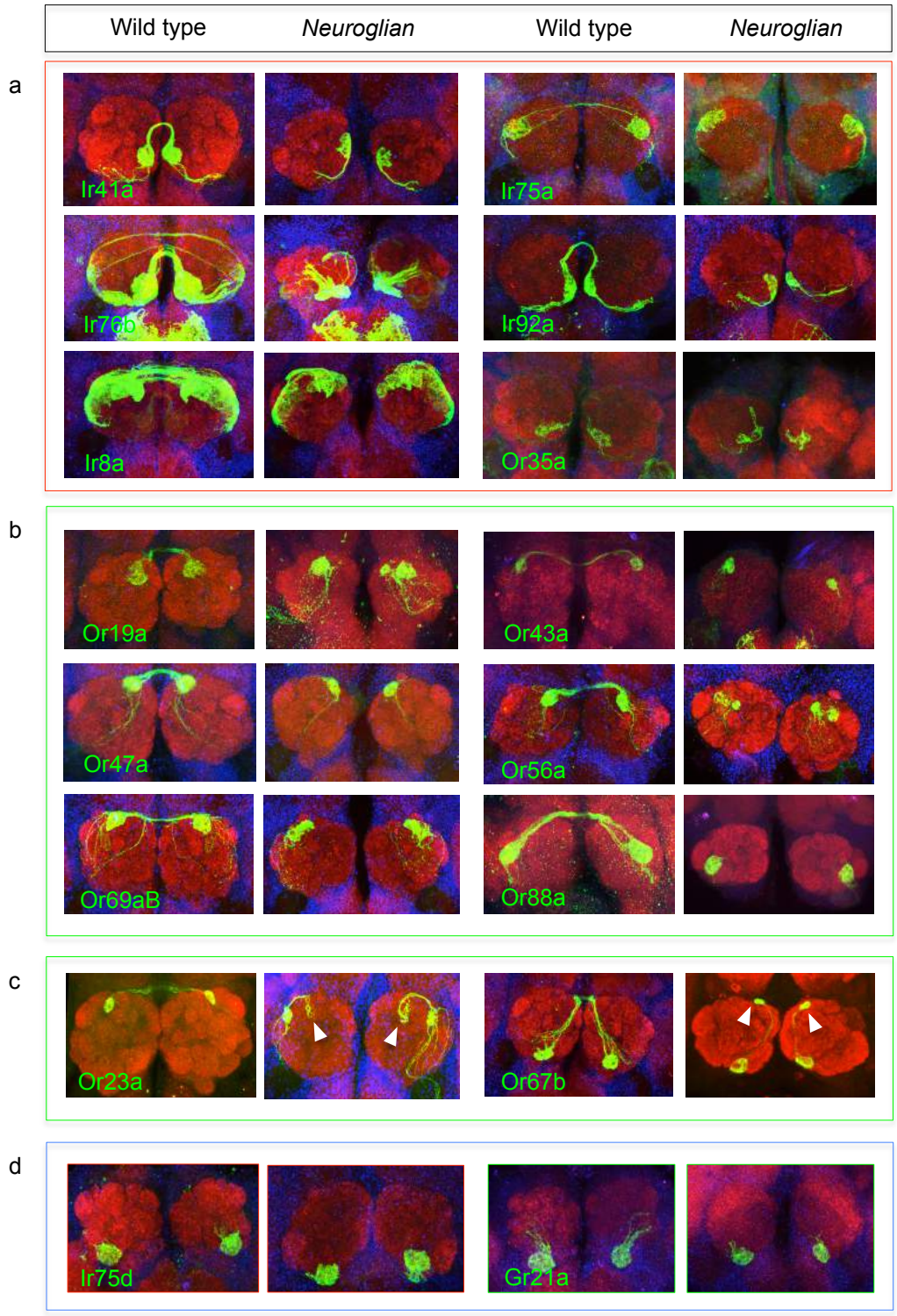

Extended Data Figure 2

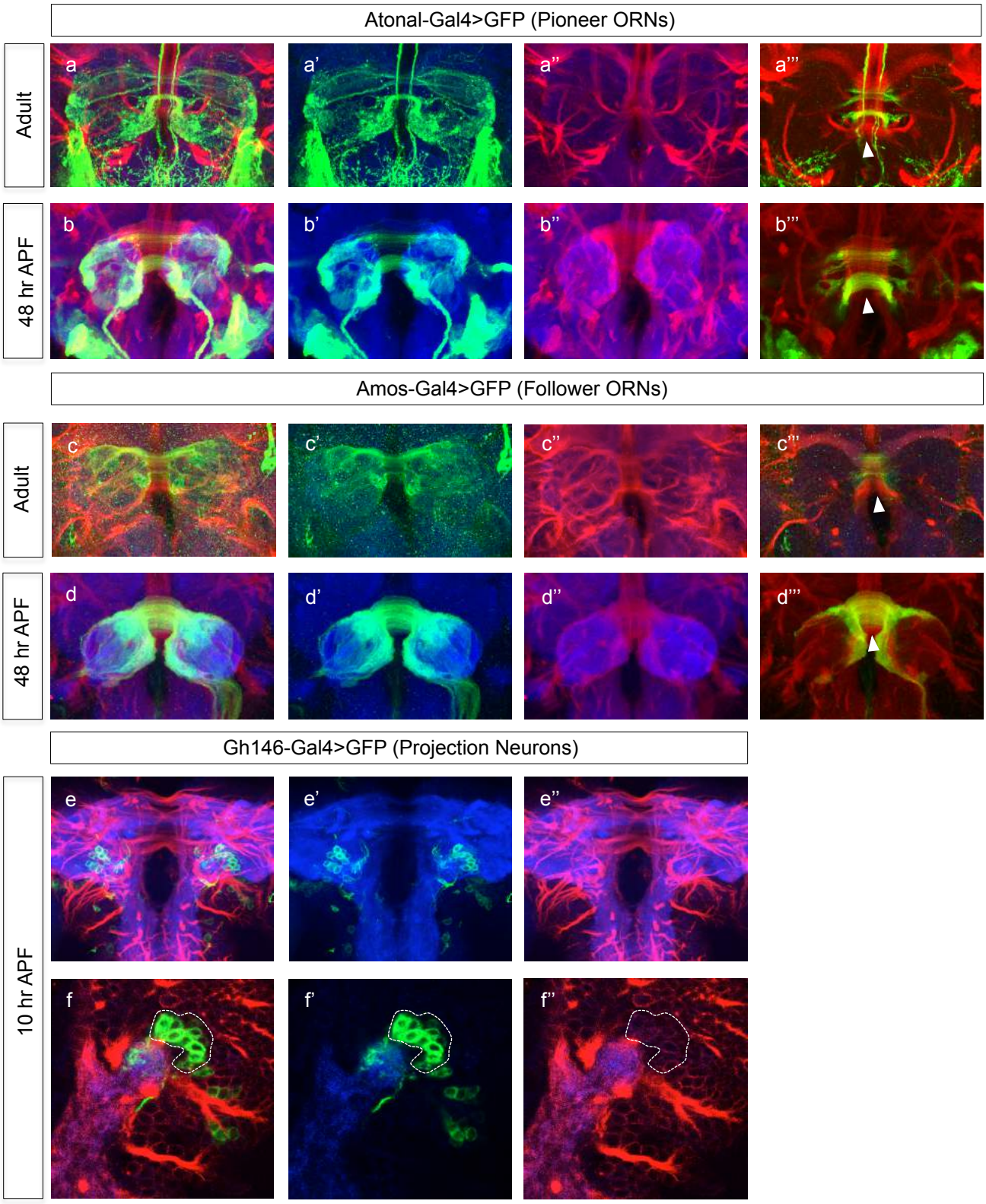

Extended Data Figure 3

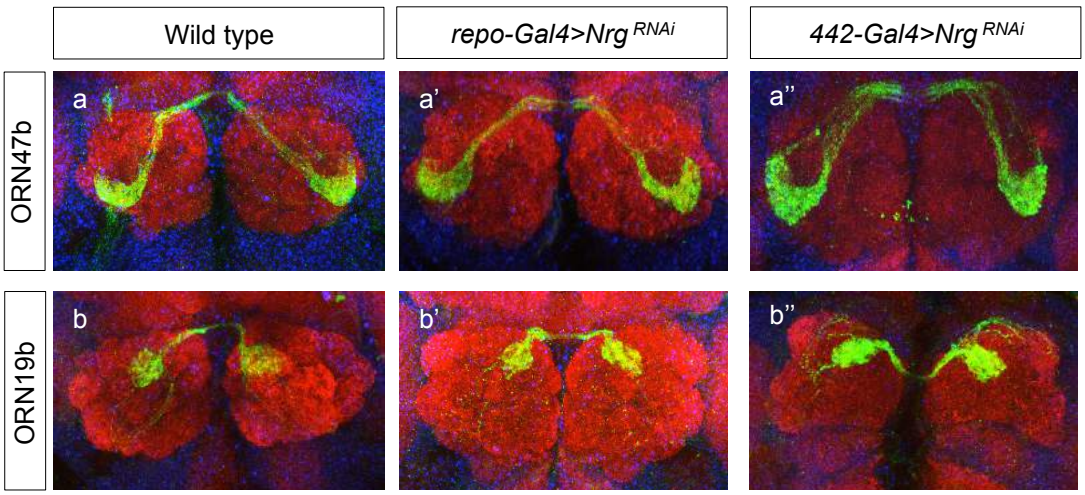

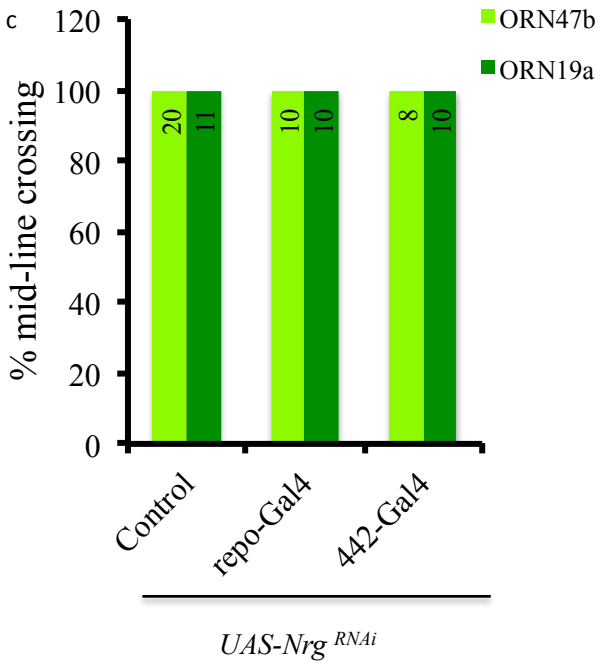

Extended Data Figure 4

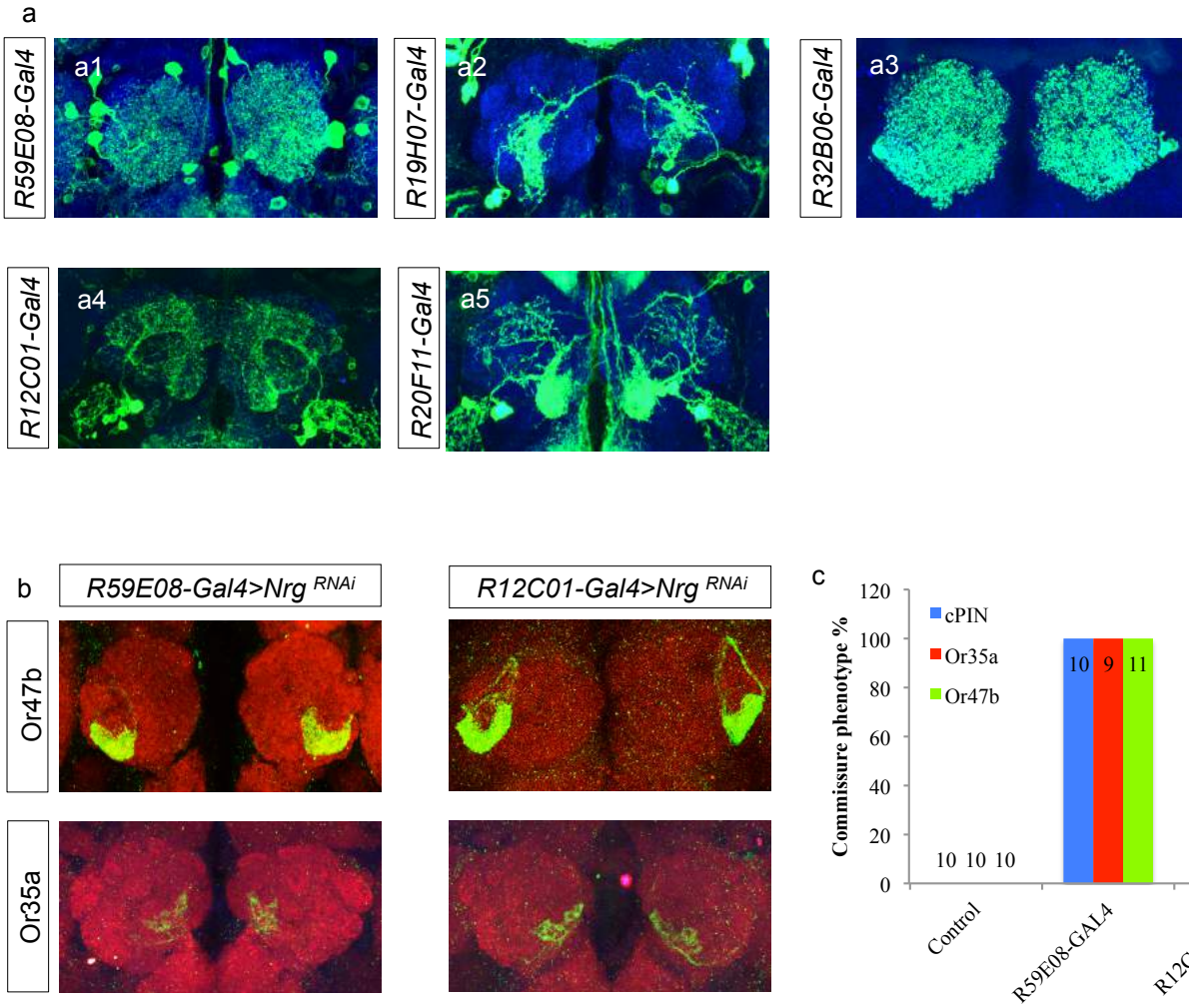

Extended Data Figure 5

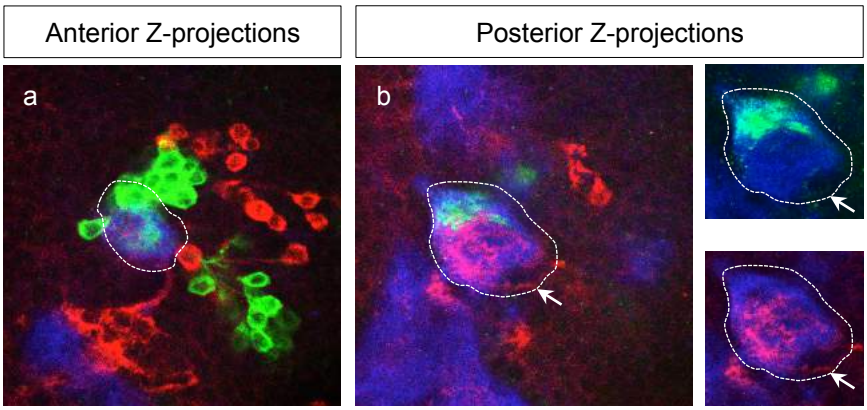

Extended Data Figure 6

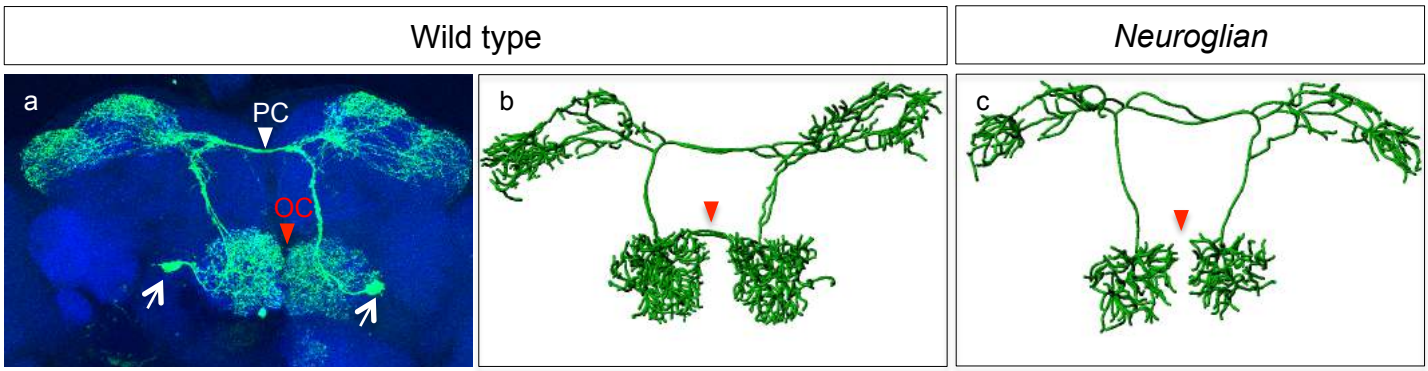

Extended Data Figure 7

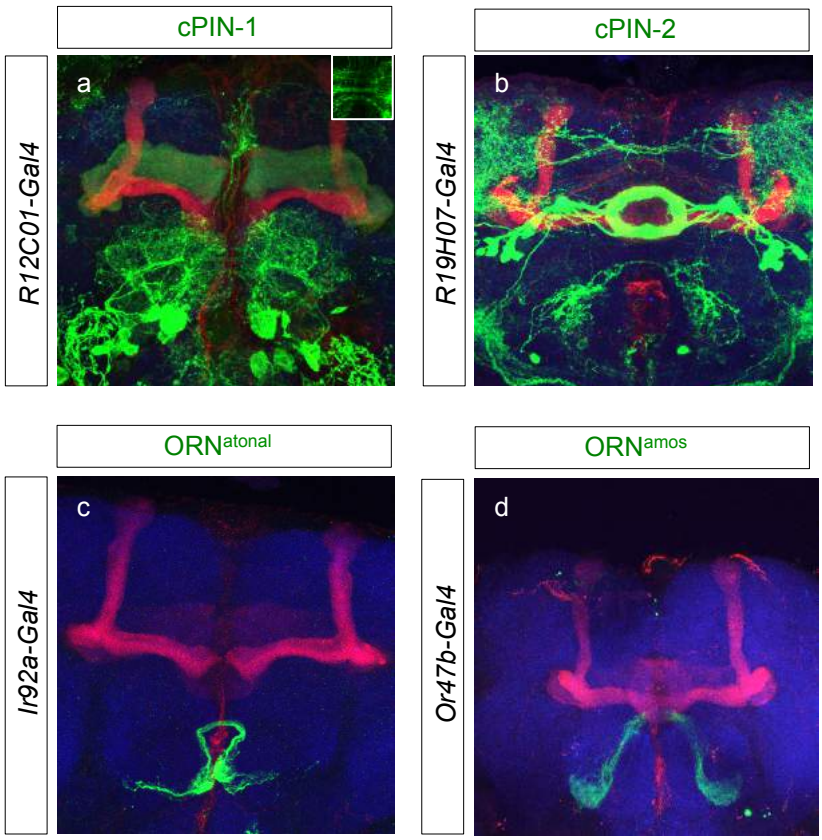

Extended Data Figure 8

Chapter 3

Synaptic recognition identity in the *Drosophila* olfactory system is mediated by non-apoptotic caspase function

Christoph Scheper[2], Rashmit Kaur[1], Lorin Timaeus[1], Sven Niehues[2], Ursula Peters[1] and Thomas Hummel[1*]

[1]Department of Neurobiology, University of Vienna, Vienna, Austria.

[2]Current address: Universität Münster, Münster, Germany.

* Corresponding author: thomas.hummel@univie.ac.at

-- manuscript form --

3.1 Summary

With more than 50 functional classes of peripheral olfactory receptor neurons (ORNs) segregating their axons into distinct synaptic glomeruli in the central brain, the development of the *Drosophila* olfactory system is challenged with a high degree of cell-cell recognition. In addition to synaptic partner recognition, sensory neurons projections in the olfactory system are organized into functional domains according to the peripheral pattern of cell body position. How gobal sensory map formation is coordinated with neuron type-specific synaptic partner recognition is largely unknown.

Here we show that non-apoptotic caspase function is a critical regulator of neuronal cell recognition in *Drosophila* olfactory system development. Mutations in the initiator caspase Dronc and its regulator Dark, the key components of the apoptosome complex, cause a specific switch in ORN axon projection and synaptic connetivity. The analysis of multiple *dark* alleles revealed a direct correlation of the cell-intrinsic level of caspase activity and the ORN connectivity phenotype. Furthermore, genetic interactions indicates a partial redundant function of Dronc and second initiator caspase Strica. Caspase-activity translates into the neuron class-specific expression of the cell adhesion molecule Connectin, which defines the domain segregation of olfactory sensory neurons. These data demonstrate a novel role of non-apoptotic caspase activity in the coordination of axon pathfinding and target recognition via the differential expression of cell surface molecules.

3.2 Introduction

The assembly of a large variety of neuronal cell types into functional brain circuits requires the recognition of connecting neurons with extraordinary precision in sequential developmental events, including axon guidance, target selection, and synapse formation. Although an array of conserved secreted and membrane bound factors have been identified that guide growing neurons through a complex extracellular environment and support unique recognition between matching synaptic partners [1,2], little is known about the spatial and temporal regulation of molecules which coordinate the sequential steps of neuronal recognition. Here, we identified a novel molecular mechanism in which graded levels of non-apoptotic caspase activity control successive steps of olfactory circuit assembly in *Drosophila*.

Proper patterning of the nervous system is mediated by progressive as well as regressive events [3,4]. Starting with neural proliferation, neurite outgrowth and synapse formation to set up a broad pattern of neural connectivity, later developmental patterning is further shaped by substantial regressive events such as axon pruning, synapse elimination and neuronal death, allowing the refinement of the pattern to a more precise and fully mature brain architecture and connectivity [5]. The programmed cell death (PCD) pathway via caspase activation has been extensively described to be involved in the regressive events that ensure precise connectivity of the brain [6,7]. In addition to their well-studied role in the execution of cell death, non-apoptotic roles of caspases have gained growing attention over recent years [8,9]. Living cells seem to be able to tolerate low levels of caspase activity without triggering the full cell death programme [10]. One strategy for evading imminent death might be a spatial restriction of caspase activation, as observed for dendrites or axons [11,12]. Also, negative feedback mechanisms have been reported, e.g. cleavage of the apoptosome unit Dark by Dronc, possibly preventing activation of the full caspase cascade when only low level caspase activity is required [13]. Furthermore, the anti-apoptotic potential of Diap1 has been shown to increase following cleavage by effector caspases, in turn buffering their destructive potential in the absence of an apoptotic stimulus [14].

To uncover mechanisms involved in axon pathfinding and synaptic specificity, the *Drosophila* olfactory system has been shown to be a suitable model system [15], where ~1300 olfactory receptor neurons can be grouped into distinct functional classes which segregate onto a specific set of synaptic target dendrites in the brain [16,17]. Various types of cell recognition molecules have been identified in the past, which control different steps in axon projection and target cell recognition [18]

In a forward genetic mosaic screen we could identify multiple genes regulating distinct steps in axon pathfinding and synaptic specificity of the *Drosophila* olfactory system, including evolutionary-conserved cell adhesion molecules and cell surface receptors [19–21]. In addition to these well-established regulators of nervous system development, other mutations affects cellular components less obviosly related to more global aspects of neuronal wiring like sphingolipid biosynthesis (Goyal et al. In revision) or the PCD pathway described above. For example, four mutant alleles defining one complementation group were identified to affect the pro-apoptotic gene *Dark (Death-associated APAF-1 related killer)*. Dark has been well characterized in the context of PCD, where it assembles together with intitiator caspases into the apoptosome to trigger caspase activation [22]. In contrast to our initial model proposing a caspase-mediated apoptosis or axon pruning underlying the ectopic connectivity phenotype of Dark mutants, further characterization revealed a direct role of inititator caspases in axon pathfinding and targeting. With the identification of the LRR-protein Connectin as one central component of the caspase-mediated recognition code, these results revealed a novel mechanism of wiring plasticity downstream of lineage-based neuronal identity.

3.3 Results

Mutations in the apoptosome components Dark and Dronc lead to a specific switch in ORN axon targeting

In the wild type antennal lobe (AL), an average of 25-30 axons of the ORN47a class converge on the ipsi- as well as contralateral DM3 glomerulus at the dorso-medial AL (Fig. 1A-A'', G) In a mosaic screen for genes controlling ORN class specific axon convergence (see Material &Methods) we identified four independent mutations defining a single complementation group called *verpeilt* (*vpt*, german for

disorientated/disorganized) that lead to a specific mistargeting of ORN47a axons (Fig. 1B). In addition to the innervation of ORN47a axons in DM3, the AL innervated by *vpt* mutant ORN axons contains an ectopic OR47a-positive glomerulus at a specific position in the dorso-lateral AL (Fig. 1B'-B''). Using recombination mapping and complementation analysis combined with sequencing of candidate genes we identified *vpt* to be allelic to the gene *dark*, which encodes an evolutionary conserved regulator of caspase activity[23]. In genetic mosacis of each of the four $dark^{vpt}$ mutations, a subset of the ORN47a axons segregates from the wild type pathway of OR47a-positive neurons at the entrance of the AL and projects along a distinct lateral pathway towards the ectopic glomerulus (Fig. 1A'', B''). Interestingly, although these ectopic ORN47a axons come in close proximity to the cognate DM3 glomerulus in the contralateral projection, we never observed a convergence of ectopic ORN47a axons onto DM3 as they organize into distinct projection tracts (Fig. 1H, H'). Independent *dark* mutations, including the defined null allele $dark^{82}$, lead to identical projection defects of ORN47a axons, and the ORN47a projection phenotype of $dark^{vpt}$ can be rescued by expression of wild type Dark in developing ORNs (data not shown).

To characterize the ectopic innervation, we performed co-labeling of ORN47a with additional ORN classes that innervate glomeruli in the dorso-lateral AL and identified a tight association of ectopic ORN47a axons with ORN23a axons (Fig. 1C-G). In wild type, ORN23a axons project along a lateral AL pathway towards the DA3 glomerulus, which appears unaffected in *vpt* mutants (Fig. 1C, D). Homozygous $dark^{vpt}$ ORN47a axons associate with ORN23a axons within the lateral projection domain but segregate into a separate ectopic glomerular unit ventrally to DA3 (Fig. 1D, F). Other ORN classes which target into synaptic glomeruli within the dorso-lateral AL, like ORN49a, are more distant to the ectopic ORN47a glomerulus (Fig. 1I-J'). In addition, ectopic ORN47a axons extend in a common fascicle with ORN23a across the dorsal midline separated from the subset of ORN47a axons which targets the medial DM3 glomerulus (Fig. 1G, H). Despite a strictly segregated convergence of the ORN23a and ectopic ORN47a axon populations into distinct domains at the glomerulus periphery, neuropil staining in the center of the glomerulus shows a common, homogeneous synaptic field with no signs of a glomerular border (Fig. 1D'', L). Furthermore, stochastic labeling of the postsynaptic projection neurons

showed that single PN dendrites cover both ORN23a and ectopically innervating ORN47a axon populations (Fig. 1M), indicating similar target cell recognition identity.

In *Drosophila*, Dark assembles into a large protein complex, called apoptosome, which supports the auto-activation of the initiator caspase Dronc [22]. To test if the Dark mutant phenotype is caused by impaired caspase activity we generated genetic mosaics of various Dronc mutations (Fig. 1N-P). Similar to Dark, loss of Dronc leads to a specific ectopic targeting of ORN47a axons at the DA3 glomerulus, in which the amount of ectopic ORN47a axons directly correlates with the allelic strength of the dronc alleles (Fig. 1N-P), indicating a level-dependent mechanism (see below). These data revealed the apoptosome complex as a critical regulator of ORN connectivity. Loss of Dark/Dronc function results in a specific switch in ORN47a axonal recognition from the DM3 to the DA3 glomerulus identity (Fig. 1Q). The co-convergence of two distinct ORN classes into a common glomerulus with intra-glomerular segregation recapitulates the projection of two ORN populations in the mouse olfactory system, which express closely related but not identical OR genes [24]. This indicates a related mechanism of ORN class-specific axon segregation via afferent interactions in *Drosophila*.

Non-apoptotic function of the apoptosome in ORN connectivity development

The apoptosome has been best characterized in the regulation of PCD, in which Dark-mediated Dronc activation results in elevated levels of effector caspases and cell fragmentation [13]. Thus we next tested if ectopic ORN47a axons in an apotosome deficient background derive from an overall increase in the number of neurons due to apoptosis blockage (Fig. 2). The following genetic approaches showed that the *dark/dronc* connectivity phenotype is indendent of the PCD pathway: First, the number of OR47a-positive neurons in the adult antenna is not changed in *dark/dronc* mutant mosaics compared to wild type (n=30 $\pm$3, Fig. 2A, B). Similarly, also ORN23a does not show any increase in overall ORN number, indicating that ORN development is not influenced by apoptosis (n=23 $\pm$3, Fig. 2A, B). Second, blocking of apoptosis in developing ORNs by targeted p35 expression, an inhibitor of effector caspases [25], does not lead to any ORN47a targeting defect (Fig. 2C, D). Third, in contrast to Dronc mutations, no effect on ORN47a axon targeting was observed

following the loss of the main effector caspase Drice, which further supports a non-apoptotic function of the apoptosome in ORN connectivity (Fig. 2F). Interestingly, the deletion of a second initiator caspase, Strica, results in a similar, although milder, ORN47a mistargeting phenotype (Fig. 2E) and genetic interaction studies revealed a partial redundant function between Dronc and Strica (Fig. 2G, H).These results support a model in which the ectopic ORN47a glomerulus in *dark/dronc* mutants is a direct consequence of reduced initiator caspase function in ORN axon guidance instead of additional neurons which survive due to developmental apoptosis defects. Here, combined activities of initiator caspases, independent of down-stream effector caspase activiation, seem to mediate axonal recognition identity.

Gradual levels of caspase activity controls ORN axon pathfinding and targeting

The results described above indicate that the amount of ectopic ORN47a fibers correlates with caspase activity as shown by different Dronc alleles (Fig. 1N-P) or Dronc/Strica interaction (Fig. 2G, H). To gain further insights into the effect of caspase activity in ORN connectivity development, we modified caspase activity in vivo by using a large collection of *dark* mutations defining an allelic series with multiple alleles of weak and strong hypomorphic as well as null mutations. These *dark* alleles were classified according to their suppression of apoptosis, e. g. the reduction of the GMR-hid induced photoreceptor degeneration, and levels of caspase activity directly correlated with levels of activated Caspase3 expression (Fig. 2I-L). In contrast to a wild type caspase activity, in which all ORN47a axons extend along the central AL pathway to converge on the dorsal DM3 (Fig. 2I, M), the loss of Dark-activated Dronc results in a lateral projection and ectopic DA3 mistargeting of ORN47a axons (Fig. 2K,L,O). Following a reduction in caspase activity in *dark* weak hypomorphic mutants, a misrouting of ORN47a axons along the lateral AL region is observed (Fig. 2J). Interestingly, although the proportion of misprojecting axons projecting along the lateral path appears similar to the *dark*-null phenotype, all ectopic axons converge onto the cognate DM3 glomerulus and no ectopic innervation in the DA3 region can be detected (Fig. 2J). A substantial reduction of caspase activity in strong hypomorphic *dark* mutants results in a lateral misrouting of ORN47a axons with partial ectopic convergence into DA3 (Fig. 2K,N).

Furthermore, dosage-sensitivity of caspase function can be observed in combining hypomorphic *dark/dronc* mutations with targeted RNAi expression (Fig. 2P, Q) or heterozygous loss-of-function mutants (Fig. 2R, S), which allows to funcionally separate the axon pathfinding and targeting process. A moderate reduction in caspase activity (weak *dark* hypomorphs, *dronc* RNAi) leads to a switch of axonal projection from the medial to the lateral AL domain but does not support their association and targeting with ORN23a axons at the DA3 glomerulus. A strong reduction in caspase activity (strong *dark* hypomorphs) induces the mistargeting of some of the lateral ORN47a axons into the DA3 glomerulus, whereas the complete loss of caspase activity (*dark*-null alleles) directs all of the lateral ORN47a axons into the DA3 glomerulus.

Apoptosome-mediated axon interactions in ORN projections

We next performed detailed clonal studies to determine how caspase function controls ORN47a axon pathfinding and targeting. As described above, homozygous mutant ORNs segregate into two main projection pathways, the cognate central pathway towards the DM3 glomerulus and the lateral pathways towards the ectopic DA3 innervation, indicating distinct subpopulations of caspase-independent and caspase-sensitive ORN47a neurons. Using the *Flybow* technique to visualize the projection of individual fibers within genetic mosaics [26], we observed a strict separation between the central and the lateral pathway for homozygous *dark* mutant compared to wild type ORN47a axons (Fig. 3A-E). Centrally-projecting mutant ORN47a axons are indistinguishable from the bi-lateral pathway of wild type neurons, indicating no role of caspases in this subpopulation (Fig. 3A, B). *dark* mutant ORN47a axons extending along the lateral pathway also show a stereotypic projection pattern with bilateral glomerular arborization fully separated from the central pathway and reminiscent of ORN23a projections (Fig. 3C-E). Interestingly, although ectopic ORN47a axons project in close proximity to their actual wild type target, the DM3 glomerulus, we did not observe lateral-projecting axons to innervate DM3 (Fig. 3D), further supporting a complete switch in ORN recognition identity following caspase inhibition.

We next determined if apoptosome function is required cell-autonomously to control ORN connectivity by generating single *dark* mutant ORNs in a wild type background

(Fig. 3F, G). Similar to ORN47a projections in large size clones, single *dark* mutant ORN axons project along the central or lateral pathway and show synaptic arborizations within the DM3 or DA3 glomerulus, respectively, supporting a mechanism by which cell-intrinsic caspase activity controls neuronal recognition . Comparing the projection pattern of different clone sizes revealed a direct correlation between the number of ectopic axons and the degree of axonal convergence: a small number of lateral ORN47a axons (< 3) show more dispersed synaptic arborizations within the DA3 area (Fig. 3I) compared to medium-sized clones of *dark* mutant neuron (> 3 axons) converge into a distinct glomerular structure (Fig. 3H).

Interestingly, in addition to the cell-autonomous function of Dark/Dronc in ORN47a connectivity, *reverse MARCM* clones, which allow to visualize the development of wild type neurons in the vicinity of homozygous mutant neighboring axons [27], showed specific cell-nonautonomous phenotypes (Fig. 3J, K). Here, the majority of homozygous wild type axons projects along the central pathways and terminates within DM3 (Fig. 3K). Additionaly, in this mosaic background a fraction of wild type axons comparable to the number of mutant axons follows the lateral pathway (Fig. 3K). However, instead of terminating in the DA3 glomerulus the wild type axons continue growing medially and recognize the cognate DM3 glomerulus (Fig. 3K). In contrast, a significant number of *dark* heterozygous ORN47a axons target within DA3 (Fig. 3K). As in *dark* heterozygous animals, where all neurons have the same genotype, an ectopic targeting could not be observed (Fig. 2S), these results indicate a context-dependent interaction of ORN axons with reduced caspase activity: in a homogenous projection field lateral ORN47a axons fail to recognise the ectopic DA3 target area but with an ectopic glomerulus, induced by homozygous caspase mutant ORNs, present, even a reduced caspase level is sufficient to trigger ectopic axon convergence. Similar "community effect" in ORN axon connectivty has been described in the development of mammalian olfactory system, in which a critical number of axon is required to induced ectopic glomerulus formation. These results show that the apoptosome functions cell-nonautonomously to control ORN47a connectivity and that the intra-cellular levels of caspase activity together with cellular identity of the co-projecting axons (also specified by caspase activity) determine the final connectivity pattern

Caspase-mediated target domain projections of ORN axons

To determine the overall requirement of apoptosome function in olfactory map formation we analyzed the axonal projections of multiple ORN classes (Fig. 4). Domain-specific projections of ORN classes are a characteristic feature of the wild type AL (visualized with the ORN-specific marker Orco-Gal4), allowing to distinguish a dorso-lateral, central and ventro-medial projection domain (Fig. 4AA). In *dark/dronc* mutants the overall axonal projection domains are no longer segregated into visible AL domains but more evenly distributed across the AL (Fig. 4AB). We next analyzed the projection of individual ORN classes in a caspase-deficient background and identified a specific domain requirement of the apoptosome (Fig. 4A-X). Whereas no axonal projection defect could be observed for *dark/dronc* mutant ORNs of the lateral domain including ORN23a (7 classes tested, Fig. 4A-F), a subset of mutant ORNs in the medial domain, including ORN47a, showed a specific shift towards the lateral domain combined with an ectopic glomerular targeting (Fig. 4G-L). For caspase-deficient ORNs of the ventro-medial domain only mild lateral shifts could be observed for antennal classes (Fig. 4M-R) but severe and specific lateral mistargeting phenotypes were detected for mutant ventro-medial ORNs coming from the maxillary palps (Fig. 4S-X). Similar to the specific association of ectopic ORN47a with lateral ORN23a axons, a specific switch in neuronal recognition could be observed for additional ORN classes which lack Dark/Dronc activity. For example, ectopic ORN67b axons target specifically to the ORN83c-positive VC3 glomerulus (Fig. 4AC, AD) and ORN56a axons shows a strong lateral shifts in its projection associated with ectopically innervating ORN47a axons (Fig. 4AE, AF).

These data show that the correct projection along a distinct nerve layer domain is critical for a subset of ORNs to prevent mistargeting to an ectopic glomerulus, suggesting existence of multiple potential target areas for caspase-sensitive ORN classes in the AL. Class-specific axonal convergence and initial axon sorting should therefor prevent the recognition of potential additional target regions.

Domain-specific expression of LRR cell adhesion molecules controls ORN axon sorting

To determine how caspase activity translates into axonal and synaptic recognition we next screened for gene expression patterns that recapitulate the ORN axon projection domains. Among them, the LRR-type cell adhesion molecule Connectin shows a

strong expression in ORN classes of the lateral projection domain but is almost absent in ORN classes which extend along the medial domain (Fig. 5A). During initial steps of ORN innervation, high levels of Connectin expression can be observed in all axon fibers extending along the lateral target area, which is fully separated by ORN axons of the central domain, visualized by an engrailed reporter line (Fig. 5B–D).

We next determined how the loss of apotosome activity affects Connectin expression. In the wild type AL, centrally projecting ORN47a axons as well as the DM3 glomerulus are Connectin-negative (Fig. 5E-E'''). In contrast, ectopic Connectin expression can be observed in *dark/dronc* mutant 47a-ORNs, which directly correlates with their domain-specific segregation (Fig. 5F). Within *dark* mutant mosaics, the centrally-projecting 47a-ORNs are still Connectin-negative whereas the laterally-projecting ORN47a axons that terminate in the ectopic DA3 glomerulus show high levels of Connectin expression (Fig. $5F^1$). Similar domain-specific misexpression of Connectin can be observed in ORN47a axons deficient for Dronc (Fig. Fig. $5F^2$). The ectopic expression of Connectin in a subpopulation of ORN47a was confirmed in the antennal sensory epithelium (Fig. 5G). During ORN innervation, axons of the neighboring DA3/4 target regions start to accumulate synaptic proteins before glomerulus formation (Fig. 5H), followed by the development of distinct glomerular boundaries (Fig. 5I). Interestingly, ventrally to the newly-formed DA3 glomerulus adjacend glomeruli are more losely assembled leaving a distinct region without a glomerular neuropil (5I', I''). Whereas, in *dark* mutants, a Connectin-positive glomerulus develops ventrally to DA3 (5 J- J'').

To determine if ectopic Connectin expression is sufficient for the lateral projection shift of ORN47a axons we combined *UAS-Connectin* with developmental *ORN-Gal4* lines (e.g. *pebbled-Gal4*). In about 40% of the analyzed brain (n=18) we could detect an ectopic ORN47a glomerulus next to DA3 (Fig. 5K, L). In addition, ectopic expression of Connectin in the central domain via *en-Gal4* not only affects the organization of axon tracts but also leads to strongly reduced Connectin levels in the lateral domain, indicating a cross-talk between these two projection domains (Fig. 5M-P). In addition to Connectin misexpression in wild type ORNs, an interference with Connectin expression in wild type and *dark/dronc* mutant background revealed a specific interaction between ORN23a and ORN47a (Fig. 5Q-X). Targeted RNA-

interference in developing ORNs leads to a substantial reduction in Connectin levels, which does not disrupt antennal nerve organization (Fig. 5Q-R), but modifies the ORN axon targeting phenotype (Fig. 5S-V). Within the ALs, reduced Connectin expression has no effect on ORN47a connectivity (Fig. 5S, T) but leads to a shift of ORN23a targeting from the lateral DA3 to the medial DM3 ectopic position (Fig. 5U, V). Finally, the downregulation of Connectin in *dark*/*dronc* mutant ORN47a axons strongly suppresses ectopic glomerulus formation (Fig. 5W, X), supporting a critical role of Connectin in mediating the caspase-controlled ORN recognition identity.

3.4 Discussion

The sensory map of the olfactory system is one of the most astonishing cases of wiring specificity independent of topographic patterning. Pioneer studies in mouse have uncovered the basic principles of olfactory system development, most importantly the identification of OR genes as central regulators of axonal recognition identity, in which OR activity translates into combinatorial expression of cell surface molecules [28]. Here, closely related OR genes trigger axonal segregation and convergence, commonly into distinct adjacent synaptic glomeruli and in cases of high molecular OR similarity even within a single glomerulus. In contrast, more different OR genes induced the formation of ectopic glomeruli, accompanied by a switch between the main projection domains in OR swap experiments [29]. How the sequential steps of domain identity and glomerulus identity are coordinated to specify unique synaptic positioning is not understood.

Here we describe a novel function of the apoptosome complex in the regulation of domain-specific sensory axon projection and glomerulus-specific axon targeting in the *Drosophila* olfactory system (Fig. 6). With a similar organization in wiring specificity but reduced cellular complexity compared to the mouse olfactory map, circuit analysis in *Drosophila* allows to determine the mechanisms underlying neuronal recognition identity at single cell resolution. Loss of the two conserved apotosome components, the caspase Dronc and its regulator Dark, leads to a class-specific switch in ORN axon identity at two consecutive developmental steps of axon sorting, the initial segregation into distinct projection domains and the subsequent

convergence into unique synaptic glomeruli. We provide experimental evidence that cell-type specific levels of caspase activity directly coordinate neuronal recognition identity at domain- and glomerulus segregation and thereby provide developmental flexibility downstream of neuronal lineage specification.

We show that the two sensory classes ORN23a and ORN47a are intermingled within the antennal epithelium but segregate their axons within the target region into two main projection domains (Fig. 6A). A moderate reduction in endogenous caspase activity leads to a switch in projection identity of ORN47a axons from the central to the lateral domain without changing the targeting identity as axons bypass the DA3 region and retour onto the medial DM3 glomerulus (Fig. 6B). Intermediate levels of caspase activity result in partial ectopic targeting of lateral ORN47a axons whereas a loss of caspase function results in a full switch of glomerulus identity due to which all lateral ORN47a axons terminate at DA3 and ignore DM3 even while bypassing the medial area during contralateral projection (Fig. 6C). This switch in recognition identity correlated with the expression of the cell adhesion molecule Connectin, which, in wild type and *dark/dronc* mutant ORN47a, is expressed in axons of the lateral projection domain but absent in the central domain. Modulation of Connectin levels in wild type and mutant caspase ORNs showed that Connectin is a critical mediator of cell type specific caspase activity as ectopic Connectin expression can shift wild type axons to the lateral domain and Connectin downregulation suppresses lateral targeting in caspase mutants.

Connectin is a family member of leucine-rich repeat (LRR) domain-containing proteins, which has been shown to be critical not only in organizing neural connectivity from axon guidance to target selection and synapse formation, but also in various nervous system disorders [30,31]. Besides Connectin, we expect additional cell recognition molecules to be targeted by the apoptosome. First, the ORN47a phenotype can only be partially rescued by suppression of ectopic Connectin expression, suggesting Connectin as part of a combinatorial code for ORN47a recognition identity. Second, the level of Connectin expression does not change in laterally displaced ORN67b axons with low Connectin expression both at the cognate target as well at the ectopic glomerulus. Interestingly, ORN67b but not ORN47a projection depends on Semaphorin-Plexin signaling further supporting an ORN class-

specific combinatorial recognition code. Furthermore, in the mammalian olfactory system, caspase-mediated regulation of Semaphorin expression controls ORN axon connectivity, suggesting a conserved developmental mechanism [32].

3.5 Material and Methods

Genetics

Fly stocks were maintained on standard medium and kept at 25°C. The *dark*^{ypt} alleles were found in a mutant screen performed in the lab. The null allele *dark*^{82}, *UAS-dark*^{wt} and *UAS-dark*^{V} stocks were provided by F. Akdemir. The mutant dark alleles *dark*^{G8}, *dark*^{D3} and *dark*^{N5} were generated by Srivastava et al [33]. The *UAS-dark*^{RNAi}, *UAS-Dronc*^{RNAi} and *UAS-connectin*^{RNAi} constructs were available in VDRC. *UAS-p35* were ordered from the Bloomington Stock Centre and *pebbled-Gal4* was a gift from L. Luo [34]. OR-markers were a kind gift from B. Dickson [16] and have been recombined with *UAS-sytGFP*, *UAS-CD8GFP* or *UAS-CD2* for labeling purposes.

For MARCM analysis [35], *FRT42* and/or *Gal80* constructs were recombined with the relevant constructs. For large clones in the antenna and maxillary palps, an *eyFLP* insertion on the X chromosome was used [36]. To generate smaller clones and for single-cell analysis, the FLYBOW1.1 construct [26] in combination with a temperature-induced *hs-mFLP* transgene on the X chromosome was used. 37°C heatshocks were given at larval stages and duration of heatshock was modulated according to the required number of labeled cells. Subsequently, larvae and pupae were restored at 25°C and dissected after eclosion.

Immunohistology

Primary antibodies used for immunohistochemistry were: rat anti-CadN (1:20; DSHB), mouse anti-con (1:20; kindly provided by Robert AH White), mouse anti-Bruchpilot (1:20; DSHB), rabbit anti-GFP (1:1000; Molecular Probes), and mouse anti-CD2 (1:1000; Molecular Probes). Secondary antibodies used were as follows (all 1:300): goat anti-rabbit F(ab)′ fragment coupled to Alexa 488 (Molecular Probes), goat anti-mouse F(ab)′ fragment coupled to Alexa 568 (Molecular Probes), and anti-HRP Cy5 (1:100; Dianova).

Immunostaining of brains of adult flies and pupae were carried out essentially as previously described [37] with the following exceptions: (1) adult brains were fixed in 2% PFA for 90 min, and (2) for the dissection of the pupal brains, the pupal cases were open, 2% PFA was added, and the brains were allowed to fix for 10 min before further dissection in 2% PFA. The overall time of fixation in 2% PFA was 90 min. Fluorescent samples were analysed using a Leica SP5 and Zeiss Meta510 confocal microscope. Software used for image processing was ImageJ Version 2.0.0 and Adobe Photoshop CS6.

3.6 Acknowledgements

We are grateful to B. Dickson, L. Vosshall, L. Luo, K. McCall, A. Bergmann and H. Stellar for providing critical reagents for this study. We would like to thank the Bloomington Drosophila Stock Center for Drosophila, Vienna Drosophila resource center for transgenic lines and Developmental Studies Hybridoma Bank and Cell Signaling Technology for antibodies. We further thank Dr. Gaurav Goyal and members of the Hummel laboratory for critical comments on the manuscript. DFG, Schram Foundation, ROL Research Platform Vienna University supported this work.

3.7 Author Contributions

C.S. performed the initial genetic mosaic screen, characterize the verpeilt alleles, analysis of Connectin expression and domain organisation. R.K. performed Flybow clonal analysis, analysed dronc alleles, analysis of engrailed expression pattern, genetic manipulation by Connectin RNAi, analysis of dark alleles with various ORN classes. L.T. generation of single cell and reverse MARCM clones, genetic manipulation of overexpression of Connectin. S.N. peformed genetic characterization of various dark alleles. U.P. performed analysis of effector caspases. C.S., R.K., L.T. and TH, concept and design. T.H. supervision, funding acquisition, analysis and interpretation of data, writing the original article.

3.8 References

1. Dickson BJ. Molecular Mechanisms of Axon Guidance. Science (80-). 2002;298: 1959–1964. doi:10.1126/science.1072165
2. Evans TA, Bashaw GJ. Axon guidance at the midline: of mice and flies. Curr

Opin Neurobiol. 2010;20: 79–85. doi:10.1016/j.conb.2009.12.006

3. Cowan WM, Fawcett JW, O'Leary DD, Stanfield BB. Regressive events in neurogenesis. Science (80-). 1984;225: 1258–65.
4. Low LK, Cheng H-J. Axon pruning: an essential step underlying the developmental plasticity of neuronal connections. Philos Trans R Soc L B Biol Sci. 2006;361: 1531–44. doi:10.1098/rstb.2006.1883
5. Luo L, O'Leary DDM. Axon Retraction and Degeneration in Development and Disease. Annu Rev Neurosci. 2005;28: 127–156. doi:10.1146/annurev.neuro.28.061604.135632
6. Cecconi F, Alvarez-Bolado G, Meyer BI, Roth KA, Gruss P. Apaf1 (CED-4 homolog) regulates programmed cell death in mammalian development. Cell. 1998;94: 727–37. doi:10.1016/S0092-8674(00)81732-8
7. Kuida K, Haydar TF, Kuan CY, Gu Y, Taya C, Karasuyama H, et al. Reduced apoptosis and cytochrome c-mediated caspase activation in mice lacking caspase 9. Cell. 1998;94: 325–37. doi:10.1016/S0092-8674(00)81476-2
8. Feinstein-Rotkopf Y, Arama E. Can't live without them, can live with them: roles of caspases during vital cellular processes. Apoptosis. 2009;14: 980–95. doi:10.1007/s10495-009-0346-6
9. Williams DW, Mukherjee A. More alive than dead: non-apoptotic roles for caspases in neuronal development, plasticity and disease. Running title: Caspases in. Nature Publishing Group; 2017;44: 1–11. doi:10.1038/cdd.2017.64
10. Kuranaga E, Kanuka H, Tonoki A, Takemoto K, Tomioka T, Kobayashi M, et al. Drosophila IKK-related kinase regulates nonapoptotic function of caspases via degradation of IAPs. Cell. 2006;126: 583–96. doi:10.1016/j.cell.2006.05.048
11. Arama E, Agapite J, Steller H. Caspase activity and a specific cytochrome C are required for sperm differentiation in Drosophila. Dev Cell. 2003;4: 687–97. doi:10.1016/S1534-5807(03)00120-5
12. Geisbrecht ER, Montell DJ. A role for Drosophila IAP1-mediated caspase inhibition in Rac-dependent cell migration. Cell. 2004;118: 111–25. doi:10.1016/j.cell.2004.06.020
13. Shapiro PJ, Hsu HH, Jung H, Robbins ES, Ryoo HD. Regulation of the Drosophila apoptosome through feedback inhibition. Nat Cell Biol. 2008;10:

1440–6. doi:10.1038/ncb1803

14. Orme M, Meier P. Inhibitor of apoptosis proteins in Drosophila: gatekeepers of death. Apoptosis. 2009;14: 950–60. doi:10.1007/s10495-009-0358-2
15. Jefferis GSXE, Hummel T. Wiring specificity in the olfactory system. Semin Cell Dev Biol. 2006;17: 50–65. doi:10.1016/j.semcdb.2005.12.002
16. Couto A, Alenius M, Dickson BJ. Molecular, anatomical, and functional organization of the Drosophila olfactory system. Curr Biol. 2005;15: 1535–1547. doi:10.1016/j.cub.2005.07.034
17. Vosshall LB, Wong AM, Axel R. An olfactory sensory map in the fly brain. Cell. 2000;102: 147–159. doi:10.1016/S0092-8674(00)00021-0
18. de Wit J, Hong W, Luo L, Ghosh A. Role of Leucine-Rich Repeat Proteins in the Development and Function of Neural Circuits. Annu Rev Cell Dev Biol. 2011;27: 697–729. doi:10.1146/annurev-cellbio-092910-154111
19. Lattemann M, Zierau A, Schulte C, Seidl S, Kuhlmann B, Hummel T. Semaphorin-1a controls receptor neuron-specific axonal convergence in the primary olfactory center of Drosophila. Neuron. 2007;53: 169–84. doi:10.1016/j.neuron.2006.12.024
20. Hummel T, Zipursky SL. Afferent induction of olfactory glomeruli requires N-cadherin. Neuron. 2004;42: 77–88. doi:10.1016/S0896-6273(04)00158-8
21. Hummel T, Vasconcelos ML, Clemens JC, Fishilevich Y, Vosshall LB, Zipursky SL. Axonal targeting of olfactory receptor neurons in Drosophila is controlled by Dscam. Neuron. 2003;37: 221–31. doi:10.1016/S0896-6273(02)01183-2
22. Yu X, Wang L, Acehan D, Wang X, Akey CW. Three-dimensional structure of a double apoptosome formed by the Drosophila Apaf-1 related killer. J Mol Biol. 2006;355: 577–89. doi:10.1016/j.jmb.2005.10.040
23. Kanuka H, Sawamoto K, Inohara N, Matsuno K, Okano H, Miura M. Control of the cell death pathway by Dapaf-1, a Drosophila Apaf-1/CED-4-related caspase activator. Mol Cell. 1999;4: 757–769. doi:10.1016/S1097-2765(00)80386-X
24. Zou D-J, Feinstein P, Rivers AL, Mathews GA, Kim A, Greer CA, et al. Postnatal refinement of peripheral olfactory projections. Science (80-). 2004;304: 1976–9. doi:10.1126/science.1093468
25. Hay BA, Wolff T, Rubin GM. Expression of baculovirus P35 prevents cell

death in Drosophila. Development. 1994;

26. Hadjieconomou D, Rotkopf S, Alexandre C, Bell DM, Dickson BJ, Salecker I. Flybow: genetic multicolor cell labeling for neural circuit analysis in Drosophila melanogaster. Nat Methods. 2011;8: 260–6. doi:10.1038/nmeth.1567
27. Kao C-F, Lee T. Reverse genetics by loss-of-function mosaic analysis in Drosophila. Cold Spring Harb Protoc. 2013;2013: 66–69. doi:10.1101/pdb.prot071670
28. Imai T, Sakano H. Odorant receptor-mediated signaling in the mouse. Curr Opin Neurobiol. 2008;18: 251–60. doi:10.1016/j.conb.2008.07.009
29. Mombaerts P, Wang F, Dulac C, Chao SK, Nemes A, Mendelsohn M, et al. Visualizing an olfactory sensory map. Cell. 1996;87: 675–686. doi:10.1016/S0092-8674(00)81387-2
30. Nose A, Umeda T, Takeichi M. Neuromuscular target recognition by a homophilic interaction of connectin cell adhesion molecules in Drosophila. Development. 1997;124: 1433–1441. Available: http://dev.biologists.org/content/124/8/1433.long%5Cnpapers3://publication/uuid/BA92BFB6-1DA6-4EE9-B8D6-BBA77C94DDD0
31. Raghavan S, White RA. Connectin mediates adhesion in Drosophila. Neuron. 1997;18: 873–80.
32. Ohsawa S, Hamada S, Kuida K, Yoshida H, Igaki T, Miura M. Maturation of the olfactory sensory neurons by Apaf-1/caspase-9-mediated caspase activity. Proc Natl Acad Sci U S A. 2010;107: 13366–71. doi:10.1073/pnas.0910488107
33. Srivastava M, Scherr H, Lackey M, Xu D, Chen Z, Lu J, et al. ARK, the Apaf-1 related killer in Drosophila, requires diverse domains for its apoptotic activity. Cell Death Differ. 2007;14: 92–102. doi:10.1038/sj.cdd.4401931
34. Sweeney LB, Couto A, Chou YH, Berdnik D, Dickson BJ, Luo L, et al. Temporal Target Restriction of Olfactory Receptor Neurons by Semaphorin-1a/PlexinA-Mediated Axon-Axon Interactions. Neuron. 2007;53: 185–200. doi:10.1016/j.neuron.2006.12.022
35. Lee T, Luo L. Mosaic Analysis with a Repressible Cell Marker for Studies of Gene Function in Neuronal Morphogenesis. Neuron. 1999;22: 451–461. doi:10.1016/S0896-6273(00)80701-1
36. Newsome TP, Asling B, Dickson BJ. Analysis of Drosophila photoreceptor

axon guidance in eye-specific mosaics. Development. 2000;127: 851–60.

37. Van Vactor DL, Cagan RL, Krämer H, Zipursky SL. Induction in the developing compound eye of Drosophila: multiple mechanisms restrict R7 induction to a single retinal precursor cell. Cell. 1991;67: 1145–55. doi:10.1016/0092-8674(91)90291-6

Figure Legends

Figure 1. Switch in olfactory axon targeting in mutations of the apoptosome components Dark and Dronc. If not otherwise stated, in all figures the antennal lobe is stained by the neuropil marker anti-Ncad. OR-specific driver lines are used to visualize ORN classes in green (endogenous GFP) or red (anti-CD2). (A-A'') Wild type ORN47a axons project across the AL to converge onto the dorso-medial DM3 glomerulus. White box indicates the position of the DA3 glomerulus, which does not receive ORN47a innervation in the wild type olfactory system (A'). (B-B'') In homozygous mutant dark clones, ORN47a axons extend along two separate projection domains towards unique glomeruli: the cognate central pathway to DM3 and the ectopic lateral pathways towards a novel glomerulus adjacent to DA3. (C-C'') In wild type, ORN47a axons (green) project along the central pathway to reach DM3 and ORN23a axons (red) target the DA3 glomerulus along the lateral projection domain. (D-D'') In dark mutant mosaics ectopic ORN47a axons associate with ORN23a axons in the lateral AL domain and converge onto a common glomerulus unit (D'') but segregate into distinct synaptic regions (D'). (E, F) Schematics of the ORN47a and ORN23a axons in wild type (E) and dark mutants (F) and quantification (phenotypic penetrance) of DM3 and DA3 innervation by wild type and dark mutant ORN47a and ORN23a axons. (G, G') For the bilateral innervation in wild type, ORN47a and ORN23a project along distinct commissural tracts (red and white asterisk). (H, H') Dark mutant ORN47a axons segregate into a distinct commissural tract to reach the ectopic glomerulus. (I) In wild type, ORN49a axons project along the lateral pathway and target the dorso-lateral DL4 glomerulus. (J, J') Although *dark* mutant ORN47a axons converge into an ectopic glomerulus in vicinity to DL4, the dorsal view reveals a close association with DA3 but not DL4 (arrowheads in J'). (K-M) Interaction of wild type and *dark* mutant OR47a axons with projection neurons (PNs). PNs are labeled by GH146-Gal4, with expression in 1/3 of the PN classes. (K) In wild type,

ORN47a axons densely innervate the PN dendrites of the DM3 glomerulus. (L) *dark* mutant ORNs arborize in a wild type pattern within DM3 but show a restricted innervation to the ventral area of the DA3 glomerulus. (M) Labeling of single projection neurons reveals a homogeneous dendritic field within the DA3 glomerulus, which covers the endogenous ORN23a axons as well as the ectopic ORN47a axons. No common PN dendrites are shared between DA3 and DM3. (N-P) Mutations in the initiator caspase Dronc result in an ectopic DA3 innervation similar to the loss of Dark. The amount of ectopic ORN47a axons targeting to DA3 correlates with the allelic strength of the *dronc* mutations: hypomorphic *dronc* mutations result in a small ectopic glomerulus (N, N'), whereas strong *dronc* alleles show a strong ectopic DA3 innervation (O, P). (Q) Schematics summarizing the ORN targeting phenotype following the loss of the apoptosome components Dronc and Dark. Sensory neuron axons of the ORN47 class with impaired Dronc caspase activity shift from the central to the lateral projection domain and co-converge onto the same PN dendrite class within the DA3 glomerulus.

Figure 2. Level-dependent caspase activity controls ORN47a connectivity development independent of apoptosis. (A, B) Loss of *dark* does not affect the number of ORN47a (red, *OR47a-Gal4 UAS-mCherry*) and ORN23a (green, *OR23a:CD8-GFP*) in the antenna. Distribution (A) and quantification (B) of ORNs in the adult antenna (n=5) is unaffected in *dark* mutant mosaics compared to wild type. (C, D) Blocking developmental cell death by the expression of viral apoptosis blocker p35 in early ORNs (*pbl-Gal4 UAS-p35*) does not result in the ectopic ORN47a targeting phenotype of dark mutants. (E-H) Initiator caspases but not effector caspases control ORN47a connectivity. (E) Mutations in the initiator caspase Strica result in a mild DA3 mistargeting phenotype of ORN47a axons. (F) Loss of the main effector caspase Drice does not induce any changes in ORN47a projection. (G, H) Simultaneous reduction in the activity of the two initiator caspases Dronc and Strica results in an increased severity of DA3 mistargeting phenotype accompanied by a strongly reduced innervation of the cognate DM3 glomerulus. (I-O) Analysis of caspase activity in controlling ORN47a axon projection and targeting by using an allelic series of *dark* mutations. The effect of *dark* mutations on the activity of initiator caspases can be determined by anti-Caspase3 staining in the 3rd instar eye discs (I, J, K, L). ORN47a with wild type levels of caspase activity project along the

central pathway and exclusively target the DM3 glomerulus (I, M). (J-J''') In the hypomorphic *dark*^{J7} background, a large fraction of ORN47a axons switches towards the lateral projection tract (arrow in J'') but bypasses the DA3 glomerulus without any sign of synaptic targeting (arrowhead in J''') and turns towards the cognate DM3 at the dorsal AL. (N-N'') The weak hypomorphic allele *dark*^{D3} results in a similar amount of ORN47a lateral axon projections, but here a small subset of ectopic ORN axons can innervate the DA3 glomerulus (arrowheads). (K, L, O) In strong hypomorphic and null *dark* mutant background all ORN47a axons, which project along the lateral pathway, converge onto the DA3 glomerulus and project as a separate contralateral fascicle, bypassing the medial DM3 glomerulus (asterisk in L''). (P-S) Dosage-sensitive Dark function in ORN47a connectivity. (P, Q) The weak *dark*^{G15} mutation does not lead to a strong DA3 mistargeting of ORN47a axons, but a further reduction of dark activity via targeted RNAi results in strong ectopic lateral targeting (arrow). (R, S) In contrast to the *dark* homozygous wild type background, in which all ORN47a axons extend along the medial pathway and terminate within DM3 (R, R'), heterozygous *dark*^{V8} mutants show a substantial amount of lateral projecting ORN47a axons but no sign of ectopic targeting (S, S') Nuclei are labeled by toto (blue).

Figure 3. Cell-autonomous and non-autonomous functions of the apoptosome in projecting ORN axons. (A-E) FLYBOW-generated mosaics (green, eGFP; white, mCitrin; red, mCherry). (A, B) Single wild type ORN47a axons project along the central pathway and arborize within the DM3 glomerulus on the ipsi- and contralateral hemisphere. (A', A'') Two examples of ORN47a single cell clones projecting from both antennae. (B', B') Two examples of ORN47a two cell clones projecting from only one antenna. (C-E) The projection of single ORN47a axons in *dark* mutants. In all cases, a spatial separation of axons of the central and lateral pathway is observed. (C'-E') Three examples of unilateral clones in which single ORN47a axons projecting either along the central pathway and target to DM3 (white arrowheads) or along the lateral pathway and target the DA3 glomerulus (red arrowheads). (C''-E'') Three examples of bilateral clones with central (white arrowheads) and lateral (green arrowheads) ORN47a axons. (F) Single-cell wild type clone of ORN47a neurons projecting along the central pathway and arborizing within DM3. (G) Two-cell *dark* mutant clone of ORN47a (G'), with one neuron projecting

along the central pathway and arborizing in a wild type pattern within DM3, whereas the other neuron extends along the lateral pathway and forms minor synaptic arborizations within the DA3 glomerulus (G'', G'''). (H, I) The formation of an ectopic glomerulus correlates with the number of *dark* mutant ORN47a axons, which project along the lateral pathway. Whereas 3 neighboring *dark* mutant axons converge into a distinct synaptic glomerular structure (H', H''), synaptic terminals of a single *dark* mutant lateral axon are less restricted in the DA3 region (I', I''). (J, K) Non-autonomous effects of *dark* mutant ORN axons on the projection of neighboring wild type axons. (J) In a wild type olfactory system, all ORN47a axons project along the central pathway and terminate with DM3. (K) In an olfactory system with homozygous *dark* mutant mosaic clones, neighboring wild type and heterozygous neurons show a distinct projection behavior. Whereas homozygous wild type ORN47a axons project only to the cognate DM3 glomerulus (K''), a fraction of *dark* heterozygous neurons terminates in the ectopic DA3 glomerulus (K'). (L) Schematics summarizing the autonomous and non-autonomous effects of caspase activity on the projection and targeting of ORN47a axons.

Figure 4. Global shift and ectopic targeting of ORN axon projections in apoptosome mutants. ORN axons in the antennal lobe show a class specific segregation into distinct projection domains: the lateral projection domain (A-C), the central projection domain (G-I) and a medial projection domain, which contain ORN axons from antennal classes (M-O) and from ORNs located in the maxillary palps (S-U). For ORN classes that project along the lateral AL domain, loss of caspase activity has no effect on their axonal connectivity (D-F) and only a mild defasciculation phenotype could be observed (arrowheads in D' and F'). In contrast, of the five ORN classes within the central projection domain tested, three showed a switch to the lateral projection domain with an ectopic targeting in a specific glomerulus (J-L). (P-R) For ORN classes of the medial projection domain, *dark* mutant antennal ORN classes show no differences to their wild type projection pattern (P'-R'). (V-X) In contrast, maxillary ORNs with reduced caspase activity display a stereotypic shift to the central domain (arrows in V'-X') accompanied by an ectopic glomerular targeting (arrowheads in V'-X'). (AA, AB) The organization of wild type ORN axons into distinct projection domains is severely disrupted in *dark* mutants lacking caspase activity. (AC-AD) Ectopic targeting of *dark* mutant central ORN classes is associated

with a distinct lateral glomerulus. As a result of the lack of caspase activity in ORN67b neurons, axons associate with ORN83c axons and target to a common glomerulus (AE, AF). Similarly, *dark* mutant ORN56a axons show a strong lateral shift, associated with ectopic ORN47a axons.

Figure 5. Connectin controls caspase-mediated ORN recognition identity. (A-A'') In the adult olfactory system, the cell-adhesion molecule Connectin is strongly expressed in the lateral projection domain (LD) and no expression can be detected in the adjacent central projection domain (CD). Weak Connectin expression can be detected in some glomeruli in medial domain (MD). The *Con-Gal4* expression (A'') recapitulates the endogenous Connectin pattern as detected by anti-Connectin (A'). (B-D) Developmental Connectin expression in the olfactory system. (B-B'') Connectin-positive ORN axons in the developing antenna project in 3 main fascicles towards the antennal lobe, inter-mingled with a non-overlapping population of *en-Gal4* positive ORNs. (C-C'') At 30h APF, Connectin-positive ORNs segregate in a large lateral (LD) and a minor medial (MD) pathway, whereas the central pathway (CD) is occupied by axons of en-positive ORNs. (D-D'') At 40h APF, newly formed Connectin-positive glomeruli accumulate in the lateral domain (LD) with the majority of en-positive glomeruli in the adjacent central domain (CD). (E-G) Loss of caspase activity in ORN47a results in ectopic expression of Connectin. (E-E''') In wild type, no expression of Connectin can be detected in ORN47a axons and the DM3 target glomerulus, whereas ORN23a axons and DA3 in the lateral domain are expressing high level of Connectin. (F^1) Loss of caspase activity in *dark* mutants leads to a specific misexpression of Connectin in ORN47a neurons: Centrally projecting ORN47a axons are still Connectin-negative (green dotted circle), whereas ORN47a axon which project along the lateral domain and target DA3 show high levels of Conncetin expression (black dotted circle),. (F^2) Similarly, in *dronc* mutants ectopic ORN47a axons that target the DA3 glomerulus misexpress Connectin. (G) Analysis of Connectin expression in the developing antenna. In wild type, Connectin-positive ORNs can be found next to ORN47a sensilla (G'). In *dark* mutants, a subset of ORN47a expresses Connectin (G''). (H, J) Development of the Connectin-positive glomeruli. Within the lateral Connectin domain, the DA3/4 glomeruli start first to differentiate synaptic regions (H', H'') with subsequently DA3 locating in a specific position dorsally to a region without a glomerular neuropil (I', I'' arrowhead). (J) In

dark mutants, a Connectin-positive glomerulus develops ventrally to DA3 (green arrowhead in J''). (K-P) Ectopic expression of Connetin in wild type ORNs. (K, L) Overexpression of Connectin in developing ORNs results in ectopic targeting of ORN47a axons with a penetrance of about 30% (arrowhead in L). (M-P) Ectopic expression of Connectin in the central projection domain using *en-Gal4* (M) results in a strong suppression of endogenous Connectin expression in the lateral domain (N-N''). (O, P) In addition, cell surface molecule expression of ORNs in the lateral domain (ORN47b>CD8GFP) is strongly reduced (P', P''). (Q-X) Targeted RNA interference of Connectin expression in wild type and *dark* mutant background. (Q, R) Strong reduction of Connectin levels in wild type antenna following *UAS-Con*^{RNAi} expression in developing ORNs via *pebbled-Gal4*. (S-V) Reduction of Connectin in developing ORN has no effect on central ORN47a projections (T) but leads to a medial shift in ORN23a targeting (V, V'). (W, X) In *dark* mutants, suppression of Connectin expression results in a reduction (X, X') or full suppression (X'') of the ectopic DA3 innervation by ORN47a axons.

Figure 6. Caspase-mediated regulation of ORN connectivity development. Zonal organization of ORNs in the periphery and the synaptic target region. (A) ORN23a neurons (red) are restricted to a single ORN domain (zone B) and target the lateral synaptic glomerulus (red). In contrast, the ORN47a class (green) is distributed in two peripheral domains (zone A, caspase independent and zone B, caspase dependent [black arrow]). High caspase expression in wild type ORN47a results in a suppression of Connectin expression allowing axon to leave the lateral domain and reach the central target glomerulus. (B) A reduction in caspase activity prevents the early segregation of ORN47a axons from the lateral into the central domain but does not change ORN targeting identity, reaching the central glomerulus via a dorsal detour route. (C) Increased Connectin expression due to a complete loss of caspase activity switches not only the projection domain but also synaptic identity of ORN47a axons, resulting in ectopic targeting to the lateral glomerulus.

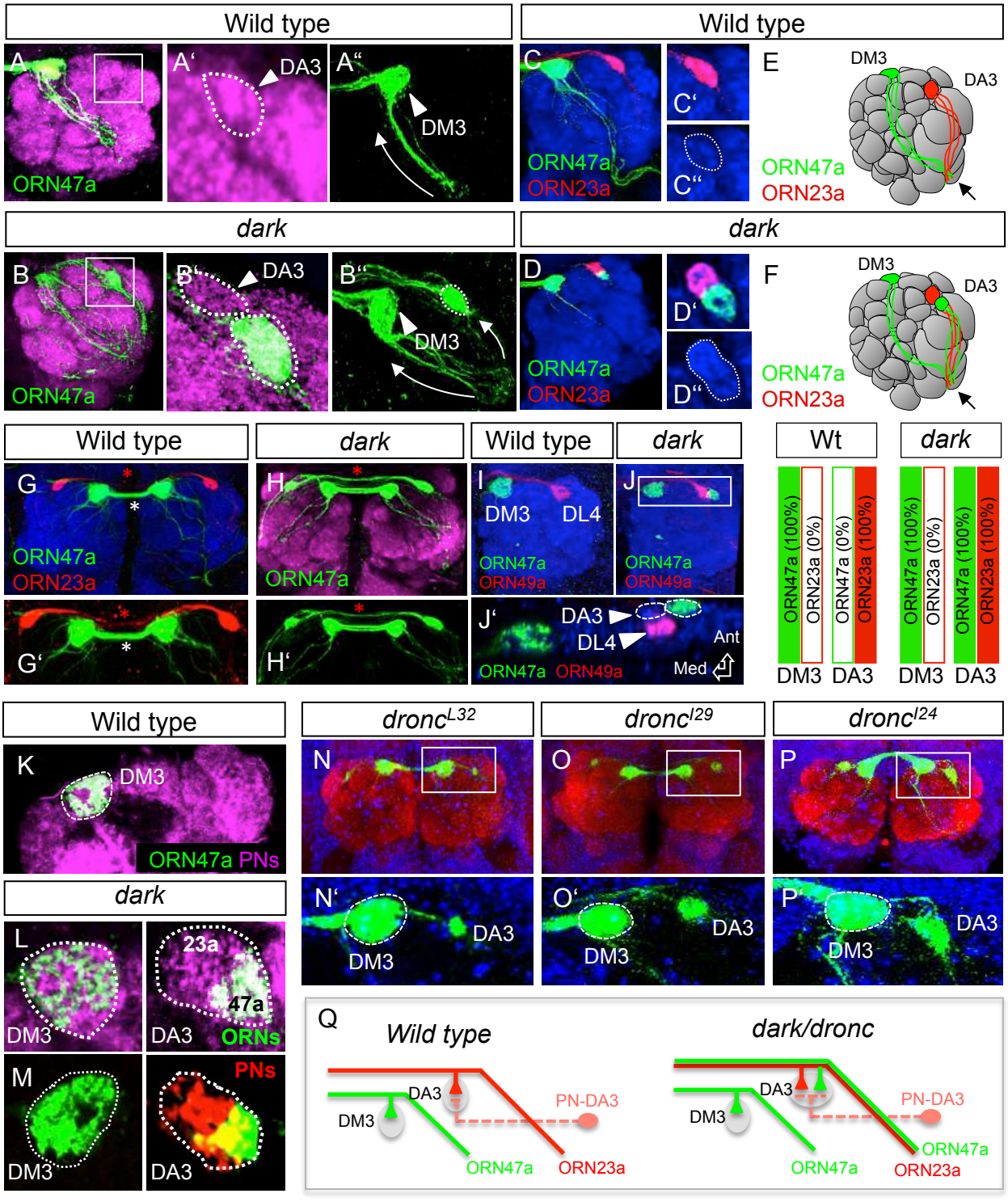
Wild type
Wild type
A
A'
DA3
A"
DM3
ORN47a
C
C'
C"
ORN47a
ORN23a
E
DM3
DA3
ORN47a
ORN23a
dark
dark
B
B'
DA3
B"
DM3
ORN47a
D
D'
D"
ORN47a
ORN23a
F
DM3
DA3
ORN47a
ORN23a
Wild type
dark
Wild type
dark
G
G'
ORN47a
ORN23a
H
H'
ORN47a
I
DM3
DL4
ORN47a
ORN49a
J
J'
DA3
DL4
Ant
Med
ORN47a
ORN49a
Wt
dark
ORN47a (100%)
ORN23a (0%)
ORN47a (0%)
ORN23a (100%)
ORN47a (100%)
ORN23a (0%)
ORN47a (100%)
ORN23a (100%)
DM3
DA3
DM3
DA3
Wild type
dronc^L32
dronc^I29
dronc^I24
K
DM3
ORN47a PNs
N
O
P
N'
DA3
DM3
O'
DA3
DM3
P'
DA3
DM3
dark
L
23a
47a
DM3
DA3
ORNs
M
PNs
DM3
DA3
Q
Wild type
dark/dronc
DA3
DM3
PN-DA3
ORN47a
ORN23a
DA3
DM3
PN-DA3
ORN47a
ORN47a
ORN23a

Figure 1

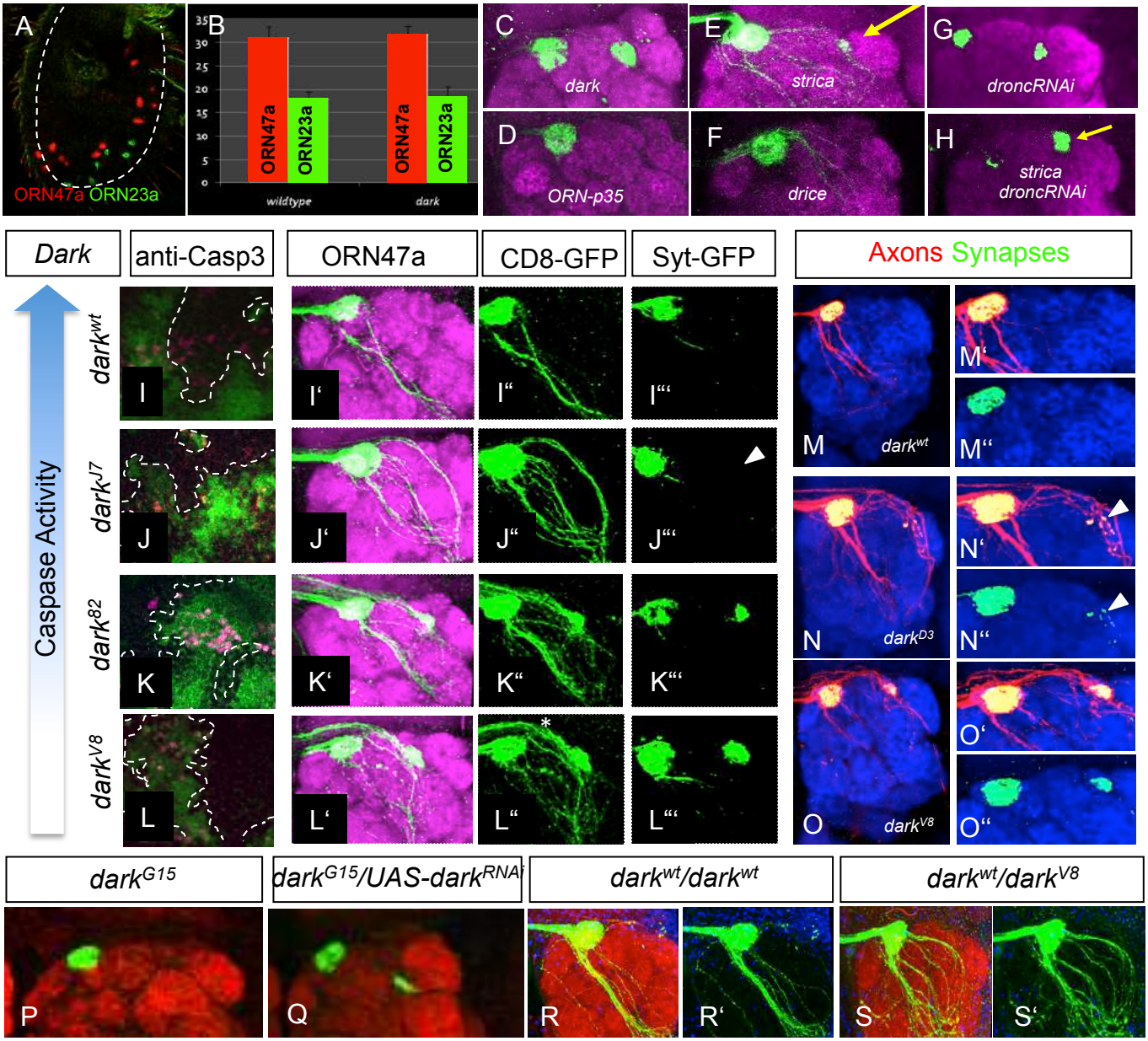
A
ORN47a ORN23a
B
ORN47a
ORN23a
wildtype
dark
C
dark
D
ORN-p35
E
strica
F
drice
G
droncRNAi
H
strica
droncRNAi
Dark
anti-Casp3
ORN47a
CD8-GFP
Syt-GFP
Axons Synapses
Caspase Activity
darkwt
darkJ7
dark82
darkV8
darkD3
darkG15
darkG15/UAS-darkRNAi
darkwt/darkwt
darkwt/darkV8

Figure 2

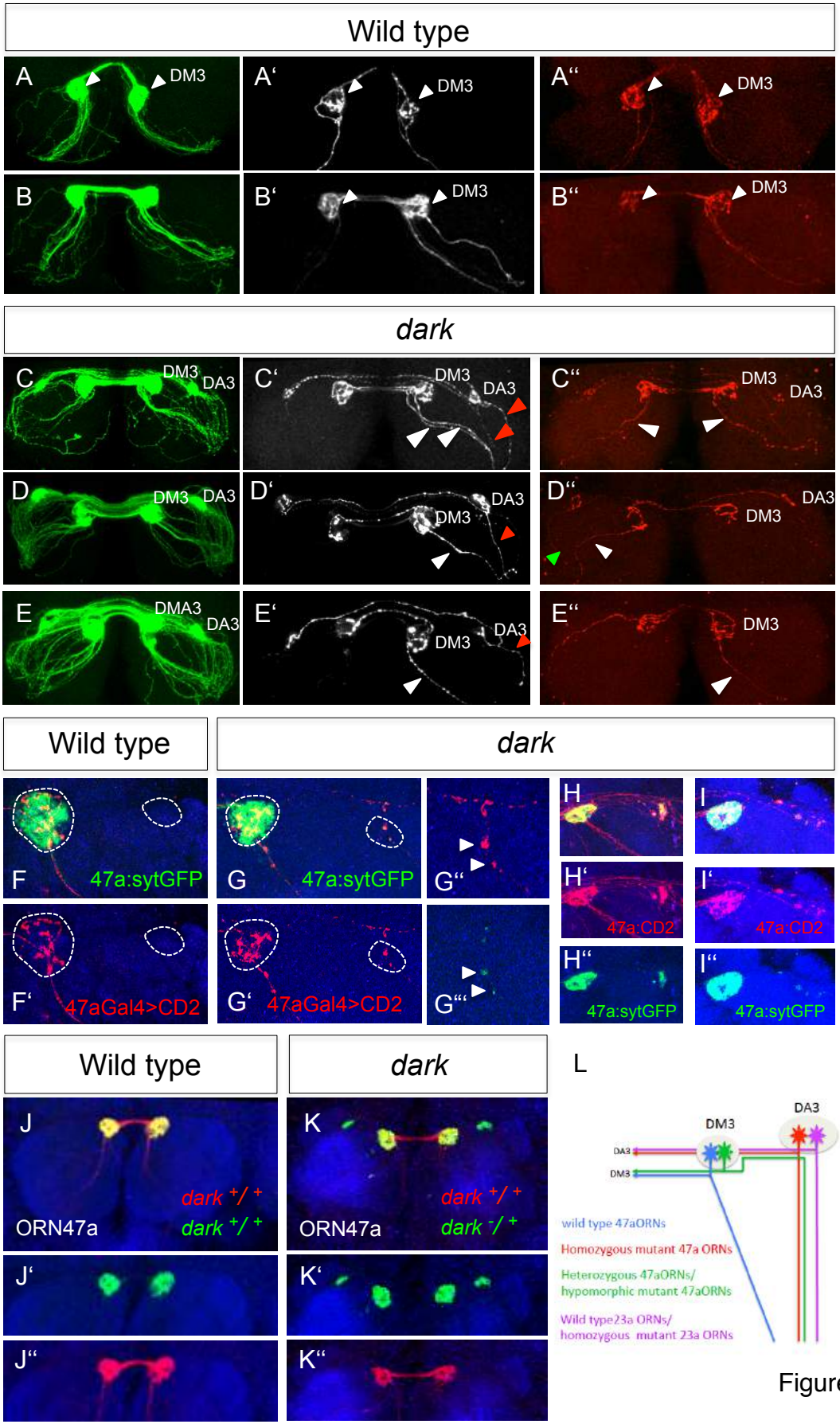
Wild type
A
DM3
A‘
DM3
A“
DM3
B
B‘
DM3
B“
DM3
dark
C
DM3
DA3
C‘
DM3
DA3
C“
DM3
DA3
D
DM3
DA3
D‘
DA3
DM3
D“
DA3
DM3
E
DMA3
DA3
E‘
DA3
DM3
E“
DM3
Wild type
dark
F
47a:sytGFP
G
47a:sytGFP
G“
H
H‘
47a:CD2
H“
47a:sytGFP
I
I‘
47a:CD2
I“
47a:sytGFP
F‘
47aGal4>CD2
G‘
47aGal4>CD2
G“‘
Wild type
dark
J
dark +/ +
ORN47a
dark +/ +
K
dark +/ +
ORN47a
dark -/ +
J‘
K‘
J“
K“
L
DA3
DM3
DA3
DM3
wild type 47aORNs
Homozygous mutant 47a ORNs
Heterozygous 47aORNs/
hypomorphic mutant 47aORNs
Wild type23a ORNs/
homozygous mutant 23a ORNs

Figure3

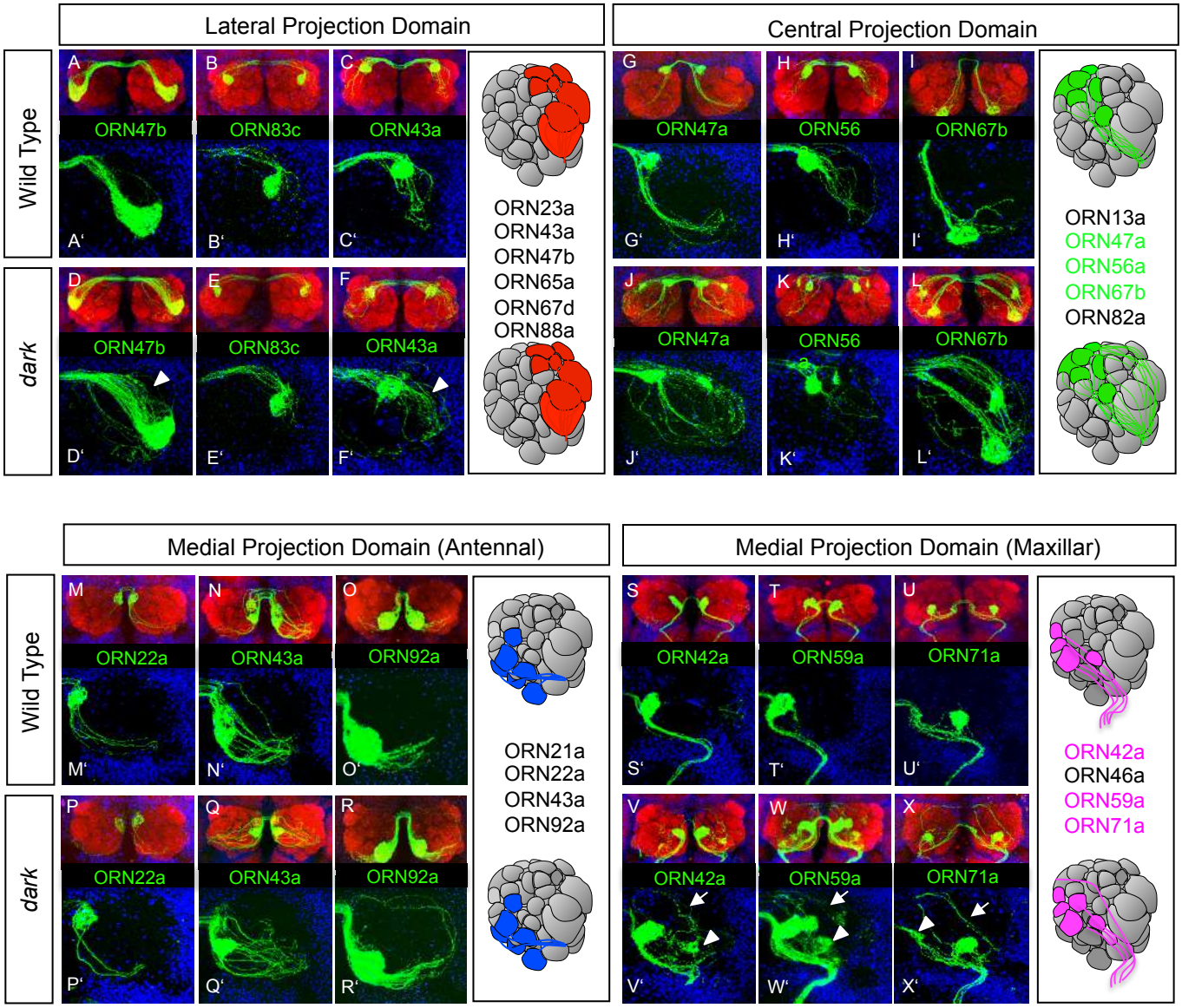
Lateral Projection Domain
Central Projection Domain
Wild Type
dark
A
B
C
ORN47b
ORN83c
ORN43a
A'
B'
C'
D
E
F
D'
E'
F'
ORN23a
ORN43a
ORN47b
ORN65a
ORN67d
ORN88a
G
H
I
ORN47a
ORN56
ORN67b
G'
H'
I'
J
K
L
J'
K'
L'
ORN13a
ORN47a
ORN56a
ORN67b
ORN82a
Medial Projection Domain (Antennal)
Medial Projection Domain (Maxillar)
M
N
O
ORN22a
ORN43a
ORN92a
M'
N'
O'
ORN21a
ORN22a
ORN43a
ORN92a
S
T
U
ORN42a
ORN59a
ORN71a
S'
T'
U'
ORN42a
ORN46a
ORN59a
ORN71a
P
Q
R
P'
Q'
R'
V
W
X
V'
W'
X'

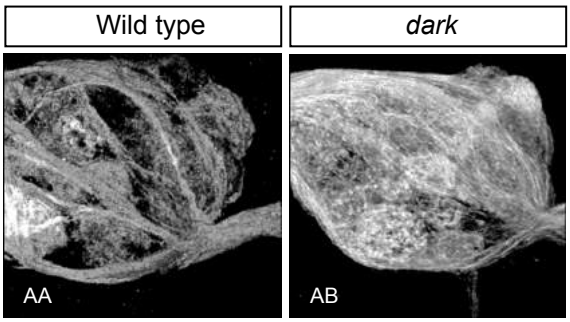
Wild type
dark
AA
AB

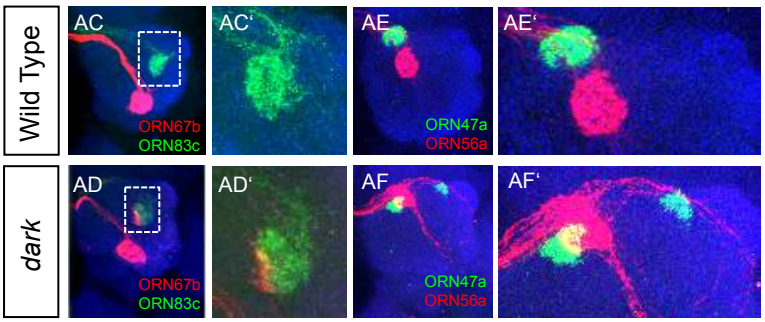
Wild Type
dark
AC
AC'
AE
AE'
ORN67b
ORN83c
ORN47a
ORN56a
AD
AD'
AF
AF'

Figure 4

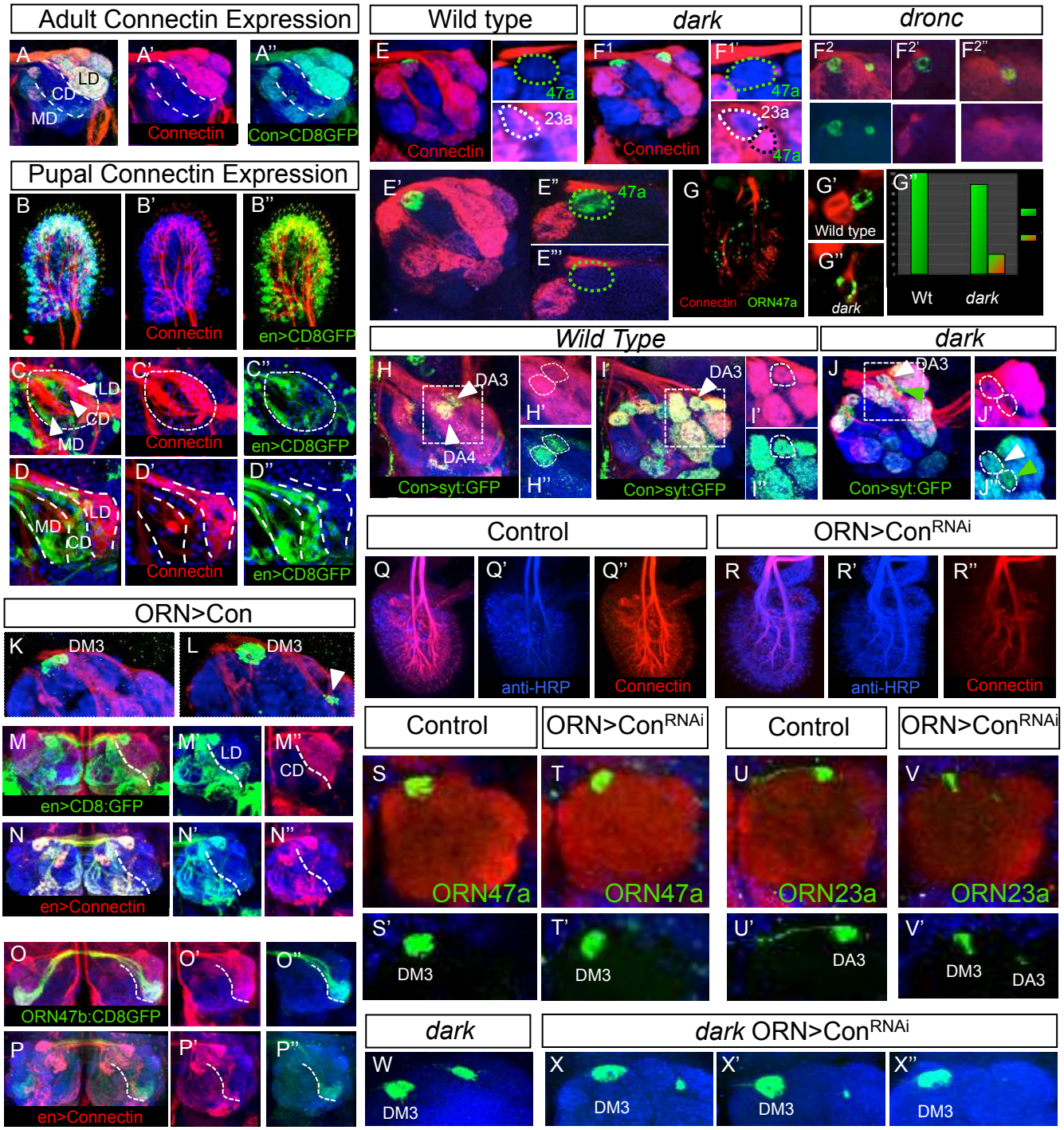
Adult Connectin Expression
A
LD
CD
MD
A'
Connectin
A''
Con>CD8GFP
Pupal Connectin Expression
B
B'
Connectin
B''
en>CD8GFP
C
LD
CD
MD
C'
Connectin
C''
en>CD8GFP
D
MD
LD
CD
D'
Connectin
D''
en>CD8GFP
ORN>Con
K
DM3
L
DM3
M
en>CD8:GFP
M'
LD
M''
CD
N
en>Connectin
N'
N''
O
ORN47b:CD8GFP
O'
O''
P
en>Connectin
P'
P''
Wild type
dark
dronc
E
Connectin
47a
23a
F1
Connectin
F1'
47a
23a
47a
F2
F2'
F2''
E'
E''
47a
E'''
G
Connectin
ORN47a
G'
Wild type
G''
dark
G''
Wt
dark
Wild Type
dark
H
DA3
DA4
Con>syt:GFP
H'
H''
I
DA3
Con>syt:GFP
I'
I''
J
DA3
Con>syt:GFP
J'
J''
Control
ORN>Con^RNAi
Q
Q'
anti-HRP
Q''
Connectin
R
R'
anti-HRP
R''
Connectin
Control
ORN>Con^RNAi
Control
ORN>Con^RNAi
S
ORN47a
T
ORN47a
U
ORN23a
V
ORN23a
S'
DM3
T'
DM3
U'
DA3
V'
DM3
DA3
dark
dark ORN>Con^RNAi
W
DM3
X
DM3
X'
DM3
X''
DM3

Figure 5

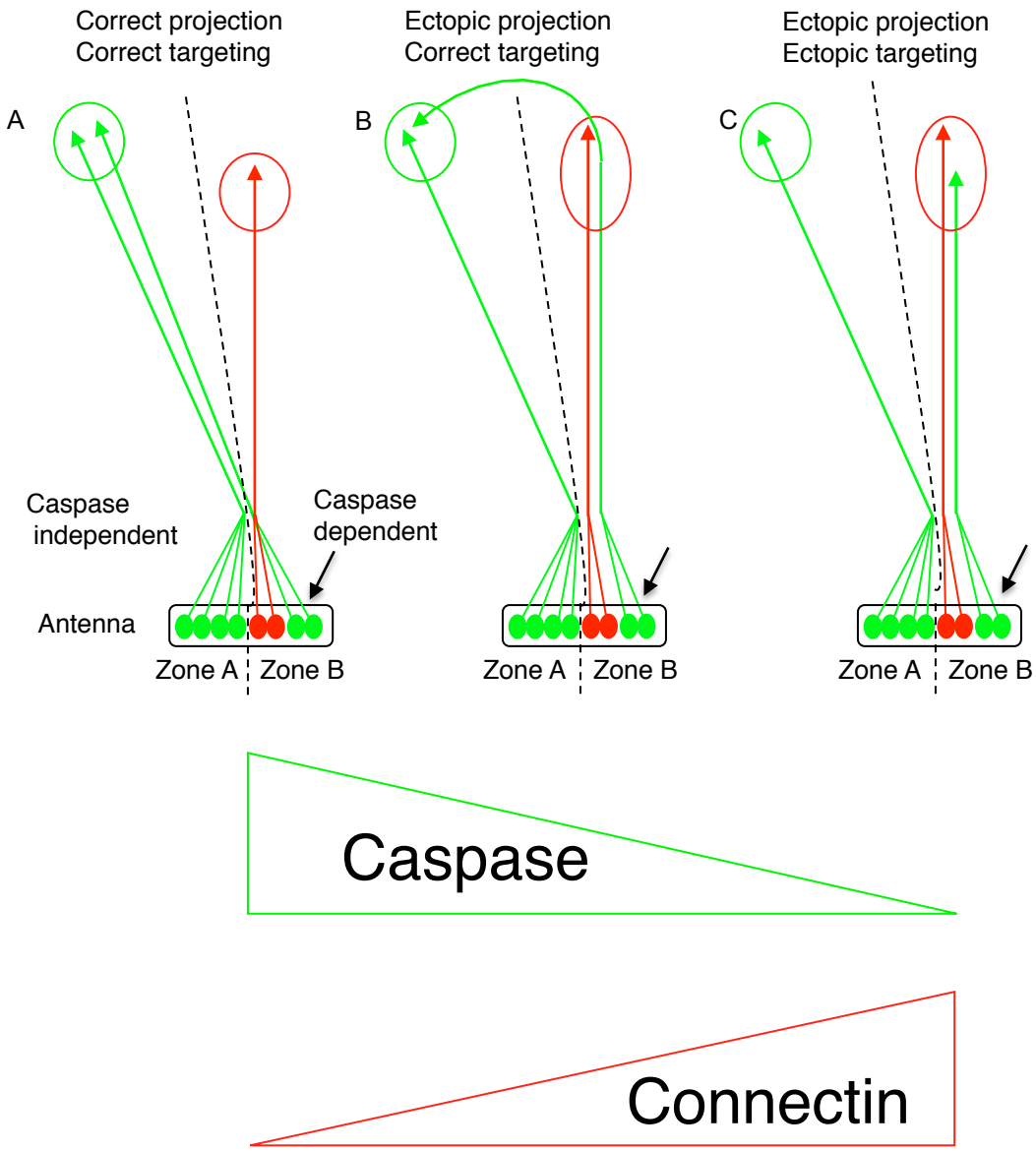
Correct projection
Correct targeting
Ectopic projection
Correct targeting
Ectopic projection
Ectopic targeting
A
B
C
Caspase
independent
Caspase
dependent
Antenna
Zone A
Zone B
Zone A
Zone B
Zone A
Zone B
Caspase
Connectin

Figure 6

Chapter 4

The chromatin modulator Psc coordinates synaptic and sensory identity in the *Drosophila* olfactory system

Özkan Aydemir[2], Rashmit Kaur[1], Georg Steffes[2], Britta Kuhlmann[2], Anna Brochtrup[2], Alexandra Grimm[1], Mathias Alenius[3], Adrian Moore[4] and Thomas Hummel[1*]

[1]Department of Neurobiology, University of Vienna, Althanstr. 14, 1090 Vienna, Austria

[2]Institut für Neurobiologie, Universität Münster, Badestr. 9, D-48149 Münster, Germany

[3]Department of Molecular Biology, 6K och 6L, SjukhusområdetUmeå universitet, 901 87 Umeå

[4]Disease Mechanism Research Core, RIKEN Brain Science Institute, Wako, Saitama, Japan

* Corresponding author: thomas.hummel@univie.ac.at

-- manuscript form --

4.1 Summary

Olfactory receptor neurons (ORNs) across the animal kingdom display a strict coupling of receptor type expression and axonal target selection. In insects and vertebrates, all sensory neurons expressing the same type of odorant receptor (OR) project their axons to specific synaptic glomerulus within the olfactory brain center. In contrast to the mouse olfactory system, where multifunctional ORs control singular receptor type expression as well as sensory axon targeting, little is known about the OR-independent mechanism underlying monospecificity of insect ORNs. Here we show that tightly coordinated differentiation of sensory and synaptic identity in a subset of Drosophila ORNs is mediated through a novel dynamic function of the chromatin regulator Psc, a component of the Polycomb repressor complex (PRC). Loss of Psc in ORN precursors does not affect initial lineage-based neuronal diversification but results in an ambiquous synaptic specificiy and a defined switch in OR gene expression. In projecting ORNs, Psc stabilizes the expression of Svp, which is critical for class-specific axon-axon segregation. In the subsequent step of OR gene selection, Psc suppresses the default OR expression thereby allowing the alternative OR gene selection. Surprisingly, during this binary OR gene choice Psc functions in a dose-dependent manner and independently of the PRC-mediated Hox gene regulation. These results revealed two independent mechanisms for the expression of axonal recognition molecules and odorant receptors, which are orchestrated through differential Psc activity during olfactory system assembly.

4.2 Introduction

A multitude of peripheral sensory neurons provides essential information about the external world to integration centers in the brain. During development, the differentiation of sensory neurons into specialized subclasses is an essential prerequisite for the discriminatory capacity of sensory systems. Differentiation diversity and specificity is most impressive in the olfactory system. In the mouse, the 10^6 sensory neurons in the nasal epithelium can be subdivided into roughly 1200 ORN classes, characterized by the selective expression of a single odorant receptor type[1,2]. All sensory neurons of the same OR class project their axons to 1-2 synaptic glomeruli in the primary olfactory brain center, thereby creating a precise odotopic map in the brain[3]. Likewise, in the Drosophila olfactory system around 1500 sensory neurons are grouped into 50 OR classes and connect in the brain according to the "One neuron-One receptor-One glomerulus" rule[4-6]. However, despite their similar morphological and functional organization, different types of control mechanisms seem to govern the development of the fly and vertebrate olfactory system[7].

In mouse, ORs are multifunctional receptors that mediate not only odor detection in the adult animals but are directly involved in the selective expression of a single OR gene and glomerulus-specific axon guidance in the developing nervous system. A negative-feedback regulation of stochastically selected ORs ensures the "One neuron - One receptor" rule[8,9].update on OR regulation! In addition, OR-derived signaling directs axonal projection of sensory neurons through the transcriptional regulation of axon-guidance and axon-sorting molecules, thereby guaranteeing the "One neuron - One glomerulus" rule[10]. During olfactory system development of Drosophila, class-specific OR expression starts after sensory neuron axons have segregated into distinct synaptic glomeruli, indicating an OR-independent mechanism in ORN connectivity[11]. Furthermore, deletion of OR genes as well as OR misexpression has no effect on the corresponding axonal glomerulus specificity[12,13] thereby excluding a central role of ORs in the regulation of sensory neuron differentiation. In contrast to the stochastic distribution of ORN subtypes in the mouse sensory epithelium, olfactory neurons in the Drosophila sensory epithelia are grouped into distinct sensilla classes, e.g. trichoid and basiconic sensilla[14], with a fixed combination of 1-4 ORNs for each sensillar subtype[5,15].

ORNs inside each sensillum derive from a common sensory organ precursor (SOP) cell, which, in a series of divisions, generates up to four neurons as well as outer support cells[16,17]. Notch-mediated cell-cell signaling among the SOP progenies controls the initial diversification of the SOP lineage[18]. For example, mutations in *numb* leads to the duplication of one ORN class at the expense of the alternative fate[18]. Genetic analysis identified a set of transcriptional regulators that affect different aspects of OR expression and axon targeting suggesting a combinatorial code for ORN subtype specification[19-22]. In addition, the characterization of OR upstream regulatory elements[20,23] and mutations in the *miR-279* micro-RNA[24] supports a model in which a combination of positive and negative factors restrict receptor gene expression to one of the two olfactory epithelia, the antenna or maxillary palps. However, the developmental control mechanisms that coordinates class-specific OR selection and axonal connectivity are still unknown.

Here we describe a novel multifunctional role of the Polycomb group gene *Posterior sex combs* (*Psc*) in the regulation of central aspects of neuronal differentiation for a subset of *Drosophila* ORNs. First, Psc coordinates ORN class-specific target glomerulus selection and odorant receptor choice . Second, differences in the level of Psc among lineage-related ORNs determine neuronal subtype diversification from a common precursor. As the Psc homologe BMI-1 has been shown to regulate the transition from pluripotent precursor cells to committed neurons in vertebrates, a conserved molecular mechanism may coordinate critical steps in neuronal differentiation.

4.3 Results

Mutations in *Psc* lead to a specific switch in ORN identity

Using a Synaptotagmin-GFP fusion protein expressed under the control of an OR47b regulatory element[5,6], the axonal convergence onto the VA1v glomerulus can be visualized in the *Drosophila* adult olfactory system (Fig. 1a, c). In a mosaic screen for mutations that affect sensory neuron development[25,26] we identified an allele of *Posterior sex combs* (Psc^{III09}), which leads to a specific change in the ORN47b>SytGFP innervation pattern (Fig. 1b, h). In addition to the VA1v innervation, *Psc* mutants show an ectopic ORN47b>SytGFP labeling in the neighboring VA1d glomerulus and the dorsally located DL3 glomerular region (n>30, 100% penetrance). In wild type, the glomeruli VA1d and DL3 are targeted by axons from the ORN88a and ORN65a classes, respectively, which are grouped together with ORN47b in the olfactory at4 sensillum (Fig. 1a, b, d, e). Similar to the ORN47b class, homozygous *Psc* mutant OR88a neurons innervate VA1d and the neighboring VA1v glomerulus (Fig. 1i). The simultaneous labeling of ORN47b and ORN88a revealed a mixing of axons of both ORN classes without any clear glomerular boundary (Fig. 1f, k). In contrast to ORN47b and ORN88a, *Psc* mutant OR65a neurons show a reduction in the DL3 innervation but no ectopic labeling of the other two glomeruli (Fig. 1e, j). Inside the DL3 glomerulus, the remaining ORN65a axons segregate from the ectopic ORN47b axons (Fig. 1g, l).

Taken together, loss of *Psc* in neighboring ORNs of the at4 sensillum leads to a characteristic switch in their neuronal identity. As previous studies have shown that ORNs occupying the same sensillum are lineage-related[18], these class-specific defects suggest a mechanism in which Psc controls the precise segregation of individual fates from a common precursor cell. The null allele $Psc^{H27\ 27}$ leads to the same changes in glomerular innervation of ORN47b, 65a, and 88a compared to Psc^{III09} (Supplementary Fig. 1) and no Psc protein expression can be detected in homozygous mutant Psc^{III09} antennal cells (Supplementary Fig. 2), indicating a loss-of-function mutation. To test if *Psc* is required for the development of other ORN classes, we analyzed additional sensilla types (Supplementary Fig. 3). Similar to the at4 ORNs we observed ectopic innervation and local axon mixing for Psc mutant ORNs most prominent in sensilla types which house more than 2 neurons, e.g. ab1 (4 neurons), at4, ac1-3 (all 3 neurons), indicating a critical role in neuronal diversification among lineage-related precursor cells.

Psc controls ORN class-specific axon sorting and axon-dendrite matching

We noticed that the even distribution of at4 ORN axon terminals among the three glomeruli in wild type has changed in *Psc* mosaics indicating defects in the ORN axon sorting (Fig. 2a, b). In genetic mosaics, which contain a smaller number (5-10) of *Psc* mutant 47b ORNs, homozygous axons often segregate out from their wild type neighbor axons and accumulate at the border between the VA1v and VA1d glomerulus (Fig. 2e, f). As we increased the amount of *Psc* mutant ORNs, their axons spread evenly across the VA1v/VA1d field and no glomerular boundaries can be detected (Fig. 2c, d). This is consistent with previous findings showing that ORN axon identity is a major determinant of glomerular integrity[28,29]. In addition, loss of *Psc* in ORNs affects the class-specific axon-dendrite matching into glomerular units (Supplementary Fig. 4). These results show that *Psc* provides critical aspects for the ORN synaptic identity.

Next we followed the projection of individual ORNs, which in wild type show a restricted elaboration of axon terminal arborization inside the target glomerulus (Fig. 2g, j). Axons of single *Psc* mutant ORN47b neurons no longer respect glomerular boundaries but extend into multiple glomeruli, most obvious in the co-innervation of VA1v and VA1d (Fig. 2h, l). Similar to the larger mosaics described above, the ectopic innervation of single mutants ORNs remains restricted to the three target glomeruli of the at4 neurons. Most strikingly, terminal branches of single *Psc* mutant ORNs often occupy the VA1v/d and the DL3 regions (Fig. 2i). Loss of *Psc* in single ORN88a also results in an axonal crossing of the VA1v/d glomerular boundary (Fig. 2k, l). These single cell phenotypes indicate that individual *Psc* mutant ORNs posses a "multiple recognition identity" that allow the corresponding axons to connect to all three target glomeruli of the at4 ORNs. From these data we conclude that Psc cell-autonomously restricts the multipotent fate of sensory precursors to defined ORN axon identities.

Loss of *Psc* leads to a switch in OR gene expression

To determine if *Psc*, in addition to regulate axon recognition identity, also controls odorant receptor choice, we analyzed OR expression in the at4 sensillum (Fig. 3). In wild type, trichoid sensilla are enriched at the lateral surface of the adult antenna (Fig. 3a). No obvious changes in the total number and distribution of at4 sensilla, visualized by the simultaneous labeling of ORN47b, 65a and 88a, can be detected in *Psc* mosaic antenna (Fig. 3d, 45+/-5 ORNs, >10 antenna) compared to the wild type antenna (Fig. 3a, 43+/-4 ORNs; >10 antenna). By visualizing

individual ORN classes, we observed a similar distribution of ORN47b in *Psc* mosaics, but accompanied by multiple OR47b-positive neurons per sensillum (Fig. 3b, e). In contrast, the total number of Or88a- and OR65a-positive ORNs in *Psc* mutant antenna is strongly reduced (Fig. 3c, f, data not shown).

To further characterize the changes in OR expression, we performed antennal sections containing sensory epithelia positively labeled using the MARCM technique[25]. In wild type antennae, the ORNs of the at4 sensillum can be identified as clusters of three Elav-positive neurons, with each cluster containing a single Or47b expressing neuron (Fig. 3g, g'). *Psc* mutant at4 sensilla still contain a total of three Elav-positive neurons, but here two or all three of them express Or47b (Fig. 3h, h'). In contrast, the remaining Or88a or Or65a positive at4 sensilla in *Psc* mosaics show no increase in the number of Or88a- or Or65a- expressing neurons (Fig. 3i, j and data not shown). To determine if the changes in OR expression is caused by a receptor switch or due to receptor co-expression we simultaneously visualized Or47b and Or88a. Compared to the precise pairing of ORN47b/88a neurons in the wild type antenna (Fig. 3k, k'), mutant antennae show an increase in the number of OR47b-positive neurons correlated with a loss of Or88-expressing neurons in the same sensillum (Fig. 3l, l'). Similarly, double labeling of Or47b- and Or65a-positive neurons show a switch of Or65a into Or47b expression with no sign of receptor co-expression (Fig. 3m, n). Together with the class-specific axon projection defects described above, these data show that Psc is a critical component in the coordination of sensory and synaptic ORN identity. In contrast to multiglomerular innervation of single *Psc* mutant ORNs, no signs of OR co-expression could be detected, suggesting distinct control mechanisms for axon identity and receptor choice downstream of Psc.

Loss of *Psc* does not affect the ORN precursor lineage

ORNs housed in the same sensillum are derived from a common precursor and generated through a series of asymmetric divisions during the first 10-20 h of pupal development[18]. The neuronal progenitors of the SOP lineage can be identified by the expression of Senseless in early dividing progenitors and Elav in post-mitotic differentiating ORN precursors (Fig. 4h). In large *Psc* mutant antennal mosaics we did not find any changes in the segregation of neuronal and non-neuronal precursors in the antennal trichoid precursor field (data not shown). In addition, the induction of single *Psc* mutant sensory organ precursor does not affect the following two

divisions leading to four Elav-positive ORN precursors (Fig. 4i/i', j/j'). These results indicate that Psc does not control early ORN precursor specification but regulates subsequent neuronal differentiation.

To follow the neuronal precursors during development, we first determined the lineage-relationship of the at4 ORNs through *hs-Flp* induced MARCM clones (Supplementary Fig. 6). In agreement with previous studies we found a preferential co-segregation of the Or47b- and Or88a-identity in 2-cell MARCM clones. Using a combination of OR reporter and developmental ORN subclass markers (e.g. *seven-up* (*svp*)[18]) we conclude that the final division of the neuronal precursor pNa give rise to the ORN47b/88a precursors (Naa/Nab) whereas ORN65a develops from the pNb precursor (Fig. 4h, k).

To further characterize the role of Psc in ORN differentiation, we followed the expression of Svp and *E132-Gal4* (enhancer trap of the *unpaired* locus) as early and late ORN88a differentiation marker, respectively (Fig. 4l, o, p). Similar to the early expression of Sens and Elav described above, the loss of *Psc* does not affect the onset of Svp expression in ORN88a precursors despite a subsequent Or gene switch (Fig. 4m, m'). However, a strong reduction in the *E132-Gal4* level could be observed in mutant 88a precursors (Fig. 4o, o', q), indicating that Psc controls specific aspects of ORN identity. Similarly, loss of Psc leads to an increase in the expression of the early ORN47b marker *fruitless* (data not shown). As we did not detect differences in the expression of general neuronal differentiation markers (Supplementary Fig. 7), the primary targets of Psc regulation are most likely ORN class specific differentiation factors.

Psc stabilizes Svp expression to support ORN synaptic identity

To further characterize the role of Psc in ORN subclass-specific differentiation, we analyzed the expression dynamics of Svp, which specifies the Psc sensitive Naa precursors in 3-neuron sensilla (Fig. 5). In the at4 sensillum, loss of Svp results in a complete switch of ORN88a into ORN47b differentiation (Fig. 5a-f). In *Svp*-mutant clones, the amount of OR88a expressing neurons is severely reduced (Fig. 5a, b) with a corresponding increase of OR47b-positive neurons in the antenna and antennal lobe (Fig. 5c, d). The wild type organization with a strict coupling of OR47a/88a expression is lost in *Svp* mutant clones accompanied with two ORN47b per sensillum (Fig. 5e,f). In contrast, no change in the expression and projection of ORN65a can be

detected in *Svp* mutants (Fig. 5g, h). In *Psc* mutant clones, we observed the complete loss of Svp expression in the adult olfactory system, indicating a critical role of Psc in maintaining Naa precursor identity (Fig. 5i,j). As described above, developmental analysis revealed that initial Svp expression during lineage divisions is not changes in Psc mutants which allowed us to follow ORN88a axonal projections (Fig. 5k-m). During midpupal development, wild type axons of Svp-positive ORNs arborize homogenously throughout the newly formed glomeruli (Fig. 5k) In Psc mosacis, axons of Svp-positive ORN classes reach their target glomeruli but fail to integrate into the dendritic field and segregate at the glomerular boundaries apart from the wild type axons in the center (Fig. 5l, m). A similar axon segregation phenotype of *Psc* mutant ORNs can be observed in the adult AL of other sensilla types, in which the endogenous OR gene expression (e.g. OR43a) is partially maintained (Fig. 5l, m). These results identified Psc as a critical regulator of neuronal diversificaiton by maintaining the initial differentiation program induced during lineage divisions.

To further determine the spatial and temporal requirement of Psc in ORN differentiation, we performed a series of *Psc* knock down experiments using targeted *Psc-RNAi* expression (Fig. 6). The expression of *Psc-RNAi* (VDRC) under the control of the pan-neuronal driver *elav-Gal4*, which starts expression during SOP division[18] results in the differentiation of up to three OR47b-positive neurons per at4 sensillum combined with an accumulation of their axons in the VA1v/d glomerular regions (Fig. 6a-d). In contrast, the expression of *PscRNAi* at the stage of subsequent neuronal differentiation (e.g. *E132-Gal4*, *Connectin-Gal4*) has only weak effects on ORN subtype differentiation (Supplementary Fig. 8 and data not shown). Similarly, the knock down of Psc in late differentiating ORNs using different *Or-Gal4/UAS-PscRNAi* combinations does not change the neuron-specific receptor selection (Supplementary Fig. 8). These data indicate a critical window of Psc activity during initial ORN differentiation.

In wild type, the onset of OR expression occurs in an ORN class-specific order[11] (see Fig. 6i) in which OR47b starts to become expressed at mid-pupal development (50h APF) followed by the onset of OR88a about a day later (70-80h APF) and OR65a expression shortly before eclosion (90-100h APF). To determine if the loss of *Psc* leads to a switch in the developmental sequence we followed ORN development throughout pupal development. In the *Psc* mutant background we could detect 2-3 ORNs starting 47b expression at mid-pupal development (45-50h APF) in

contrast to a single 47b-positive ORN per sensillum in wild type (Fig. 6g', e'). Similarly, axonal innervation of 47b-positive neurons occupies both VA1v and VA1d protoglomeruli (Fig. 6e-g). These data shows that Psc activity during initial ORN precursor development triggers subtype-specific differentiation programs.

Instructive role of the Psc expression level in ORN subclass specification

The temporally-restricted function of Psc in ORN differentiation is supported by rescue experiments using a wild type *Psc* transgene in the mutant mosaic nervous system (Fig. 7). Similar to the targeted *Psc-RNAi* studies described above, we observed a narrow temporal window of *Psc* requirement for at4 ORN development between 10-20h APF, at which we could rescue the Or47b phenotype (Fig. 7a-c). In the course of these rescue experiments we detected a dose-dependent effect of *Psc* on ORN subtype differentiation (Fig. 7d-f). In contrast to additional OR47b differentiation in the loss-of-function situation, an increased level of Psc during the time of ORN precursor division leads to the reduction in the number of OR47b- and a gain of OR88a- and OR65a-neurons (Fig. 7g-i,data not shown). These experiments suggest that the Psc level in dividing sensory neuron precursors directly controls their OR subclass identity (Fig. 7s). In agreement with this model, mosaics of the Psc^{E22} allele, which has been described as a gain-of-function mutation[27] and displays an increase in Psc expression (Fig. 7l, Supplementary Fig. 2), showed a strong reduction in the number of ORN47b accompanied by a gain of OR88a neurons (Fig. 7o-r, Supplementary Fig. 1).

In developing sensory epithelium we observed a highly dynamic expression of Psc (Fig. 8). First, during cell division of the SOP lineage, Psc becomes enriched in the neuronal precursors compared to the outer support cells (Fig. 8a-d). Second, different levels of Psc can be detected between Sens- and early Elav-positive neurons, with enriched Psc-positive accumulations in one of the ORN precursors compared to its sensillum neighbors (Fig. 8d-e). The higher Psc accumulation correlates with the level of Sens expression in the pNb precursor (Fig. 8f, f'). Thus, the differential Psc expression among lineage-related ORN precursors is in agreement with phenotypic data, where a low Psc activity supports ORN47b differentiation and high Psc expression induce ORN88a/65a differentiation. From these data we propose a model in which Psc not only stablizes intial differentiation programs but directly triggers divergent differentiation programs in ORN precursors (Fig. 8g).

A novel dynamic Psc function independent of canonical PRC gene regulation

As Polycomb group genes are known to control segment identity [30], we analyzed the organization of the antennal anlage (Fig. 4). No difference in the polarity of the antennal disc as well as the early specification of the 3rd antennal segment can be observed in *Psc* mutant clones (Fig. 4a, data not shown), confirming earlier findings that the loss of *Psc* does not affect patterning of the disc epithelial field due to redundant gene function [27,31].

The *in vivo* function of Psc has been analyzed so far in the context of a conserved Polycomb repressor complex (PRC), which regulates Hox gene expression during development [30,32]. As we did not detect a mis-expression of Hox genes in *Psc* mutant ORN precursors (Fig. 4b), we analyzed ORN identity in mutants affecting other components of the PRC1/2 repressor complex (Fig. 9e-g, Supplementary Fig. 5). Although genetic mosaics for some of the PRC genes show changes in the arrangement of glomerular organization (e.g. *Pc*, *E(z)* Fig. 4f, g) and ORN labeling (e.g. *esc* Fig. 4e), we did not observe the characteristic switch in ORN47b/65a/88a differentiation typical of *Psc* mutants (compare to Fig. 1). This is not due to the perdurance of gene function in the mosaic tissue, because we could detect, in contrast to *Psc* (Fig. 4b), ectopic Hox gene expression in olfactory epithelium mosaics for the PRC1/2 components (Fig. 4c, d, data not shown). These results indicate a novel dynamics Psc function during ORN differentiation distinct from the canonical PRC mechanism of Hox target gene regulation.

4.4 Discussion

The precise coordination of sensory and synaptic specificity in the peripheral olfactory system is an essential prerequisite for proper information processing. In contrast to the OR-mediated regulation of mouse sensory neuron differentiation [10], little is known about the activity-independent mechanism underlying the strict linkage of OR type and synaptic target selection in the insect olfactory system. In Drosophila, a couple of mutations have been described that lead to the loss of OR expression in a sub-population of sensory neurons [19,21,22], but these genes seem to mediate the onset or maintenance of receptor expression rather than OR gene choice. Similarly, loss of axonal cell surface molecules such as Dscam and Semaphorin leads to a random glomerular mistargeting instead of a specific switch in ORN synaptic target selection [26,28]. Here we show that the chromatin modulator Psc defines a critical component in the coordinated

differentiation of Drosophila ORNs. During a narrow developmental period of early olfactory system development, Psc not only mediates the restriction of a multipotent precursor to a single ORN identity, but also organizes the sensory neuron-subclass specific assembly of the olfactory sensillar unit. In contrast to a complete ORN identity switch in mutants affecting Notch signaling[18], *Psc* mutant ORNs posses multiple axon recognition identities, which represent all differentiation features of the sensillum cluster. From these data we are proposing a model in which the developmental potential of pluripotent ORN progenitors segregating from different epithelia position is restricted to a small set of alternative fates and the level of Psc triggers distinct differentiation programs that lead to the subclass-specific sensory and synaptic identity (Fig. 8g).

As a central part of the Polycomb-Repressor-Complex (PRC), Psc has been characterized so far in the regulation of Hox gene expression during embryonic patterning[27]. Recent studies have revealed that PRC-mediated Hox gene regulation controls different aspects of neuronal development in *Drosophila*, including neuroblast proliferation[33], neuronal differentiation in the CNS[34] and the PNS[35]. The data presented here show that in the *Drosophila* olfactory system, Hox genes are not the targets of *Psc*-mediated gene regulation. First, we did not find a deregulation of Hox genes in the *Psc* mosaic tissue. Second, *Su(z)2* and *Psc* do not function in a redundant fashion in at4 ORN differentiation. Third, the loss of other PRC genes cause only mild defects on ORN differentiation despite the fact that a strong ectopic expression of Hox gene can be observed. In addition to the control of gene expression via Hox gene regulation, recent genomic profiling of PRC targets indicate that >1–5% of genes in mice, humans and flies are directly regulated via chromatin modification[36-39]. The vast majority of these PRC targets encode transcription factors that are important for specifying cell fates during development.

Studies in vertebrates identified novel dynamic Polycomb targets that behave very different to the Hox-mediated long term repression[39]. For example, in an in vitro differentiation model for neurogenesis, many neuron-specific genes that become activated upon terminal differentiation are Polycomb targets only in progenitor cells[40]. Our analysis revealed a narrow developmental window of Psc function in ORN progenitors during the transition from proliferation to early differentiation, which could mediate a subclass-specific and transient target gene repression that is released through further induction signals. Interestingly, two classes of PRC genes can be

distinguished depending on whether their elimination leads to a rapid derepression of Hox genes, or a slow and spatially more complex destabilization of Hox gene silencing that occurs over many cell generations[41]. In contrast to the long-term stability of the Pc-mediated silenced state, the deletion of *Psc/Su(z)2* leads to rapid misexpression of Hox genes, suggesting a continuous requirement for transcriptional repression. In humans, Iwama et al. showed that Bmi-1 but not the other PcG components has a central role in the maintenance of hematopoietic stem cells, suggesting that Bmi-1 can behave as a core component of the PcG-independent complex in recruiting molecules essential for gene silencing[42]. In an in vitro model for chromatin remodeling, Psc has been shown to induce chromatin compaction independent of the other PRC1 components[27,43,44]. Further structure-function studies will provide crucial insights into the mechanisms of Psc/BMI-1 regulatory dynamics and its interaction with other PcG components in neuronal differentiation.

Bmi-1, the mouse homologue of Psc, is required for the self-renewal of several types of normal and cancer stem cells, including neural crest stem cells[45]. Interestingly, in addition to the transcriptional control of cell cycle regulators, Bmi-1 also seems to be involved in the specification of neuronal lineages in the resulting tumors[46,47]. Furthermore, recent studies have presented strong evidence that Bmi-1 expression levels exert an instructive influence on lineage commitment by I-type neuroblastoma cells, in which a BMI-1 reduction facilitates Schwann/glial cell differentiation and BMI-1 overexpression promotes I-type cell development along the neuronal lineage[48]. We found that Psc acts in a similar concentration-dependent manner to control ORN sub-class diversification in the Drosophila olfactory system. These observations suggest that graded activity of Psc/BMI-1 within individual progenitors could trigger divergent developmental programs responsible for neuronal heterogeneity.

Despite the fact that olfactory systems in vertebrates and insects share many anatomical and functional similarities, a distinct evolutionary origin of their odorant receptors as well as different developmental strategies to control sensory neuron identity suggest convergent evolutionary pathways[7]. In vertebrates stochastically selected OR genes ensure monospecificity in OR gene expression and axonal convergence, but the developmental control mechanisms underlying both differentiation processes are poorly understood. On the other hand, the chromatin regulator Psc acts as an initial coordinator of neuronal sensory and synaptic identity for each ORN as well as

neuron subclass combination within the Drosophila olfactory sensillar unit. Interestingly, transcriptional coordination of sensory and guidance receptor expression has recently identified in the *Drosophila* visual system[49]. These regulators of initial gene expression will provide a direct experimental approach to identify the relevant downstream components underlying neuron-specific differentiation pathways.

4.5 Material and Methods

Genetics

Fly stocks were maintained in standard medium at 25°C unless stated otherwise. The *Posterior sex combs* allele Psc^{III09} was identified in a histological mosaic screen using the *eyFlp/FRT* technique[26,29]**;** details of the mutagenesis screen will be published elsewhere. The stocks used were as follows: *FRT42* Psc^{III09} [this study]; Psc^{H27}, Psc^{e22}, *E132-Gal4* (*upd-Gal4*), $Psc^{CB05083}$ (*Psc-GFP*), *C155-Gal4*, *hsp70-FLP* [Bloomington Stock Center]; $P\{lacW\}svp^{S000512}$ [Szeged Drosophila Stock Centre]; *MZ19-Gal4*[50]; *hs-Psc* (N. Francis); *con-Gal4* [28], *Or47b-Gal4* [6], *OR47b::sytGFP*, *Or65a-Gal4*, *OR88a::mCD8GFP* [5], *Or88a-Gal4* [21], *UAS-mCD8GFP* [25], *UAS-rCD2*, *UAS-sytGFP*. *UAS-RNAi* lines were obtained from VDRC and NIG-Fly stock centers.

To label ORN projections *Or-Gal4>UASmCD8GFP/UASrCD2* and *Or-Gal4> UAS:sytGFP* combinations were used. *Or::GFP* fusions are used in RNAi knock down experiments as well as in combination with *Or-Gal4* lines for simultaneous labeling of two ORN classes. An *Or47b-Gal4 Or65a-Gal4 Or88a-Gal4 UAS-sytGFP* recombinant chromosome was generated for simultaneous labeling of all at4 neurons. Stocks for mosaic analysis were the following: Small size MARCM clones (1-5 ORNs) of *Psc* mutants and wild type were induced during larval stages with *hsFlp/FRT* system. Large MARCM clones were induced utilizing *eyFlp/FRT* system. A minute mutation (*PCNA*) was used to increase the clone size. Dissection and immunostaining of adult or pupal brains were performed according to standard procedures. For mosaic analysis in the 3rd antennal segment: 1) whole mount antenna expressing *Or::mCD8GFP* or *Or-Gal4>UAS-mCD8GFP* were dissected without fixation and visualized with confocal microscopy. 2) Cryostat sections of adult antenna were performed using *Or-Gal4>UAS-rCD2* for single ORN analysis or in combination with *Or::CD8GFP/Or::sytGFP* for double labeling experiments. SOP lineage

analysis were performed as previously described [18]. For rescue and overexpression experiments flies containing *hs-Psc* were heat-shocked for 30 min at 37°C at various stages.

Immunohistology

Primary antibodies used for immunohistochemistry were: rabbit anti-Psc (1:300; kindly provided by V. Orlando, rat anti-N-Cadherin extracellular domain (DN-Ex #8; 1:20; DSHB); rabbit anti-GFP (1: 1000; Molecular Probes); mouse anti-GFP(1:100; Molecular Probes), rat anti-Elav (1:10; DSHB); guinea pig anti-Senseless (1:1000; kindly provided by Hugo Bellen; mouse anti-Svp (1:100; kind gift of Y. Hiromi); mouse anti-Neuroglian (1:10; DSHB), mouse anti-Ubx and mouse anti-Connectin (kind gift of R.A. White); mouse anti-CD2; mouse anti-Cut; mouse anti-Beta-galactosidase (Cappel), mouse anti-Dachshund (1:10; DSHB), mouse anti-Invected (DSHB). Secondary antibodies: Secondary antibodies used were coupled to Alexa488, Alexa568 or Alexa647 (Molecular Probes). In cases where anti-mouse and anti-rat or anti-guinea pig antibodies were simultaneously used, Alexa coupled cross-adsorbed anti-mouse antibodies (Molecular probes) were preferred. Fluorescent samples were analyzed using a Zeiss Meta510 confocal microscope and images were processed with ImageJ and Adobe Photoshop.

4.6 Acknowledgments

We are grateful to B. Dickson and L. Vosshall for providing various OR reporter transgenes. We like to thank H. Bellen, G. Cavalli, N. Francis, Y. Hiromi, J. Müller, V. Orlando, R. Paro for providing mutants, transgenes and antibodies, R. Stilling for establishing *Psc* transgenes, H. Aberle, S. Bogdan, C. Klämbt and members of the Hummel and Klämbt lab for their very helpful comments on the manuscript.

4.7 Author Contributions

Ö. A. performed all the functional characterization of Psc in ORN development (MARCM analysis, RNA interference, gain-of-function studies, generation of transgenes, confocal imaging). R.K. analysed the Psc/Svp interactions. G. S. conducted the mosaic screen and identified the Psc^{III09} allele. A. B. contributed to the RNAi screen. B. K. performed the initial OR expression studies of Psc loss- and gain-of-function mutants. A.G. performed the Svp mosaic studies. M. A. and A. M. provided critical ideas and reagents. T. H. coordinated the work and wrote the manuscript.

4.8 References

1. Buck, L. & Axel, R. A novel multigene family may encode odorant receptors: a molecular basis for odor recognition. *Cell* 65, 175-87 (1991).
2. Mombaerts, P. Axonal wiring in the mouse olfactory system. *Annu Rev Cell Dev Biol* 22, 713-37 (2006).
3. Mombaerts, P. et al. Visualizing an olfactory sensory map. *Cell* 87, 675-86 (1996).
4. Fishilevich, E. & Vosshall, L.B. Genetic and functional subdivision of the Drosophila antennal lobe. *Curr Biol* 15, 1548-53 (2005).
5. Couto, A., Alenius, M. & Dickson, B.J. Molecular, anatomical, and functional organization of the Drosophila olfactory system. *Curr Biol* 15, 1535-47 (2005).
6. Vosshall, L.B., Wong, A.M. & Axel, R. An olfactory sensory map in the fly brain. *Cell* 102, 147-59 (2000).
7. Fuss, S.H. & Ray, A. Mechanisms of odorant receptor gene choice in Drosophila and vertebrates. *Mol Cell Neurosci* (2009).
8. Serizawa, S. et al. Negative feedback regulation ensures the one receptor-one olfactory neuron rule in mouse. *Science* 302, 2088-94 (2003).
9. Serizawa, S., Miyamichi, K. & Sakano, H. One neuron-one receptor rule in the mouse olfactory system. *Trends Genet* 20, 648-53 (2004).
10. Imai, T. & Sakano, H. Odorant Receptor Gene Choice and Axonal Projection in the Mouse Olfactory System. *Results Probl Cell Differ* (2008).
11. Vosshall, L.B., Amrein, H., Morozov, P.S., Rzhetsky, A. & Axel, R. A spatial map of olfactory receptor expression in the Drosophila antenna. *Cell* 96, 725-36 (1999).
12. Dobritsa, A.A., van der Goes van Naters, W., Warr, C.G., Steinbrecht, R.A. & Carlson, J.R. Integrating the molecular and cellular basis of odor coding in the Drosophila antenna. *Neuron* 37, 827-41 (2003).
13. Elmore, T., Ignell, R., Carlson, J.R. & Smith, D.P. Targeted mutation of a Drosophila odor receptor defines receptor requirement in a novel class of sensillum. *J Neurosci* 23, 9906-12 (2003).
14. Stocker, R.F. The organization of the chemosensory system in Drosophila melanogaster: a review. *Cell Tissue Res* 275, 3-26 (1994).

15. Hallem, E.A., Ho, M.G. & Carlson, J.R. The molecular basis of odor coding in the Drosophila antenna. *Cell* 117, 965-79 (2004).
16. Ray, K. & Rodrigues, V. Cellular events during development of the olfactory sense organs in Drosophila melanogaster. *Dev Biol* 167, 426-38 (1995).
17. Reddy, G.V., Gupta, B., Ray, K. & Rodrigues, V. Development of the Drosophila olfactory sense organs utilizes cell-cell interactions as well as lineage. *Development* 124, 703-12 (1997).
18. Endo, K., Aoki, T., Yoda, Y., Kimura, K. & Hama, C. Notch signal organizes the Drosophila olfactory circuitry by diversifying the sensory neuronal lineages. *Nat Neurosci* 10, 153-60 (2007).
19. Tichy, A.L., Ray, A. & Carlson, J.R. A new Drosophila POU gene, pdm3, acts in odor receptor expression and axon targeting of olfactory neurons. *J Neurosci* 28, 7121-9 (2008).
20. Ray, A., van der Goes van Naters, W. & Carlson, J.R. A regulatory code for neuron-specific odor receptor expression. *PLoS Biol* 6, e125 (2008).
21. Komiyama, T., Carlson, J.R. & Luo, L. Olfactory receptor neuron axon targeting: intrinsic transcriptional control and hierarchical interactions. *Nat Neurosci* 7, 819-25 (2004).
22. Clyne, P.J. et al. The odor specificities of a subset of olfactory receptor neurons are governed by Acj6, a POU-domain transcription factor. *Neuron* 22, 339-47 (1999).
23. Ray, A., van Naters, W.G., Shiraiwa, T. & Carlson, J.R. Mechanisms of odor receptor gene choice in Drosophila. *Neuron* 53, 353-69 (2007).
24. Cayirlioglu, P. et al. Hybrid neurons in a microRNA mutant are putative evolutionary intermediates in insect CO2 sensory systems. *Science* 319, 1256-60 (2008).
25. Lee, T. & Luo, L. Mosaic analysis with a repressible cell marker for studies of gene function in neuronal morphogenesis. *Neuron* 22, 451-61 (1999).
26. Hummel, T. et al. Axonal targeting of olfactory receptor neurons in Drosophila is controlled by Dscam. *Neuron* 37, 221-31 (2003).
27. King, I.F. et al. Analysis of a polycomb group protein defines regions that link repressive activity on nucleosomal templates to in vivo function. *Mol Cell Biol* 25, 6578-91 (2005).
28. Lattemann, M. et al. Semaphorin-1a controls receptor neuron-specific axonal convergence in the primary olfactory center of Drosophila. *Neuron* 53, 169-84 (2007).

29. Hummel, T. & Zipursky, S.L. Afferent induction of olfactory glomeruli requires N-cadherin. *Neuron* 42, 77-88 (2004).
30. Ringrose, L. & Paro, R. Polycomb/Trithorax response elements and epigenetic memory of cell identity. *Development* 134, 223-32 (2007).
31. Gaytan de Ayala Alonso, A. et al. A genetic screen identifies novel polycomb group genes in Drosophila. *Genetics* 176, 2099-108 (2007).
32. Bantignies, F. & Cavalli, G. Cellular memory and dynamic regulation of polycomb group proteins. *Curr Opin Cell Biol* 18, 275-83 (2006).
33. Bello, B., Holbro, N. & Reichert, H. Polycomb group genes are required for neural stem cell survival in postembryonic neurogenesis of Drosophila. *Development* 134, 1091-9 (2007).
34. Wang, J., Lee, C.H., Lin, S. & Lee, T. Steroid hormone-dependent transformation of polyhomeotic mutant neurons in the Drosophila brain. *Development* 133, 1231-40 (2006).
35. Parrish, J.Z., Emoto, K., Jan, L.Y. & Jan, Y.N. Polycomb genes interact with the tumor suppressor genes hippo and warts in the maintenance of Drosophila sensory neuron dendrites. *Genes Dev* 21, 956-72 (2007).
36. Oktaba, K. et al. Dynamic regulation by polycomb group protein complexes controls pattern formation and the cell cycle in Drosophila. *Dev Cell* 15, 877-89 (2008).
37. Tolhuis, B. et al. Genome-wide profiling of PRC1 and PRC2 Polycomb chromatin binding in Drosophila melanogaster. *Nat Genet* 38, 694-9 (2006).
38. Schwartz, Y.B. et al. Genome-wide analysis of Polycomb targets in Drosophila melanogaster. *Nat Genet* 38, 700-5 (2006).
39. Bracken, A.P., Dietrich, N., Pasini, D., Hansen, K.H. & Helin, K. Genome-wide mapping of Polycomb target genes unravels their roles in cell fate transitions. *Genes Dev* 20, 1123-36 (2006).
40. Mohn, F. et al. Lineage-specific polycomb targets and de novo DNA methylation define restriction and potential of neuronal progenitors. *Mol Cell* 30, 755-66 (2008).
41. Beuchle, D., Struhl, G. & Muller, J. Polycomb group proteins and heritable silencing of Drosophila Hox genes. *Development* 128, 993-1004 (2001).
42. Iwama, A. et al. Enhanced self-renewal of hematopoietic stem cells mediated by the polycomb gene product Bmi-1. *Immunity* 21, 843-51 (2004).

43. Francis, N.J., Saurin, A.J., Shao, Z. & Kingston, R.E. Reconstitution of a functional core polycomb repressive complex. *Mol Cell* 8, 545-56 (2001).
44. Francis, N.J., Kingston, R.E. & Woodcock, C.L. Chromatin compaction by a polycomb group protein complex. *Science* 306, 1574-7 (2004).
45. Jacobs, J.J., Kieboom, K., Marino, S., DePinho, R.A. & van Lohuizen, M. The oncogene and Polycomb-group gene bmi-1 regulates cell proliferation and senescence through the ink4a locus. *Nature* 397, 164-8 (1999).
46. Bruggeman, S.W. et al. Bmi1 controls tumor development in an Ink4a/Arf-independent manner in a mouse model for glioma. *Cancer Cell* 12, 328-41 (2007).
47. Zencak, D. et al. Bmi1 loss produces an increase in astroglial cells and a decrease in neural stem cell population and proliferation. *J Neurosci* 25, 5774-83 (2005).
48. Cui, H. et al. Bmi-1 regulates the differentiation and clonogenic self-renewal of I-type neuroblastoma cells in a concentration-dependent manner. *J Biol Chem* 281, 34696-704 (2006).
49. Morey, M. et al. Coordinate control of synaptic-layer specificity and rhodopsins in photoreceptor neurons. *Nature* 456, 795-9 (2008).
50. Jefferis, G.S. et al. Developmental origin of wiring specificity in the olfactory system of Drosophila. *Development* 131, 117-30 (2004).

Figure legends

Figure 1. Loss of Psc disrupts ORN class-specific innervation of olfactory glomeruli.

(a) Schematics illustrating the organization of the *Drosophila* olfactory system. Stereotype combination of sensory neuron classes inside each sensillar unit (e.g. OR47b, 88a, 65a for the at4 sensillum) and class-specific axon convergence onto synaptic glomeruli (VA1v, VA1d and DL3) in the antennal lobe. (b) In contrast to the innervation of glomeruli by a single ORN class in wild type, axons of *Psc* mutant ORNs show a characteristic mixture in glomerular targeting. (c-e) ORNs of the at4 sensillum display class-specific convergence onto single synaptic glomeruli in the wild type antennal lobe. (h-j) Multi-glomerular innervation of *Psc* mutant ORN47b and ORN88a but not ORN65a axons. (f, g, k, l) Axonal labeling of two different ORN classes shows a non-overlapping axon segregation into neighboring glomeruli in wild type but heterogeneous intra-glomerular intermingling of *Psc* mutant ORNs . Schematics of the right column illustrate

the ORN specific innervation defect in *Psc* mosaics. Genotypes: (c-e) *eyFlp; FRT42/FRT42 Gal80; Or-Gal4 UAS-sytGFP* (h-j) *eyFlp; FRT42 Psc/FRT42 Gal80; Or-Gal4 UAS-sytGFP* (f, g) *eyFlp; FRT42 Or:sytGFP/FRT42 Gal80; Or-Gal4 UAS-CD2* (k, l) *eyFlp; FRT42 Psc Or:sytGFP/FRT42 Gal80; Or-Gal4 UAS-CD2*. (C, D, E, H, I, J) anti-GFP (green), anti-Ncadherin (red), TOTO-3 (blue); (f, g, k, l) anti-GFP (green), anti-CD2 (red). Scale bar in C is 20mm.

Figure 2. Cell-autonomous function of Psc in ORN axon sorting

(a, b) Axonal projections of all three ORN classes (47b, 65a, 88a) located in the at4 sensillum shows an even glomerular distribution in the wild type antennal lobe (a) but glomeruli innervated by *Psc* mutant ORNs show a patchy axon segregation pattern (arrowheads) (b). (c, d) In *Psc* mosaics in which the majority of the at4 ORNs are homozygous mutant, the morphological boundary between the VA1v/d glomeruli (arrowheads in c) is no longer detectable leading to a large VA1 glomerulus (dotted line in d) whereas other glomeruli are not affected. (e, f) In small *Psc* mosaics with up to five mutant 47b-ORNs the corresponding axons segregate out from the surrounding heterozygous axons and accumulate at the glomeruli borders. (g-i) Single cell analysis of *Psc* mutant ORN47b revealed innervation of two (h) or three (i) glomeruli by terminals of a single axon in contrast to the singular glomerulus innervation in wild type (g). (j, k) Similarly, single *Psc* mutant 88aORNs elaborate in the VA1v/d area. (l) Quantification of the axon segregation phenotypes in *Psc* single cell mosaics. Genotypes: (a) *eyFlp; FRT42/FRT42 Gal80; Or47b-Gal4 Or65a-Gal4 Or88a-Gal4 UAS-sytGFP*; (b) *eyFlp; FRT42 Psc/FRT42 Gal80; Or47b-Gal4 Or65a-Gal4 Or88a-Gal4 UAS-sytGFP*; (c) *eyFlp; FRT42/FRT42 PCNA; Or47b-Gal4 UAS-sytGFP*; (d) *eyFlp; FRT42 Psc/FRT42 PCNA; Or47b-Gal4 UAS-sytGFP*; (e, g) *hsFlp UAS-CD2; FRT42/FRT42 Gal80; Or47b:sytGFP Or47b-Gal4 UAS-CD2* (f, h, i) *hsFlp UAS-CD2; FRT42 Psc/FRT42 Gal80; Or47b:sytGFP Or47b-Gal4 UAS-CD2* (j) *hsFlp UAS-CD2; FRT42/FRT42 Gal80; Or47b:sytGFP Or88a-Gal4 UAS-CD2* (k) *hsFlp UAS-CD2; FRT42 Psc/FRT42 Gal80; Or47b:sytGFP Or88a-Gal4 UAS-CD2.* (a-d) anti-GFP (green), anti-NCadherin (red), TOTO-3 (blue); (e-k) Or:sytGFP (green), OR-Gal4/UAS-CD2 (red), anti-NCadherin (blue).

Figure 3. Loss of *Psc* leads to a switch in odorant receptor expression

(a-f) Distribution of at4 ORNs in the 3rd antennal segment containing wild type (a-c) or *Psc* mutant (d-f) mosaics. (a, b) No changes in the overall distribution and number of at4 sensilla in antennal Psc mosaics (d) compared to wild type antenna (a). (b, e) No change in the spatial distribution of Or47b neurons but increase in the number of OR47b-positive neurons inside the at4 sensilla (arrowheads in insets). (c, f) Strong reduction in the number of Or88a-positive neurons in *Psc* mosaic antennae. (g, h) Antennal sections of adult antennae containing *Psc* mosaics show an increase in the Or47b number of up to three positive neurons per sensillum (h, h') whereas the remaining Or88a-positive sensilla show a wild type pattern (i, j). Double labeling of ORN47b/88a (k, l) and ORN47b/65 (m, n) revealed that the loss of Or88a and Or65a neurons is accompanied by a gain of Or47b neurons in the same sensillum. Genotypes: (a-c) *eyFlp; FRT42/FRT42; Or-Gal4 UAS-CD8GFP*; (d-f) *eyFlp; FRT42 Psc/FRT42; Or-Gal4 UAS-CD8GFP*; (g, h) *eyFlp; FRT42/FRT42 Gal80; Or-Gal4 UAS-CD8GFP* (j, k) *eyFlp; FRT42 Psc/FRT42 Gal80; Or-Gal4 UAS-CD8GFP*; (i) (l) *eyFlp; FRT42/FRT42 Gal80; Or88a:CD8GFP Or47b-Gal4 UAS-CD2* (l) *eyFlp; FRT42 Psc/FRT42 Gal80; Or88a:CD8GFP Or47b-Gal4 UAS-CD2* (a-f) anti-GFP (green); (g, h, j, k) anti-GFP (green), anti-Elav (red), TOTO-3 (blue); (i, l) anti-GFP (green), anti-CD2 (red), TOTO-3 (blue). Scale bar in A' is 20mm.

Figure 4. Loss of Psc does not affect ORN lineage specification

(a-d) Loss of Psc does not affect imaginal disc patterning. No changes were observed in the expression of Dachshund (Dac) (a) and Ultrabithorax (Ubx) (b) in the antennal disc containing GFP-negative *Psc* mutant clones compared to GFP-positive heterozygous cells. In contrast, loss of the PRC components E(z) (c) and Pc (d) leads to ectopic Ubx expression. (e-g') Mutations affecting the PRC components Esc (e, e'), E(z) (f, f') and Pc (g, g') do not show a switch in ORN identity. (h) Scheme of ORN lineage and differentiation in the at4 sensillum. (i, j) *Psc* mutant sensory organ precursors (SOPs) display a normal formation of lineage-related precursor specification with two Cut-positive and two Senseless (Sens)-positive precursors at the 4-cell stage (i and i' represent different optical sections of the same SOP clone) and four Cut-positive and four Elav-positive precursors at the 8-cell stage (j and j' represent different optical sections of the same SOP clone). (k, l) During subsequent ORN differentiation, ORN47b can be identified by receptor expression while the ORN88a precursors can be initially recognized by Seven-up (Svp) expression and during later stages by their *E132-G4* expression. (m-q') Loss of *Psc* in the SOP

does not change Svp expression (m, m') but leads to a strong reduction in the *E132-G4* level in the ORN88a precursors (o, arrowheads in o') and antennal lobe (q, q'). Genotypes: (a-d) *eyFlp; FRT42 Psc/FRT42 Ubi-GFP* (e-g') (i-j) *hsFlp elav-Gal4 UAS-CD8GFP; FRT42 Psc/FRT42 Gal80* (k) *eyFlp; FRT42 Or47b:CD8GFP/FRT42; svp-lacZ* (l) *eyFlp/E132Gal4; FRT42 /FRT42*; *svp-lacZ* (m, m') *eyFlp; FRT42 Psc Or47b:CD8GFP/FRT42; svp-lacZ;* (o, o') *eyFlp/E132Gal4; FRT42 Psc/FRT42 Ubi-GFP; UAS-CD2.* (p) *eyFlp/E132Gal4; FRT42/FRT42 Gal80* (q) *eyFlp/E132Gal4; FRT42 Psc/FRT42 Gal80* (a-f) anti-GFP (green); (e-g') anti-GFP (green), anti-Ncadherin (red), TOTO-3 (blue) (i-q) anti-GFP (Green).

Figure 5. Psc stabilizes Svp expression to support neuronal differentiation of the Naa precursor cell

(a-h) Loss of Svp results in a switch of ORN88a into ORN47b differentiation. In Svp-mutant clones, the amount of OR88a expressing neurons is severely reduced in the antenna lobe (b) and antenna (b') compared to the wild type expression (a, a'). In contrast to a single ORN47b in wild type at4 sensilla (c'), Svp mutants show two neighboring OR47b-positive neurons in the antenna (d'), which leads to a strong increase in the corresponding glomerulus (d) compared to the wild type innervation (c). The wild type organization with a strict coupling of OR47a/88a expression (e) is lost in *svp* mutant clones accompanied with an ORN47a increase (f). No change in the expression and projection of ORN65a can be detected (g, h). (i-o) Svp expression is initiated but not maintained in Psc mutants. (i) In the adult wild type, Svp-positive ORNs label the Naa identity of all 3-neuron sensilla, which innervate four distinct glomeruli in the lateral AL. (j) Loss of Psc leads to a complete absence of Svp expression in the adult olfactory system. (k,k') During midpupal development, wild type axons of Svp-positive ORNs arborize homogenously throughout the newly formed glomeruli. (l,m) In Psc mosacis, axons of Svp-positive ORN classes reach their target glomeruli but fail to integrate into the dendritic field and segregate at the glomerular boundaries apart from the wild type axons in the center. (n,o) A similar axon segregation phenotype of *Psc* mutant ORNs can be observed in the adult AL, in which the endogenous OR gene expression is partially maintained. Genotypes: (a, c, g) *eyFlp, UAS-mTomato; Or-Gal4; FRT82 Gal80/ FRT82* (b, d, h) *eyFlp, UAS-mTomato; Or-Gal4; FRT82 Gal80/ FRT82, Svp^{e22}* (e) *eyFlp, UAS-mTomato; Or47b-Gal4, Or88a-CD8GFP; FRT82 Gal80/ FRT82* (f) *eyFlp, UAS-mTomato; Or47b-Gal4, Or88a-CD8GFP; FRT82 Gal80/ FRT82, Svp^{e22}* (i, k) *eyFlp, UAS--CD8GFP; FRT42, UAS-CD8GFP /FRT42 Gal80; FRT82,Svp-Gal4* (j, l, m)

eyFlp, UAS-CD8GFP; FRT42, UAS-CD8GFP, Psc /FRT42 Gal80; FRT82,Svp-Gal4 (n) *eyFlp, UAS-CD8GFP; FRT42, UAS-CD8GFP/ FRT42 Gal80; Or43a-Gal4* (o) *eyFlp, UAS-CD8GFP FRT42, UAS-CD8GFP, Psc/ FRT42 Gal80; Or43a-Gal4* (a-h) UAS-mTomato (red), anti-Ncadherin (green) (i-o) anti-GFP (green); anti- Ncadherin (red), TOTO-3 (blue).

Figure 6. Loss of Psc leads to a switch in the ORN differentiation program

(a-d) The knock-down of Psc in the SOP using *elav-Gal4* driven *Psc-RNAi* expression leads to an increase in ORN47b accompanied by a reduction in ORN88a in the AL (inserts in a and b show at4 sensilla in the antenna). Development of the axon targeting (e-g) and OR expression (e'-g') phenotype of *Psc* mutant ORNs. In wild type antenna at 50h APF (After Pupae Formation), ORN47b axons have segregated from the ORN88a precursor axons (e, e'), but Or88a expression has not started yet (f, f'). Loss of *Psc* leads to an activation of Or47b in all three sensillar ORNs at 50h APF (g') and multi-glomerular innervation in the early antennal lobe (g). (i) Schematics illustrating the sequential onset of Or expression in the wild type antenna compared to *Psc* loss-of-function (LOF) background. Genotypes: (a, e, e') *elav-Gal4; OR47b:sytGFP,* (b, g, g') *elav-Gal4; UAS-> Psc; OR47b:sytGFP* (c, f, f') *elav-Gal4; OR88a:GFP,* (d, h, h') *elav-Gal4; UAS-> Psc; OR88a:GFP* . anti-GFP (green); anti-Elav (red), TOTO-3 (blue).

Figure 7. Dose-dependent activity of Psc in ORN subclass specification

(a-c) *Psc* mutant rescue experiments at different development stages. Expression of a wild type *Psc* transgene in a *Psc* mutant background leads to a rescue of the multiple ORN47 phenotype in a narrow temporal window (18h-20h APF). (d-i) The temporally-restricted overexpression of a *Psc* transgene in wild type leads to a strong reduction in the number of ORN47b (e, g) and a gain of ORN88a (h, i). (j-o) ORN subclass differentiation in the loss-of-function Psc^{H27} (k) and gain-of-function Psc^{E22} (l) mutants. In contrast to the Psc^{H27} mutations, which lead to an increase in the ORN47b and decrease in ORN88a number (k, n), the Psc^{E22} mosaics show a gain in ORN88a accompanied by the loss of ORN47b (l, o). (p-r) Antennal sections of Psc^{E22} mosaics show two OR88a neurons per sensillum (p) and the switch of OR47 neurons into OR88a neurons (r). (s) Schematics summarizing the dose-dependent Psc function in ORN subclass specification. Genotypes: (a-c) *eyFlp hs-Psc; FRT42 Psc 47bSytGFP/FRT42 Gal80.* (d-g) *eyFlp hs-Psc; FRT42 47bSytGFP/FRT42 Gal80.* (h, i) *eyFlp hs-Psc; FRT42/FRT42 Gal80;88a:CD8GFP.* (j) *hsFlp elav-Gal4 UAS-CD8GFP; FRT42/FRT42 Gal80*. (k, l) *hsFlp elav-Gal4 UAS-CD8GFP;*

FRT42 Psc/FRT42 Gal80. (m, q) *eyFlp; FRT42/FRT42 Gal80; Or88a:CD8GFP Or47b-Gal4 UAS-CD2* (n, o, r) *eyFlp; FRT42/FRT42 Gal80; Or88a:CD8GFP Or47b-Gal4 UAS-CD2* (p) *eyFlp; FRT42Psc/FRT42 Gal80; Or88aGal4 UAS-CD8GFP*. Labeling (a-i) anti-GFP (green), anti-NCadherin (red); (j-l) anti-GFP (green), anti-Psc (red), anti-Elav (blue); (m-o, q, r) anti-GFP (green), anti-CD2 (red), anti-NCadherin (blue);

Figure 8. Dynamic expression of Psc in the peripheral olfactory nervous system

(a, b) Differential expression of *Psc* in the developing antenna (20h APF). The level of *Psc-GFP* is higher in the inner layer containing the neuronal precursors compared to the outer support cells (a). In addition, different levels of Psc can be detected among neighboring ORNs (b). (c-f) Analysis of Psc expression in the SOP lineage. At the 4-cell stage, the two neuronal precursors express higher amounts of Psc compared to the support cells (c). By the time ORN precursors have stopped dividing, differential accumulation of Psc among lineage-related ORNs can be detected (d, e; anti-Psc staining intensity in false color mode in e'). (f, f') Accumulation of Psc correlates with the level of Sens in the pNa/pNb precursors. (g) Model of ORN subtype diversification through different Psc levels in the precursor cells. The pluripotent SOP has the potential to differentiate into each AT4 neuron. During subsequent cell divisions, Psc determines the OR choice in a dose dependent fashion as well as restricts the axonal tageting to correct glomerulus. Genotypes: (c-f) *hsFlp elav-Gal4 UAS-CD8GFP; FRT42/FRT42 Gal80.* Labeling (a-f) anti-GFP (green).

Supplimentary Figure legends

Supplimentary Figure 1. Loss of Psc disrupts ORN class-specific innervation of olfactory glomeruli. (a-c) Phenotypic analysis of the defined null mutation Psc^{H27} in ORN differentiation. Ectopic OR47b labeling in VA1d and DL3 glomeruli (a, a'), OR88a labeling in VA1d (b, b') and reduction in OR65a (c, c'). (d, f) Ectopic ORN innervation of the gain-of-function allele Psc^{E22}. A reduction in OR47b labeling in the VA1v glomerulus (d,d') and ectopic Or88a (e, e') and OR65a (f,f') labeling in VA1v.

Supplimentary Figure 2. Analysis of Psc mutants revealed different expression levels. Psc antibody staining of different alleles showed a loss of Psc protein in homozygous Psc^{III09} clones

(b) similar to defined null allele Psc^{H27} (a). In contrast, homozygous mutant Psc^{E22} cells show a highly enriched Psc expression (c).

Supplimentary Figure 3. Loss of Psc affects ORN development of trichoid sensilla. Psc mutant ORN in at3 sensillum (a-g) and at2 sensillum (h-l) display axon projection defects in the antennal lobe. In wildtype, ORN19a (b), ORN43a (c), ORN83c (i) and ORN23a (j) neurons innervate distinct glomeruli in a uniform and space filling manner. Double labeling of ORN19a and ORN43a shows distinct adjacent glomeruli in the wildtype (d). In *Psc* mutans, glomerular innervation of ORN19a/ORN43a is dispersed (e, f, g) and axons of the two classes do not sort out properly. Similarly, *Psc* mutant ORN23a axons enter the ORN83c target area (arrowhead in k and l).

Supplimentary Figure 4. Axon-dendritic interaction in Psc mosaics. Defects in seggregation of *Psc* mutant ORN47b/88a axon affect ORN-PN matching. (a, c) Inthe wild type antennal lobe, *Mz19*-positive PN dendrites occupy the VA1d glomerulus and interact with ORN88a axons (c) but are excluded from the ORN47b-positive VA1v glomerulus. (b, d) Axons of *Psc* mutant ORN47b interact with the *Mz19*-positive PN dendrites in the VA1d glomerulus (b), which is only partially innervated by ORN88a axons (d).

Supplimentary Figure 5. The function of Pc/Trx genes in ORN differentiation. Memebers of the Polycomb group (a-h) and Trithorax group (i-n) genes were tested in genetic mosaics (MARCM) for theit effect on ORN differentiation. A variety of phenotypes raning from a decrease in the amount of labeled neurons (e.g. *Su(z)2, Osa),* to different degrees of mistargeting (e.g. *Asx, trx*) and disruption of glomerular structure (*brm*) can be observed.

Supplimentary Figure 6. Lineage analysis of the at4 ORNs. Hs-Flp induced MARCM clones in the SOP or the following two cell division (1-3) in the wild type flies indicate the lineage relationship among the at4 neurons. SOP mosaics clones generate three labeled cells that innervate DL3, VA1d and VA1v glomeruli (1), showing the ORN65a, ORN88a and ORN47b are derived from the same precursor cell. PIIb mosaic clones generated two labeled cells innervating VA1d and VA1v glomeruli (2) showing ORN88a and ORN47b ar derived from the same precursor cell. Single ORN mosaics innervating VA1v (3) or VA1d (3).

Supplimentary Figure 7. General neuronal differentiation is not affected in *Psc* mutant antennae. Pan-neuronal knock down of Psc (*elav-Gal4> UAS-Psc RNAi*) does not lead to changes in the overall differentiation as indicated by HRP (a-d), Connectin (a-b) and Neuroglian (c-d).

Supplimentary Figure 8. Psc knock down in differentiating ORNs. Expression of *Psc-RNAi* at 30-40 hr APF with *E132-Gal4* (a) leads to mild ectopic Or47b labeling in VA1d glomerulus, wheras a knock down of *Psc* at around 50 hr APF with *Or47b-Gal4* (b, d) and 70 hr APF with *Or88a-Gal4* (c) has no effect on ORN differentitaion.

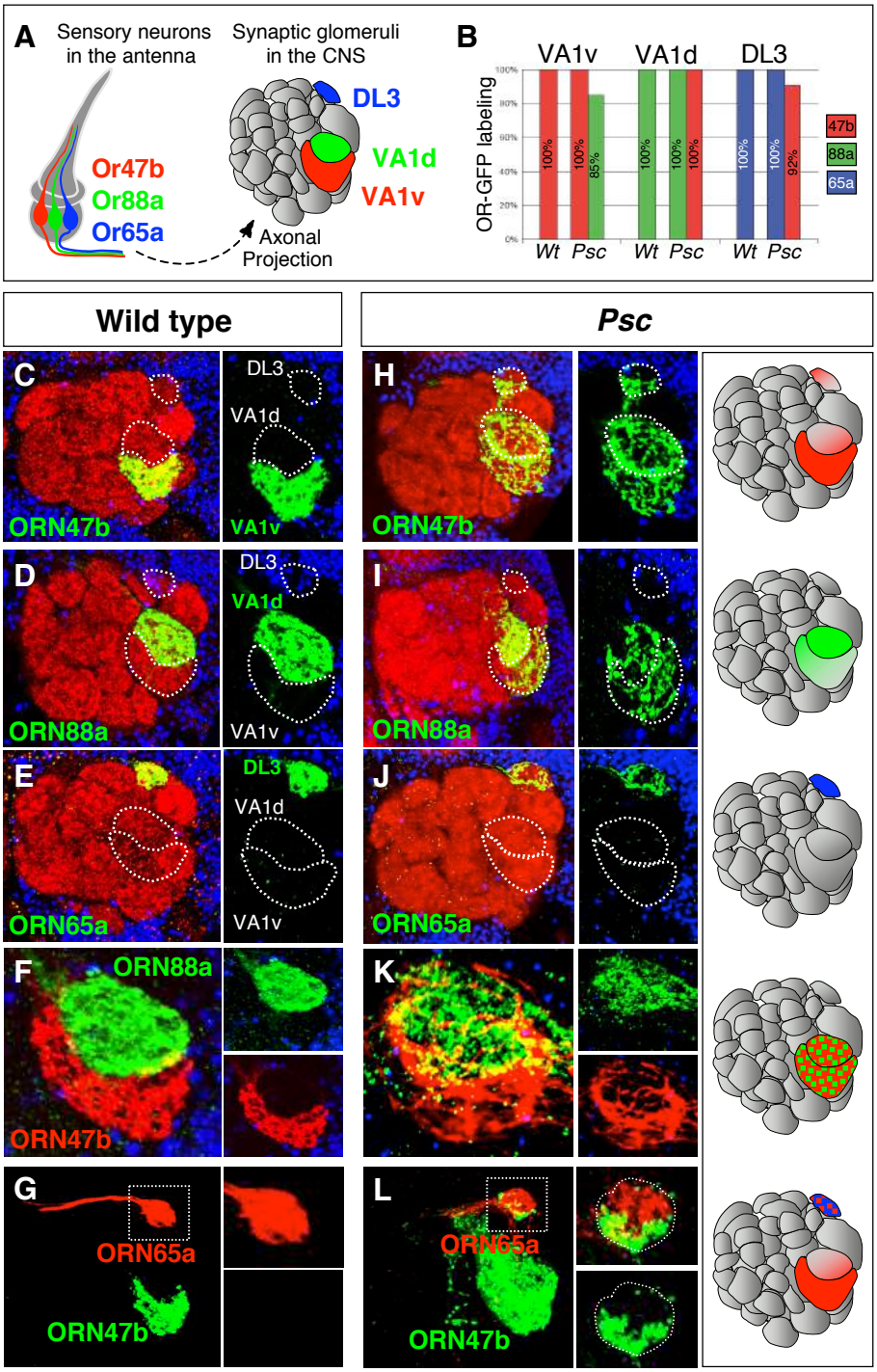
A
Sensory neurons in the antenna
Synaptic glomeruli in the CNS
Or47b
Or88a
Or65a
DL3
VA1d
VA1v
Axonal Projection
B
VA1v
VA1d
DL3
OR-GFP labeling
100%
100%
85%
100%
100%
100%
100%
100%
92%
47b
88a
65a
Wt Psc Wt Psc Wt Psc
Wild type
Psc
C
ORN47b
DL3
VA1d
VA1v
H
ORN47b
D
ORN88a
DL3
VA1d
VA1v
I
ORN88a
E
ORN65a
DL3
VA1d
VA1v
J
ORN65a
F
ORN88a
ORN47b
K
G
ORN65a
ORN47b
L
ORN65a
ORN47b

Figure 1

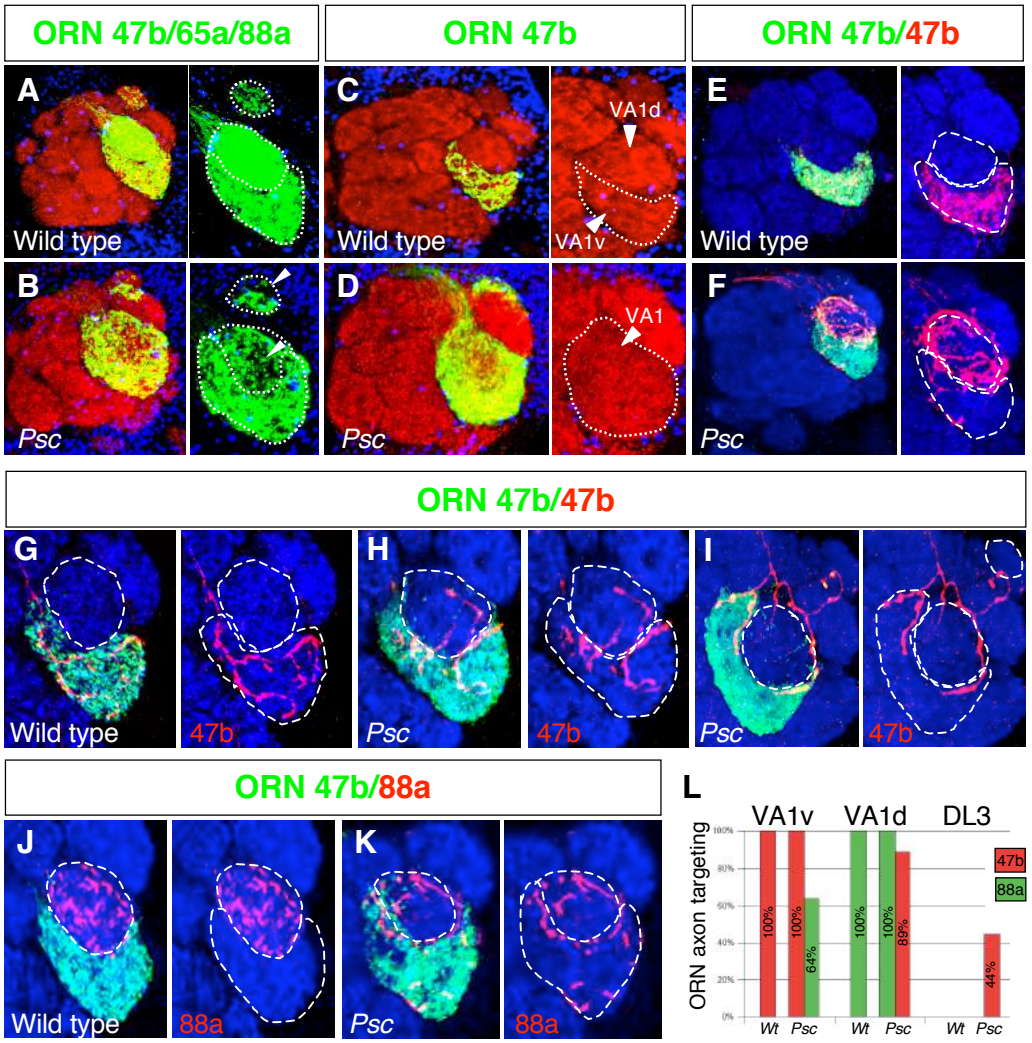
ORN 47b/65a/88a
ORN 47b
ORN 47b/47b
A
Wild type
C
Wild type
VA1d
VA1v
E
Wild type
B
Psc
D
Psc
VA1
F
Psc
ORN 47b/47b
G
Wild type
47b
H
Psc
47b
I
Psc
47b
ORN 47b/88a
J
Wild type
88a
K
Psc
88a
L
VA1v
VA1d
DL3
47b
88a
ORN axon targeting
100%
100%
64%
100%
100%
89%
44%
Wt
Psc
Wt
Psc
Wt
Psc

Figure 2

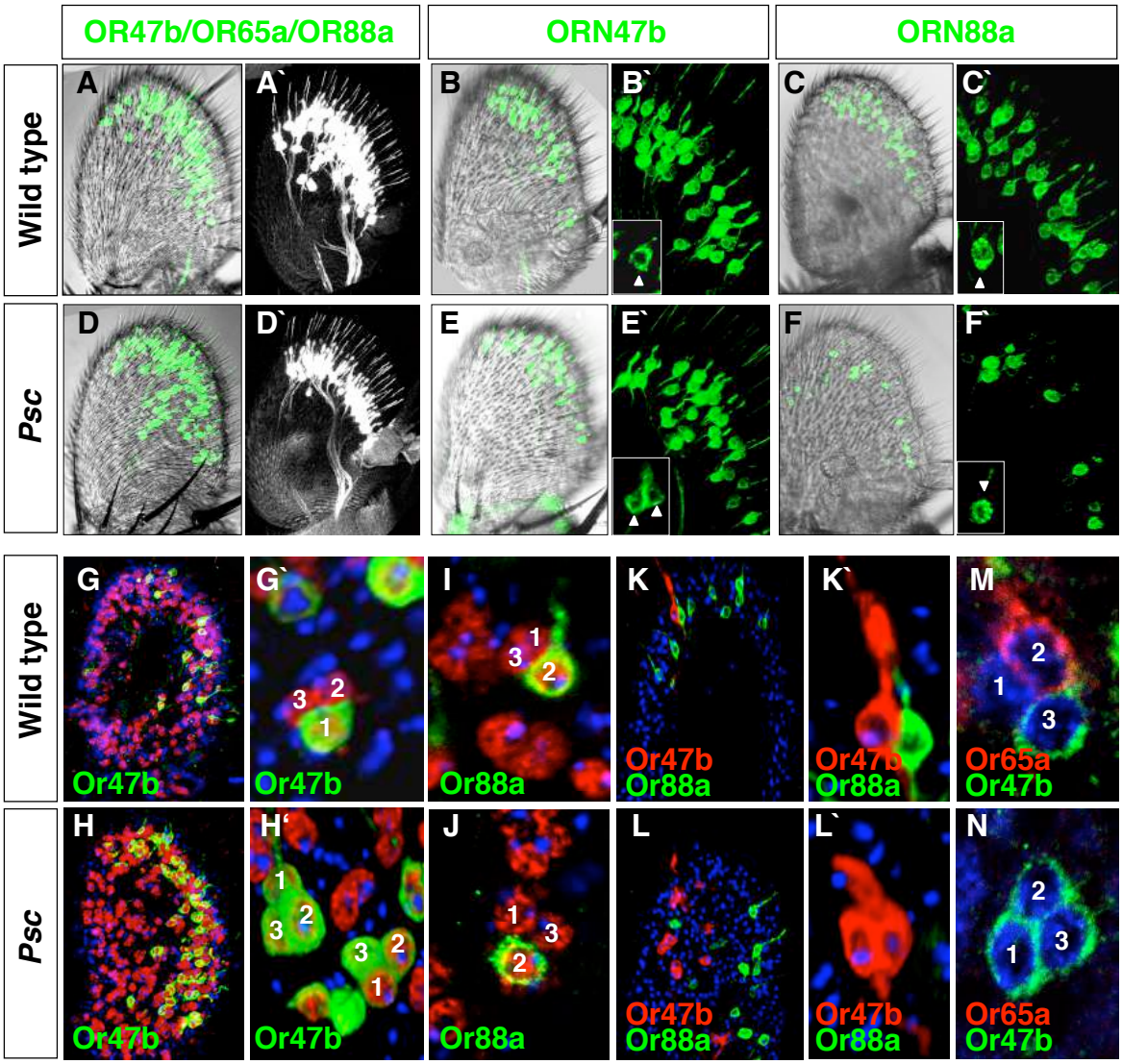
OR47b/OR65a/OR88a
ORN47b
ORN88a
Wild type
Psc
A
A`
B
B`
C
C`
D
D`
E
E`
F
F`
G
G`
I
K
K`
M
H
H`
J
L
L`
N
Or47b
Or88a
Or65a
1
2
3

Figure 3

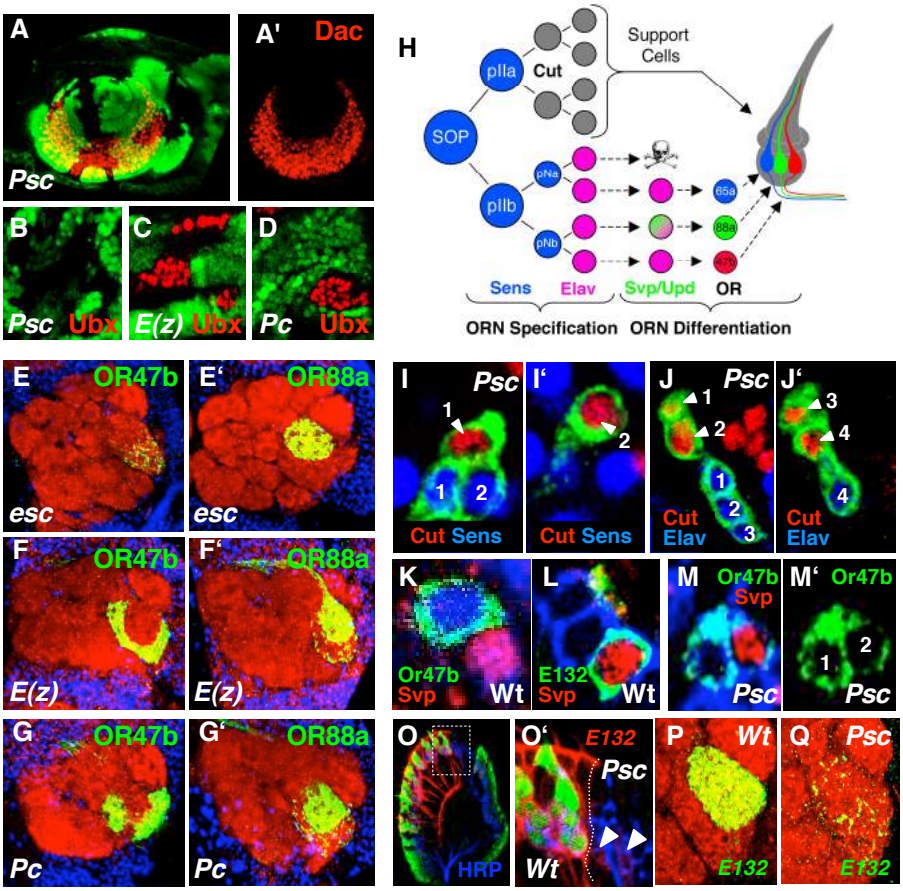
A
Psc
A'
Dac
B
Psc
Ubx
C
E(z)
Ubx
D
Pc
Ubx
H
Support
Cells
pIIa
Cut
SOP
pIIb
pNa
pNb
65a
88a
47b
Sens
Elav
Svp/Upd
OR
ORN Specification
ORN Differentiation
E
OR47b
esc
E'
OR88a
esc
F
OR47b
E(z)
F'
OR88a
E(z)
G
OR47b
Pc
G'
OR88a
Pc
I
Psc
1
2
Cut Sens
I'
2
Cut Sens
J
Psc
1
2
1
2
3
Cut
Elav
J'
3
4
4
Cut
Elav
K
Or47b
Svp
Wt
L
E132
Svp
Wt
M
Or47b
Svp
Psc
M'
Or47b
2
1
Psc
O
HRP
O'
E132
Psc
Wt
P
Wt
E132
Q
Psc
E132

Figure 4

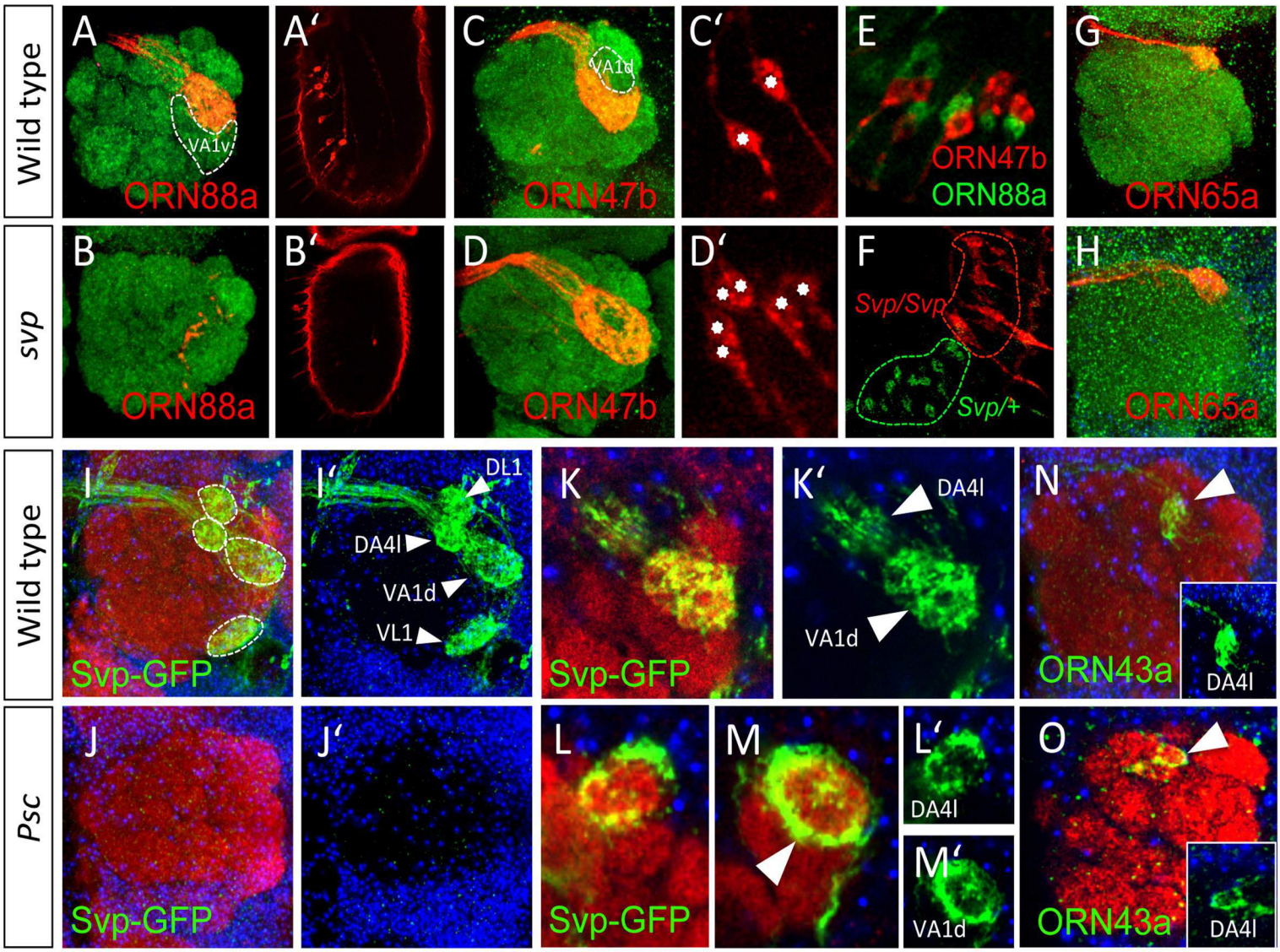
Wild type
svp
Wild type
Psc
A
A'
C
C'
E
G
VA1v
VA1d
ORN88a
ORN47b
ORN47b
ORN88a
ORN65a
B
B'
D
D'
F
H
Svp/Svp
Svp/+
ORN88a
ORN47b
ORN65a
I
I'
K
K'
N
DL1
DA4l
VA1d
VL1
DA4l
VA1d
Svp-GFP
Svp-GFP
ORN43a
DA4l
J
J'
L
M
L'
M'
O
Svp-GFP
Svp-GFP
DA4l
VA1d
ORN43a
DA4l

Figure 5

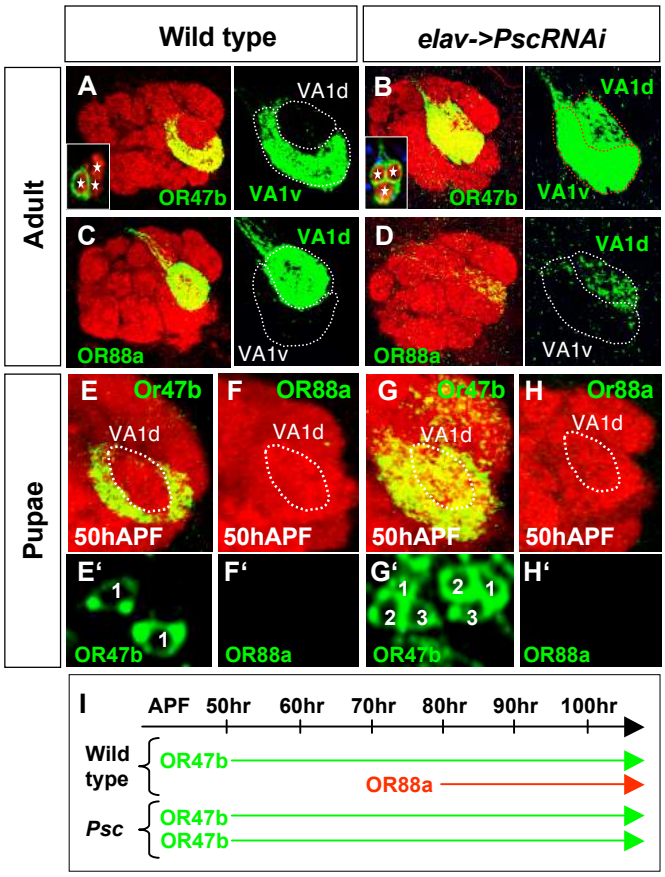
Wild type
elav->PscRNAi
Adult
Pupae
A
B
C
D
E
F
G
H
E'
F'
G'
H'
VA1d
VA1v
OR47b
OR88a
Or47b
Or88a
50hAPF
I
APF
50hr
60hr
70hr
80hr
90hr
100hr
Wild type
Psc
OR47b
OR88a
OR47b
OR47b

Figure 6

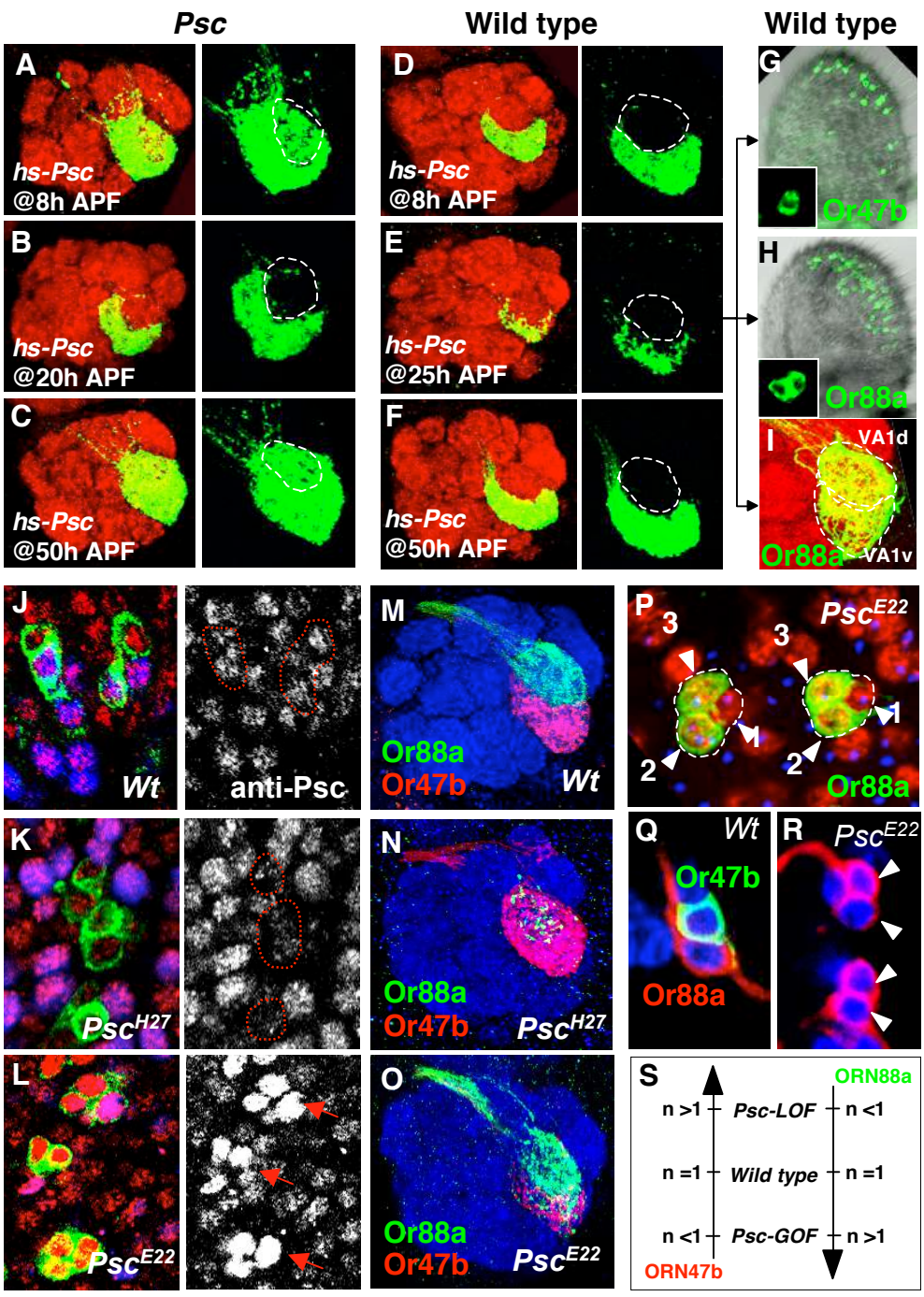
Psc
Wild type
Wild type
A
hs-Psc
@8h APF
B
hs-Psc
@20h APF
C
hs-Psc
@50h APF
D
hs-Psc
@8h APF
E
hs-Psc
@25h APF
F
hs-Psc
@50h APF
G
Or47b
H
Or88a
I
VA1d
Or88a
VA1v
J
Wt
anti-Psc
K
Psc^H27
L
Psc^E22
M
Or88a
Or47b
Wt
N
Or88a
Or47b
Psc^H27
O
Or88a
Or47b
Psc^E22
P
Psc^E22
3
3
1
2
2
Or88a
Q
Wt
Or47b
Or88a
R
Psc^E22
S
ORN88a
n >1
Psc-LOF
n <1
n =1
Wild type
n =1
n <1
Psc-GOF
n >1
ORN47b

Figure 7

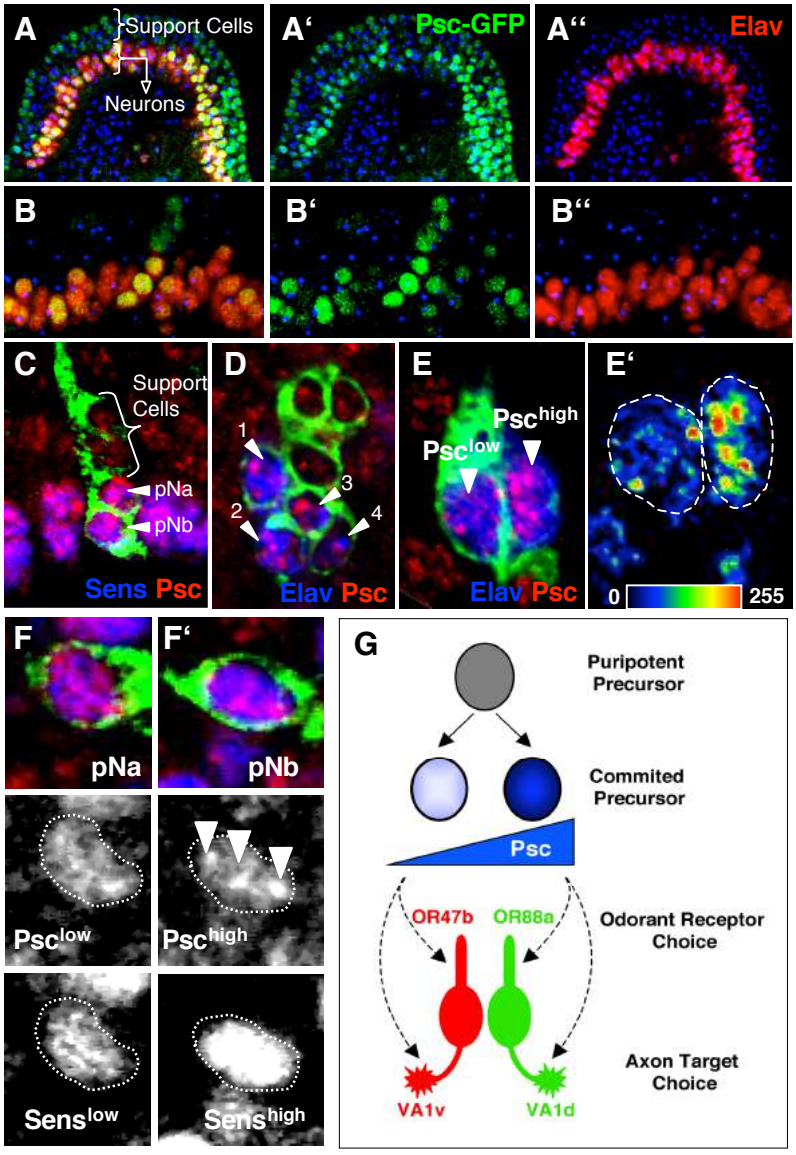
A
Support Cells
Neurons
A'
Psc-GFP
A''
Elav
B
B'
B''
C
Support Cells
pNa
pNb
Sens Psc
D
1
2
3
4
Elav Psc
E
Psc high
Psc low
Elav Psc
E'
0
255
F
pNa
F'
pNb
Psc low
Psc high
Sens low
Sens high
G
Puripotent Precursor
Commited Precursor
Psc
OR47b
OR88a
Odorant Receptor Choice
Axon Target Choice
VA1v
VA1d

Figure 8

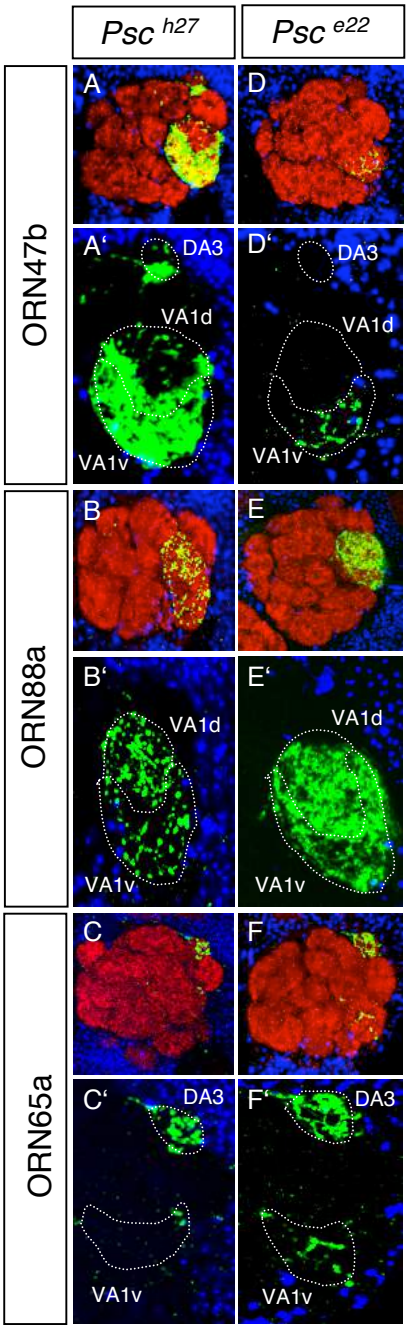

Suppl. Figure 1

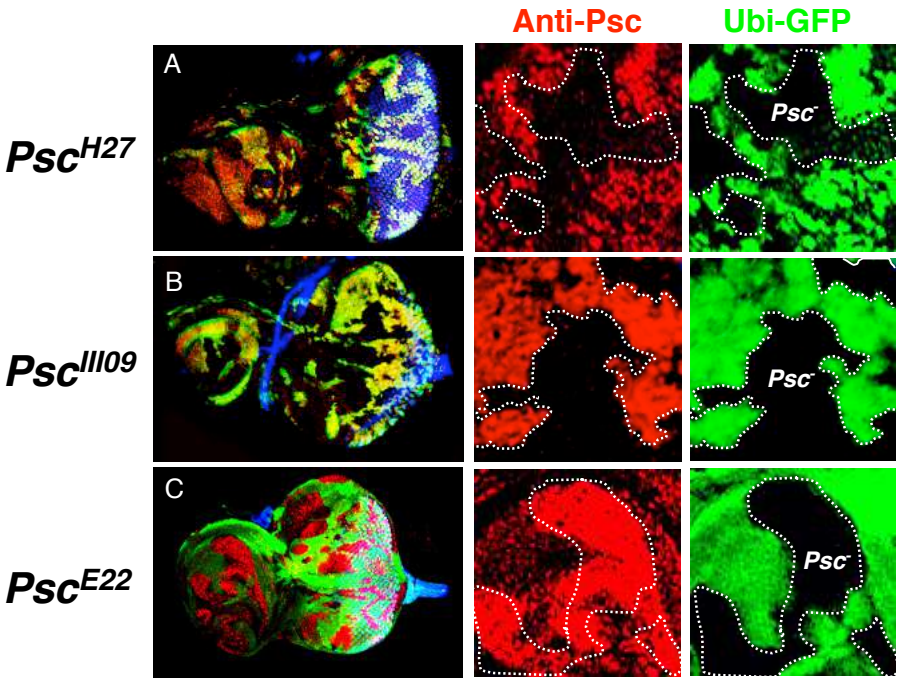

Suppl. Figure 2

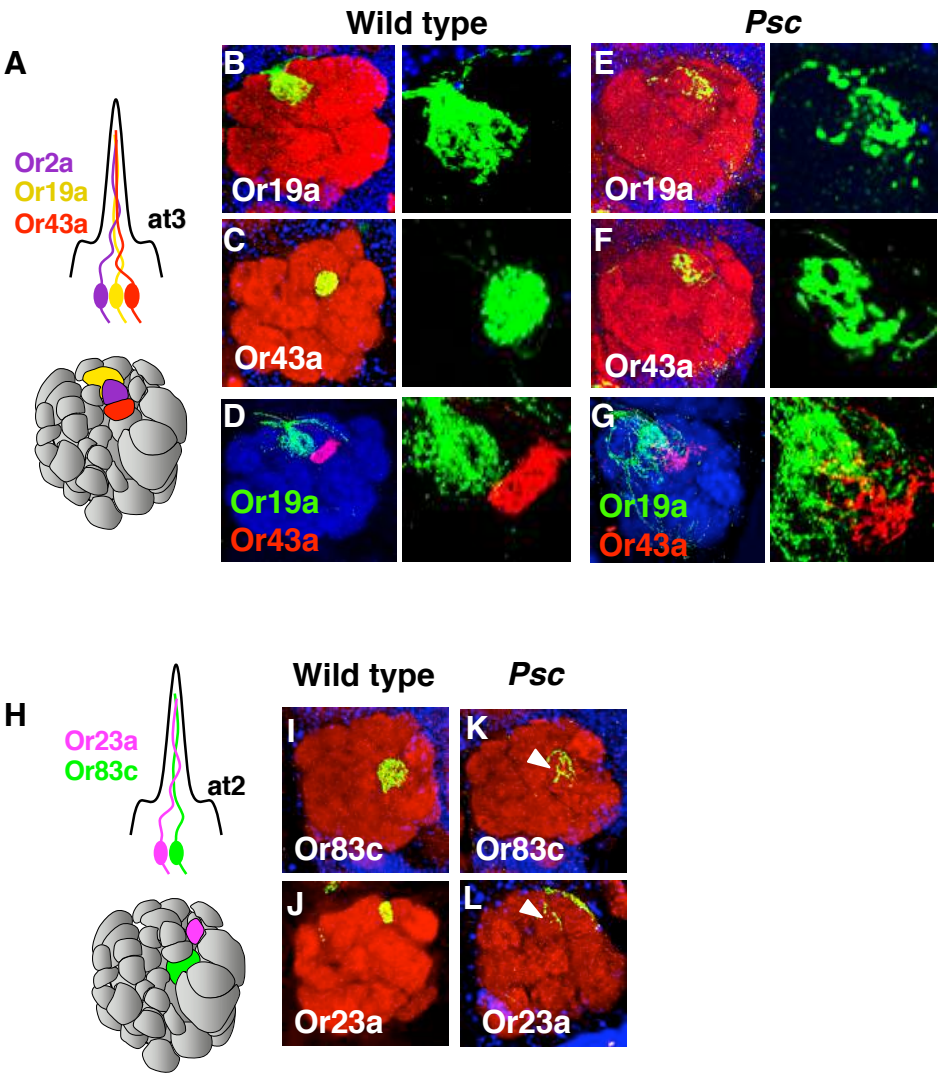

Suppl. Figure 3

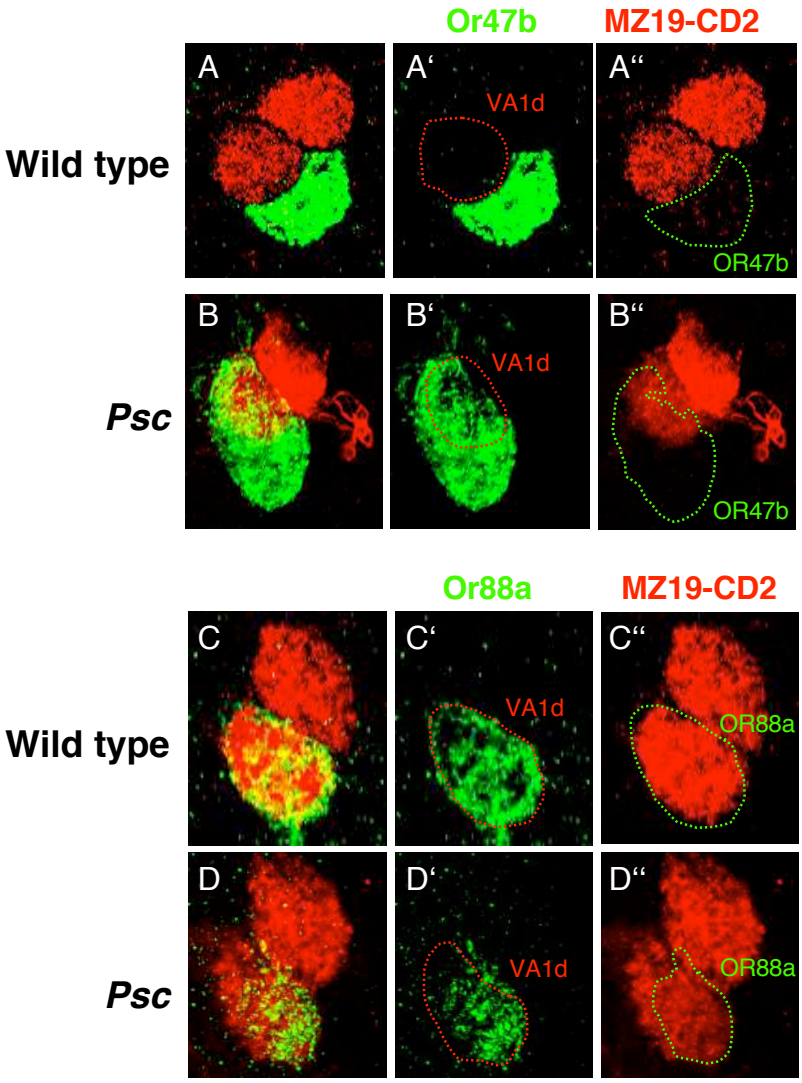

Suppl. Figure 4

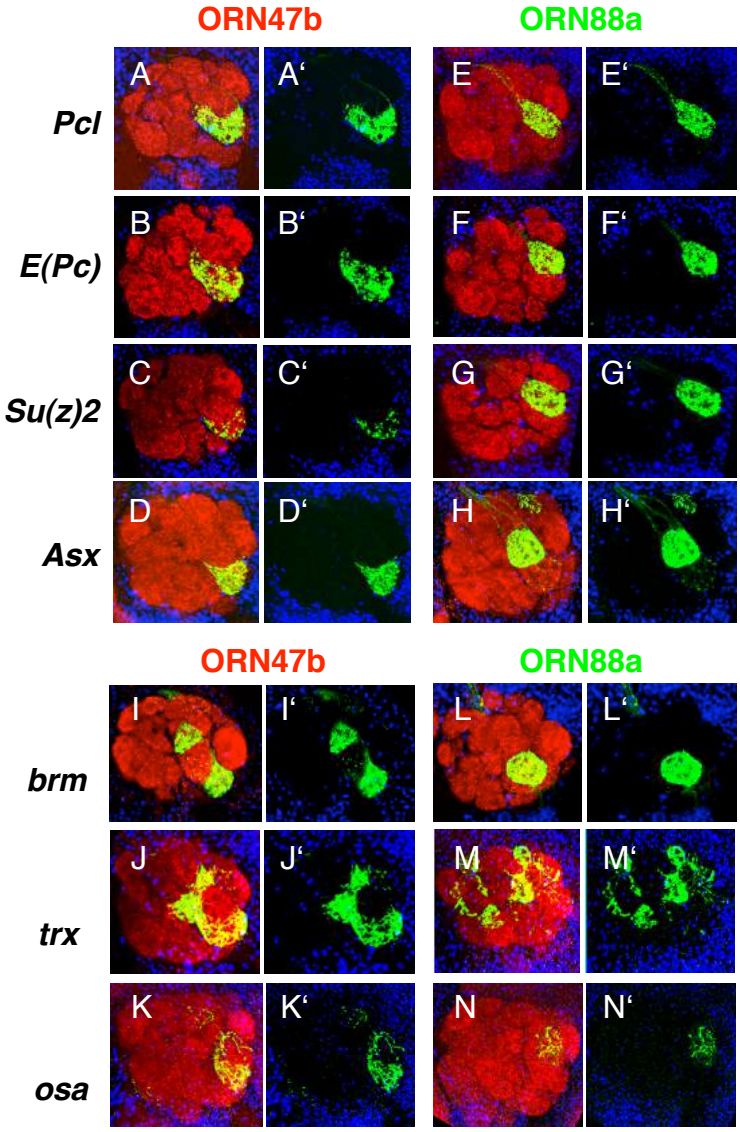

Suppl. Figure 5

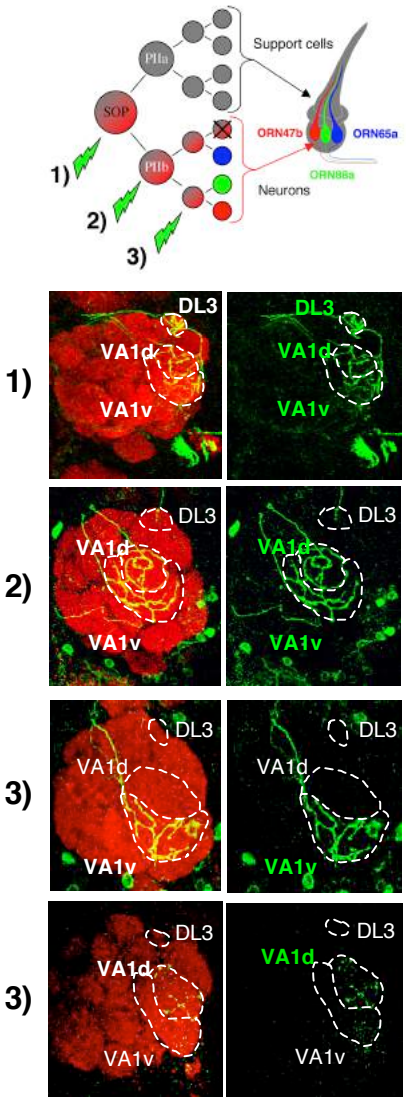

Suppl. Figure 6

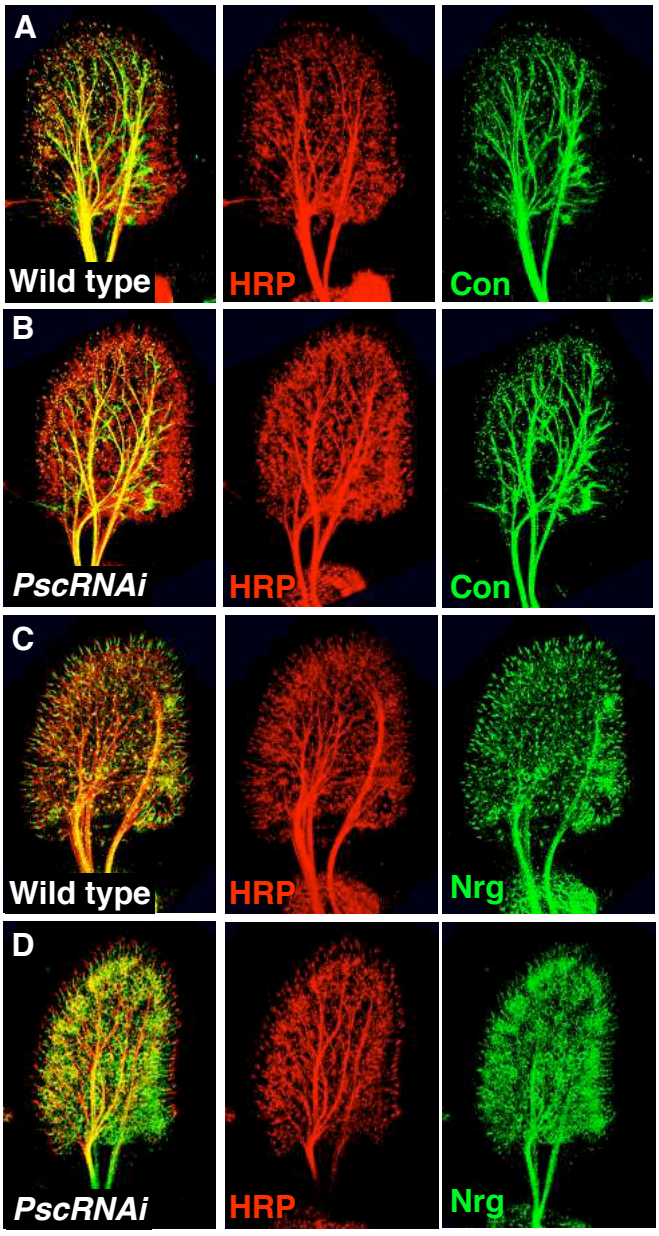

Suppl. Figure 7

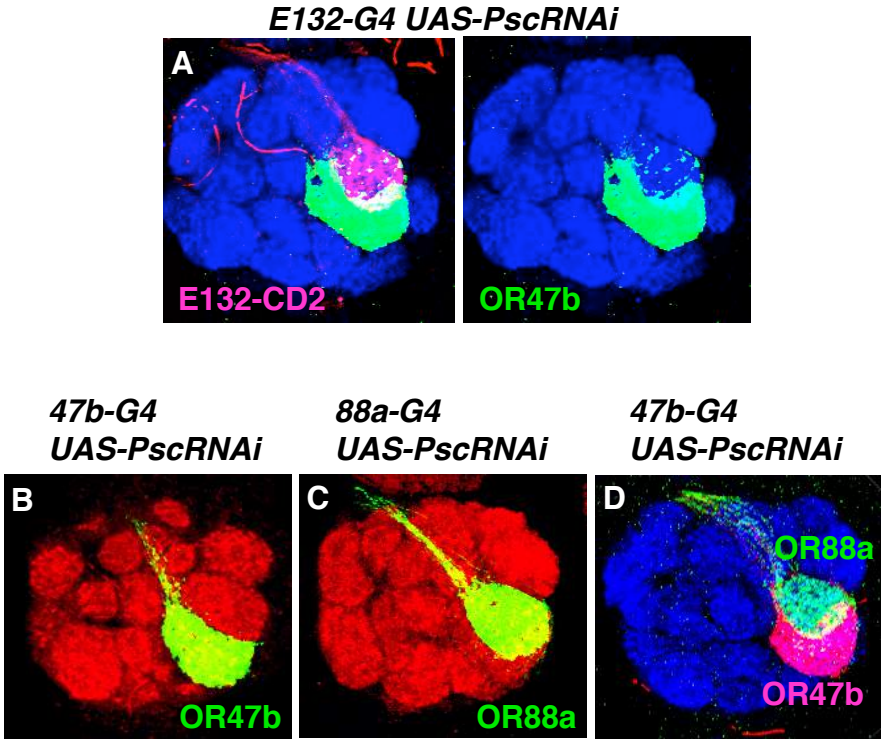

Suppl. Figure 8

Chapter 5

High-resolution ultramicroscopy of the developing and adult nervous system in optically cleared *Drosophila melanogaster*

Marko Pende[1,2*+], Klaus Becker[1,2+], Martina Wanis[1,3], Saiedeh Saghafi[1], Rashmit Kaur[3], Christian Hahn[1,2], Nika Pende[4], Massih Foroughipour[2],Thomas Hummel[3] and Hans-Ulrich Dodt[1,2*]

[1] Department for Bioelectronics, FKE, Vienna University of Technology, Gußhausstraße 25-25A, building CH, 1040 Vienna, Austria

[2] Department for Bioelectronics, Center for Brain Research, Medical University of Vienna, Spitalgasse 4, 1090 Vienna, Austria

[3] Department of Neurobiology, University of Vienna, Althanstrasse 14, 1090 Vienna, Austria

[4]Department of Ecogenomics and Systems Biology, Archaeal Biology and Ecogenomics Division, University of Vienna, Althanstrasse 14, 1090 Vienna, Austria

*Correspondence:

marko.pende@tuwien.ac.at

hans.ulrich.dodt@tuwien.ac.at

+These authors contributed equally to this work

5.1 Summary

With constantly improving technologies to visualise and genetically manipulate individual neurons in the brain, the fruit fly *Drosophila melanogaster* is an important experimental model to address central questions in neuroscience at an organismic level. However, microscopic imaging of neural circuits in intact flies, especially the combined representation of peripheral and central components, has been quite limited due to structural properties of the cuticle. Here we present a novel approach combining tissue clearing, ultramicroscopy, and data analysis which enables the complete visualisation of neuronal networks with single-cell resolution from the larval stage up to the adult *Drosophila*. FlyClear, the signal preserving clearing technique we developed, stabilises tissue integrity and signal intensity from endogenously expressed fluorescent proteins for over a month and efficiently removes the overall pigmentation. In combination with an aspheric ultramicroscope setup utilising an improved light-sheet generator, this allows us to visualise long-range connections of various sensory and central neuron types in the intact *Drosophila* visual and olfactory system. High-resolution 3D reconstructions with isotropic resolution from entire GFP-expressing flies are obtained by applying image fusion from orthogonal directions. This methodological integration of novel chemical, optical, and computational techniques allows a major advance in the analysis of global neural circuit organisation.

5.2 Introduction

In recent years, the fast development of tissue-clearing approaches has offered a wide range of tools for studying deep-tissue structures, large neuronal projections, entire organs[1-14], and even whole animals[15-20]. The main focus of these approaches was to visualise tissue organisation in vertebrate model organisms and humans. If animals genetically modified for tissue-specific fluorescence transgene expression were not available, the samples had to be immunohistochemically labeled, which is a difficult, laborious, and time consuming task for large specimens[21-24].

Regarding the fast generation time, large numbers of externally laid embryos, and the capability of being genetically modified in numerous ways, the fruit fly *Drosophila melanogaster* has proved to be a valuable model organism to address fundamental questions in a variety of biological processes[25]. In multiple disciplines of *Drosophila* research, the most commonly used imaging technique is confocal microscopy following tissue dissection[26]. However, when large undissected volumes are recorded, the drawbacks of confocal microscopy are the low imaging depth, the long recording time, and the occurrence of photo bleaching. Without clearing of the sample, strong absorption and scattering of photons occur by interaction with the tissue, especially with the pigments located in the eyes and the cuticle. These aberrations result in a decrease of signal intensity and non-uniform spatial resolution[27, 28]. Tissue transparency is usually achieved by reducing the refractive index (RI) gradient at the borders between different cellular components.

Commercially available mounting media, such as DPX, Glycerol, 2,2'-Thiodiethanol (TDE)[29], VECTASHIELD®, FocusClear®, ProLong™Gold, RapidClear®, Histodenz™ or recently published direct immersion media such as FRUIT[12], ClearT[6], ScaleS[13], SeeDB[8], SeeDB2[10] and RTF[11] have such RI matching properties. However, each of these solutions has some limitations regarding the preservation of morphology, fluorescent stability, viscosity, penetration depth and the capacity to render tissue transparent[10, 11, 13]. Further, none of these media has been reported to have depigmentation properties. Therefore, heavily pigmented organisms, such as *Drosophila* require sample preparation including the dissection of organs before mounting and imaging, which leads to tissue damage and deformation. For example, sensory neurons located in peripheral structures like the eye, antenna, or legs, establish long-range projections via various nerves to the central brain, where they segregate into distinct synaptic regions. Following the dissection and mounting of peripheral and central brain tissues the location of sensory neurons and their brain connections cannot be visualised in

total so far. Here, critical information about overall neural map organisation, especially the spatial relationship between cell body position and synaptic contacts, is lost by animal dissection. Furthermore, digital reconstruction of separate images is known to be quite labor-intensive and error-prone.

The importance of visualising distinct cell types in their organismal context has led to various attempts to image tissue organisation during development in intact *Drosophila* in the past[30-32]. Despite some progress in the field, previous approaches in whole fly imaging have shown some critical drawbacks, including the limitations of specific cell labeling[33-35], the loss of fluorescent signal, the necessity of immunohistological labeling, low spatial resolution, and the need for specialised equipment e.g. the head-array preparation[30]. As previous studies have shown that the auto fluorescence of optically cleared flies can be imaged with micrometer-resolution in a short period of time by light-sheet microscopy[36], an efficient tissue-clearing technique which preserves the stability of endogenously expressed fluorescent proteins would be a key innovation to overcome current technological disadvantages.

Here, we present a novel clearing protocol, FlyClear, which results in optical transparency of intact *Drosophila* while preserving the fluorescence of endogenously expressed GFP and mCherry.

To gain higher spatial resolution during ultramicroscope imaging, we used an improved light-sheet generator that produces a thinner light-sheet with a much-extended length of uniformity along the propagation axis compared to a standard light-sheet generator system composed of a slit aperture and a cylindrical lens[36].

In order to achieve a virtual isotropic resolution of the recorded data in all spatial directions, we implemented a multi-view combining algorithm computing a 3D Fast Fourier Transformation (FFT) to identify the sharper regions in a set of image stacks recorded from different spatial directions. Although combining multi-view microscopy image stacks has been done before[37-43], to the best of our knowledge, it was never used in optically cleared specimens.

By combining our innovations in clearing technique, light-sheet imaging, and computational multi-view combining, we show for the first time the systemic 3D imaging of endogenous fluorescent markers in intact *D. melanogaster* for multiple developmental stages and adult flies with isotropic spatial resolution and long-term signal stability.

5.3 Results

FlyClear leads to highly transparent samples with long-term signal preservation

D. melanogaster is a challenging subject for optical tissue clearing using previously established protocols[3, 5, 7, 8, 44]. The *s*tructural features of the chitinous exoskeleton and various kinds of pigmentation, including the photopigments within the compound eye, impede the clearing process as well as the RI matching to obtain optical transparency. Furthermore, expressed fluorescent proteins in transgenic fruit flies are more sensitive to chemical treatment than in other model organisms such as mice[32, 36].

To overcome these drawbacks, we developed a clearing method called FlyClear. Starting with the CUBIC protocol[7], we applied additional tissue treatment steps, depending on the developmental stage of the flies, and several modifications to the original reagent-1. For larva and prepupa we used a 0.03% Protease treatment step prior to formaldehyde fixation. In addition, a permeabilisation step with acetone was applied for prepupa after formaldehyde fixation (Fig. 1a). The concentrations of the detergent and the used aminoalcohol in the new solution were significantly decreased (hereafter termed as *Solution-1*). A substantial change in *Solution-1* (see Methods) from the original CUBIC reagent-1 was the replacement of Quadrol® (N,N,N',N'-tetrakis(2-hydroxypropyl)-ethylenediamine) by THEED (2,2′,2″,2‴-(Ethylenedinitrilo)-tetraethanol) which was also tested in the original CUBIC paper. This adjustment not only accelerates the clearing process, but also results in a complete depigmentation of the compound eye (Supplementary Fig. 1a) and a sufficient decrease in the cuticle pigmentation (Fig. 1b).

To test, whether the signal quenching effect caused by THEED, as described before[7], is too strong for transgenic fly lines with a low fluorescence expression level we directly compared the signal stability in uncleared and *Solution-1* cleared half's of same flies with weak GFP expression in the antenna (50 neurons).

Compared to the control half's we observed a significant loss of GFP signal. However, due to the increased transparency and reduced autofluorescence we had no difficulties to image the neurons with the same settings as the uncleared ones (Supplementary Fig.1b, c).

The fluorophore quenching effect of *Solution-1* led us to test alternative RI matching media (Fig. 1b, Supplementary Fig. 1d, e and 2). Ultramicroscope image quality is dependent on the uniformity and viscosity of the imaging medium e.g. streaks in the liquid can have distortion effects on the light-sheet. Furthermore, viscous liquids can cause tissue deformation due to

high osmolarity difference between the tissue and its surrounding. To prevent such effects we decided to use an aqueous solution of meglumine diatrizoate, a component which is also used in FocusClear™[45]. Among the tested RI media, this solution gave us the best results regarding, morphology preservation, sample transparency and liquid viscosity (Supplementary Fig. 1e and 2). Meglumine diatrizoate is an aromatic iodine compound that can be easily dissolved in water or PBS to create a solution with a final RI of 1.45 (hereafter termed *Solution-2*). Additionally, it has to be mentioned that no volume change could be observed when comparing cleared with the corresponding uncleared side of the flies (Supplementary Fig. 1d, e).

We tested the signal stability of GFP following incubation in *Solution-2* (see Methods) by recording samples at three different time points under the same conditions (Supplementary Fig. 3 and 4a). We did not observe any significant changes in fluorescence intensity of individual flies even after 30 days (Supplementary Fig. 4b, c). Further, we tested the protocol on mCherry labelled samples and demonstrated the signal preservation of an alternative fluorophore (Supplementary Fig. 5a, b). With the resulting final protocol, we were able to generate significantly improved transparency of larval and pupal specimens and highly transparent samples of adult flies (USAF1951-chart: group 7, element 6 = 2.19 µm resolution) (Fig. 1b and Supplementary Table 1) with stable fluorescence intensities over several weeks (Supplementary Fig 4).

New aspheric ultramicroscope system improves light-sheet by using a soft-aperture

A thinner light-sheet gives a better resolution in z-direction. Therefore we tried to decrease the full width half maximum (FWHM) of our light-sheet to increase the isotropy of imaging in x,y and z, allowing to view the sample from different directions with similar resolution.

We used ultramicroscopy for virtual sectioning to achieve high resolution images from our cleared *Drosophila* samples (Supplementary Fig. 6a, b). A cylindrical lens in combination with a rectangular slit aperture is the most common approach for generating a thin light-sheet in ultramicroscopy. Therefore, we refer to this as the standard ultramicroscope setup. The process of the optimisation of the ultramicroscope involves the usage of various optical components (Fig. 2a). These components change the phase and other related factors of the incident beam to reshape it to an ultra-thin beam with improved characteristics. Combinations of two or three cylindrical lenses can affect the orbital angular momentum of the laser beam and enables us to alter the distribution of the output beam[46]. However, some limitations and side effects may arise if aberration and related parameters are not controlled during this

process[36]. One of the most significant reasons for using Aspheric elements in any optical design is their ability to form a distortion-free image with minimal aberration. A laser beam with a symmetrical Gaussian intensity profile can be converted into a semi-uniform beam by using two identical Aspheric lenses with a particular surface design[36] (Fig. 2a (1) and (3)). Placing a Meso-Aspheric element, such as a Powell lens (Fig. 2a (2)), that generates a beam with semi-uniform intensity distribution between two Aspheric lenses facing each other enabled us to produce an elliptical beam with a uniform intensity profile. A thin light-sheet can be produced if this beam is incident on a unit containing two identical Acylinder lenses of focal length f that are separated by $\sqrt{2}f$ (Fig. 2a (5) and (6)) [36].

The output beam can be further improved by using a custom-made elliptical apodising soft-aperture (Fig 2a (4)). A mathematical function representing an elliptical Bullseye filter was obtained by using the size and shape of the elliptical uniform beam when the beam radius was at its minimum value before the beam changed the direction of its distribution toward the converting unit containing two Acylindrical lenses. Thus, a custom-made soft-aperture was designed and allocated at a distance of $2F_c$, with F_c being the focal length of the third optical element i.e. the condenser aspheric lens. The soft aperture enables us to eliminate the unwanted intensity distribution in our optical system without creating the hard-edge aperture effects that we encounter in the conventional truncation. This alteration is primarily dependent on the transmission gradient of the aperture. The combination of these complex optical elements redistributes the amplitude and phase of the beam in a way that generates a light-sheet with a highly localised intensity at the focal point and a vastly extended length of uniformity along all axes. This is achieved while simultaneously minimising the power loss when compared with the standard ultramicroscope setup.

Using LaserCam-HRTM (Coherent, Germany), the intensity profiles across the x-y plane produced by the standard ultramicroscope setup and the aspheric ultramicroscope at three different positions (focus, 1000µm, and 2000 µm away from the focus) were measured (Fig. 2b, c). Based on these measured data, the FWHM values were determined (Fig. 2b, c).

FlyClear enables whole-system interrogation from larval up to adult stages

We reasoned that the characterisation of complex organisms require methods for imaging multi-tissue interactions of distant connections in intact samples. We used FlyClear in combination with the improved ultramicroscope setup and confocal microscopy to visualise structures of the sensory-, secretory-, respiratory- and reproductive system of intact *Drosophila* expressing *UAS-mCD8::GFP* under the developmental driver line Pebbled-

Gal4[47]. In 3rd instar larvae internal tissues like trachea, mid gut and salivary glands can be visualised (Supplementary Fig. 7a, b and Supplementary Movie 1). In prepupa the projection of photoreceptors in the developing visual system (Fig. 3a, b) and the innervation of the segmental nerves into the ventral nerve cord become visible (Fig. 3b-e and Supplementary Movie 2). In mid pupal stages we demonstrated the high spatial resolution by imaging neurons of the visual-, reproductive- and the olfactory system (Supplementary Fig. 8a-e). Additionally, we visualised the neurons in various appendages of pupae and adult flies (Supplementary Fig. 8f and 9a, b and Supplementary Movie 3).

FlyClear allows precise mapping of neuronal circuit elements in developing and adult nervous system of *Drosophila*

A major advantage of FlyClear is the complete removal of eye pigments in *Drosophila* pupal and adult stage, thereby allowing a detailed analysis of individual neuronal populations and their connectivity without brain dissection. To demonstrate the spatial resolution at different levels of the central brain we imaged two neuron types in the *Drosophila* visual system, the Dorsal Cluster Neurons (DCNs) and Medulla Columnar Neurons (MCNs). In wild type, a bilateral cluster of DCNs in the dorso-lateral central brain forms an interhemispheric commissural tract to innervate the medulla and lobula synaptic neuropils in the fly optic lobes (Fig. 4a, c)[48]. In homozygous mutants of the neuronal cell adhesion molecule Neuroglian the specific loss of the commissural tract can be detected following the FlyClear treatment of intact *Drosophila* (Fig. 4b, d and Supplementary Movie 4). Similarly, for a homogenous group of MCNs in the adult visual system a single synaptic layer in the central medulla can be separated from the neuronal cell bodies in the peripheral medulla cortex (Fig. 4e, f) further illustrating the high spatial resolution in the analysis of neural circuit organization in the intact fly.

In addition, we showed with our aspheric ultramicroscope system the organisation of the undissected visual system of pupa (Supplementary Fig. 8a, b and Supplementary Movie 5). Until now, the majority of protocols for investigating neuronal connections in *D. melanogaster* involve brain dissection[49]. This leads to disrupted connections of peripheral neurons into the central brain, impeding a complete understanding of sensory map formation. Therefore, high-resolution phenotypic analysis of wild type and mutant neural circuit organisation is impaired. Applying the FlyClear protocol in combination with improved

ultramicroscopy, we are able to obtain a complete visualisation of neuronal structures leading from the cell bodies in the periphery to the synaptic target regions in the central brain (Fig. 5). For the first time, it was possible to visualise the undissected projection of sensory neurons from their receptors in eyes, antennae, maxillary palps and labellum (Fig. 5a) to their respective central processing areas in the brain (Fig. 5b and Supplementary Movie 6).
We could clearly resolve small neuronal connections (Fig. 5a, b and Supplementary Fig. 10). We were also able to follow the projections of the antennal nerve up to the antennal lobe in detail (Fig. 5c-d and Supplementrary Movie 7). Furthermore, we demonstrated that the protocol enables counting of individual cell bodies in the intact *Drosophila* (Fig. 4c, d and e, 5a, b and Supplementary Fig. 8 b-f and 10).

Multi-view combining provides virtual isotropic resolution of stacks obtained with ultramicroscopy

Generally, the axial resolution is lower than the lateral resolution in both confocal and light-sheet microscopy[37, 39, 40]. To achieve 3D-reconstructions with virtual isotropic resolution, we recorded flies from two orthogonal directions and combined the stacks using a multi-view combining approach[37, 39, 40] (Supplementary Fig. 11). The algorithm for this method uses a 3D FFT to identify parts that are sharper in one of the two pre-aligned image stacks. Once these parts are identified, it combines them to a fused image stack. As already suggested by Shaw et al.[38] and Sätzler and Eils[37], frequency components with higher magnitudes are assumed to represent the sharper image structures. Therefore, the multi-view combined stack was obtained by an inverse FFT after selecting for the frequency components with these higher magnitudes and adjusting the corresponding phase values (Fig. 6, Supplementary Fig. 11). The better resolution in 3D can be best appreciated in the movie in the Supplementary (Supplementary Movie 8).

5.4 Discussion

Here we present a novel experimental approach that allows the visualisation of the distinct peripheral and central components of neuronal networks in intact, optically-cleared *Drosophila* flies in high spatial resolution.

The FlyClear protocol provides several advantages: (1) it is a fast and simple procedure that only requires brief immersion of the flies in two solutions. If confocal microscopy is used, *Solution-2* can be replaced by VECTASHIELD®. (2) It completely maintains the morphology of the fly tissue along with high transparency and concomitant depigmentation. The strong pigmentation of the compound eye is a major obstacle as it causes absorption and diffraction of the light. FlyClear overcomes this drawback without the use of bleaching reagents that quench endogenously expressed fluorescent proteins. (3) Using this clearing protocol, the endogenous fluorescence signal is preserved for at least a month without significant changes in intensity. Some dehydration-based immersion clearing approaches for *Drosophila* have previously been published[32, 36, 50]. However, it was not proven whether they are able to stabilise transgenic fluorescent markers such as GFP. The images presented in these publications show neither detailed structures nor GFP signal clearly distinguished from autofluorescence[32]. Therefore, our protocol represents a major breakthrough in the field of optical tissue clearing for insects.

We utilised an aspheric ultramicroscope system, which was improved with a soft-aperture. With this optimised system we could exhibit a light-sheet with a very low thickness at the focus with a strongly extended length of uniformity along the propagation axis and an almost uniform intensity distribution along the imaging plane.

Unlike other fluorescence based imaging techniques such as knife-edge scanning-, confocal- or two-photon excitation microscopy, ultramicroscopy of optically cleared samples allows the visualisation of intact neuronal networks without mechanical disruptions. Neurites can be imaged and traced along their projections from their receptor to their interconnections in the central brain with single-cell resolution. As a proof of principle, we visualised axonal projections of various sensory receptor neurons and central brain populations in the adult *Drosophila* head and associated appendages to their synaptic regions in the central nervous system. Furthermore, due to the limited exposure to laser light, a sample can be repetitively imaged over a long period of time. X-ray based methods such as MicroCT X200 or synchrotron x-ray tomography could provide a powerful alternative for whole system

imaging. However, at the current state such approaches still have limitations regarding the labelling of specific cell types, tissue morphology preservation and the accessibility to a broad group of scientists.

We achieved an isotropic resolution in the 3D-reconstruction by recording cleared samples from orthogonally tilted directions and subsequently combining these tilted views into a single image stack by an FFT-based multi-view fusion algorithm. Due to the uniform resolution, it is possible to quantify cell bodies of the receptors. Our approach suggests that image fusion can be an efficient tool in general for creating isotropic resolution in ultramicroscope recordings from optically cleared samples.

We anticipate that the powerful combination of optical tissue clearing, light-sheet imaging, and multi-view combining will provide major benefits in different applications. It will fill the void of whole system approaches in *D. melanogaster* by enabling isotropic imaging from single neuronal projections to the entire nervous system. Therefore, the described protocol could potentially provide answers to questions addressing neuronal map formation. Additionally, other cell populations within and outside of the nervous system could be visualised in intact flies. This could enable better approaches to study various biological questions such as neurodegenerative diseases. Complete new mechanistic insights should also be possible within the field of developmental biology.

5.5 Methods

Animal

All fly stocks were maintained in standard fly food and kept on 25°C. Adult flies of 4-5 days were used in this study. Six different Gal4 drivers were analysed:

Pebbled-Gal4 UAS-mCD8::GFP ; ;

; dscam-Gal4/CyO ; UAS-mCD8::GFP

nrg849/+ ; UAS-mCD8::GFP ; atonal-Gal4,

nrg849/y ; UAS-mCD8::GFP ; atonal-Gal4,

; 10x UAS-mCD8::GFP ; R47G08-Gal4,

; UAS-mCD8::GFP ; Or47b-Gal4

; ; R88E12-Gal4 UAS-mCherry.

These Gal4 drivers were kindly provided by Thomas Hummel, Department of Neurobiology, University of Vienna, Austria.

FlyClear solution preparation

Solution-1 was prepared by mixing 8 wt% THEED (2,2′,2″,2‴- (Ethylenedinitrilo)-tetraethanol) (Sigma-Aldrich, 87600-100ML), 5wt % Triton® X 100 (Roth, 3051.2) and 25 wt% Urea (Roth, X999.2).

Solution-2 consists of 50 wt% Meglumine diatrizoate (Sigma-Aldrich M5266) in PBS (pH 8.5) adjusted to a refractive index of 1,45.

FlyClear Protocol (larva)

Samples were treated at 37°C for 1h with 0,03% proteinase (Sigma, P8038-250MG) in prewarmed PBS to digest the larva superficially. For optical clearing, larva were fixed in 50ml of 4% PFA (pH 8.5) at 4°C for 2h under gentle shaking followed by 3x washing with PBS at 4°C for 20min each. The samples were then immersed in 10ml of *Solution-1* at 37°C under gentle shaking for 4-5 days. The animals were then washed 3x with PBS for one day at 25°C. To avoid deformation of the sample, the larva were incubated for 3h in a diluted

Solution-2 (25 wt% Meglumine diatrizoate). Finally, the samples were immersed in *Solution-2* for 24 hours at 25°C and kept in *Solution-2* at 25°C for storage.

FlyClear Protocol (prepupa)

A small cut was made between T1 and T2 of each prepupal case to enable better penetration of chemicals and to avoid tissue deformation which can be caused by the later clearing procedure. Samples were treated at 37°C for 1h with 0,03% proteinase (Sigma, P8038-250MG) in prewarmed PBS to digest the pupal case superficially. Prepupa were then fixed in 50ml of 4% PFA (pH 8.5) at 4°C for 2h under gentle shaking followed by 3x washing with PBS at 4°C for 20min each. To permeabilise the prepupal case, the samples were treated for 2h at -20°C in aceton before immersion in 10ml of *Solution-1* at 37°C under gentle shaking for 4-5 days. The animals were then washed 3x with PBS for one day at 25°C. Finally, the samples were immersed in *Solution-2* for 24 hours at 25°C and kept in *Solution-2* at 25°C for storage.

FlyClear Protocol (pupa)

First the pupal case was removed while the pupa was immersed in PBS. For optical clearing, pupa were fixed in 50ml of 4% PFA (pH 8.5) at 4°C for 90min under gentle shaking followed by 3x washing with PBS at 4°C for 20min each. The samples were then immersed in 10ml of *Solution-1* at 37°C under gentle shaking for 3-5 days. The animals were subsequently washed 3x with PBS for one day at 25°C. Finally, the samples were immersed in *Solution-2* for 24 hours at 25°C and kept in *Solution-2* at 25°C for storage.

FlyClear Protocol (adult)

For optical clearing, the adult flies were fixed in 50ml of 4% PFA (pH 8.5) at 4°C for 90min under gentle shaking followed by 3x washing with PBS at 4°C for 20min each. The samples were then immersed in 10ml of *Solution-1* at 37°C under gentle shaking for 3-5 days, depending on the depigmentation level of the compound eyes. The animals were then washed 3x with PBS for one day at 25°C. Finally, the samples were immersed in *Solution-2* for 24 hours at 25°C and kept in *Solution-2* at 25°C for storage.

Ultramicroscopy

Cleared samples were illuminated from two sides using one of two Sapphire lasers, 488nm/200mW and 532nm/200mW (Coherent, Germany), producing a beam with Gaussian intensity distribution. A 50% beam splitter is used to divide the incident beam into two identical beams. They are guided towards two light-sheet generator units. The details of the light-sheet generators units and the custom-made soft aperture are (1) Aspheric lens (f=20mm, Linus, Germany), (2) Powell lens (10° Fan-angle, Edmund optics, Germany), (3) Aspheric lens (f=20mm, Linus, Germany), (4) Bullseye filter with elliptical aperture (Reynard Cooperation, USA), (5) Acylindrical lens (f=80mm, Linos, Germany), (6) Acylindrical lens (f=80mm, Linos, Germany). The description of the light sheet generator is given in the patent DE 102010046133B4 and in Saghafi et.al[36].

The light-sheet generators are placed on a computer-controlled linear stage (LS-65, PI-Micos, Germany), which can be moved along the beam propagation axis generating a light-sheet with an optimal line of focus propagating through the sample.

A computer-controlled elevation stage with an adjustable precision less than 100nm (Es-100, PI-Micos GmbH, Germany), and a manually adjustable xy-cross table for horizontal adjustment is used to scan the sample vertically.

The light detection part includes a customised microscope with modified objectives for refractive index mismatch, a computer-controlled filter wheel with different optical band pass filters for blocking the fluorescence excitation light, and a scientific grade sCMOS camera (Neo, Andor, Ireland).

A custom made software allows us to perform an automatised recording of stacks of images.

Objectives used:

- 4x objective (Olympus, XLFluor4x/340, 0.28 NA, WD = 29.5mm) using custom-made correction of optics for a refractive index of 1.45 (WD = 10mm after correction)
- 10x water-immersion objective (Olympus, UMPlanFLN, 0.3 NA, WD = 3.5mm) with custom-made correction of optics for a refractive index of 1.45 (WD = 3.5mm after correction)
- 25x objective (Olympus, XLPlanN, 1.0 NA, WD = 8mm) with adjustable refractive index
-

Fluorescence stereomicroscopy

Cleared and uncleared *D. melanogaster* were immersed in *Solution-2* and imaged with Leica MZ 16F fluorescence stereomicroscope using a one fold magnifying, long distance objective (Planapo 1x, 0.28 NA, WD=55mm).

Laser-scanning confocal microscopy

Samples treated with *Solution-1* and washed with PBS were mounted in VECTASHIELD® antifading mounting medium (Vector laboratories, H-1200). *D. melanogaster* were imaged with an inverted laser-scanning confocal microscopy system (Leica, SP5) using a 20x immersion objective (Leica, HCX PL APO CS, 0.7 NA, 260µm WD), 40x Oil-immersion objective (Leica, HCX OL APO CS, 1.25 NA, 100µm WD) and a 63x glycerol objective (Leica, HCX PL APO CS, 1.3 NA, WD 280µm µm).

Image processing

Image processing and 3D reconstruction was done using Amira (FEI, USA) and Photoshop (Adobe, USA) running on a Dell workstation equipped with two 8 core Xeon processors with 256GB RAM and a Nvidia Quadro M6000 graphics card.

The images were post processed by blind maximum likelihood deconvolution, adaptive histogram equalisation, and final unsharp masking. Stripes originating from the image recording procedure were removed using a Fast-Fourier-Transform-based spatial filtering approach.

Multi-view combining

To achieve a virtual isotropic resolution from all directions, we applied a multi-view combining approach. For this purpose, a fly was recorded from different orthogonal directions resulting in pairs of image stacks, I_1 and I_2, which were tilted by approximately 90° (Supplementary Fig. 11). Using Amira 5.3, the two corresponding stacks were visually pre-aligned and then precisely registered with the volume registration tool. The image stack I_2 was re-sampled to obtain virtual slices that were coplanar with respect to the recording planes from stack I_1. After registration, the non-overlapping parts were removed from both stacks (Supplementary Fig. 11). To this purpose, a binary mask was generated from Stack I_1 by thresholding the intensity values. Then stack I_2 was multiplied with this mask. A second mask

was obtained in the same way from stack I_2 and multiplied with stack I_1 (Supplementary Fig. 11).

To correct possible brightness differences, we normalised the processed data sets to their 95% intensity percentile before further processing. We then applied a 3D FFT to obtain the two 3 D arrays, M_1 *and* M_2, and the two 3 D arrays that comprise the phase values, j_1 and j_1, from the transformed data sets F_1 and F_2:

$$M(F_{x,y,z}) = \sqrt{\mathrm{Re}^2(F_{x,y,z}) + \mathrm{Im}^2(F_{x,y,z})}\ , \tag{1}$$

and

$$\varphi(F_{x,y,z})\ = \arctan\left(\frac{\mathrm{Im}(F_{x,y,z})}{\mathrm{Re}(F_{x,y,z})}\right) \tag{2}$$

(Re: real parts of the FFT data, Im: imaginary parts of the FFT data)

Assuming that the highest magnitude value at corresponding positions x, y, z within M_1 and M_2 represents the sharper structural information[37, 38], the magnitudes M_{comb} of the multi-view combined image were calculated as:

$$M_{comb} = \max(M_{I_1}, M_{I_2})\,. \tag{3}$$

The corresponding phases were obtained by adding the complex numbers from F_1 and F_2:

$$\varphi_{comb} = \arctan\left(\frac{\mathrm{Im}(I_1) + \mathrm{Im}(I_2)}{\mathrm{Re}(I_1) + \mathrm{Re}(I_2)}\right). \tag{4}$$

The FFT F_{comb} of the multi-view combined stack is obtained from the recombined magnitudes M_{comb} (eq. 3) and the recombined phases j_{comb} (eq. 4.):

$$\mathrm{Re}_{comb} = \mathrm{Mag}_{comb} \cdot \cos\left(\varphi_{comb}\right), \tag{5}$$

and

$$\mathrm{Im}_{comb} = \mathrm{Mag}_{comb} \cdot \sin\left(\varphi_{comb}\right). \tag{6}$$

The results from eq. 5 and eq. 6 were transformed back into the spatial domain, rescaled, and saved back as 16-bit tiff-files. The images were reloaded into Amira and used for generating the final multi-view reconstructed image stack.

Quantification of transparency

We placed the sample in *Solution-2* on a USAF1951-chart. A grayscale picture was recorded with a 4x objective (Olympus, XLFluor4x/340, 0.28 NA, WD = 29.5mm) using custom-made correction of optics for a refractive index of 1.45 (WD = 10mm after correction). The transparency was determined by examination of an USAF1951 chart through the optically cleared fly according to Supplementary Table 1. This allowed the quantification of the resolution that was possible in the specimen.

Quantification of fluorescence signals in *Solution-1*

We fixed adult flies, with a weak GFP expression in the antenna (about 50 neurons), in 4% PFA pH 8.5. We then embedded them in 2% of low melting agarose and cut them with a vibratome in two almost identical half's. One of each half was incubated for four days in *Solution-1* the other was stored in PBS pH 8.5 on 4°C. Because light-sheet imaging of large samples needs a certain degree of transparency, we used a confocal microscope to quantify and compare the fluorescent signal loss. We mounted the untreated and *Solution-1* treated samples (n=3) on one slide in VECTASHIELD®, because of its fluorescence stabilising properties, and imaged them with the same settings. It has to be mentioned, that we adjusted the laser intensity always on the untreated samples to avoid overexposure. The recorded image stacks were 3D reconstructed using Amira software. For signal quantification, we calculated brightness intensity histograms within regions of interest, each comprising areas in the antenna of uncleared and solution-1 treated half's of the same fly (Supplementary Fig. 1b). We plotted the averaged intensities of the image stacks recorded at the two different conditions and calculated the standards deviations. Significance was assessed with the unpaired t-test.

Quantification of fluorescence signals in *Solution-2*

We mounted Dscam-Gal4/ CyO; UAS-mCD8::GFP flies on a needle tip with UV-glue (Bondic®, Canada) and immersed them in a cuvette filled with *Solution-2* (Supplementary Fig. 3,4). To obtain standard conditions, we recorded stacks of 550 images from each entire fly using constant laser power utilising an ultramicroscope -system equipped with an improved light-sheet generator and a 4x objective (Olympus, XLFluor4x/340, 0.28 NA, WD = 29.5mm) using custom-made correction of optics for a refractive index of 1.45 (WD =

10mm after correction). We repeated the recordings after one week and one month using identical illumination and camera settings. The recorded image stacks were 3D reconstructed and spatially registered using Amira software. For signal quantification, we calculated brightness intensity histograms within regions of interest, each comprising identical areas of the same fly recorded at three subsequent time points. (Supplementary Fig. 4).

We calculated the average intensity of all image stacks recorded at subsequent days from each fly. To represent identical exposure conditions, these results were averaged for each group of samples and plotted against the day of exposure (Supplementary Fig. 4c).

Statistical analysis

In Figure 1c, data are presented as average ± S.D. For significance, P-values were calculated using a one-way ANOVA with IBM SPSS statistics software.

Data availability

The data supporting the findings of this study are available from the corresponding authors upon reasonable request.

Code availability

The source code to perform the multi-view combining in this study is available in the Supplementary Data.

5.5 Acknowledgments

We thank all lab members at the Center for Brain Research, Medical University Vienna, the Department of Bioelectronics, Technical University Vienna and the Department of Neurobiology, University of Vienna, in particular T. Zrzavy and S. Hametner for the help with the statistics, M. Bradl and H. Lassmann for providing the incubators, A. Tröscher and J. Bauer for the help with the confocal microscope, G. Goyal, L. Timaeus, L. Geid for discussion and B. Woller, B. Camurdanoglu, S. Papadopoulos and L. Hogdskiss for proofreading. The study was funded by the Austrian Science Fund (FWF), Project P 23102-N22 and Project P 25134.

5.6 Author Contributions

H.U.D, T.H and M.P. designed the study. M.P. developed the FlyClear protocol and performed most of the experiments. K.B. implemented the multi-view combining. M.W. developed the *Drosophila* fixation protocol. S.S. optimised the ultramicroscope and corrected the objectives for a refractive index of 1.45. R.K. provided the *Drosophila* lines. C.H. did the movies. N.P. made the *Drosophila* illustrations and M.F. made the light-sheet generator illustrations. H.U.D., T.H., M.P., K.B., M.W., N.P., C.H. and S.S. wrote the manuscript. All authors discussed the results and commented on the manuscript text.

Competing financial interests

The authors H.U.D., S.S. and K.B. hold a patent on the light-sheet generator (DE 102010046133B4).

5.8 References

1. Dodt, H.U. et al. Ultramicroscopy: three-dimensional visualization of neuronal networks in the whole mouse brain. *Nature methods* **4**, 331-336 (2007).
2. Becker, K., Jahrling, N., Saghafi, S., Weiler, R. & Dodt, H.U. Chemical clearing and dehydration of GFP expressing mouse brains. *PloS one* **7**, e33916 (2012).
3. Erturk, A. et al. Three-dimensional imaging of solvent-cleared organs using 3DISCO. *Nature protocols* **7**, 1983-1995 (2012).
4. Chung, K. et al. Structural and molecular interrogation of intact biological systems. *Nature* **497**, 332-337 (2013).
5. Hama, H. et al. Scale: a chemical approach for fluorescence imaging and reconstruction of transparent mouse brain. *Nature neuroscience* **14**, 1481-1488 (2011).
6. Kuwajima, T. et al. ClearT: a detergent- and solvent-free clearing method for neuronal and non-neuronal tissue. *Development (Cambridge, England)* **140**, 1364-1368 (2013).
7. Susaki, E.A. et al. Whole-brain imaging with single-cell resolution using chemical cocktails and computational analysis. *Cell* **157**, 726-739 (2014).
8. Ke, M.T., Fujimoto, S. & Imai, T. SeeDB: a simple and morphology-preserving optical clearing agent for neuronal circuit reconstruction. *Nature neuroscience* **16**, 1154-1161 (2013).
9. Murakami, T.C. et al. A three-dimensional single-cell-resolution whole-brain atlas using CUBIC-X expansion microscopy and tissue clearing. *Nature neuroscience* **21**, 625-637 (2018).
10. Ke, M.T. et al. Super-Resolution Mapping of Neuronal Circuitry With an Index-Optimized Clearing Agent. *Cell reports* **14**, 2718-2732 (2016).
11. Yu, T. et al. RTF: a rapid and versatile tissue optical clearing method. *Sci Rep* **8**, 1964 (2018).
12. Hou, B. et al. Scalable and DiI-compatible optical clearance of the mammalian brain. *Frontiers in neuroanatomy* **9**, 19 (2015).
13. Hama, H. et al. ScaleS: an optical clearing palette for biological imaging. *Nature neuroscience* **18**, 1518-1529 (2015).
14. Chen, F., Tillberg, P.W. & Boyden, E.S. Optical imaging. Expansion microscopy. *Science (New York, N.Y.)* **347**, 543-548 (2015).
15. Susaki, E.A. et al. Advanced CUBIC protocols for whole-brain and whole-body clearing and imaging. *Nature protocols* **10**, 1709-1727 (2015).

16. Yang, B. et al. Single-cell phenotyping within transparent intact tissue through whole-body clearing. *Cell* **158**, 945-958 (2014).
17. Tainaka, K. et al. Whole-body imaging with single-cell resolution by tissue decolorization. *Cell* **159**, 911-924 (2014).
18. Pan, C. et al. Shrinkage-mediated imaging of entire organs and organisms using uDISCO. *Nature methods* **13**, 859-867 (2016).
19. Treweek, J.B. et al. Whole-body tissue stabilization and selective extractions via tissue-hydrogel hybrids for high-resolution intact circuit mapping and phenotyping. *Nature protocols* **10**, 1860-1896 (2015).
20. Jing, D. et al. Tissue clearing of both hard and soft tissue organs with the PEGASOS method. *Cell research* **28**, 803-818 (2018).
21. Lai, H.M. et al. Rationalisation and Validation of an Acrylamide-Free Procedure in Three-Dimensional Histological Imaging. *PloS one* **11**, e0158628 (2016).
22. Murray, E. et al. Simple, Scalable Proteomic Imaging for High-Dimensional Profiling of Intact Systems. *Cell* **163**, 1500-1514 (2015).
23. Renier, N. et al. Mapping of Brain Activity by Automated Volume Analysis of Immediate Early Genes. *Cell* **165**, 1789-1802 (2016).
24. Belle, M. et al. A simple method for 3D analysis of immunolabeled axonal tracts in a transparent nervous system. *Cell reports* **9**, 1191-1201 (2014).
25. Jennings, B.H. Drosophila – a versatile model in biology & medicine. *Materials Today* **14**, 190-195 (2011).
26. Chiang, A.S. et al. Three-dimensional reconstruction of brain-wide wiring networks in Drosophila at single-cell resolution. *Current biology : CB* **21**, 1-11 (2011).
27. Lichtman, J.W. & Conchello, J.A. Fluorescence microscopy. *Nature methods* **2**, 910-919 (2005).
28. Richardson, D.S. & Lichtman, J.W. Clarifying Tissue Clearing. *Cell* **162**, 246-257 (2015).
29. Staudt, T., Lang, M.C., Medda, R., Engelhardt, J. & Hell, S.W. 2,2'-thiodiethanol: a new water soluble mounting medium for high resolution optical microscopy. *Microscopy research and technique* **70**, 1-9 (2007).
30. Lin, C.W. et al. Automated in situ brain imaging for mapping the Drosophila connectome. *Journal of neurogenetics* **29**, 157-168 (2015).

31. Arranz, A. et al. In-vivo Optical Tomography of Small Scattering Specimens: time-lapse 3D imaging of the head eversion process in Drosophila melanogaster. *Scientific Reports* **4**, 7325 (2014).
32. McGurk, L., Morrison, H., Keegan, L.P., Sharpe, J. & O'Connell, M.A. Three-dimensional imaging of Drosophila melanogaster. *PloS one* **2**, e834 (2007).
33. Sombke, A., Lipke, E., Michalik, P., Uhl, G. & Harzsch, S. Potential and limitations of X-Ray micro-computed tomography in arthropod neuroanatomy: a methodological and comparative survey. *The Journal of comparative neurology* **523**, 1281-1295 (2015).
34. Hwu, Y., Margaritondo, G. & Chiang, A.S. Q&A: Why use synchrotron x-ray tomography for multi-scale connectome mapping? *BMC biology* **15**, 122 (2017).
35. Ng, J. et al. Genetically targeted 3D visualisation of Drosophila neurons under Electron Microscopy and X-Ray Microscopy using miniSOG. *Sci Rep* **6**, 38863 (2016).
36. Saghafi, S., Becker, K., Hahn, C. & Dodt, H.U. 3D-ultramicroscopy utilizing aspheric optics. *Journal of biophotonics* **7**, 117-125 (2014).
37. Sätzler, K. & Eils, R. Resolution improvement by 3-D reconstructions from tilted views in axial tomography and confocal theta microscopy. *Bioimaging* **5**, 171-182 (1997).
38. Shaw, P.J., Agard, D.A., Hiraoka, Y. & Sedat, J.W. Tilted view reconstruction in optical microscopy. Three-dimensional reconstruction of Drosophila melanogaster embryo nuclei. *Biophysical Journal* **55**, 101-110 (1989).
39. Wu, Y. et al. Spatially isotropic four-dimensional imaging with dual-view plane illumination microscopy. *Nat Biotech* **31**, 1032-1038 (2013).
40. Swoger, J., Verveer, P., Greger, K., Huisken, J. & Stelzer, E.H. Multi-view image fusion improves resolution in three-dimensional microscopy. *Optics express* **15**, 8029-8042 (2007).
41. Chhetri, R.K. et al. Whole-animal functional and developmental imaging with isotropic spatial resolution. *Nature methods* **12**, 1171-1178 (2015).
42. Preibisch, S. et al. Efficient Bayesian-based multiview deconvolution. *Nature methods* **11**, 645-648 (2014).
43. Temerinac-Ott, M. et al. Multiview deblurring for 3-D images from light-sheet-based fluorescence microscopy. *IEEE transactions on image processing : a publication of the IEEE Signal Processing Society* **21**, 1863-1873 (2012).

44. Tomer, R., Ye, L., Hsueh, B. & Deisseroth, K. Advanced CLARITY for rapid and high-resolution imaging of intact tissues. *Nat. Protocols* **9**, 1682-1697 (2014).
45. Chiang, A.S. et al. Three-dimensional mapping of brain neuropils in the cockroach, Diploptera punctata. *The Journal of comparative neurology* **440**, 1-11 (2001).
46. Laabs, H., Gao, C. & Weber, H. Twisting of three-dimensional Hermite—Gaussian beams. *Journal of Modern Optics* **46**, 709-719 (1999).
47. Joo, W.J., Sweeney, L.B., Liang, L. & Luo, L. Linking cell fate, trajectory choice, and target selection: genetic analysis of Sema-2b in olfactory axon targeting. *Neuron* **78**, 673-686 (2013).
48. Srahna, M. et al. A signaling network for patterning of neuronal connectivity in the Drosophila brain. *PLoS biology* **4**, e348 (2006).
49. Wu, J.S. & Luo, L. A protocol for dissecting Drosophila melanogaster brains for live imaging or immunostaining. *Nature protocols* **1**, 2110-2115 (2006).
50. Jahrling, N., Becker, K., Schonbauer, C., Schnorrer, F. & Dodt, H.U. Three-dimensional reconstruction and segmentation of intact Drosophila by ultramicroscopy. *Frontiers in systems neuroscience* **4**, 1 (2010).

Figure Legends

Figure 1 | Workflow and properties of the FlyClear procedure. **a** Main steps of the FlyClear protocol. **b** Upper panel shows wide-field image of optically cleared specimens placed on top of a USAF1951-chart in *Solution-2* demonstrates the level of overall transparency. Middle panel shows higher magnification of red rectangular areas indicating the highest level of transparency reached in the corresponding sample. Lower panel shows GFP signal after RI matching. Bright field images were acquired with a 4x objective (Olympus, XLFluor4x/340, 0.28 NA, WD = 29.5mm) using custom-made correction of optics for a refractive index of 1.45 (WD = 10mm after correction). Fluorescent images were acquired with a stereomicroscope with a 1x objective (Leica, Plan APO 1.0X, WD 61,5mm). Genotype: *Peb-Gal4 UAS-mCD8::GFP;;*. Scale bars represent 500µm in **b**

Figure 2 | Characterisation of the improved aspheric ultramicroscope system. **a** Illustration of the shaping of the laser beam to a light-sheet by the optimised optical unit containing complex optical components. Plano-convex aspheric cylinder lenses (1, 3), Powell lens (2), an elliptical soft aperture (4) and Acylinder lenses (5, 6). **b, c** Difference between the intensity distributions across the z-y plane measured at the position x on the light-sheet by LaserCam-HRTM. Standard ultramicroscope with a 8mm-wide slit aperture **b** and the aspheric ultramicroscope system optimised with a soft aperture **c** measured at the focus x = 0, x = 1,000µm, and x = 2,000µm.

Figure 3 | Imaging of FlyClear treated prepupa using confocal and optimised aspheric ultramicroscope system. **a-c** Light-sheet images and **d**, **e** confocal images of GFP expression in the developing visual system, segmental nerves (SN), and trachea (Tr). **a** Imaging of whole prepupa. **b** Clipping plane shows higher magnification of boxed area in **a** displaying the eye discs of prepupa. **c** Dorsal view of a clipping plane in undisected prepupa showing mid gut (MG), salivary glands (SG), segmental nerves (SN) and the ventral nerve cord (VNC). **d** Higher magnification showing the innervation of the SN into the VNC. **e** Higher magnification showing trachea (Tr) and salivary glands (SG). Images in **a-c** were acquired with a 10x water-immersion objective (Olympus, UMPlanFLN, 0.3 NA, WD = 3.5mm) with custom-made correction of optics for a refractive index of 1.45 (WD = 3.5mm after correction). Images **d**, **e** were acquired with a 20x immersion objective (Leica, HCX PL APO CS, 0.7 NA, 260µm WD). Genotype: *Peb-Gal4 UAS-mCD8::GFP*. Scale bars represent 500µm in **a**, **c**, 200µm in **c**, **d** and **e**.

Figure 4 | Imaging of the *Drosophila* visual system of a FlyClear treated intact adult fly using optimised aspheric ultramicroscope system. **a-f** Light-sheet images of GFP expression in visual system. **a-d** Analysis of interhemispheric circuit defects in Neuroglian mutants. **a**, **c** In wild type, clusters of commissural neuron (arrowhead indicate Dorsal cluster neurons, DCNs) in the visual system project across the midline in the central brain (dashed box). Loss of Neuroglian does not affect the ipsilateral organisation of visual neurons but deletes the commissural projections (arrowheads in **b**), with a few single fibres sending short processes towards the midline (arrowheads in **d**). **e**, **f** Synaptic layer organization in the visual system. Collumnar interneurons innervating a single medulla layer (SML) are visualized **e**. Different optical sections indicate separated synaptic (SL) and cell body layers (CBL) **f**. Images in **a**, **b** and **e** were acquired with a 10x water-immersion objective (Olympus, UMPlanFLN, 0.3 NA, WD = 3.5mm) with custom-made correction of optics for a refractive index of 1.45 (WD = 3.5mm after correction). Images in **c**, **d** and **f** were acquired with a 25x objective (Olympus, XLPlanN, 1.0 NA, WD = 8mm). Genotypes: **a**, **c** *Control – nrg849/+ ; UAS-mCD8::GFP ; ato-Gal4 (Females)*, **b**, **d** *Mutant - nrg849/y ; UAS-mCD8::GFP ; ato-Gal4 (Males)* and **e**, **f** *; 10x UAS-mCD8::GFP ; R47G08-Gal4.* Scale bars represent 200µm in **a**, **b** and **e**, 100µm in **c**, **d**, 50µm in **f** and 10µm in insets in **f**.

Figure 5 | Imaging of the *Drosophila* chemosensory system of a FlyClear treated intact adult fly using optimised aspheric ultramicroscope. **a-d** Light-sheet images of GFP expression in sensory neurons. **a** Lateral view of olfactory and gustatory receptor neurons in antenna (ANT), maxillary palp (MX), and labellum (LB). The inset shows a higher magnification of the maxillary palp. **b** Pharynx and the connection of the pharyngeal nerve (PhN) with the ventral cibarial sense organ (vcso), the labral sense organ (lso), and the connection of the labellum with the labial nerve (lbn). The inset shows a higher magnification of the vcso with single neurons. **c** Dorsal view of antennal receptor neurons, which are connected with the antennal lobe (AL) (dashed box) through the antennal nerve (AN). **d** Lateral view of the connection described in **c**. Images in **a-c** were acquired with a 10x water-immersion objective (Olympus, UMPlanFLN, 0.3 NA, WD = 3.5mm) with custom-made correction of optics for a refractive index of 1.45 (WD = 3.5mm after correction). In **a**, **b** a post magnification of 2x was used. Image in **d** was acquired with a 0.5x post-demagnification in combination with a 25x objective (Olympus, XLPlanN, 1.0 NA, WD = 8mm). Genotype: **a, b** *dscam-Gal4/CyO;*

UAS-mCD8::GFP and **c-e** *Peb-Gal4 UAS-mCD8::GFP*. Scale bars represent 200 µm in **a-d** and 50 µm in the magnified areas of **a**, **b**.

Figure 6 | Multi-view combining of ultramicroscope recordings from orthogonal directions. **a, b** Illustration of the two sided light-sheet illumination through the specimen. Illumination direction is indicated by blue arrows **c, d** Lateral (upper panel) and dorsal (lower panel) view of ultramicroscope recordings from FlyClear processed, GFP expressing samples. Unsharp areas are indicated by arrowheads. **a** Scheme of the lateral illumination plan and **c** corresponding recording of *D. melanogaster*. Insets show bigger magnification of antenna. **b** Scheme of the 90° tilted illumination plane and **d** corresponding recording of the specimen. Insets show higher magnification of the antenna. **e** Multi-view combined reconstructions of the stacks in **c** and **d**. Insets show higher magnification of the antenna. GFP signal is represented in green and auto fluorescence is represented in grey. All images were acquired with 2x post-magnification in combination with a 4x Objective (Olympus, XLFluor4x/340, 0.28 NA, WD = 29,5mm) with custom-made correction of optics for a refractive index of 1.45 (WD after correction 10mm). Scale bars represent 200µm.

a

		Digestion	Fixation	Permeabilization	Depigmentation	RI matching
		0.03%Proteinase	4%PFA	Aceton	*Solution-1*	*Solution-2*
Larva		1h 37°C	2h 4°C		4-5 days 37°C	1 day RT
Prepupa	small cut in pupal case	1h 37°C	2h 4°C	2h -20°C	4-5 days 37°C	1 day RT
Pupa	removal of pupal case		90min 4°C		3-5 days 37°C	1 day RT
Adult			90min 4°C		3-5 days 37°C	1 day RT

b

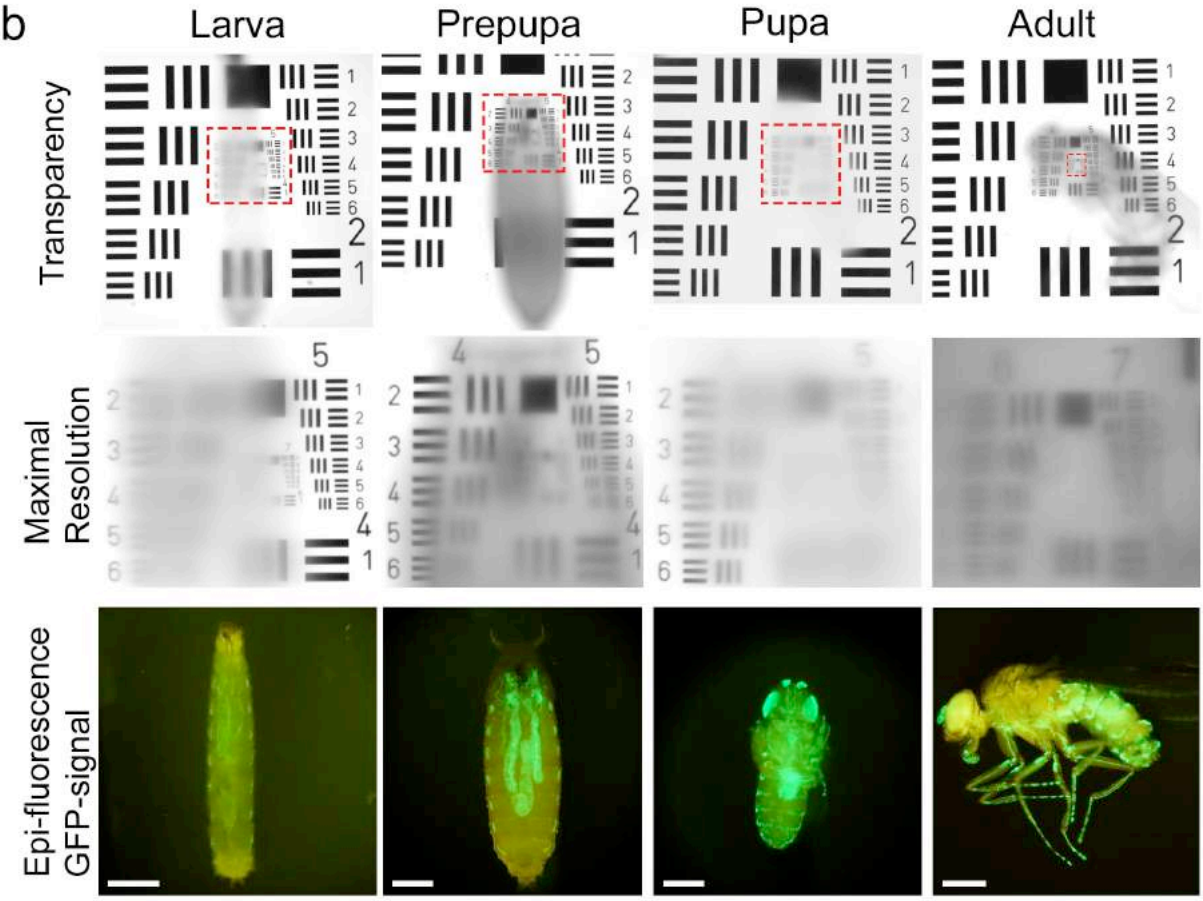

Figure 1

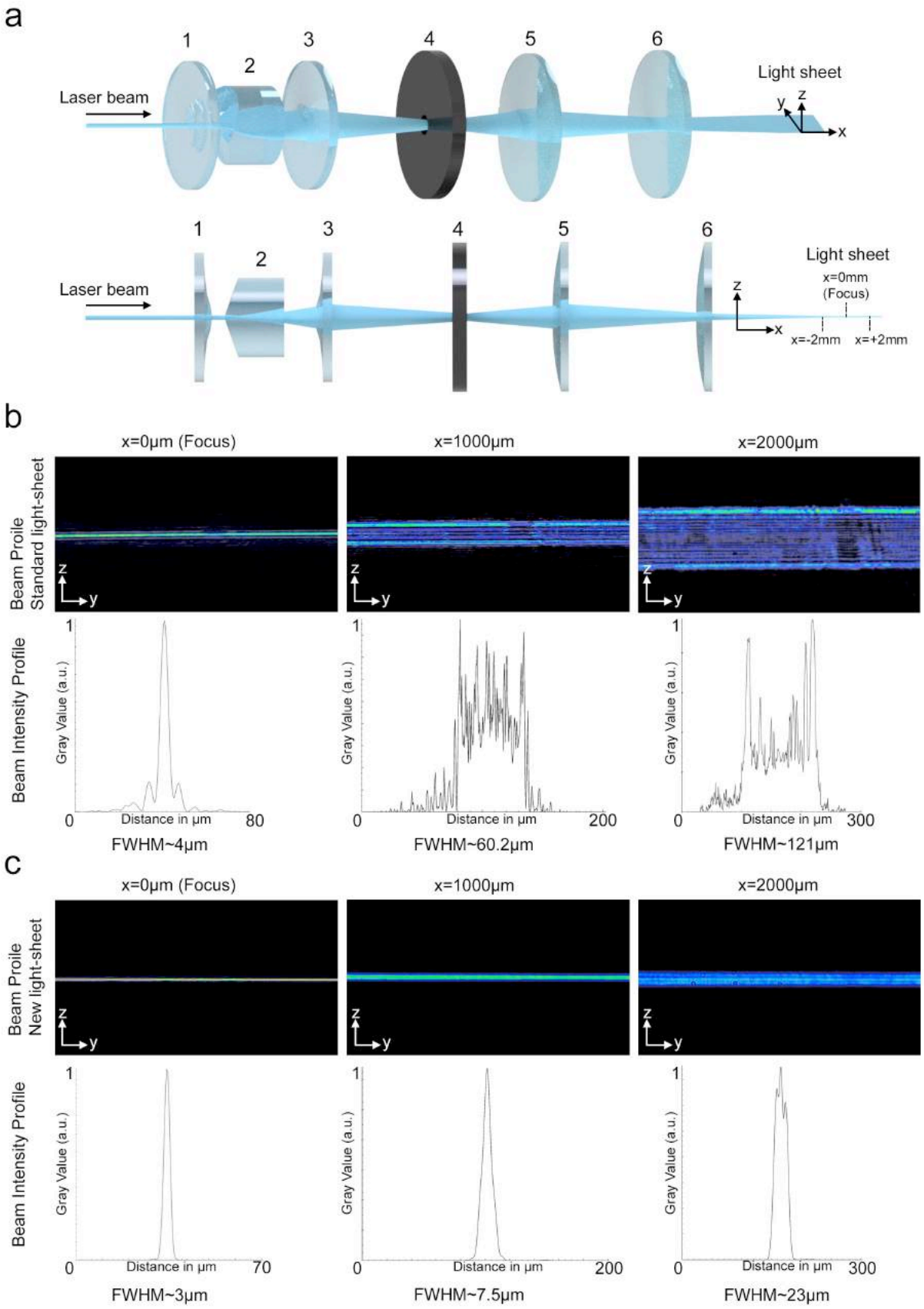
a
1
2
3
4
5
6
Laser beam
Light sheet
y
z
x
x=0mm
(Focus)
x=-2mm
x=+2mm
b
x=0μm (Focus)
x=1000μm
x=2000μm
Beam Proile
Standard light-sheet
Beam Intensity Profile
Gray Value (a.u.)
Distance in μm
FWHM~4μm
FWHM~60.2μm
FWHM~121μm
c
Beam Proile
New light-sheet
FWHM~3μm
FWHM~7.5μm
FWHM~23μm

Figure 2

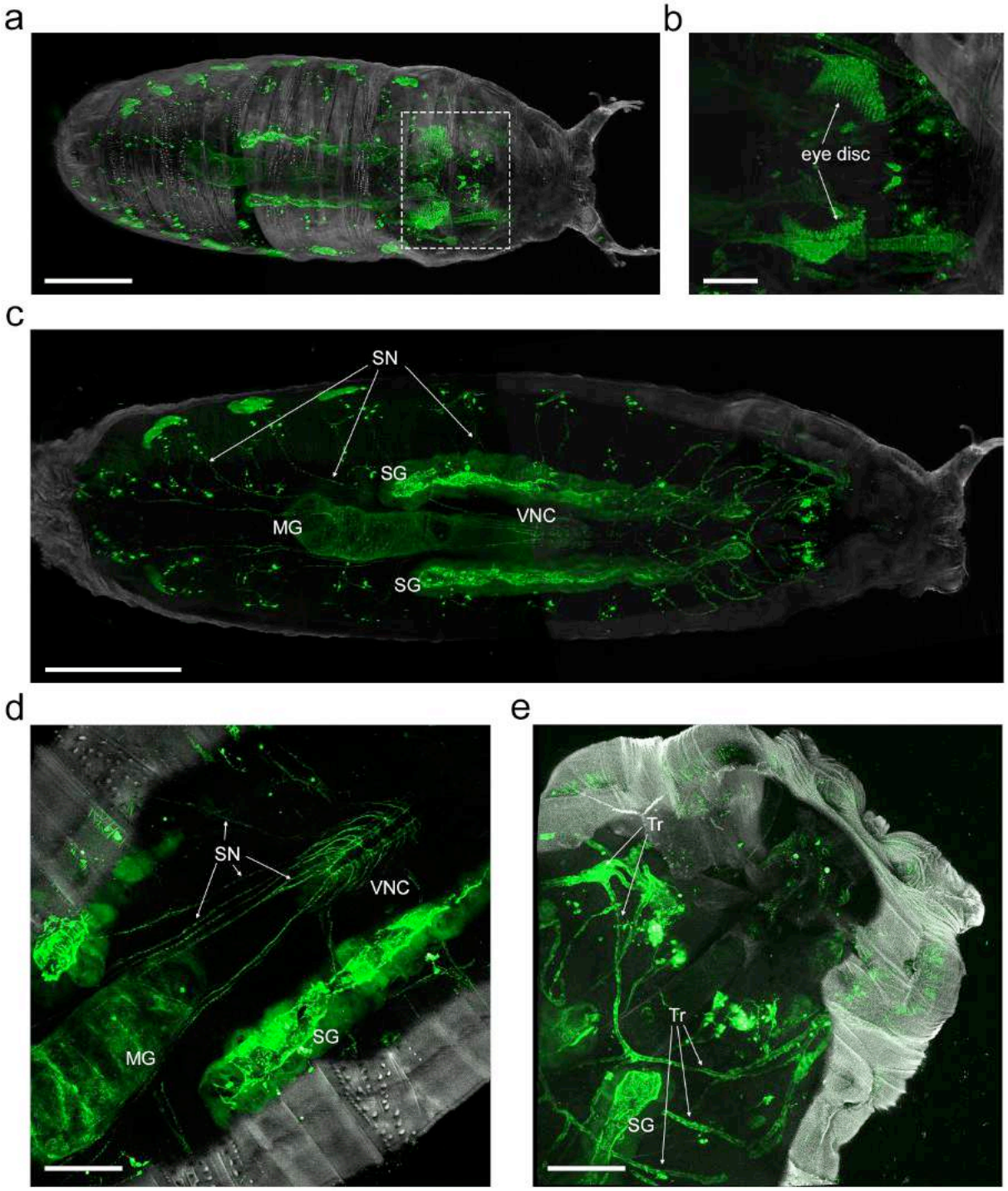

Figure 3

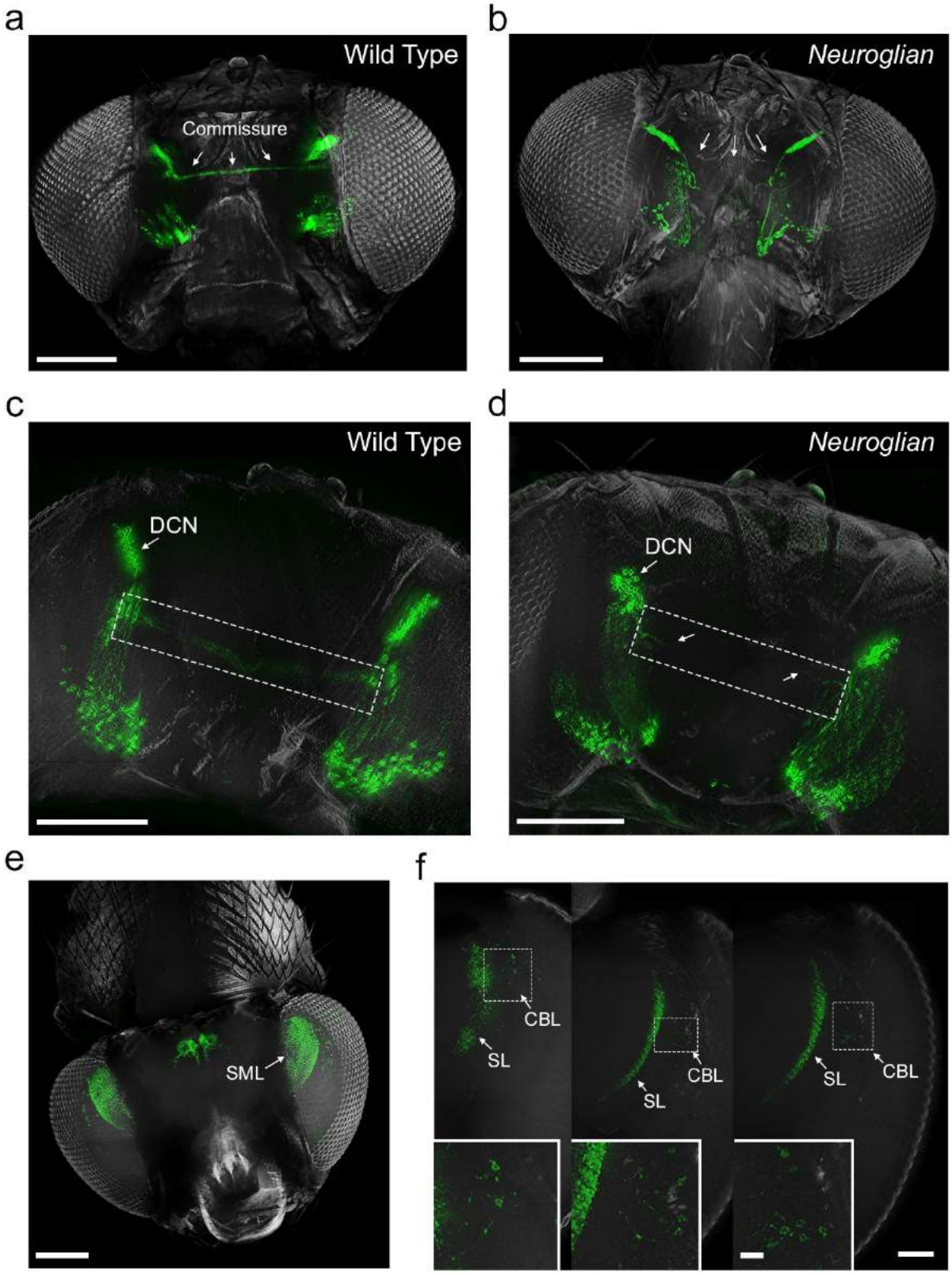
a
Wild Type
Commissure
b
Neuroglian
c
Wild Type
DCN
d
Neuroglian
DCN
e
SML
f
CBL
SL
CBL
SL
SL
CBL

Figure 4

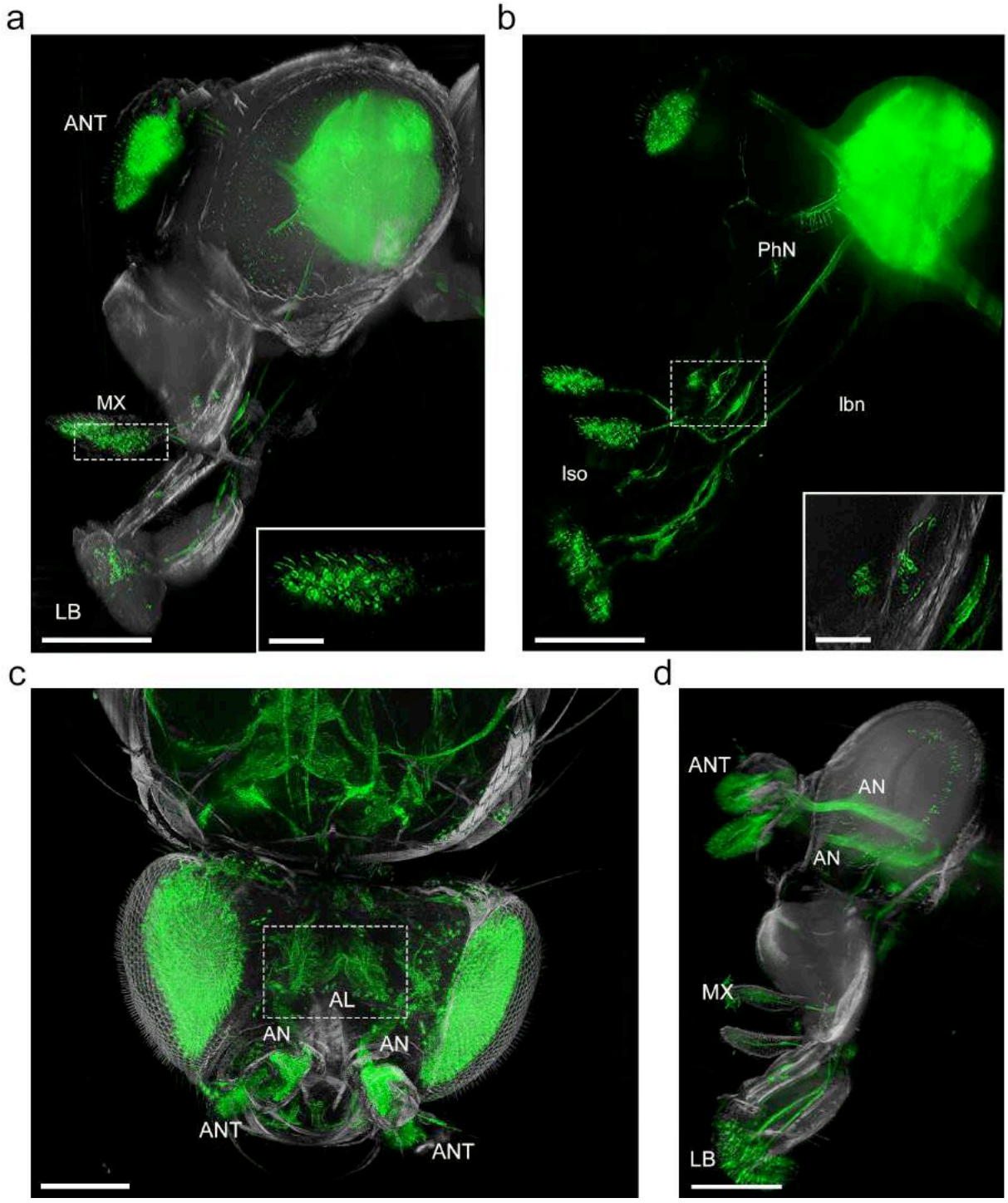

Figure 5

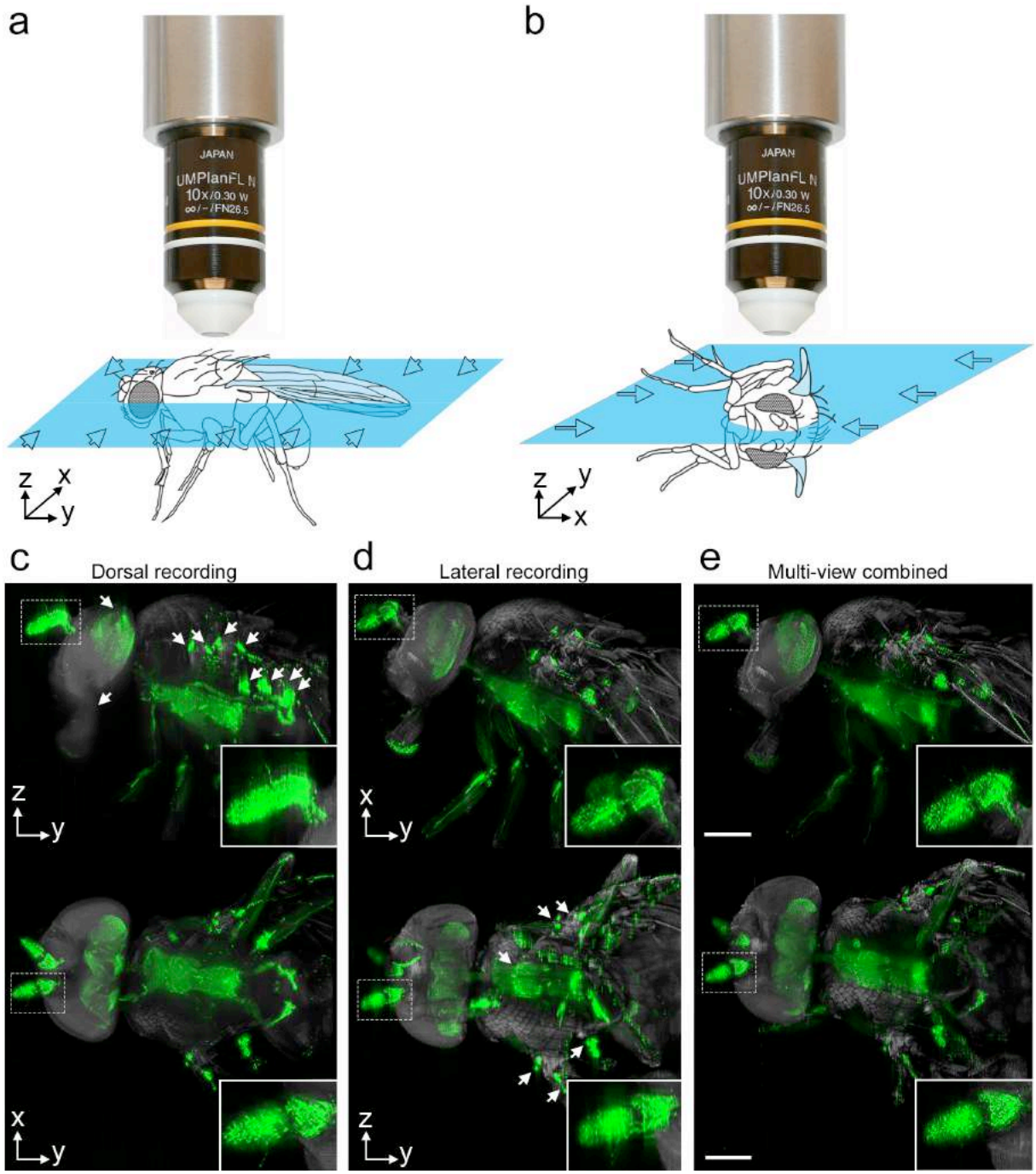
a
b
JAPAN
UMPlanFL N
10x/0.30 W
∞/– /FN26.5
z x
y
z y
x
c
Dorsal recording
d
Lateral recording
e
Multi-view combined
z
y
x
y
x
y
z
y

Figure 6

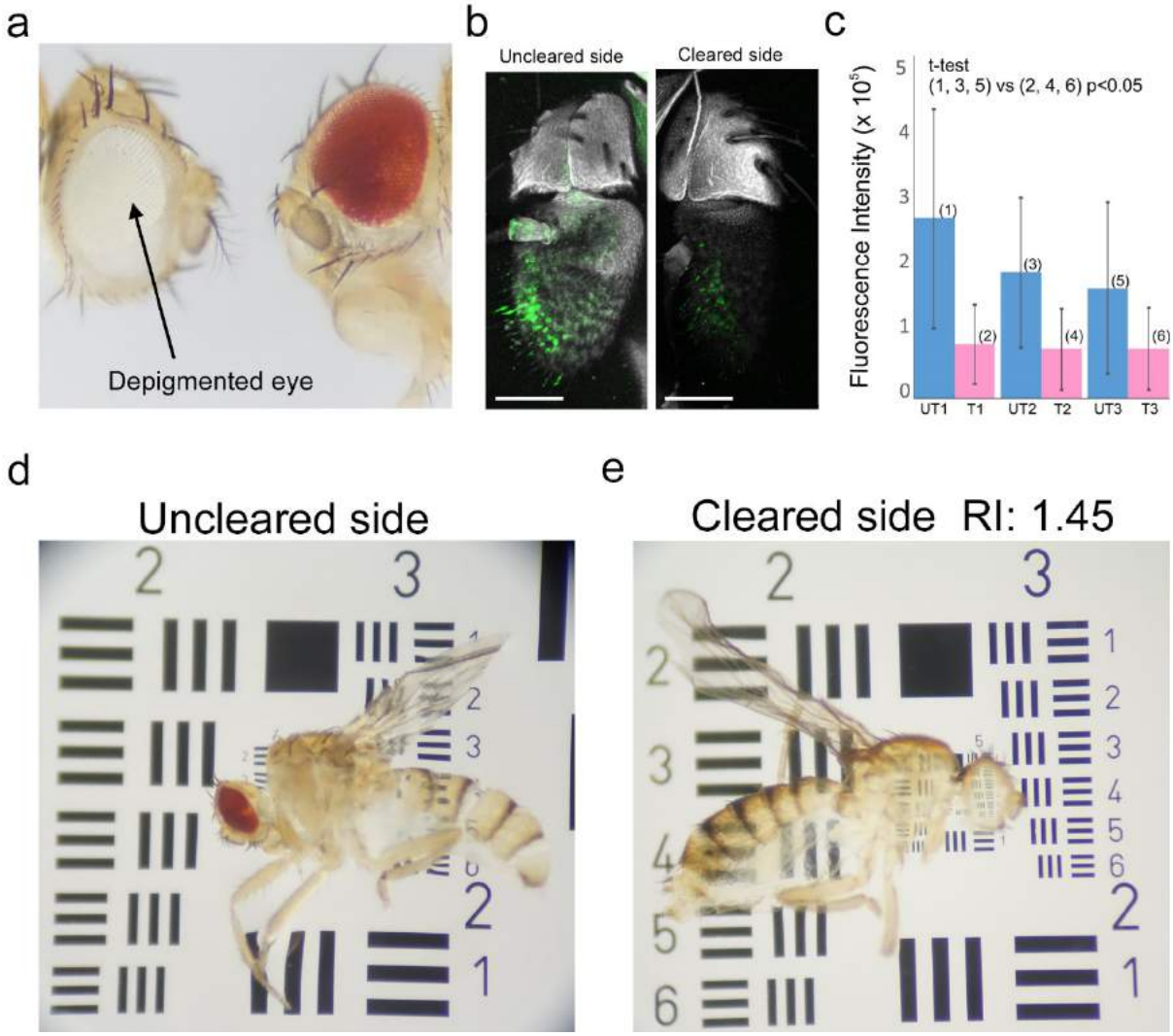

Supplementary Figure 1 | Comparison of uncleared and FlyClear treated adult flies. **a**, **d** and **e** Incident light image showing comparison of uncleared and cleared sides of the same fly. **b** Confocal image of weak GFP signal in the maxillary palp of uncleared and cleared sides of the same fly. **a** Comparison of the depigmentation properties of *Solution-1*. *Solution-1* treated side shows complete depigmentation of the adult eye (image was taken in PBS). **b** Comparison of GFP signal in Uncleared and four days in *Solution-1* cleared sample. Both sides of the same fly were mounted on one slide in Vectashield.and recorded with the same laser intensity. **c** Diagram shows the results from three independent experiments comparing the intensities (± s.d.) of untreated (UT) and *Solution-1* treated (T) sides of flies (n=3). Significance was assigned with unpaired t-test ($p<0.05$). **d** Uncleared right side of adult fly **e** FlyClear processed cleared left side of the same fly. Images in **a**, **d** and **e** were acquired with a stereomicroscope with a 1x objective (Leica, Plan APO 1.0X, WD 61,5mm). Images in **b** were acquired with a 20x immersion objective (Leica, HCX PL APO CS, 0.7 NA, 260µm WD). Genotype: *; UAS-mCD8:GFP ; Or47b-Gal4*. Scale bars in **b** represent 50µm.

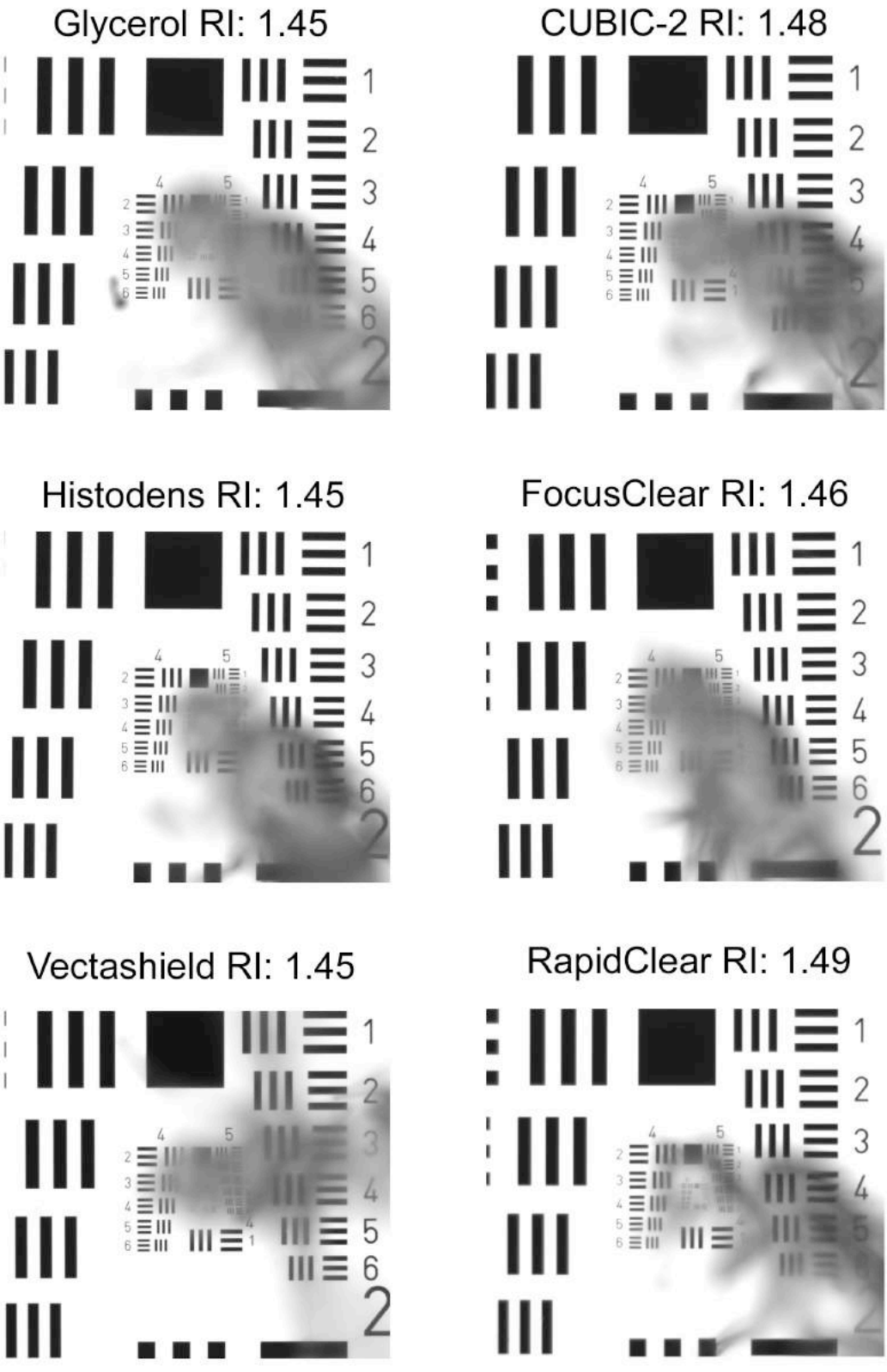

Supplementary Figure 2 | Comparison of transparency achieved after treatment with *Solution-1* and commercial refractive index (RI) matching media. Wide-field image of optically cleared specimens placed on top of a USAF1951-chart.

Supplementary Figure 3 | Mounting of optically cleared flies for signal quantification. Optically cleared flies were mounted with a UV glue on a needle tip, immersed in a cuvette filled with *Solution-2,* and sealed for imaging and storage.

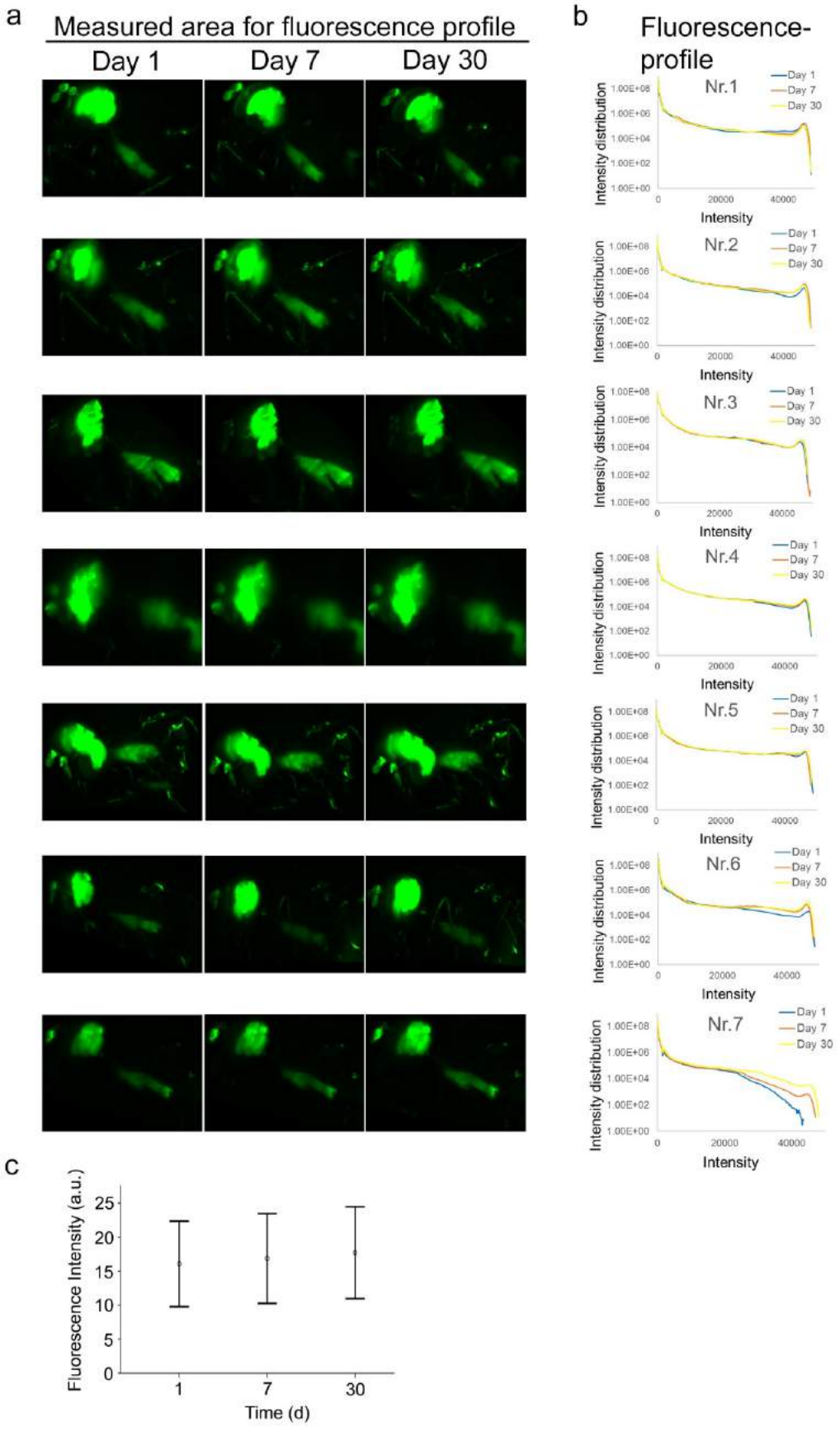
a
Measured area for fluorescence profile
Day 1
Day 7
Day 30
b
Fluorescence-profile
Nr.1
Nr.2
Nr.3
Nr.4
Nr.5
Nr.6
Nr.7
Day 1
Day 7
Day 30
Intensity distribution
Intensity
c
Fluorescence Intensity (a.u.)
Time (d)

Supplementary Figure 4 | Stability of the GFP signal in adult fly after FlyClear procedure. **a** Light-sheet stacks of 600 images show GFP signal in *Drosophila melanogaster* measured with the same settings in the same areas at three different time points (n=7). **b** Histogram data showing the comparison of fluorescence level profiles within these areas over time. **c** Dotplot representing the average ± s.d. of the intensity distribution from seven independent measurements after one day, one week, and one month. For measuring significance, p-values were assessed with one-way ANOVA (P<0.911). All images were acquired with a 4x Objective (Olympus, XLFluor4x/340, 0.28 NA, WD = 29,5mm) with custom-made correction of optics for a refractive index of 1.45 (WD after correction 10mm). Genotype: *dscam-Gal4/CyO; UAS-mCD8::GFP*

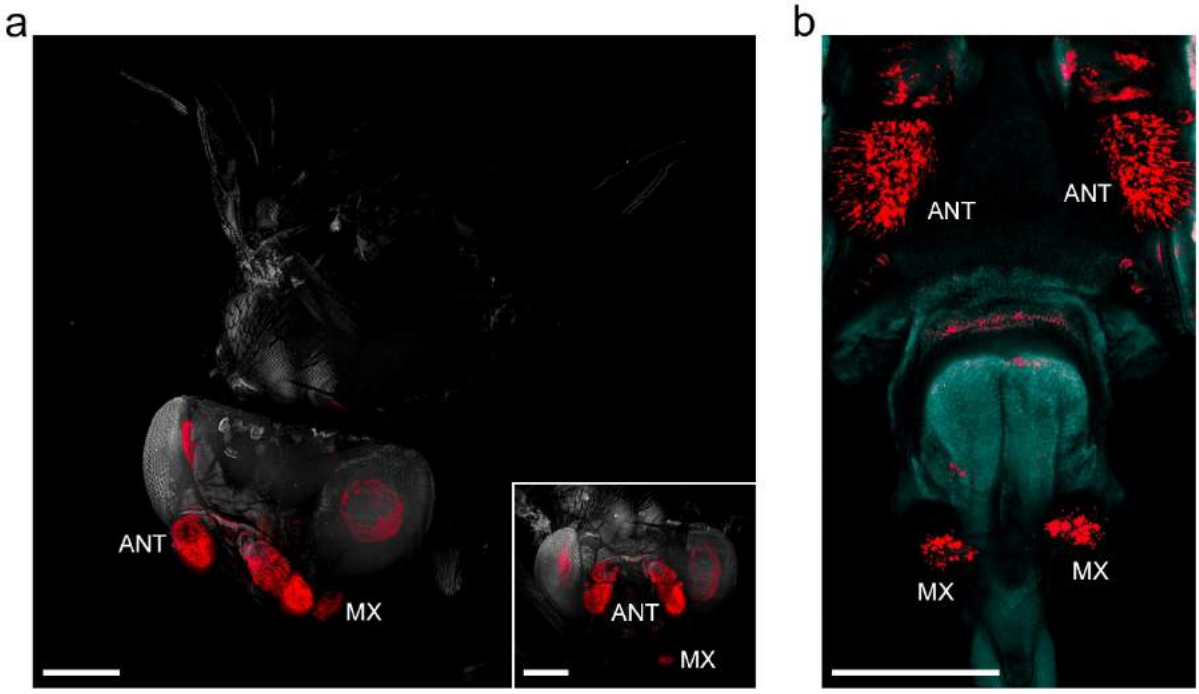

Supplementary Figure 5 | Visualisation of mCherry labeled adult *Drosophila* chemosensory system using FlyClear with confocal- and optimised ultramicroscope. **a** Light-sheet images and **b** confocal images of mCherry expression. **a** Olfactory neurons in antenna (ANT) and maxillary palp (MX). Inset shows coronal view of fly head. **b** Higher magnification of ANT and MX. Images in **a** were acquired with 0.5x post-magnification in combination with a 10x water-immersion objective (Olympus, UMPlanFLN, 0.3 NA, WD = 3.5mm) with custom-made correction of optics for a refractive index of 1.45 (WD = 3.5mm after correction). Image in **b** was acquired with a 20x immersion objective (Leica, HCX PL APO CS, 0.7 NA, 260µm WD). Genotype: *;;R88E12-Gal4 UAS-mCherry.* Scale bars represent 200µm.

a

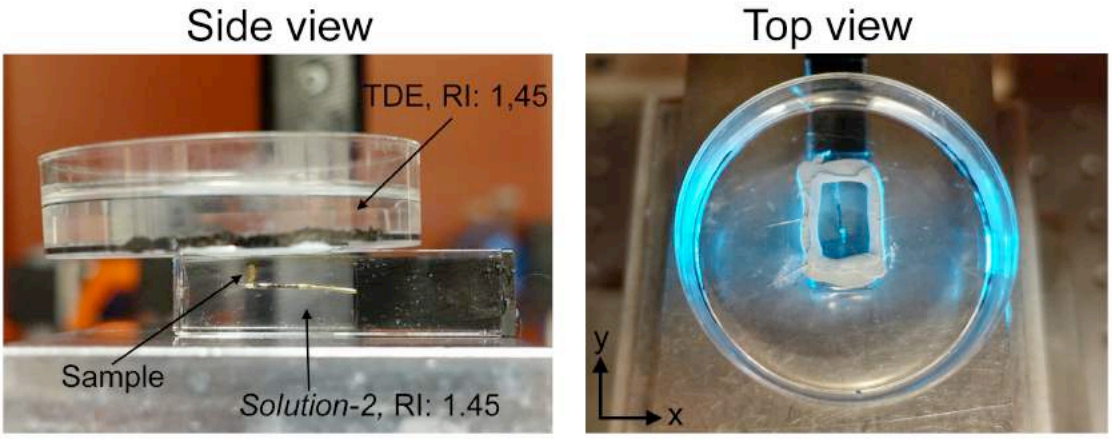
Side view
Top view
TDE, RI: 1,45
Sample
Solution-2, RI: 1.45
y
x

b

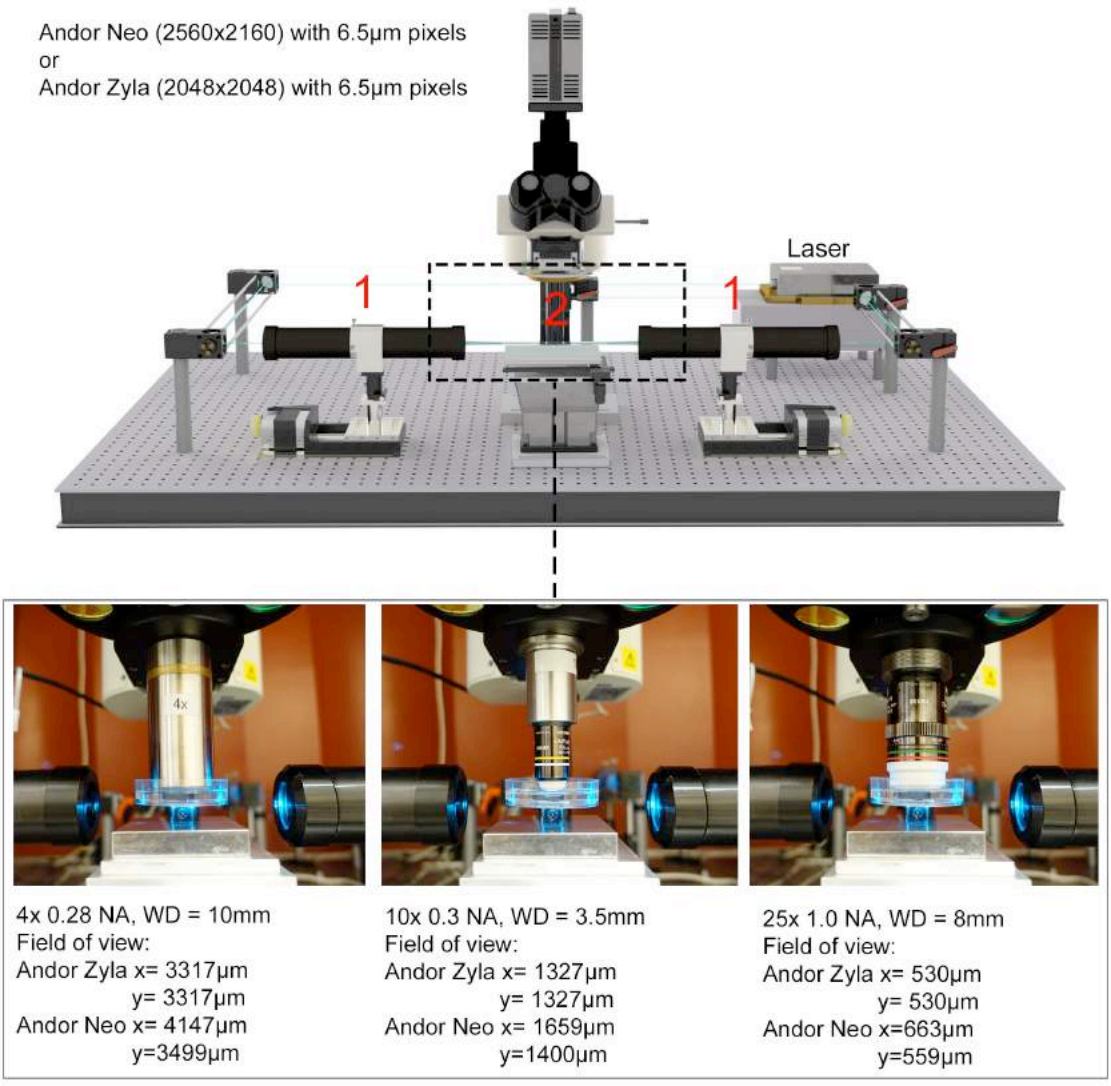
Andor Neo (2560x2160) with 6.5µm pixels
or
Andor Zyla (2048x2048) with 6.5µm pixels
Laser
1
2
1
4x
4x 0.28 NA, WD = 10mm
Field of view:
Andor Zyla x= 3317µm
y= 3317µm
Andor Neo x= 4147µm
y=3499µm
10x 0.3 NA, WD = 3.5mm
Field of view:
Andor Zyla x= 1327µm
y= 1327µm
Andor Neo x= 1659µm
y=1400µm
25x 1.0 NA, WD = 8mm
Field of view:
Andor Zyla x= 530µm
y= 530µm
Andor Neo x=663µm
y=559µm

Supplementary Figure 6 | Ultramicroscope system and imaging chamber (a) Side and top view of the imaging chamber. The sample containing chamber is filled with *Solution-2* (RI: 1,45) the objective immersion chamber is filled with aqueous Thiodiethanol solution (RI: 1,45). (b) Scheme of the ultramicroscope system. (1) Light-sheet generator (illumination lens), (2) detection lenses. Boxed area indicates different detection lenses used for imaging. (From left to right) 4x Objective (Olympus, XLFluor4x/340, 0.28 NA, WD = 29,5mm) with custom-made correction of optics for a refractive index of 1.45 (WD after correction 10mm), 10x water-immersion objective (Olympus, UMPlanFLN, 0.3 NA, WD = 3.5mm) with custom-made correction of optics for a refractive index of 1.45 (WD = 3.5mm after correction), 25x objective (Olympus, XLPlanN, 1.0 NA, WD = 8mm)

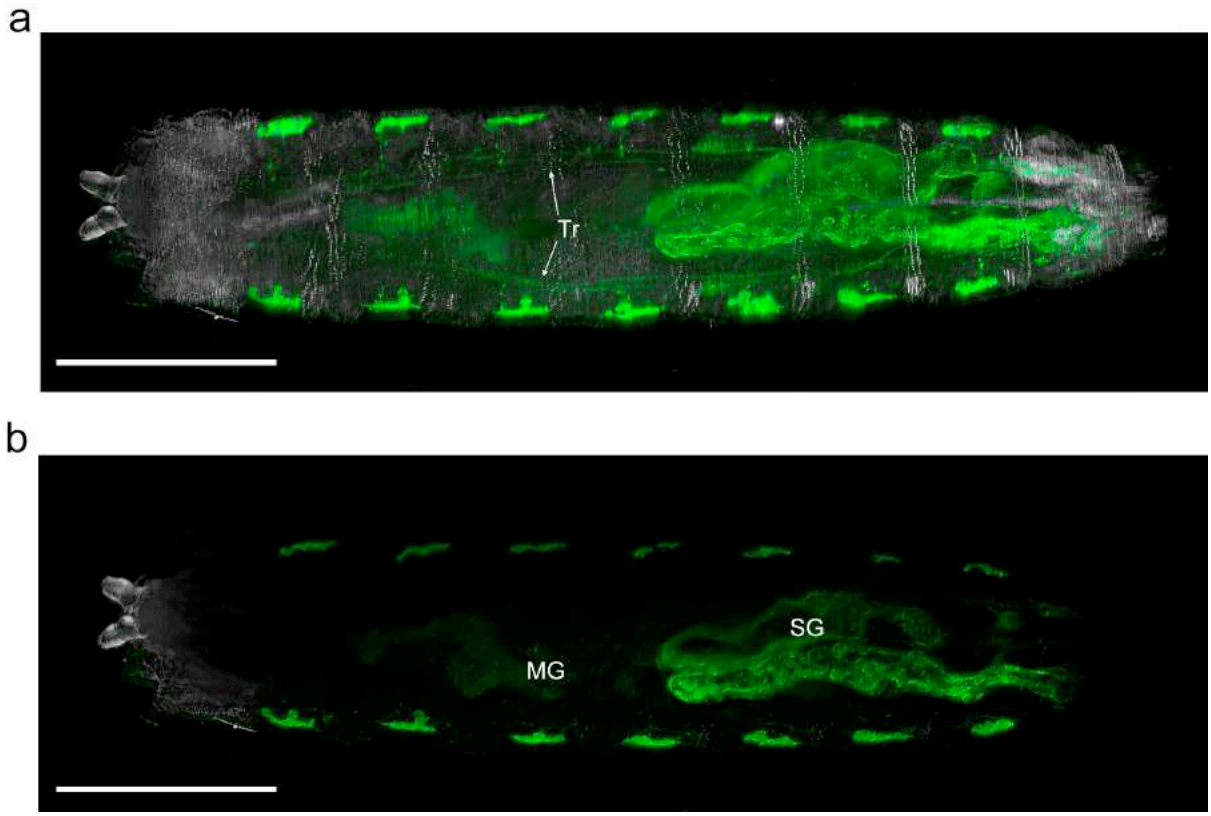

Supplementary Figure 7 | Imaging of FlyClear treated second instar larva using optimised ultramicroscope system. **a, b** Light-sheet images of GFP expression in larval organs. **a** Imaging of whole larva showing the trachea (Tr). **b** Dorsal view of a clipping plane in undisected larva showing mid gut (MG) and salivary glands (SG). All images were acquired with a 10x water-immersion objective (Olympus, UMPlanFLN, 0.3 NA, WD = 3.5mm) with custom-made correction of optics for a refractive index of 1.45 (WD = 3.5mm after correction). Genotype: *Peb-Gal4 UAS-mCD8::GFP.* Scale bars represent 500µm.

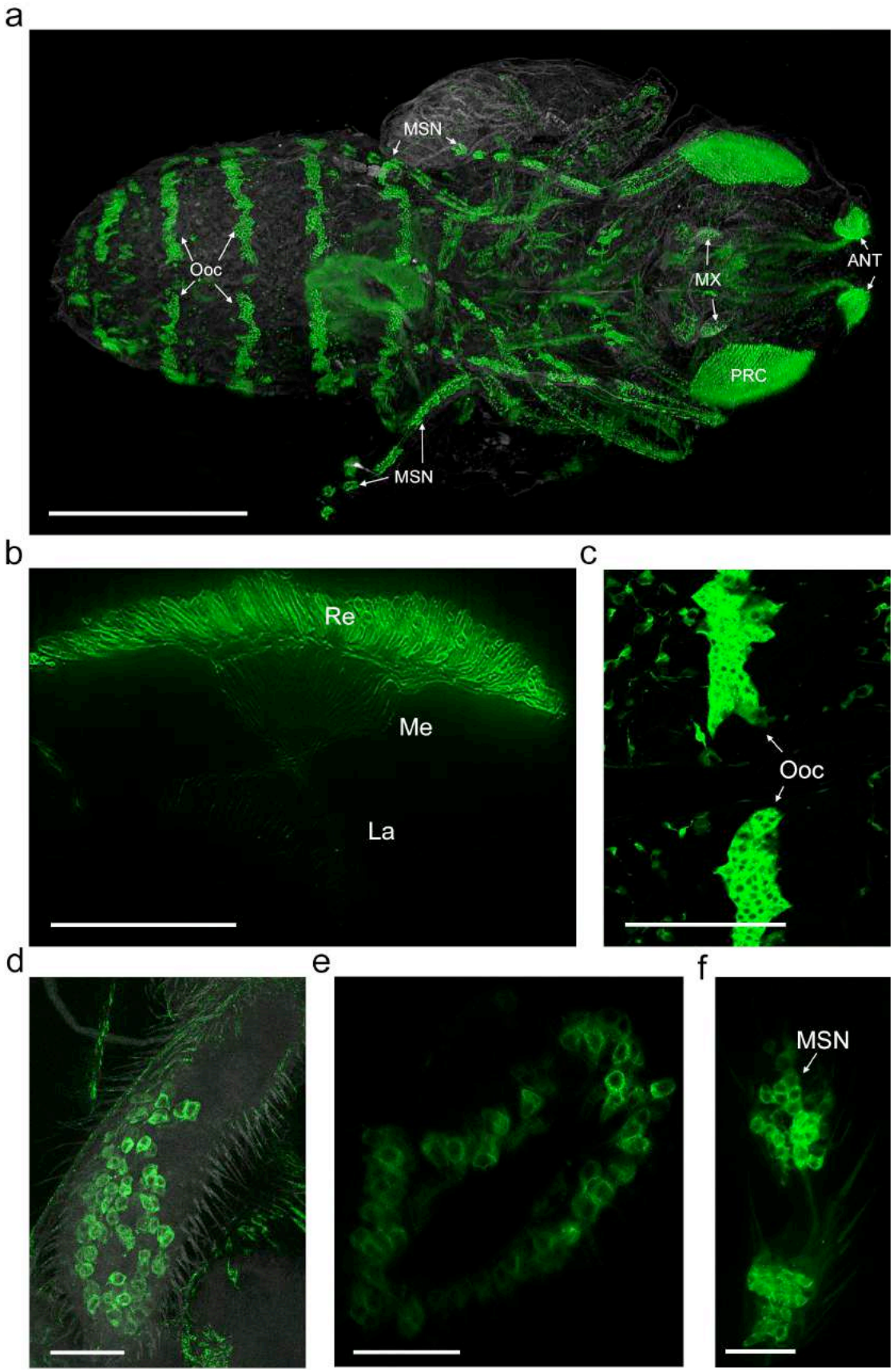
a
MSN
Ooc
MX
ANT
PRC
MSN
b
Re
Me
La
c
Ooc
d
e
f
MSN

Supplementary Figure 8 | Imaging of reproductive, visual and sensory system of an intact pupa using confocal- and optimised aspheric ultramicroscope. **a**, **b** Light-sheet images and **c**-**f** confocal images of GFP expression. **a** Ventral view of Pebbled expression in whole pupa. Arrows indicate oocytes (Ooc) in abdomen, mechanosensory neurons (MSN) in the lags, photoreceptor cells (PCR) in the eyes and olfactory neurons in the maxillary palps (MX) and antenna (ANT). **b** Photoreceptor projecting from the retina (Re) through the lamina (La) into the medulla (Me). **c** oocytes, olfactory neurons in **d** maxillary palp and **e** antenna and **f** mechansensory neurons in leg tip. Image **a** was acquired with 0.5x post-magnification in combination with a 10x water-immersion objective (Olympus, UMPlanFLN, 0.3 NA, WD = 3.5mm) with custom-made correction of optics for a refractive index of 1.45 (WD = 3.5mm after correction). Image in **b** was acquired with a 2x post-magnification in combination with a 25x objective (Olympus, XLPlanN, 1.0 NA, WD = 8mm). Confocal images in **c**, **d** were acquired with a 40x Oil-immersion objective (Leica, HCX OL APO CS, 1.25 NA, 100µm WD) and in **e**, **f** with a 63x Glycerol-immersion objective (Leica, HC PL APO, 1.3 NA, WD 280µm). Genotype: *Peb-Gal4 UAS-mCD8::GFP.* Scale bars represent 500µm in **a**, 100µm in **b**, **c** and 25µm in **d**-**f**.

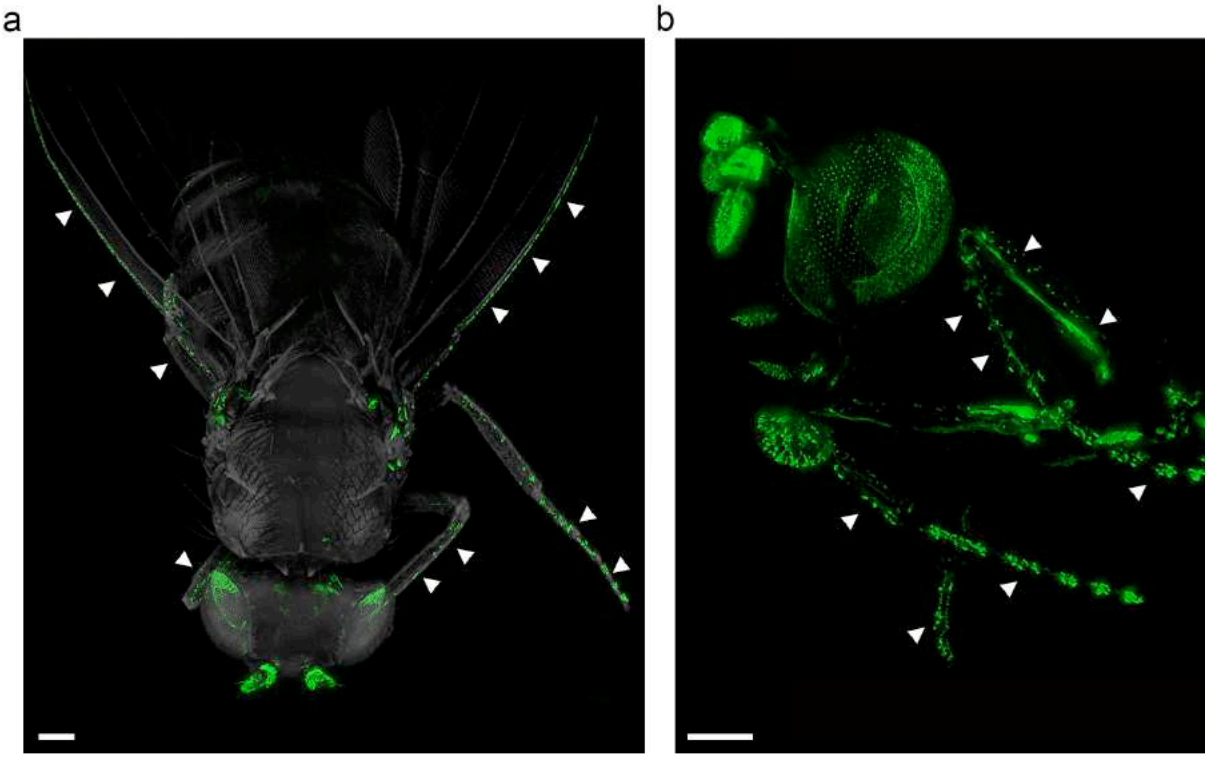

Supplementary Figure 9 | Distribution of mechanosensory neurons in legs and wings visualised using optimised aspheric ultramicroscope system. **a, b** Light-sheet images of GFP expression. **a** Dorsal view of sensory neurons in legs and wings marked with arrowheads. **b** Lateral view of sensory neurons in legs and wings marked with arrowheads. Images in **a** was acquired with 0.5x post-magnification in combination with a 10x water- immersion objective (Olympus, UMPlanFLN, 0.3 NA, WD = 3.5mm) with custom made correction of optics for a refractive index of 1.45 (WD after correction 3.5mm). Image in **b** was acquired with 2x post-magnification in combination with a 4x Objective (Olympus, XLFluor4x/340, 0.28 NA, WD = 29,5mm) with custom-made correction of optics for a refractive index of 1.45 (WD after correction 10mm). In **a** a post magnification of 0.5x was used. Genotype: *Peb-Gal4 UAS-mCD8::GFP.* Scale bars represent 200µm.

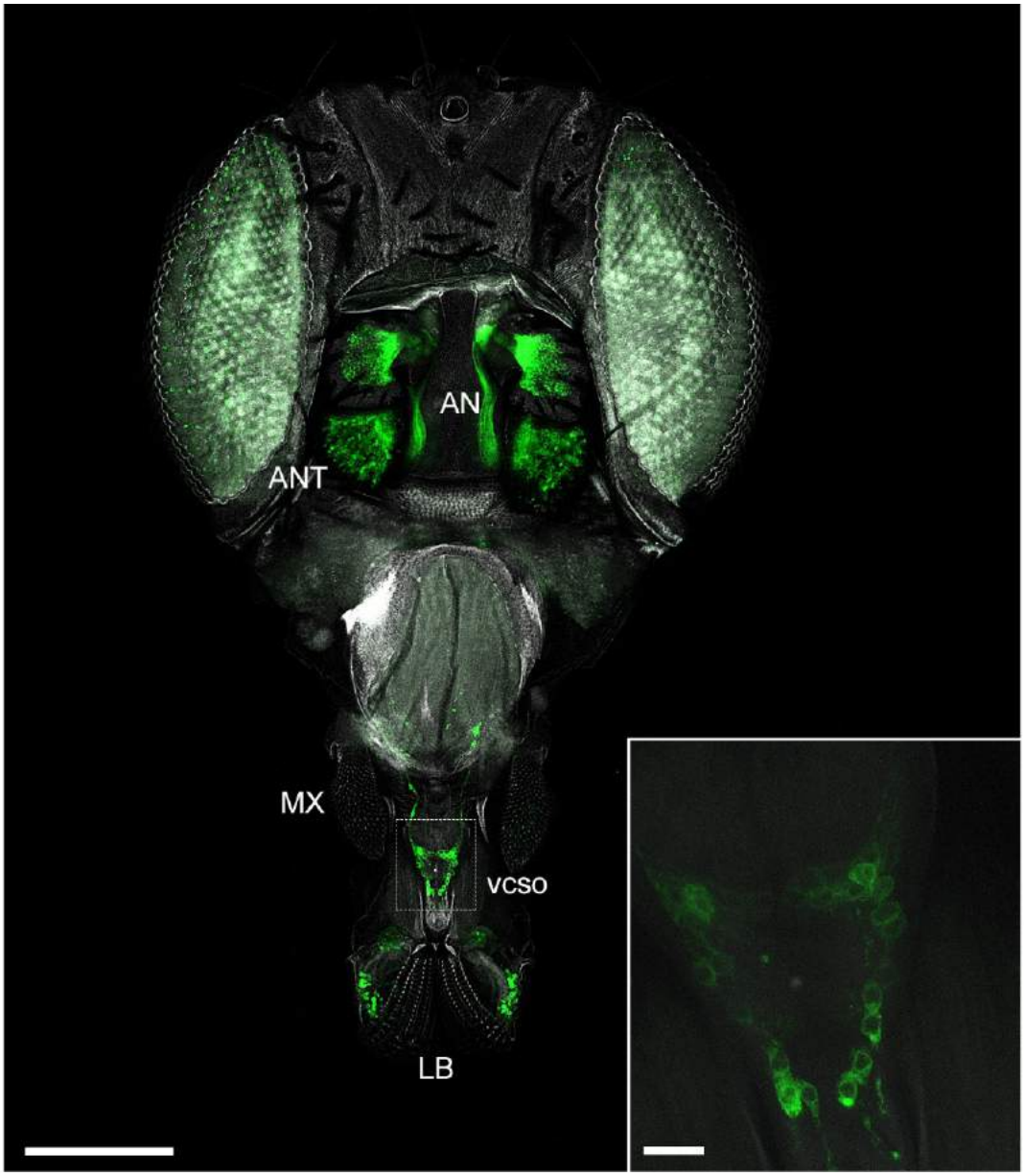

Supplementary Figure 10 | Visualisation of the connections in adult fly olfactory receptor system using confocal microscopy. Coronal view of olfactory receptor neurons in antenna (ANT), maxillary palp (MX), labellum (LB), and part of the antennal nerve (AN) projecting from the ANT. Inset shows a higher magnification image of ventral cibarial sense organ (vcso). Images were acquired with a 20x immersion objective (Leica, HCX PL APO CS, 0.7 NA, 260µm WD). Genotype: *Peb-Gal4 UAS-mCD8::GFP.* Scale bars represent 200µm and 10µm in the main figure and inset respectively.

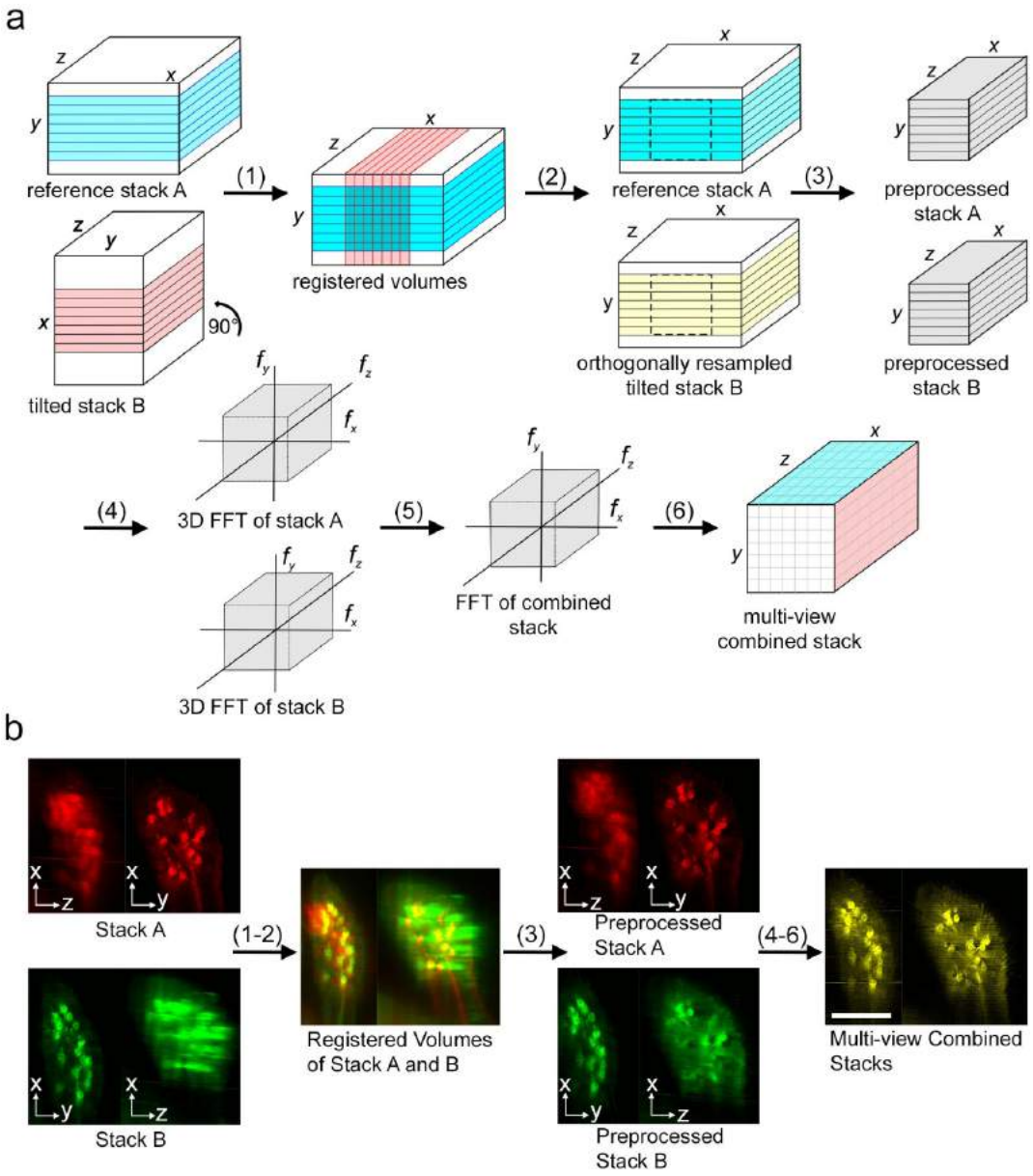

Supplementary Figure 11 | Principle of multi-view combining of ultramicroscope-recordings from 90°tilted directions. **a** Scheme of the workflow of multi-view combining. **b** GFP-labelled neurons in maxillary palp processed with multi-view combining. **a, b** (1) Two image stacks, A (reference stack) and B (tilted stack) were recorded from orthogonally tilted directions and spatially registered using Amira software. (2) After registration, stack B was virtually resliced to generate computed section planes that are coplanar with respect to stack A. (3) Non-overlapping regions were removed from stacks A and B using a binary masking operation. The remaining parts were scaled to approximately the same average brightness by scaling to the 95% percentile. (4) A 3D Fast Fourier Transformation was applied to both stacks and the calculated magnitudes and phases were recombined according to eq. *(3)* and *(4)* in the methods section. (5) The multi-view combined stack comprising the sharper components of A and B was obtained by applying the inverse Fourier transformation.

(6) Finished multi-view combined stack. Scale bar represents 50µm and is representative for all images in **b**.

Supplementary Table 1 | Resolution of the USAF1951-chart in µm

	Group Number						
Element	1	2	3	4	5	6	7
1	250	125	62.5	31.25	15.63	7.81	3.91
2	222.72	111.36	55.68	27.84	13.92	6.96	3.48
3	198.43	99.21	49.61	24.8	12.4	6.2	3.1
4	176.78	88.39	44.19	22.1	11.05	5.52	2.76
5	157.49	78.75	39.37	19.69	9.84	4.92	2.46
6	140.31	70.15	35.08	17.54	8.77	4.38	2.19

Supplementary Table 2 | Imaging specifications

Figure	Animal	System	Objective	Postmagnification	Image pixel size	z-step	Number of channels	Imaging depth	Number of merged stacks	Data volume	Imaging Time
3a	Prepupa	UM	corr. 10x RI: 1.45		0.651µm x 0.651µm	0.651µm	2	936µm	2	19GB	2h
3b	Prepupa	UM	corr. 10x RI: 1.45		0.651µm x 0.651µm	0.651µm	2	Clipped plane of 3a		n.a	n.a
3c	Prepupa	UM	corr. 10x RI: 1.45		0.651µm x 0.651µm	0.651µm	2	Clipped plane of 3a	2	n.a	n.a
3d	Prepupa	Confocal	Leica 20x Gly		0.757µm x 0.757µm	2.01µm	2	247µm		190MB	11min
3e	Prepupa	Confocal	Leica 20x Gly		0.757µm x 0.757µm	1.3µm	2	119µm		260MB	8min
4a	adult *Drosophila*	UM	corr. 10x RI: 1.45		0.651µm x 0.651µm	0.651µm	2	563µm		4GB	40min
4b	adult *Drosophila*	UM	corr. 10x RI: 1.45		0.651µm x 0.651µm	0.651µm	2	546µm		4GB	40min
4c	adult *Drosophila*	UM	Olympus 25x RI:1.45		0.259µm x 0.259µm	0.259µm	2	226µm		12GB	45min
4d	adult *Drosophila*	UM	Olympus 25x RI:1.45		0.259µm x 0.259µm	0.259µm	2	196µm		10GB	40min
4e	adult *Drosophila*	UM	corr. 10x RI: 1.45		0.651µm x 0.651µm	0.651µm	2	459µm		4GB	35min
4f	adult *Drosophila*	UM	Olympus 25x RI:1.45		0.259µm x 0.259µm	0.259µm	2	248µm		16GB	45min
5a	adult *Drosophila*	UM	corr. 10x RI: 1.45	2x	0.324µm x 0.324µm	1.539µm	2	672µm	2	4GB	40min
5b	adult *Drosophila*	UM	corr. 10x RI: 1.45	2x	0.324µm x 0.324µm	1.539µm	1	672µm	2	2GB	20min
5c	adult *Drosophila*	UM	corr. 10x RI: 1.45		0.651µm x 0.651µm	0.651µm	2	601µm		4GB	40min
5d	adult *Drosophila*	UM	Olympus 25x RI:1.45	0.5x	0.54µm x 0.54µm	1.08µm	2	844µm		7GB	55min
6c	adult *Drosophila*	UM	corr. 4x RI: 1.45	2x	0.81µm x 0.81µm	1.62µm	2	1313µm		3GB	30min
6d	adult *Drosophila*	UM	corr. 4x RI: 1.45	2x	0.81µm x 0.81µm	1.62µm	2	2198µm	2	10GB	55min
6e	adult *Drosophila*	UM	corr. 4x RI: 1.45	2x	0.81µm x 0.81µm	1.62µm	2	Dorsal 1313µm; Sag. 2198µm	2 (multiview combined)	25GB	1h 15min
Supp. Figure	**Animal**	**System**	**Objective**	**Postmagnification**	**Image pixel size**	**z-step**	**Number of channels**	**Imaging depth**	**Number of merged stacks**	**Data volume**	**Imaging Time**
1b	adult *Drosophila*	Confocal	Leica 20x Gly		1.250µm x 1.250µm	1µm	2	74µm		100MB	11min
4a	adult *Drosophila*	UM	corr. 4x RI: 1.45		1.642µm x 1.642µm	1.642µm	1	500µm-800µm		n.a.	n.a.
5a	adult *Drosophila*	UM	corr. 10x RI: 1.45	0.5x	1.302µm x 1.302µm	2.432µm	2	1884µm		6GB	45min
5b	adult *Drosophila*	Confocal	Leica 20x Gly		0.757µm x 0.757µm	2.01µm	2	267µm		280MB	11min
7a	Larva	UM	corr. 10x RI: 1.45		0.651µm x 0.651µm	0.651µm	2	895µm	2	16GB	1h20min
7b	Larva	UM	corr. 10x RI: 1.45		0.651µm x 0.651µm	0.651µm	2	Clipped plane of 7a	2	n.a	n.a
8a	Pupa	UM	corr. 10x RI: 1.45	0.5x	1.302µm x 1.302µm	0.651µm	2	801µm	2	12GB	60min
8b	Pupa	UM	Olympus 25x RI:1.45	2x	0.129µm x 0.129µm	0.4µm	1	clipping plane of stack of 422µm		6GB	30min
8c	Pupa	Confocal	Leica 40x Oil		0.378µm x 0.378µm	1.09µm	2	one image		1MB	<1min
8d	Pupa	Confocal	Leica 40x Oil	1.8x Zoom	0.215µm x 0.215µm	0.59µm	2	44µm		160MB	6min
8e	Pupa	Confocal	Leica 63x Gly	1.8x Zoom	0.135µm x 0.135µm	0.04µm	1	one image		1MB	<1min
8f	Pupa	Confocal	Leica 63x Gly	1.8x Zoom	0.137µm x 0.137µm	0.71µm	1	52µm		80MB	6min
9a	adult *Drosophila*	UM	corr. 10x RI: 1.45	0.5x	1.302µm x 1.302µm	2.916µm	2	2145µm		6GB	50min
9b	adult *Drosophila*	UM	corr. 4x RI: 1.45	2x	0.81µm x 0.81µm	1.62µm	1	1061µm		800MB	12min
10a	adult *Drosophila*	Confocal	Leica 20x Gly		0.757µm x 0.757µm	2µm	2	136µm	2	288MB	25min

UM = ultramicroscope, corr. =corrected

Supplementary Table 3 | Video specifications

Supp. Video	Animal	System	Objective	Postmagnification	Image pixel size	z-step	Imaging direction	Imaging depth
1	Larva	UM	corr. 10x RI: 1.45		0.651µm x 0.651µm	0.651µm	Dorsal	895µm
2	Prepupa	UM	corr. 10x RI: 1.45		0.651µm x 0.651µm	0.651µm	Dorsal	936µm
3	adult *Drosophila*	UM	corr. 10x RI: 1.45	0.5x	1.302µm x 1.302µm	2.916µm	Dorsal	2145µm
4 (Multiview)	adult *Drosophila*	UM	Olympus 25x RI:1.45		0.259µm x 0.259µm	0.259µm	Coronal	196µm
	adult *Drosophila*	UM	Olympus 25x RI:1.45		0.259µm x 0.259µm	0.259µm	Sagittal	318µm
5	Pupa	UM	Olympus 25x RI:1.45		0.259µm x 0.259µm	0.259µm	Dorsal	512µm
6	adult *Drosophila*	UM	corr. 10x RI: 1.45	2x	0.324µm x 0.324µm	1.539µm	Sagittal	672µm
7	adult *Drosophila*	UM	corr. 10x RI: 1.45		0.651µm x 0.651µm	0.651µm	Sagital	601µm
8 (Multiview)	adult *Drosophila*	UM	corr. 4x RI: 1.45	2x	0.81µm x 0.81µm	1.62µm	Dorsal	1313µm
	adult *Drosophila*	UM	corr. 4x RI: 1.45	2x	0.81µm x 0.81µm	1.62µm	Sagital	2198µm

UM = ultramicroscope, corr. = corrected

6. Conclusions

A fundamental aspect of brain organization and development is the precise connectivity between different brain regions with multitudes of neuronal population, which forms the underlying biological substrate for organismal behavior. How such a feat of extraordinary neuronal complexity and wiring specificity could be achieved from initially distinct sets of progenitor cells is one of the most intriguing questions? The development of *Drosophila* olfactory map offers a well-suited model system to decipher the cellular and molecular mechanisms specifying neural ensembles into a functional circuit.

In my PhD, I studied how cell-intrinsic differentiation programs, cellular interactions generate a stereotyped olfactory map in *Drosophila.* The precise coordination of sensory and synaptic differentiation is an essential feature of olfactory system, key for proper information processing. Building on the previous findings showing that the chromatin regulator Psc, a component of Polycomb repressor complex, affects the tight coordination of olfactory receptor expression and axonal targeting in lineage-related ORNs, I extended the analysis to multiple ORN classes and determined the role in ORN diversification and is required in the sensilla that give rise to three different ORN classes. Notch dependent final division of intermediate precursor cell pNa leads to two distinct terminal daughter cells: Nab [$Notch^{OFF}$] and Naa [$Notch^{ON}$]. This follows the expression of transcription factor Seven up [Svp], specifically in ORNs deriving from Naa identity [see figure 3 and 9]. Further, I probe the role of Svp in ORN specification and found that loss of Svp specifically leads to switch in axonal targeting preference, from Naa to Nab. This was also accompanied by changes in the identity of the expressed OR type, suggesting a qualitative switch. Moreover, Psc also regulates synaptic and sensory specificity, likely by distinct mechanisms. In Psc loss of function a mixed or patchy axonal innervation was observed where axons fail to innervate within the glomerular boundary with a switch in OR specificity. Interestingly, Psc functions in a dose dependent manner; loss of Psc in lineage-related ORNs express OR specific to Nab identity whereas a gain in Psc level results in an opposite effect. In a detailed lineage study, I could show that Psc stabilizes the synaptic identity and suppress Nab specific fate in Naa derived ORNs by maintaining

the Svp expression. This work thus provides insights into the role of Psc in the diversification of ORN classes derived from single SOP. Unlike mouse olfactory system, in *Drosophila* olfactory receptor function is not required for ORN axon targeting [1], Psc plays an important role in coordinating both the synaptic specificity and sensory identity.

The non-apoptotic function of activator of the programmed cell death, Dark [Death associated apaf-1 related killer], in sensory map formation [2], highlighted a novel regulatory principle in axon guidance. Although non-apoptotic functions of caspases during development have gained growing attention [3], our results for the first time showed its unique role in sensory axon pathfinding and targeting. In this part of the study, I determined the role of Dronc [initiator caspase], the main component of apoptosome complex, along with its regulator Dark in the development of olfactory circuit. Loss of Dark and Dronc affect the same subset of ORN classes and leads to a stereotypic switch in axonal projection domain as well as ectopic targeting by aberrant target recognition. As both Dark and Dronc show clear correlation in the targeting of ORN classes, this implies that Dark exhibit direct positive regulation of Dronc. In order to test the potential targets and to confirm the non-apoptotic function of apoptosome complex in axon targeting, we analyzed the downstream targets of Dronc in apoptotic pathway. Interestingly, mutation in DrICE, the main downstream apoptotic target of Dronc, showed no targeting defects implying a non-apoptotic function of the apoptosome in ORN innervation. Further characterization of other initiator caspases, Strica and Dredd, showed an exclusive class-specific effect for ORN47a axon targeting with partial redundancy of Dronc and Strica, whereas Dredd is dispensable for targeting. Analysis of hypomorphic alleles [2] and RNAi interference against Dark/Dronc lead to the conclusion that level of caspase activity is the key determinant of the innervation pattern of ORNs, as weak reduction in caspase activity leads to shift in projection domain whereas strong reduction in ingrowing ORNs shows both domain switch and ectopic innervation. These experiments revealed that differential caspase activity controls the spatial segregation of axons into different projection domains and its requirement in glomerulus-specific axonal convergence. In order to analyze the cell-autonomous function of apoptosome complex, I generated several *dark* mutant single cell clones, which indicated that cell intrinsic level of caspase activity determines the projection of individual ORN.

However, reverse *MARCM* studies (manuscript 2) showed that the ectopic convergence of the mutant ORNs is influenced by the surrounding ORN axons. These results indicate that cell-intrinsic caspase activity controls axon targeting in two ways: 1) the differential activity of caspase controls initial axon sorting into domains and 2) it mediates synaptic identity by subsequent target recognition. In relation to the molecular nature of this recognition code, Connectin, which is expressed in domain restricted manner, was identified as a potential downstream target of the caspase [2]. Connectin expression was observed in the ectopically innervating caspase mutant ORN axons. Interestingly, neuronal knockdown of Connectin also displayed projection and targeting defect of ORN classes, which belongs to Connectin positive domain. Altogether this work provided novel insights into the non-apoptotic function of caspases in the development of olfactory circuit wiring where the cell adhesion molecule Connectin is controlled via caspases to provide neuronal recognition identity. Interestingly, in aged mouse olfactory bulb Sema7A has been shown as a non-apoptotic target of an initiator caspase, caspase-9 [4]. Sema7A harbors an evolutionary conserved motif, which are the putative caspase-cleavage sites and mutating such sites blocked the cleavage activity by caspase-9 [4]. Both *apaf-1* [vertebrate homologue of Dark] and *caspase-9* [vertebrate homologue of Dronc] mutant mouse ORNs shows pathfinding, maturation and synaptic formation defects [4]. Oshawa et al predict that caspase cleaved Sema7A is inactive and Apaf-1/Caspase-9 signaling regulates ORN development by modulating the functional amount of Sema7A. Likewise, in *Drosophila*, Sema-2b has been shown to play an important role for the selection of correct projection domain [5]. It is evident that the apoptosome signaling controls neuronal wiring by regulating molecules related to axon guidance. Only subset of ORN classes getting affected in apoptosome mutant background, which indicates that Caspase control the expression of subset of recognition molecule and wiring specificity is product of several molecular code working in a combinatorial manner. However, it remains to study how caspases could negatively regulate the Connectin expression and what are the other non-apoptotic targets of caspases? Is Sema also one of the non-apoptotic targets of caspase in *Drosophila* ORNs? This would be an important follow-up of this study.

Besides neuronal differentiation and domain targeting, I investigated the molecular underpinnings of bilateral neural circuit formation. Unlike other sensory system,

olfactory system is ipsilaterally organized in most invertebrates. However, ORNs in *Drosophila* exhibit bilateral mirror symmetric connections in the primary olfactory centers via olfactory commissure, a feature unique to Dipteran. In order to identify the molecular players responsible for the emergence of this bilateral connectivity, I set up a large-scale RNAi screen. Results of this screen showed that ORN specific knockdown of Neuroglian [Nrg], a cell adhesion molecule, during development not only perturb the interhemispheric connectivity of ORNs but also switched the bilateral sensory map to unilateral connectivity pattern. I further confirmed the phenotype by analyzing a strong hypomorphic Nrg allele in which the homophilic adhesion property is perturbed due to a missense mutation in the extracellular second Ig C2 type domain. Developmental analysis of Atonal specified pioneer and Amos specified follower ORNs revealed that both ORN types fail to project contralaterally and is restricted ipsilaterally to their cognate target domains. Targeted Nrg RNAi revealed a specific interaction of ingrowing sensory axons with a distinct class of bilateral glutamatergic LNs. The removal of Nrg from LNs triggers unilateral targeting of all bilateral ORN classes whereas Nrg mutant ORNs have no effect on the bilateral organization of LNs. To determine the number of neurons critical for bilateral olfactory map formation, Nrg-RNAi screen in subsets of bilateral LNs revealed Nrg functions in a small population of ventro-lateral LNs from which Nrg removal completely switched the bilateral map to unilateral. Hence, we named these neurons as commissural Pioneering Interneurons [cPINs]. Developmental characterization of cPINs revealed several novel features and their prospective role in bilateral neuronal targeting and patterning: 1) cPINs are part of ventro-lateral neuroblast lineage, 2) cPINs can be divided into two morphological classes lateral and medial cPINs, 3) cPINs innervate the developing AL right from the beginning of pupa formation and innervate bilaterally prior to the arrival of ORNs, and 4) cPINs prefigure the early ORN projections. Altogether, my results indicated that Nrg could act by cell-cell adhesion between developing cPINs and ORNs, and prevent sensory axons from recognizing their respective ipsilateral targets during the olfactory map development. This may be crucial for the extension of the ORN axons that eventually initiates the contralateral connectivity. To get further insights into the molecular mechanism of Nrg function, we analyzed a series of deletion construction for their ability to rescue the Nrg-mutant uni-lateral map phenotype. I found that during hierarchical axon targeting there is differential requirement of adhesion and signaling domains in different cell types. At

the cellular level axon-axon mediated interaction between different cell types is necessary for bilateral organization, whereas at the molecular level, my data shows that intracellular association with Moesin is independently required in all cell types, whereas Ankyrin-binding domain is mainly required for the innervation of Amos positive follower ORNs. Therefore, our findings reveal how an ipsilateral map could evolve into a bilateral one by recruiting a key molecule in the developmental programs, thereby fundamentally changing the brain circuit organization.

Inter-hemispheric connections are present in several animals with a bilateral body plan, and this could play important function in coordinating lateralized cognitive and sensory-motor functions [6]. Such commissural fiber tracts, most obvious in the formation of corpus callosum, are believed to appear suddenly, highlighting possible evolutionary jumps [6,7]. However, the behavioral relevance of several of these commissures, such as the olfactory commissure studied here, are not yet clear. Do they increase the ability of the organism to interact efficiently with its environment? Possibly yes, but the utility of such additional machinery may be specific to the stage of the organism correlated to their environment. For example, unlike adult flies, larval olfactory system is unilateral in nature [8]. A possible explanation for this could be that larvae often reside in a homogenous and restricted environment. Unlike adult flies, they do not often traverse through complex and temporally unpredictable aerial olfactory space at high velocity. On the other hand, adult flies are confronted with the task to take real-time decisions during their flight though complex olfactory landscapes [9–12]. The commissural olfactory projection might assist them to detect small changes in odor gradient. The ability to detect minute odor differences could be critical for Dipteran flies, where commissural olfactory projections are observed, considering the small distance between their two antennae. Various studies have hypothesized that insects could detect olfactory gradients by detecting odor differences between their two antennae [13–15] but an underlying assumption to this must be that the two antennae are well-separated in distance. However, this assumption does not necessarily apply to flies with short inter-antennal distance, such as *Drosophila*, and in such case the existence of commissural tract could assist in odor gradient detection. A proposal in this regard is that the existence of commissural olfactory tract could amplify small inter-antennal odor differences at the level of olfactory projection neurons. A possible way to achieve such amplification could be

by having differential postsynaptic targeting properties of the ipsi- and contra-lateral innervations. For example, if the contralateral projection has higher tendency to target inhibitory local interneurons that target ORNs, then this could lead to a higher suppression of the activity of ORNs arriving from antenna that is exposed to lower odor concentration. This would result in a contrast enhancement between the activity of ORNs in the two hemispheres. In this regard, a computer modeling exercise on the activity of this neural circuitry could shed important insights. Furthermore, electrophysiological measurement of the postsynaptic responses from interneuron on ipsi- and contra-lateral sides could confirm functional differences in the preferential interneuron targeting of the contralateral projections.

If indeed contralateral projection enhances the contrast between the activity of ORNs in the two AL, thereby conferring the flies with the ability to detect minute odor differences, then this must be reflected in its flight pattern [12]. A possible way to confirm this is by undertaking behavioral analysis in the future. Specifically, test the ability of flies, which possess [wild type] or lack [Nrg mutant] commissural projections to detect a shallow olfactory gradient. Comparing the ability of other non-Dipteran flies that lack this commissure will provide further clues on the physiological relevance of the inter-hemispheric olfactory projections.

In general, the developmental mechanisms underlying the formation of homotopic connections between the two brain hemispheres are mostly unknown. What are the molecular mechanisms involved in the formation of *such* novel structures? This raises the question regarding the functional and molecular constrains which give rise to such evolutionary innovation? *Drosophila* develops two olfactory systems during its lifecycle: larva specific and adult specific. As compared to adult the larval olfactory system shows unilateral organization [8]. During metamorphosis few of the larva specific neurons survive and gets integrated into the adult olfactory system [16,17]. We found in our detailed developmental analysis of cPINs that they start to project contralaterally across the midline right from the early pupa development. It has been recently reported that interneurons during development emerge into three different groups, larval interneurons, adult specific interneurons and interneurons which innervate the AL after the establishment of synaptic specificity and gets integrated in the adult specific olfactory system [17]. What molecular changes in cPINs during the transition from larva to adult trigger the bilateral connectivity? It could be possible

that such molecular changes leads to small variations in molecular interaction involving functional modification of preexisting components, a process known as “exaptation” [18], which might play a key role during this transition. Further, this change may also include modification of several molecular and cellular events like cell fate determination, spatial - temporal constrains during circuit formation and midline axon guidance in context “interhemispheric connectivity”.

Transcription factors and cell adhesion molecules are widely thought to provide cell-type identity and cell surface molecules establish neuronal wiring. It has been proposed that the transcription factors act within lineage to specify different projection neurons classes and cell surface molecules acts downstream of such transcription factors to provide targeting specificity [19,20]. By performing Single-cell RNA sequencing [RNA-seq], Li et al showed that the neuronal transcriptome change dynamically during development of projection neurons [20]. RNA-seq of larval interneurons and developing cPINs could help to determine the expression of such molecular profile in larval vs developing adult specific cPINs and details of transcription factors and/or cell surface molecule would help us to deduce the molecular changes leading to the adult specific interhemsiphric connectivity. In support to this notion, Sen et al. showed that deleting the *orthodenticle* gene from a central complex neuroblast causes it to develop into olfactory neuroblast which give rise to projection neurons with morphological similarity and molecular properties [21], hence it is possible to significantly modify the neuronal circuit. This indicates that new neuronal connection can form relatively easily [21], and this could help us to address how novel brain structures or circuits evolved.

Besides the role of inter-hemispheric olfactory projections, the general importance of bilateral connectivity is further emphasized by a wide spectrum of neurological disorders observed in human patients with abnormal commissural tracts, specifically corpus callosum [22,23]. These subjects harbor mutations in the vertebrate homolog of Nrg, L1 [22,23]. This highlights the high degree of evolutionary conservation in the developmental role of Nrg. In general, L1CAM in vertebrates and Nrg in *Drosophila* has been shown to involved in similar biological processes like neurite outgrowth, axon guidance, fasciculation and synapse formation [24–27]. Mutations on extra- and intracellular domains can result in hypoplasia of corpus callosum and mental retardation, and are often accompanied by additional developmental defects

summarized as CRASH or L1 syndrome [23,28]. In humans, more than 120 mutations dispersed throughout the entire L1 gene have been registered affecting both adhesion and signaling [23]. One of the pathological human mutation $L1^{H210Q}$ is similar to nrg^{849} allele [23,25], where they show a striking defect in the corpus callosum and olfactory commissure formation, respectively.

Despite the genetic linkage, the precise molecular mechanisms by which L1 controls contralateral guidance are unknown. Several pathogenic L1 missense mutations have been addressed *in-vitro* in respect to homophilic and heterophilic binding interactions and their effects on neurite outgrowth and axon branching in cell culture [29,30]. However the *in vivo* consequences of these mutations at cellular level are less well addressed. In *Drosophila* giant fiber circuit, nrg^{849} mutants exhibit axonal guidance as well as synaptic defects that can be rescued by transgenic expression of human L1-CAM, depicting its conserved role from flies to humans [25,31]. Moreover, in vertebrates the L1family of cell adhesion molecules has four protein members [L1, NrCAM, CHL1 and Neurofascin] with functional redundancies, which can complicate the analysis of L1CAM function in vertebrates [24]. Generating endogenous CRASH syndrome mutations in *Drosophila* using *Crisper/cas9* could prove as an invaluable diseases model to probe molecular signaling defects associated with this neuropathology.

As mentioned above, this study finds Nrg to be centrally placed in a sequential developmental patterning of the bilateral olfactory map formation. Nrg in ORNs utilizes its interaction with cPINs, which serve as a path for the contralateral ORN projection. However it remains interesting how the developing bilateral ORNs axons innervate the ipsi- as well as contralateral target during the development, given that the projection neurons the main postsynaptic partners of ORNs innervate the proto-AL prior to ORN innervation? Our detailed developmental analysis shows that both cPINs and Atonal ORNs innervate the proto-AL posteriorly and Nrg mediated interaction between these two cell types prevents ORN axons to recognize their postsynaptic partners, therefore preventing the ipsilateral target recognition. cPINs prefigured the commissural pathway which later innervating ORN axons use for their contralateral innervation. During development, ORN axons show exuberance in filopodia all along the axon at ipsi- and contralateral side and later as the development progress, filopodia seems to be restricted precisely to their cognate target region. This

phenomenon has been observed in vertebrates too, which is known as interstitial branching. Interstitial branching occurs through the formation of collateral branches all along the axon shaft and axon thereby bypass the target region and innervate the target region days after the growth-cone has surpass the target [32,33]. Even though we confirmed the specific Nrg domains required for different cell types during olfactory map development, it is not clear what exact intracellular signaling is recruited in this process. It has been shown that Nrg is involved in the regulation of RTK signaling, where Nrg autonomously increases the activity of both the FGFR and EGFR or repress the EGFR signaling [27,34]. Although considerable knowledge has been gained in L1CAM function, it is not yet understood how L1-family CAMs act in different molecular complexes and integrate signals to control various cellular processes. It would be interesting to elucidate the molecular signaling involved in this interaction.

Moreover, a cell-autonomous Nrg function is required for the formation of initial contralateral cPIN projection, which we view as a guidance tract of subsequent mid-line crossing of ORNs. However, it is still not clear what is the corresponding cell-type with which cPINs interacts with during the initial contralateral projection. It will be interesting to further investigate this aspect. A possible substrate for this could be patterning of midline glia. In *Drosophila*, alternate splicing results in non-neuronal specific isoform of Nrg [35], glial knockdown of Nrg did not disrupt the contralateral projections in our experiments. An RNAi screen for the partner adhesion molecule in glia would be an important future extension to this work. This could possibly imply that Nrg in cPINs engage in heterophilic interaction. Nrg has been shown to elicit a direct heterophilic interaction in *trans* with Echinoid, another Ig-domain containing cell adhesion molecule [34,36]. Nrg can activate Echinoid which antagonize the EGFR signaling pathway during *Drosophila* eye development [34]. In addition to this, Sema1a and Nrg have been also suggested to physically interact in *cis* during gaint fiber development and synapse formation and influence each other's signaling [37]. However the interaction between these two molecules result in different responses during different developmental stages of targeting [37]. It would be interesting to determine the interaction of aforementioned trans-membrane molecules in context of the bilateral axonal innervation of cPINs as well as ORNs.

Taken together, the studies presented in this PhD thesis identified various novel regulators that are central to different aspects of neural circuit development. Furthermore, it highlighted the temporal sequence of these developmental events and attempted to provide mechanistic insights into olfactory system development. Many of these mechanisms may be conserved across different species and other brain regions. Revealing their generality in nervous system formation would indeed be enlightening.

References

1. Dobritsa AA, Van Der Goes Van Naters W, Warr CG, Steinbrecht RA, Carlson JR. Integrating the molecular and cellular basis of odor coding in the Drosophila antenna. Neuron. 2003;37: 827–841. doi:10.1016/S0896-6273(03)00094-1
2. Scheper C. The Role of Drosophila Apaf-1-related-killer (dark) in Establishing Synaptic Specificity in the Olfactory System. WWU Münster. 2009.
3. Williams DW, Mukherjee A. More alive than dead: non-apoptotic roles for caspases in neuronal development, plasticity and disease. Running title: Caspases in. Nature Publishing Group; 2017;44: 1–11. doi:10.1038/cdd.2017.64
4. Ohsawa S, Hamada S, Kuida K, Yoshida H, Igaki T, Miura M. Maturation of the olfactory sensory neurons by Apaf-1/caspase-9-mediated caspase activity. Proc Natl Acad Sci U S A. 2010;107: 13366–71. doi:10.1073/pnas.0910488107
5. Joo W, Sweeney L, Liang L, Luo L. Linking cell fate, trajectory choice, and target selection: Genetic analysis of sema-2b in olfactory axon targeting. Neuron. 2013;78: 673–686. doi:10.1016/j.neuron.2013.03.022
6. Suárez R, Gobius I, Richards LJ. Evolution and development of interhemispheric connections in the vertebrate forebrain. Front Hum Neurosci. 2014;8: 497. doi:10.3389/fnhum.2014.00497
7. Aboitiz F, Montiel J. One hundred million years of interhemispheric communication: The history of the corpus callosum. Brazilian J Med Biol Res. 2003;36: 409–420. doi:10.1590/S0100-879X2003000400002
8. Thum AS, Leisibach B, Gendre N, Selcho M, Stocker RF. Diversity, variability, and suboesophageal connectivity of antennal lobe neurons in D.

melanogaster larvae. J Comp Neurol. 2011;519: 3415–32. doi:10.1002/cne.22713

9. Stocker RF. The olfactory pathway of adult and larval Drosophila: conservation or adaptation to stage-specific needs? Ann N Y Acad Sci. 2009;1170: 482–6. doi:10.1111/j.1749-6632.2009.03896.x
10. Wasserman S, Salomon A, Frye MA. Drosophila tracks carbon dioxide in flight. Curr Biol. Elsevier Ltd; 2013;23: 301–306. doi:10.1016/j.cub.2012.12.038
11. Warren TL, Weir PT, Dickinson MH. Flying *Drosophila* maintain arbitrary but stable headings relative to the angle of polarized light. J Exp Biol. 2018; doi:10.1242/jeb.177550
12. Duistermars BJ, Chow DM, Frye MA. Flies require bilateral sensory input to track odor gradients in flight. Curr Biol. 2009;19: 1301–7. doi:10.1016/j.cub.2009.06.022
13. Borst A, Heisenberg M. Osmotropotaxis in Drosophila melanogaster. J Comp Physiol □ A. 1982; doi:10.1007/BF00612013
14. Martin H. Osmotropotaxis in the Honey-Bee. Nature. 1965;208: 59–63. doi:10.1038/208059a0
15. Duistermars BJ, Frye M. A Magnetic Tether System to Investigate Visual and Olfactory Mediated Flight Control in Drosophila. J Vis Exp. 2008; 3–5. doi:10.3791/1063
16. Tissot M, Gendre N, Hawken A, St??rtkuhl KF, Stocker RF. Larval chemosensory projections and invasion of adult afferents in the antennal lobe of drosophila. J Neurobiol. 1997;32: 281–297. doi:10.1002/(SICI)1097-4695(199703)32:3<281::AID-NEU3>3.0.CO;2-3
17. Liou N-F, Lin S-H, Chen Y-J, Tsai K-T, Yang C-J, Lin T-Y, et al. Diverse populations of local interneurons integrate into the Drosophila adult olfactory circuit. Nat Commun. Springer US; 2018;9: 2232. doi:10.1038/s41467-018-04675-x
18. Gould SJ, Vrba ES. Exaptation—a Missing Term in the Science of Form. Paleobiology. 1982;1: 4–15. doi:10.1017/S0094837300004310
19. Li H, Shuster SA, Li J, Luo L. Linking neuronal lineage and wiring specificity. Neural Dev. Neural Development; 2018;13: 5. doi:10.1186/s13064-018-0102-0
20. Li H, Horns F, Xie Q, Xie Q, Li T, Luginbuhl DJ, et al. Classifying Drosophila

Olfactory Projection Neuron Subtypes by Single-Cell RNA Sequencing. Cell. Elsevier Inc.; 2017;171: 1206.e22-1207. doi:10.1016/j.cell.2017.10.019

21. Sen S, Biagini S, Reichert H, VijayRaghavan K. Orthodenticle is required for the development of olfactory projection neurons and local interneurons in Drosophila. Biol Open. 2014;3: 711–717. doi:10.1242/bio.20148524
22. Bieber AJ, Snow PM, Hortsch M, Patel NH, Jacobs JR, Traquina ZR, et al. Drosophila neuroglian: A member of the immunoglobulin superfamily with extensive homology to the vertebrate neural adhesion molecule L1. Cell. 1989;59: 447–460. doi:10.1016/0092-8674(89)90029-9
23. Fransen E, Van Camp G, Vits L, Willems PJ. L1-associated diseases: Clinical geneticists divide, molecular geneticists unite. Hum Mol Genet. 1997;6: 1625–1632. doi:10.1093/hmg/6.10.1625
24. Hortsch M. Structural and functional evolution of the L1 family: are four adhesion molecules better than one? Mol Cell Neurosci. 2000;15: 1–10. doi:10.1006/mcne.1999.0809
25. Godenschwege TA, Kristiansen L V., Uthaman SB, Hortsch M, Murphey RK. A conserved role for Drosophila Neuroglian and human L1-CAM in central-synapse formation. Curr Biol. 2006;16: 12–23. doi:10.1016/j.cub.2005.11.062
26. Nagaraj K, Kristiansen L V., Skrzynski A, Castiella C, Garcia-Alonso L, Hortsch M. Pathogenic human L1-CAM mutations reduce the adhesion-dependent activation of EGFR. Hum Mol Genet. 2009;18: 3822–3831. doi:10.1093/hmg/ddp325
27. García-Alonso L, Romani S, Jiménez F. The EGF and FGF receptors mediate neuroglian function to control growth cone decisions during sensory axon guidance in Drosophila. Neuron. 2000;28: 741–752. doi:10.1016/S0896-6273(00)00150-1
28. Zhang L. CRASH syndrome: does it teach us about neurotrophic functions of cell adhesion molecules? Neuroscientist. 2010;16: 470–4. doi:10.1177/1073858410365561
29. Schäfer MKE, Frotscher M. Role of L1CAM for axon sprouting and branching. Cell Tissue Res. 2012;349: 39–48. doi:10.1007/s00441-012-1345-4
30. De Angelis E, MacFarlane J, Du JS, Yeo G, Hicks R, Rathjen FG, et al. Pathological missense mutations of neural cell adhesion molecule L1 affect homophilic and heterophilic binding activities. EMBO J. 1999;18: 4744–4753.

doi:10.1093/emboj/18.17.4744

31. Kudumala S, Freund J, Hortsch M, Godenschwege TA. Differential Effects of Human L1CAM Mutations on Complementing Guidance and Synaptic Defects in Drosophila melanogaster. PLoS One. 2013;8. doi:10.1371/journal.pone.0076974
32. Lewis TL, Courchet J, Polleux F. Cell biology in neuroscience: Cellular and molecular mechanisms underlying axon formation, growth, and branching. J Cell Biol. 2013;202: 837–48. doi:10.1083/jcb.201305098
33. Kalil K, Dent EW. Branch management: mechanisms of axon branching in the developing vertebrate CNS. Nat Rev Neurosci. Nature Publishing Group; 2013;15: 7–18. doi:10.1038/nrn3650
34. Islam R, Wei S-Y, Chiu W-H, Hortsch M, Hsu J-C. Neuroglian activates Echinoid to antagonize the Drosophila EGF receptor signaling pathway. Development. 2003;130: 2051–2059. doi:10.1242/dev.00415
35. Hortsch M, Bieber AJ, Patel NH, Goodman CS. Differential splicing generates a nervous system-specific form of Drosophila neuroglian. Neuron. 1990;4: 697–709. Available: http://www.ncbi.nlm.nih.gov/pubmed/1693086
36. Bai J, Chiu W, Wang J, Tzeng T, Perrimon N, Hsu J. The cell adhesion molecule Echinoid defines a new pathway that antagonizes the Drosophila EGF receptor signaling pathway. Development. 2001;
37. Godenschwege TA, Murphey RK. Genetic interaction of Neuroglian and Semaphorin1a during guidance and synapse formation. J Neurogenet. 2009;23: 147–155. doi:10.1080/01677060802441380